BARC
N E W S L E T T E R

RIPE BANANA POWDER
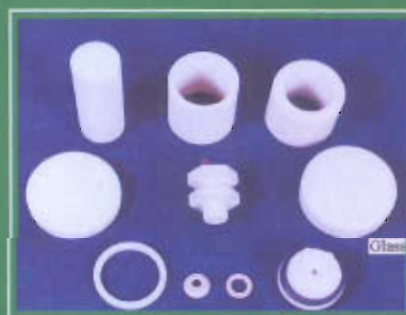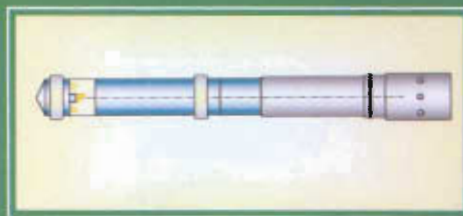
BHABHA ATOMIC RESEARCH CENTRE

FOUNDER'S DAY SPECIAL ISSUE

INDIGENOUS DEVELOPMENT OF MINIATURE UNDERWATER RADIATION RESISTANT CCTV CAMERA FOR REMOTISED INSPECTION OF COOLANT CHANNELS OF PHWRS

R.K. Puri, A.K. Haruray, M. Padmanabhan, H.M. Bapat and Manjit Singh
Division of Remote Handling & Robotics
Bhabha Atomic Research Centre

Introduction

Under IX-Plan project, "Development of Tools and Techniques" (Power-6), development of state-of-art technologies for in-service inspection of coolant channels of PHWRs was taken up at DRHR. Under this project, a Miniature Underwater Radiation Resistant CCTV Camera for visual inspection of coolant channels has been developed. The camera has been designed to be compatible with BARCIS delivery system. The development has resulted in achieving self-reliance in high tech area and substantial savings in cost.

Fig. 1 shows the CCTV camera system. The system consists of Camera Head, Camera Control Unit and the Monitor. The Camera is specially designed with only minimum electronic components (Pick-up tube & pre-amplifier PCB) working in high radiation environment. All other electronic components needed for camera operation are built in the Camera Control Unit, which is located outside radiation environment. The optical and electronic components of the Camera have been specially developed and qualified for use in radiation field of 10^6 Rads/hr for an integrated dose of 10^8 Rads. Gamma Chamber 5000 has been used for irradiation testing of optical and electronics components. CG&CRI and ECIL have helped in the fabrication of optical and electronics components respectively.

Fig. 1 - Miniature Underwater Radiation Resistant CCTV Camera System

Camera Head

Fig. 2 shows the Camera Head. The Camera Head consists of 2/3 inches Yoke Assembly, 2/3 inches Pick-up Tube, Tube Socket PCB, Pre-amplifier and Macro Motor for focus, a Rotating Mirror for radial viewing, a motor for rotating the mirror, and Illumination Head at the front end of camera and water sealing arrangements and centring provisions. The Camera Head is designed to be interchangeable with BARCIS Inspection Head. The assembly of Camera Head and BARCIS Sealing Plug is loaded into the coolant channel using Fuelling Machine. Fig.3 shows the assembly of Camera Head and BARCIS Sealing Plug.
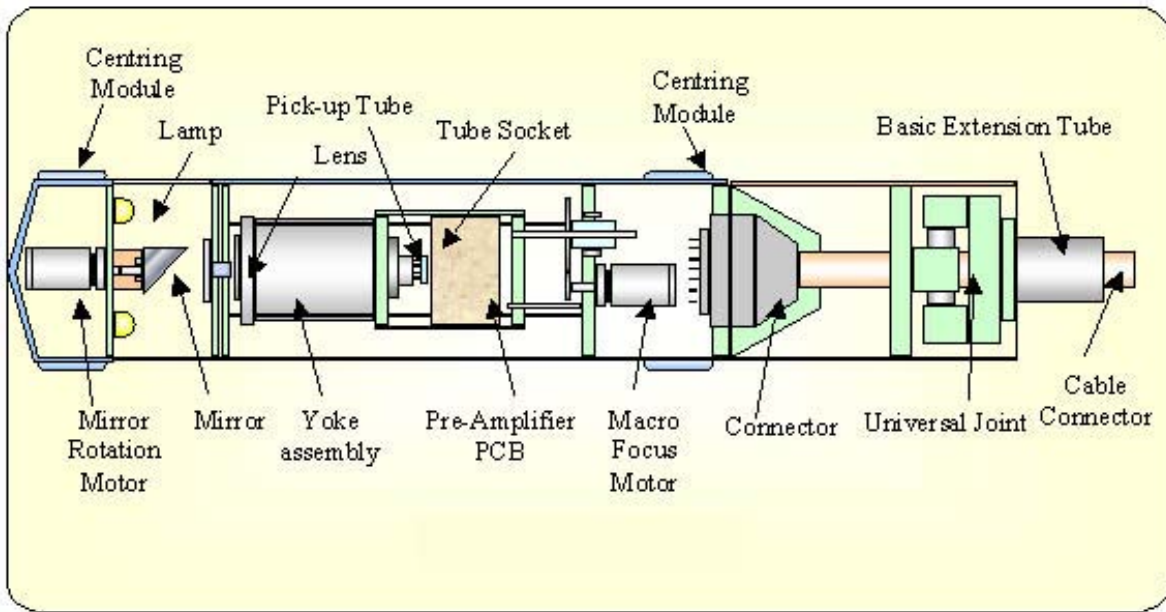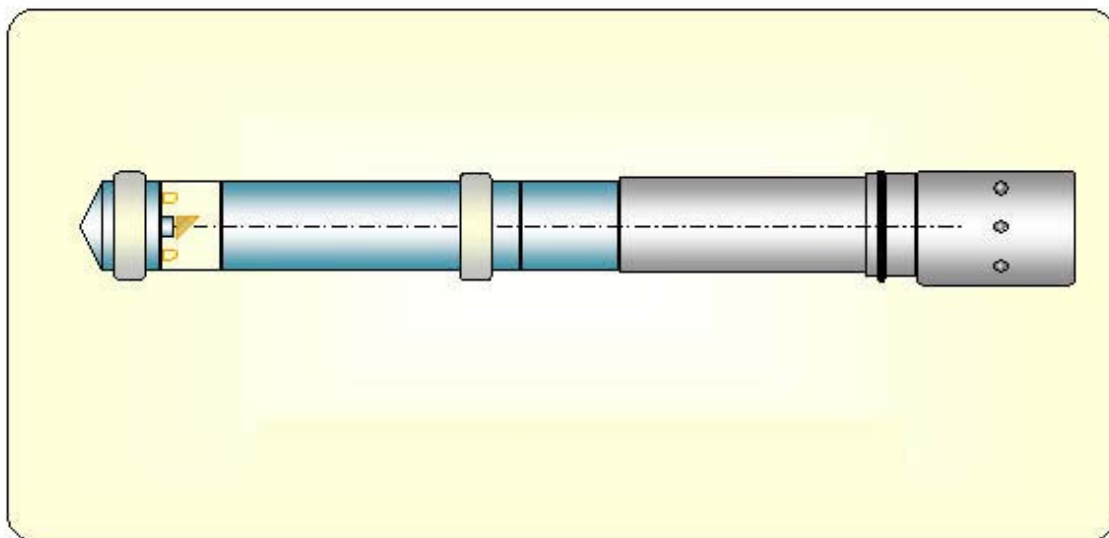

Fig.2 Camera Head

Fig. 3 Camera Head with Special Sealing Plug

Specification of Camera Head

Radiation tolerance	:	100 M Rad @ 1 M Rad per hour
Pickup element	:	2/3" non-browning vidicon tube
Resolution	:	Better than 600 lines at the centre
Sensitivity	:	10 lux on face plate
Illumination	:	3 Halogen bulbs rated at 6 V, 20 W
Controls		Macro focus control
		Illumination control
		Mirror rotation control
Environment (underwater)	:	Rated at 10 Kgs/Sq cm; Working pressure 5 Kgs/Sq cm
Cable	:	Radiation resistant cable length 100 metres

Parts of Camera Head

- Yoke Assembly: The yoke consists of the vertical and horizontal deflection coils for the scanning of the beam in the pick-up tube and a focus coil, which controls the beam current for sharp focus.
- Pick-Up Tube: The Pick-up Tube is the heart of the camera. This is a 2/3 inches radiation hardened pickup tube. It picks up the image signal and supplies it to the Pre-amplifier.
- Tube Socket PCB: The Tube Socket PCB is on the rear side of the Pick-up tube. This PCB supplies the filtered voltages to the electrodes of the Pick-up tube.
- Pre-amplifier: The Pre-amplifier is situated next to the Tube Socket PCB. The signals picked up by the tube are fed to the Pre-amplifier before they are given the main video amplifier. This Pre-amplifier PCB is housed in a shielded copper box to avoid stray noise pick-ups. All the components in the PCB can withstand an integrated of dose of 100 MRads.
- Focus Motor: The Focus Motor is used to adjust the focus. This is done by moving the pick-up tube and yoke assembly on a fixed horizontal axis using the Macro Motor. The motor moves the yoke assembly near or away from the lens depending the focusing required.
- Illumination Head and rotating mirror: The Illumination Head is designed to illuminate the dark inside surface of the pressure tube. The Rotating Mirror is provided to obtain radial view of the internal surface of the pressure tube.
- Multi-component Lens System: The multi-component lens system is provided to obtain focussed image. Fig. 4 shows optical components. The Optical Components are radiation resistant.

Camera Control Unit (CCU)

CCU provides the user with the following facilities
- Focus control
- Illumination control
- Radial mirror rotation control

Apart from fulfilling the usual functions of a camera control unit i.e. focus control, illumination control and mirror rotation, this unit also houses the following camera electronics.
- Signal Generator
- Horizontal Scanning circuit
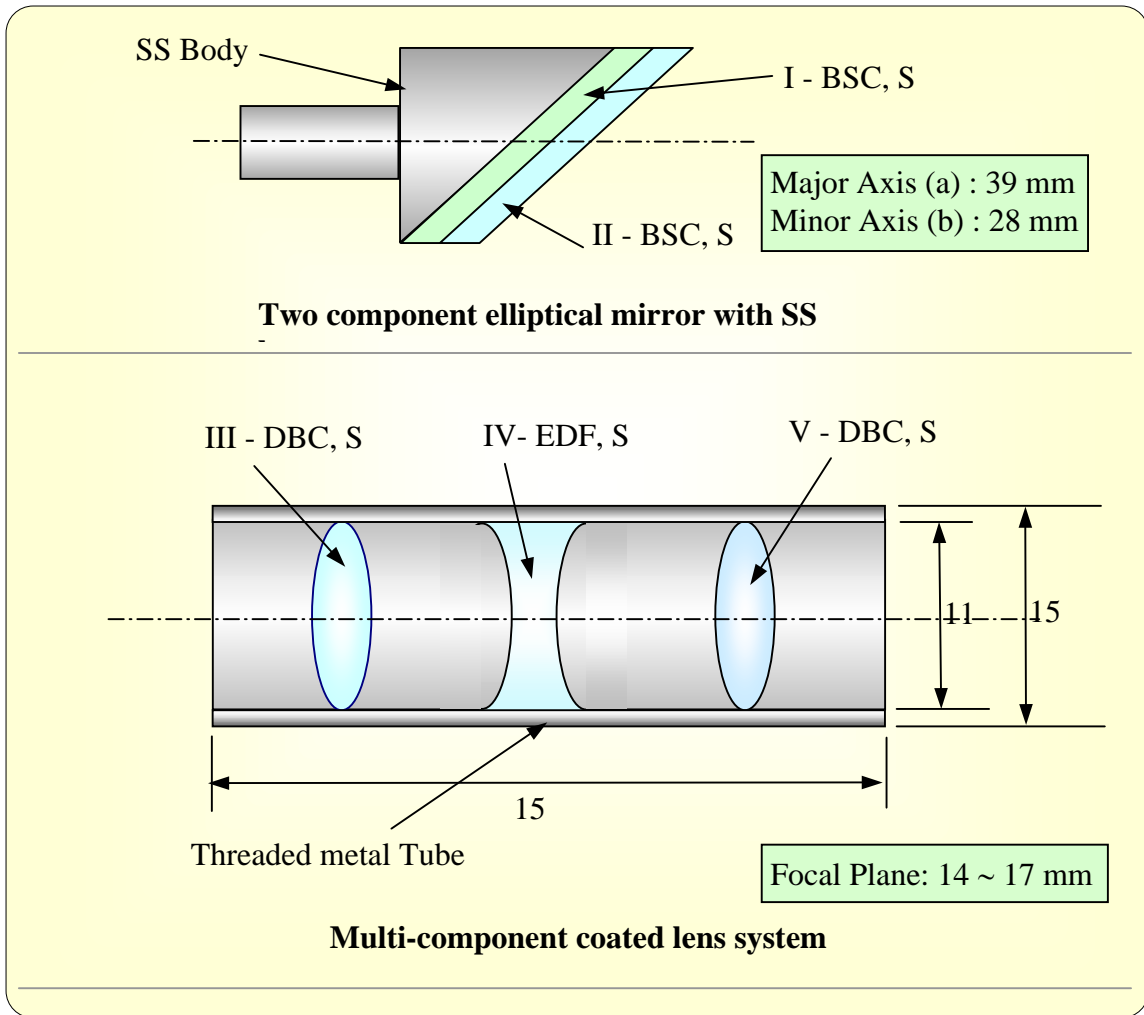- HV Converter
- Video Amplifier

Fig. 4 Optical component of camera

Sr. No.	Glass type	Lens dimensions in mm	%CeO$_2$ Doping
I	BSC, S *(Borosilicate)*	39 (a) x 28 (b) x 4	0.5
II	BSC, S *(Borosilicate)*	39 (a) x 28 (b) x 2	1.8
III	DBC, S *(Dense Barium Crown)*	ϕ 10 x 5	0.5
IV	EDF, S *(Extra Dense Flint)*	ϕ 10 x 6	0.5
V	DBC, S *(Dense Barium Crown)*	ϕ 10 x 5	0.5

Specification of Camera Control Unit:

Standards	:	CCIR-B
Bandwidth	:	> 5.5 MHz @ 3 db
Sensitivity	:	10 Lux
AGC	:	10/1
Signal to noise ratio	:	40 db
Power supply	:	230 V Ac 50 Hz
Power Consumption	:	50 VA
Video Output	:	1 V p-p with 75 Ω termination

Normally these components would have been housed inside the camera itself. In order to make the camera radiation resistant only essential electronics is housed inside the camera and the all the above-mentioned circuits have been moved into the CCU, which will be situated in the control room.

Applications

It was decided to visually inspect the Calandria tubes before installing the new coolant tubes in MAPS-2. The camera was successfully used for inspection of 16 Calandria tubes in August 2002. Fig.-5 shows broken pieces of garter springs in the calandria tube and Fig.-6 shows marks of garter springs (at GS location) on the calandria tube. Fig.-7 shows the camera being inserted into the calandria tube through Lattice Tube Protection Sleeve in MAPS mock-up station.
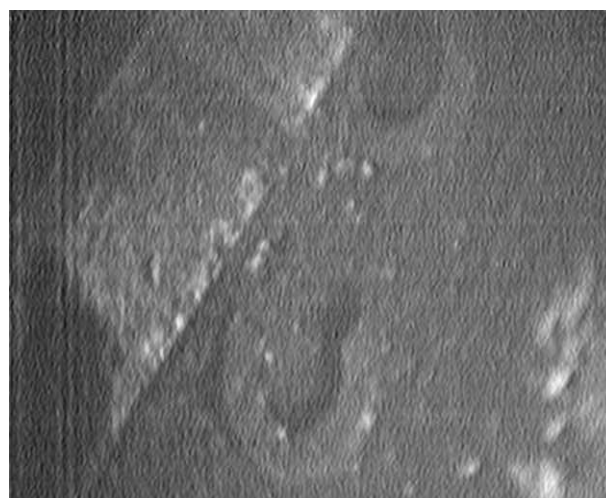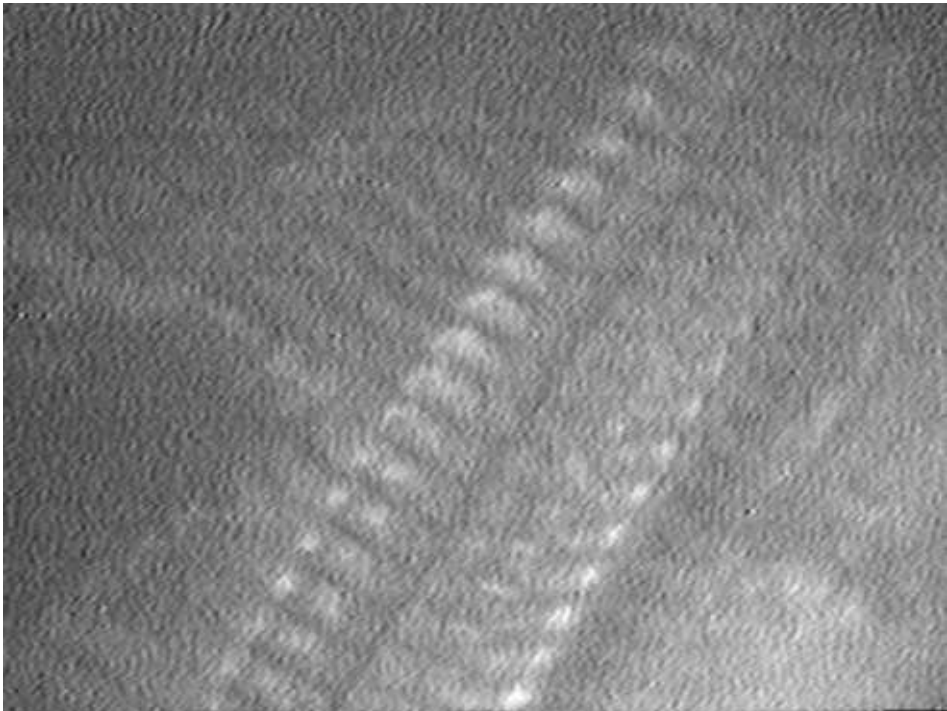

Fig. 5 Broken garter spring pieces

Fig. 6 Garter spring marks on calandria tube

Fig. 7 Camera being inserted into the calandria tube

The camera was also successfully used for visual inspection of ID surface of K-11 coolant channel of KGS-1 reactor in February 2003. Presently the camera is being adopted for visual inspection of Calandria vault of KAPS -1.

Conclusion

The indigenous development of Miniature Underwater Radiation Resistant CCTV Camera for Remotised Inspection of Coolant Channels of PHWRs has been completed. The camera has been designed to be compatible with BARCIS

delivery system. The camera can be used for radial viewing of inside surface of pressure tubes of 220 MWe/500 MWe PHWRs during in-service inspection. The camera can also be used for in-situ inspection of inside surface of calandria tubes prior to installation of pressure tubes. This development has resulted in self-reliance in high tech area and substantial savings in cost. With the experience gained during the development, it will be possible to develop radiation resistant CCTV camera with pan, tilt and zoom for use in hot cells & water pools.

Mr Mahadeva Padmanabhan is the recipient of the DAE Technical Excellence Award for the year 2002 for his outstanding contributions in the development of Minature Underwater Radiation Resistant CCTV Camera for Remote Inspection of Coolant Channels of Pressurised Heavy Water Reactors (PHWRs), computer-controlled Single Crystal X-ray Diffractometer (SCXRD) and BARC Channel Inspection System (BARCIS)

About the authors ...

R.K. Puri *of Division of Remote Handling and Robotics, BARC, is heading the In-Service Inspection Section. He is involved in the development of BARCIS system and Radiation Resistant CCTV camera system. He has also developed micro-arrayer for DNA chip making, sag-measuring tool for pre-service inspection of coolant channels of PHWRs.*

A.K. Haruray *of DRHR, has worked on the development of BARCIS and Radiation Resistant CCTV Camera system. He has developed a number of devices, tools and fixtures for various NDT applications.*

M. Padmanabhan *of DRHR has worked on the development of BARCIS and Radiation Resistant CCTV Camera system. He has also worked on the development of Single Crystal X-ray Diffractometer system. He is the recipient of Indian Physics Association's S.N. Seshadri Memorial Instrumentation Award for 1999.*

H.M. Bapat *of DRHR has worked on the development of BARCIS, Radiation Resistant CCTV Camera system and Performance Testing & Evaluation system for reactivity control mechanisms of TAPP-3&4.*

Manjit Singh *is Head, Division of Remote Handling and Robotics, BARC. He joined the BARC Training School in 1972. Mr. Manjit Singh is the recipient of Homi Bhabha award for securing 1st rank in BARC Training School. He has also received 'BARC Technical Excellence Award 1997'. He has pioneered the development of remotised tools for in-service inspection of coolant channels of 220 MWe PHWRs in India. He has been responsible for the design, development and supply of BARCIS (BARC Channel Inspection System) systems to NPCIL. He has pioneered the development of reactivity control mechanisms for use in research and power reactors. He has been responsible for the development of Cobalt-60 Teletherapy machine, Mobile Robot, Rugged Duty Manipulator & KRUSHAK (POTON – Potato & Onion Irradiator).*

FLUCTUATIONS IN ATMOSPHERIC PRESSURE ARC PLASMA DEVICES : A THEORETICAL INVESTIGATION SUPPORTED WITH EXPERIMENTS

S. Ghorui, S.N. Sahasrabudhe, P.S.S. Murty and A.K. Das
Laser & Plasma Technology Division
Bhabha Atomic Research Centre

A b s t r a c t

Fluctuations in atmospheric pressure arc plasma devices play important role in plasma processing applications. A number of experimental investigations are reported in literature to characterize dynamic behavior of such systems. Recently, experimental works by the authors established existence of chaotic behavior in such systems. Investigation, presented in the paper, addresses possible theoretical explanation of the behavior observed experimentally. Starting from the basic governing equations, a third order nonlinear amplitude equation is obtained through systematic development for dynamic evolution of such systems. Coefficients of this equation depend on thermo-physical properties of the system that in tern depend on plasma temperature, arc current and flow rate of plasma gas. System has been found to follow period doubling route to chaos under change in value of control parameter in agreement with that observed experimentally. For higher value of control parameter, system is found to exhibit catastrophic behavior in terms of sudden extinction of arc. A number of interesting facts about the dynamics are obtained through study of coefficients that matches with experimental observations. The developed theory for fluctuation is fairly general to explain dynamic behavior of atmospheric pressure arc plasma devices. Outcome of the theory has been compared with reported experiments performed by the authors in terms of time series, power spectra, Lyapunov exponents, fractal dimension, phase portrait and response under variation in control parameters. Nice match is observed between experiment and theory in all cases. The theory has also been applied to explain observed behavior in most of the important experiments on fluctuation reported in literature performed by various experimentalists. The theory reproduces observed behavior to a reasonably good extent in all the cases. Details of these results are reviewed in this paper. Possible impacts of the obtained results are also discussed.

Introduction

Arc plasma fluctuations are inherent part of most laboratory as well as industrial plasma devices and have been a cause of major worry to researchers due to their adverse impact on plasma processing [1]. In terms of literature, except for experimental data on arc electrode erosion, no systematic work to understand the nature of fluctuation has been carried out. Present work looked at the problem from this viewpoint and performed an in-depth study for the first time. A number of new facts about arc plasma fluctuations are found out through experimental and theoretical investigations and presented in this paper.

The complete work can be broadly categorized into two parts: experimental and theoretical. The systematic experimental study and rigorous analyses of the associated signals confirmed existence of chaos in such systems as well as determined possible controlling parameters of dynamics and route of transition from regular to

chaotic behavior. Experimental estimates of a number of dynamic quantities of the system are also obtained through this study. Values of these dynamic quantities are reproduced to a closed proximity from the developed theory. On the other hand, the theoretical analyses model the near arc root region using standard conservation equations and Maxwell's equations and evolve to a third order nonlinear amplitude equation for describing dynamics of the system. Coefficient of this amplitude equation depends on thermo-physical properties of the plasma realized under given operating condition and hence determines dynamic behavior of the system. System behavior is studied in detail through this amplitude equation. Finally, results obtained from the theory are compared with experiments performed in the laboratory as well as with experiments performed by various experimentalists worldwide. Most of the important experiments reported in literature are covered and good match is observed in all cases. Possible impacts of these new findings are discussed.

Experimental

Arc voltage fluctuation, acoustic emission and optical output are the three easily measurable signals generated from any arc plasma discharge that caries most of the information about underlying dynamics. Experimental measurement of such signals in a typical arc plasma device is presented in Fig.1. Arc is

initiated and stabilized to form plasma jet, emanating from ends of anode. A microphone [bandwidth: 100 Hz-13kHz] is used for receiving the acoustic signal, a photomultiplier tube [bandwidth 0-120 MHz] is used for detecting optical signal and voltage drop across the arc (termed as voltage signal) is measured using a potential divider circuit. All the three signals are recorded electronically using a two-channel digital oscilloscope having maximum sampling capacity of 10 megasamples per second.
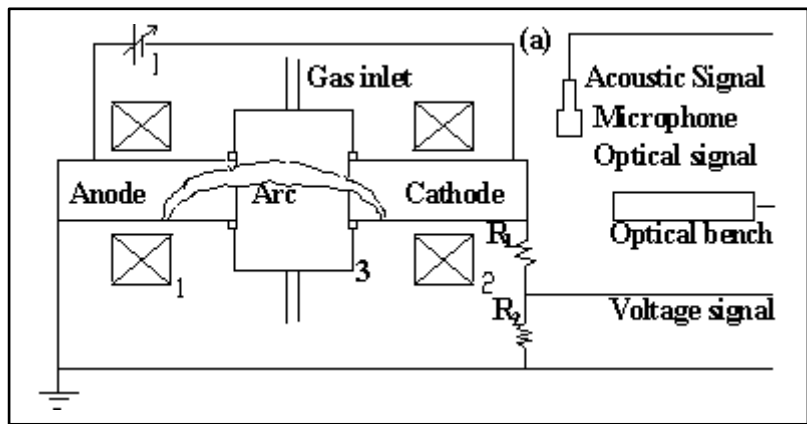

Fig.1 (a) Schematic of experimental setup [1,2 magnetic coils; 3 vortex chamber ,R_1 = 220 kΩ, R_2 =22 kΩ]
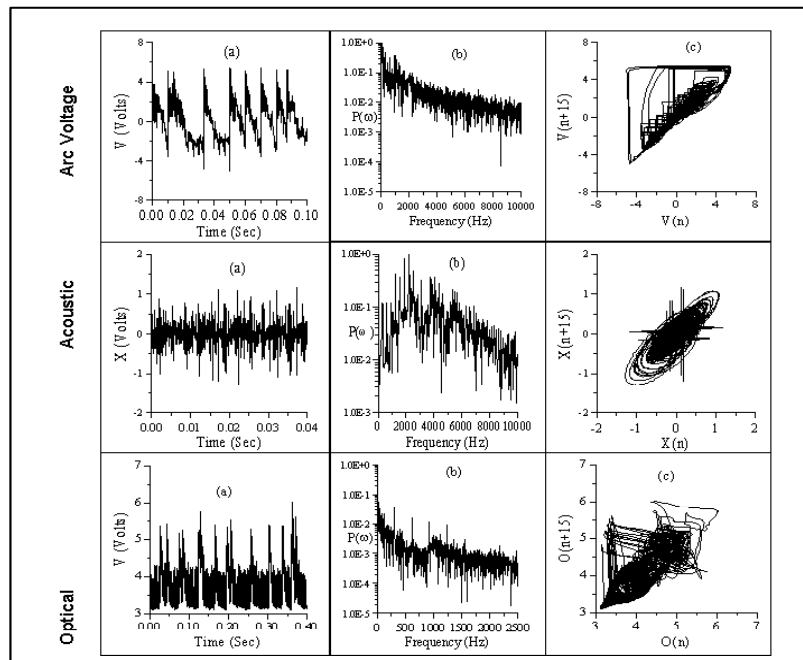

Fig.2 Typical fluctuation in various experimental signals (a) time series, (b) Power spectra, and (c) phase space attractor
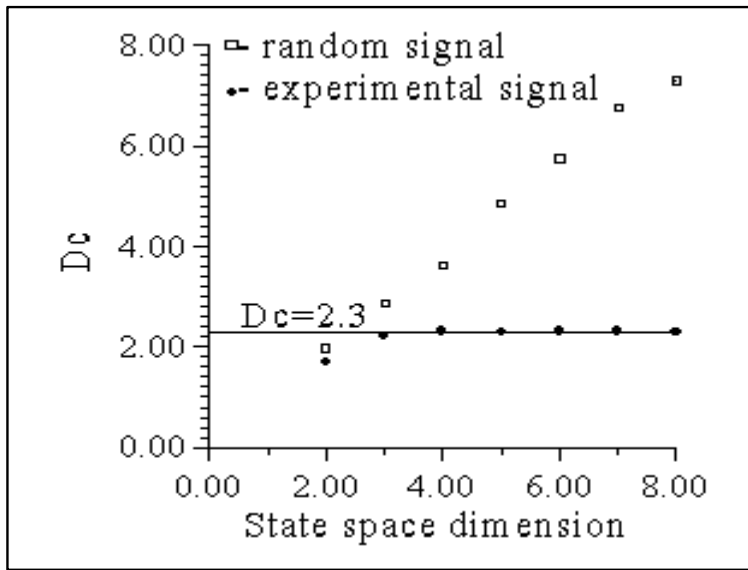
Fig.3 Correlation dimension for the attractor of voltage signal and a random signal in different state space
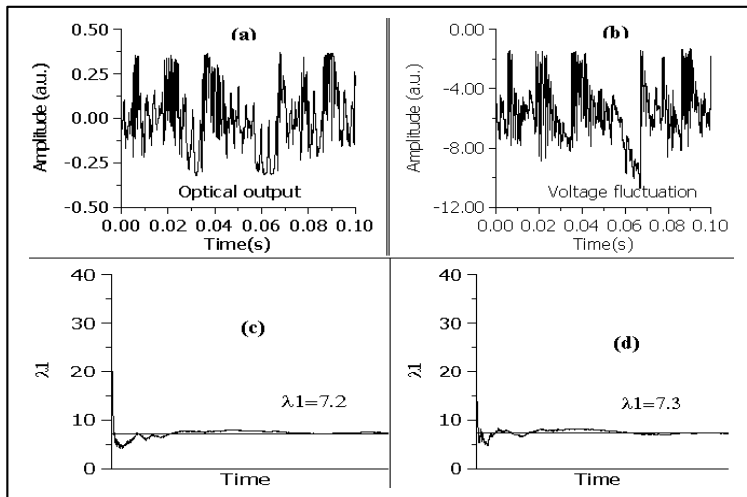

Fig.4 (a) and (b) simultaneously recorded Optical and Voltage signals (c) Computation of Lyapunov exponent for the Optical output (d) Computation of exponent for the voltage fluctuation. [Argon flow rate: 120 lpm, arc current: 300A]

Typical time series, power spectra and phase portrait of voltage, optical and acoustic signals are presented in Fig.2. Current and flow rate of the plasma gas have been found to be potential chaos controlling parameters. External axial magnetic field mainly influences stability of the arc without affecting much of the dynamical aspects. Composition of plasma gas is found to influence the jump in magnitude of

voltage signal without seriously affecting nature of dynamics of the system. The fluctuations in arc voltage have been always found to follow a reverse saw-tooth signal with sudden and irregular jumps in amplitude, when the system operates in chaotic regime. Attractors [2], found for these signals, all have similar appearances. Similar behavior is observed for other signals also. As current increases in magnitude from lower to a higher value, a gradual transition from quasi-periodic to chaotic regime is observed. Real time behavior, power spectra and phase space behavior of the recorded signals exhibit this unambiguously [2]. However, explicit period doubling is not observed in the experiments. In another experiment, together with voltage signal, optical and acoustic signals generated from usual arc plasma discharge are also found to be chaotic for the first time. Origin of each of these signals, their mutual correspondence and various dynamical properties are investigated in depth [3]. Complex real time behavior, continuous power spectra, together with definite phase portraits, low fractal dimension [Fig.3], positive Lyapunov exponent [Fig.4] and dependence of system behavior on control parameters identified themselves distinctly different from random and proved all of them to be chaotic [3]. Analysis reveals identical fractal dimensional [3,4] and identical Lyapunov exponent [Fig.4] for all simultaneously recorded voltage, optical and acoustic signals. It establishes that all the three signals are macroscopic outburst of the same

underlying chaotic phenomenon, i.e. movement of arc root [3].

To develop theory for arc plasma fluctuation, it is assumed that the observed fluctuations originate from the underlying instability in the near arc root region [Fig.3]. The region is modeled in terms of conservation of mass, momentum and heat coupled with the Maxwell's equation and equation of state [5,6]. The set of nonlinear differential equations for fluctuating plasma field quantities reduces to the following after nondimensionalization, removal of pressure term taking curl and introduction of stream function ψ such that:

$$u = \frac{dr}{dt} = \frac{\partial \psi}{\partial z}, w = \frac{dz}{dt} = -\frac{\partial \psi}{\partial r}, \Gamma(\psi,\phi) = -\vec{V}.\vec{\nabla}\phi, \eta = \frac{\partial u}{\partial z} - \frac{\partial w}{\partial r} = \nabla^2\psi \tag{1}$$

$$\frac{\partial \eta}{\partial t} = \Gamma(\psi,\eta) + \sigma\nabla^2\eta - R_l\sigma\partial_r T + R_s\sigma\tau\partial_r S - \frac{2}{R}\sigma\xi Q\partial_z B$$

$$\frac{\partial T}{\partial t} = \Gamma(\psi,T) - \partial_r\psi + \nabla^2 T \tag{2}$$

$$\frac{\partial S}{\partial t} = \Gamma(\psi,S) - \partial_r\psi + \tau\nabla^2 S$$

$$\frac{\partial B}{\partial t} = \phi(v,B) - 2dR^{-1}\partial_z\psi + \xi\nabla^2 B$$

where, all the parameters are dimensionless and R_l, R_s, σ, ξ, τ and Q are Rayleigh number, solute Rayleigh number, Prandtl number, Magnetic Prandtl number, ratio of solute to thermal diffusivities and Chandrasekhar number [6]. r and z are radial and axial coordinates. u and w are radial and axial velocities.

Plasma field quantities are expressed in vector form, which transforms according to associated operators in the plasma field. The reduced set of governing equations depends on number of non-dimensional numbers like Raylleigh number, Prandtl number, Lewis number and Chandrasekhar number. Coupling of electromagnetic effects into this problem comes through the Chandrasekhar number. In plasma parameter space, there is a critical hypersurface, where, the growth rate of linear theory vanishes. When plasma parameters are very near to this polycritical condition, the temporal behavior of the system becomes complicated and may be chaotic. Components of the plasma field vector in this region are split into two parts: one in stable space and other in critical space. Temporal behavior of amplitude of the plasma field vector is studied near the polycritical condition. Behavior of the system under such condition is determined, first finding the linear amplitude equation and then computing the leading nonlinear terms. Critical polynomial and parameter values for the onset of lowest order instability are determined and system behaviors under different parametric conditions are generated from the resulting nonlinear amplitude equation for amplitude of plasma field vector [5,6]:

$$A + C_2 A + C_1 A + C_0 A = C_4 A^3 \tag{3}$$

where, the coefficients are defined as [6]:

$$c_0 = \frac{q^2(q^6 - a^2m^2R_l + a^2m^2R_S - 4d\pi^2R^{-2}n^2Q)\sigma\tau\xi}{q^2(1+\tau+\sigma+\xi)}$$

$$c_1 = \frac{-a^2\sigma(\tau+\xi)m^2R_l + a^2\sigma\tau(1+\xi)m^2R_S - 4d\pi^2R^{-2}\sigma\xi(1+\tau)n^2Q + (\sigma\tau+\sigma\xi+\tau\xi+\sigma\tau\xi)q^6}{q^2(1+\tau+\sigma+\xi)}$$

$$- \frac{q^2(q^6 - a^2R_l + a^2R_S - 4d\pi^2R^{-2}n^2Q)\sigma\tau\xi}{[q^2(1+\tau+\sigma+\xi)]^2} \tag{4}$$

$$c_2 = \frac{-a^2\sigma q^{-2}m^2R_l + a^2\sigma\tau q^{-2}m^2R_S - 4d\pi^2R^{-2}\sigma\xi q^{-2}n^2Q + (\sigma+\tau+\xi+\sigma\tau+\sigma\xi+\tau\xi)q^4}{q^2(1+\tau+\sigma+\xi)} -$$

$$- \frac{-a^2\sigma(\tau+\xi)m^2R_l + a^2\sigma\tau(1+\xi)m^2R_S - 4d\pi^2R^{-2}\sigma\xi(1+\tau)n^2Q + (\sigma\tau+\sigma\xi+\tau\xi+\sigma\tau\xi)q^6}{[q^2(1+\tau+\sigma+\xi)]^2}$$

$$+ \frac{q^2(q^6 - a^2m^2R_l + a^2m^2R_S - 4d\pi^2R^{-2}n^2Q)\sigma\tau\xi}{[q^2(1+\tau+\sigma+\xi)]^3}$$
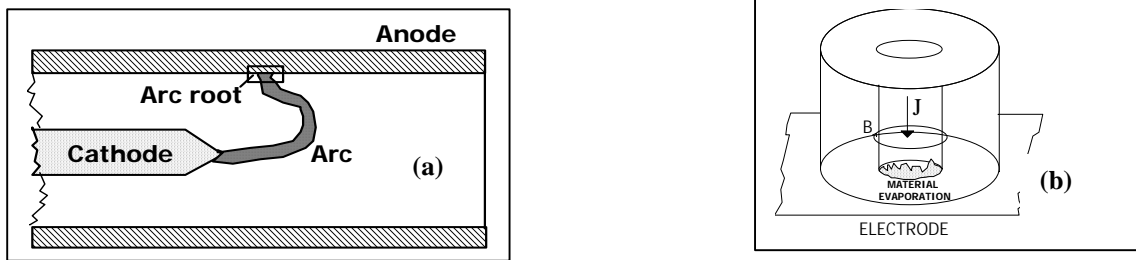
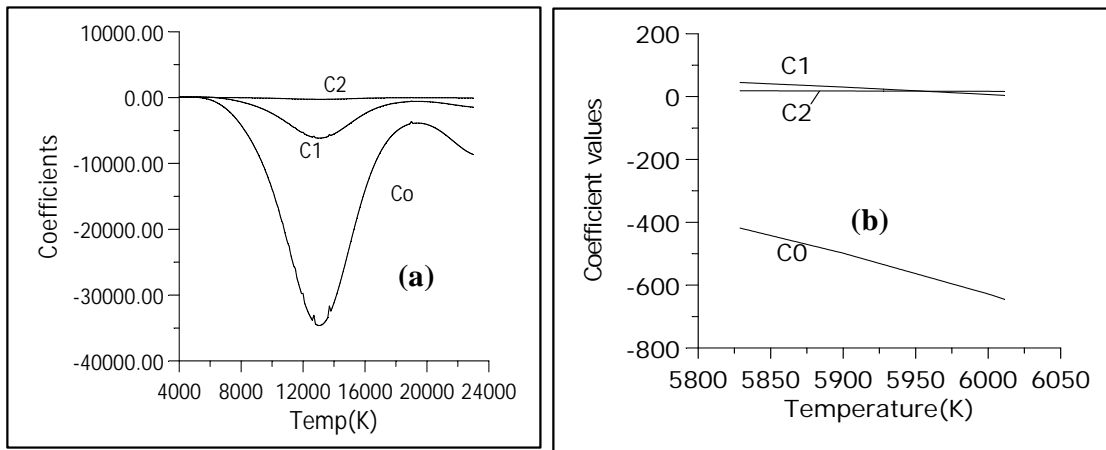Fig.5 (a) Formation of arc in an arc plasma torch, (b) Schematic of the model of near arc root region.

Fig.6. Variation of coefficients with temperature for Argon plasma (a) An overall view,(b) Near criticality

Quantities on right side of the above expressions relates to various parameters of the plasma like density, electrical conductivity, thermal conductivity, viscosity, specific heat, diffusivity etc. realized under a given state. Details of these parameters are available in Ref.6. Behavior of the coefficients with temperature and expanded view of the near criticality zone is presented in Fig.6. For a given plasma operating condition, coefficients in the nonlinear amplitude equation ultimately depend on arc current and various thermo-physical properties of the plasma realized under that condition. Once temperature of the instability zone and gas forming the plasma are identified, all mentioned thermo-physical properties of the generated plasma are known from property table of respective plasma gases available in literature and coefficients can be computed. As all the coefficients (c_0, c_1, c_2) are known for a given plasma operating condition, Eqn. (3) can be solved to get time dependence of amplitude of plasma field vector.

The underlying instability will be reflected in all measurable signals emitted from the plasma subjected to associated other conditions.

All basic experimentally observed signals and their origins are identified from theory [6]. Similar to experiments, the theory predicts a gradual transition from non-oscillatory to regular oscillatory to chaotic regime through period doubling route [6]. Theory recognizes arc current and gas flow rate as the major externally controlling parameters in agreement with experiment. Coefficient regimes where an experimental system reaches near criticality are obtained from theory and found to be fairly within the experimentally achievable zone. All theoretically obtained signals are studied for time series, phase portrait, power spectra, dimension and Lyapunov exponent [7,8]. In agreement with experimental signals, the theoretical voltage signal is found to produce saw-tooth time series and self-similar (saw-tooth
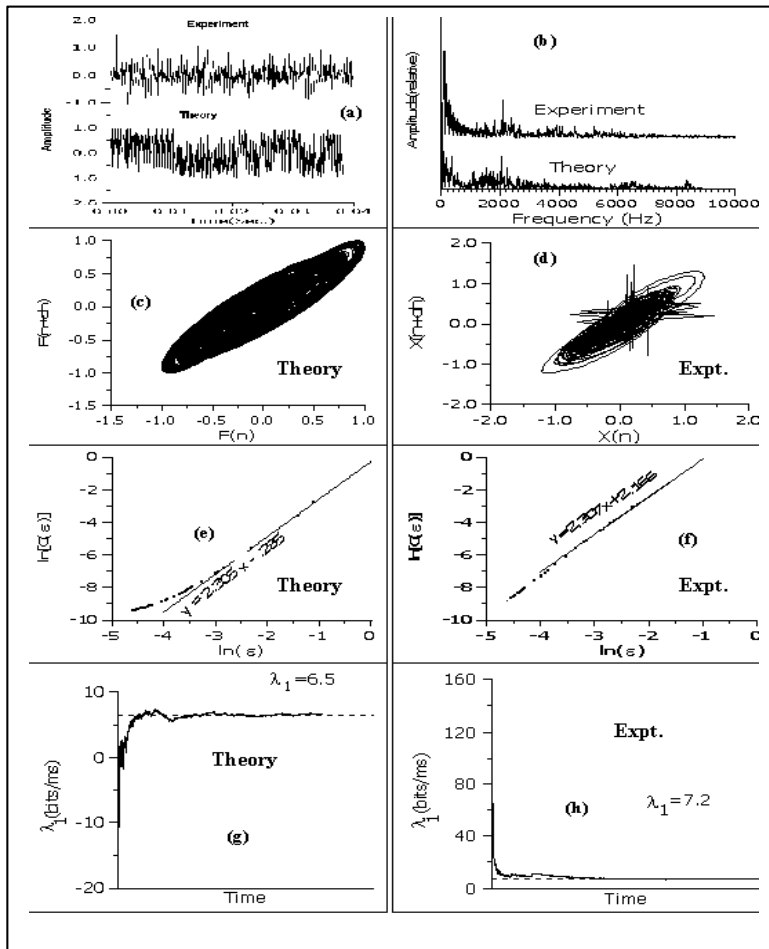
Fig.7. Experiment and theory for I=400A: (a) time series, (b) Power spectra, (c) Theoretically obtained phase portrait, (d) Experimental phase portrait, (e) dimension computation of the theoretical signal, (f) dimension computation of the experimental signal, (g) Evolution of Lyapunov exponent for theoretical signal, and (h) Evolution of Lyapunov exponent for experimental signal

Theoretically obtained voltage and acoustic signals both provide a correlation dimension of 2.3 in complete agreement with that obtained experimentally [Fig.7]. A detail dimensional analysis is carried out on the theoretical and corresponding experimental signals on various reconstruction state spaces having dimension ranging from 2 to 7. This study established that phenomena modeled by the theory essentially take place in same state space, where experimental phenomena happen [8]. A detail study on Lyapunov exponent is carried out on regular oscillatory, random, experimental and corresponding theoretical signals, all having similar number of data points and same sampling interval. Investigation is carried out in reconstruction state space dimension ranging from 3 to 8. The study established that both theoretical and experimental signals definitely present chaotic signal [8]. Possible excitations of higher order modes in arc plasma instability have also been investigated. It is observed that for typical operations, excitation of fundamental mode is the most probable and that few modes near to fundamental may also be excited. However, when one mode is excited, possible other modes are damped. Higher order modes, if excited, offer similar dynamics but in different operating zone [6,8].

It has been observed that under certain operating regimes current attractor suddenly disappears from state space and the post bifurcation response jumps to remote unbounded attractor

inside saw-tooth) behavior [8]. Both theoretical and experimental voltage signals exhibit similar nature of power spectra and phase portrait [Fig.7]. Acoustic signal generated from theory matches well with experimental data on time series, dimension and Lyapunov exponent [Fig.7]. A comparison of theoretical and experimental power spectrum indicates existence of an envelope function in the frequency domain for response [7]. Form of this envelope function, demanded by the developed theory, matches excellently with the form predicted by theory of acoustic wave generation in thermal plasma.

[6,8]. In pre-bifurcation state, system exhibits usual oscillatory behavior. Such catastrophic behavior is similar to well known "Blue sky catastrophe" in nonlinear dynamics. Existence of such inbuilt catastrophic behavior in arc plasma systems is an extremely important finding. Over decades, development of high power plasma devices is facing unmanageable difficulty arising due to sudden device failure. Sudden extinction of arc, often encountered in certain operating regime of arc operation can be explained using this fact. Poor dependence on gravity related terms indicates that the phenomenon will be observed irrespective of alignment of the device (vertical/horizontal), a true fact observed in practice.

Fig.8. Comparison with experiments by Brilhac et. al. (a) Acoustic fluctuation, (b) Voltage fluctuation, (c) Power spectra of acoustic signal, and (d) Power spectral of voltage signal. In each figure, upper curve presents ES and lower curve presents TS. [I=260A, V=77V, Flow =50slpm]

Because of non-dimensional nature of the formulation, the developed theory inherits general applicability and can be used to predict nature of instability in other experimental systems too. Literature is surveyed to identify important experiments worldwide on arc plasma instabilities and the developed arc instability theory has been applied to all of them. Results obtained are compared with the published experimental results. Nice mach has been observed in each case [7,8]. Atypical match with experiments by the authors [4,7] is shown in Fig.7. A similar match with experiments experiments by Brilhac et. al.[9,7] is shown in Fig.8 .

Conclusion

The present work not only establish occurrence of chaos in arc plasma devices for the first time but also identifies chaotic and non-chaotic operating regime, chaos control parameters, and offers a concrete theoretical basis for the first time for observed fluctuations in arc plasma devices. Establishment of the phenomenon of fluctuation in arc plasma devices as chaotic and not random is an important outcome of the work. Unlike random systems, chaotic systems are controllable. Obtained results indicate that fluctuations in arc plasma devices can be controlled. Primary importance of the present work is introduction of this new approach to a wider circle of researchers in the area of arc plasma jets and other related devices. Chaotic behavior in low pressure plasmas have already been found useful. The observed chaotic behavior in high pressure plasma beams may be linked to a number of possible physical effects within the torch like electrode losses due to erosion, puncturing of device, sudden extinction of arc, change of surface conditions of the electrodes, change in operati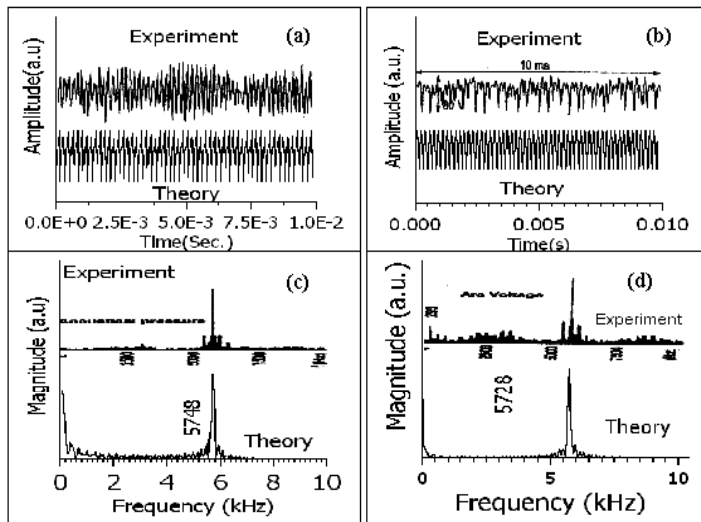ng characteristics of torch, etc. The present work is a first attempt of its kind at searching a path to control all these non-linear interactions occurring in arc plasma devices employing knowledge of nonlinear dynamics. Once geometry, arc current, plasmagen gas and its flow rate are specified, static and dynamic behavior of any arc plasma device is frozen. So far, standard fluid dynamic simulations were able to predict steady state behavior of the system for these inputs but not dynamic

behavior. The developed theory makes it possible for the first time to predict associated dynamic behavior also once these inputs are specified. Although, there are definite scopes for further development, it is believed that outcome of the work will be extremely useful to thermal plasma applications in future.

The present theory is developed for marginal instability only. Excellent agreement between experimental and theoretical behavior suggests that the fluctuations observed in most of the arc plasma devices arise out of marginal instability in such systems. Such tendency may be a natural outcome of the non-equilibrium dynamics in arc plasma systems. However, issues regarding reason behind such tendency remains to be clarified.

References

1. E. Pfender, Plasma Chem. Plasma Process.19 1 (1999).
2. S. Ghorui et. al., IEEE Trans. Plasma Sci. 28 253 (2000)
3. S. Ghorui, et. al., IEEE trans. Plasma Sci. 28 2179 (2000).
4. S. Ghorui, A.K. Das, and N. Venkatramani, PRAMANA-J. Phys. 54 L331 (2000).
5. S.Ghorui and A.K. Das, Phys. Rev. E 69 026408 (2004).
6. S. Ghorui and A.K. Das, IEEE trans. Plasma Sci. 32 296 (2004).
7. S. Ghorui et. al., IEEE trans. Plasma Sci. 32 308 (2004).
8. S. Ghorui, Ph.D. Thesis, University of Mumbai, Jan, (2004).
9. J.F. Brilhac, et. al., Plasma Chem. Plasma Process., 15 231 (1995).

This paper was adjudged as the Best Paper at the 18th National Symposium on Plasma Science & Technology, Plasma-2003, held at BIT, Mesra, during December 8-11, 2003

About the authors ...

Mr S. Ghorui obtained his Master's degree in physics with specialization in radio physics and electronics from the University of Burdwan in 1995. He graduated from BARC Training School, in 1997. He is presently involved in research and development work in Laser and Plasma Technology Division, BARC. His current research interest is non-linear plasma dynamics, heat transfer and fluid flow.

Mr S.N. Sahasrabudhe received his Master's degree in physics in 1977. He joined Plasma Physics Division, BARC, in 1980. His research interest is laser doppler velocimetry and plasma diagnostics.

Mr P.S.S. Murthy is a Member of Institute of Engineers, India. He joined Plasma Physics Division, BARC, in 1968. His current research interest is development of high power plasma devices.

Dr A. K. Das is a Life Member of the Plasma Science Society of India and ICTP Indian chapter. He joined Plasma Physics Division, BARC, in 1973 after graduating from the BARC Training School. He received his Ph.D. degree on "Thermal MHD generator grade plasmas" from University of Bombay in 1979. Currently, he heads the Power Plasma Device Section at BARC and is a Ph.D. guide in Plasma Physics at the Mumbai University. His research interests include basic plasma science, computational plasma physics, development of high power plasma sources and non-linear plasma dynamics.

THERMAL ANALYSIS OF A CHEMICAL REACTOR FOR UF$_6$ REDUCTION

A.K. Tiwari, C.S. R. Prasad and V.K. Kansal
Chemical Technology Division
Bhabha Atomic Research Centre

and

S. Ghorui and A.K. Das
Laser & Plasma Technology Division
Bhabha Atomic Research Centre

A b s t r a c t

Thermal plasma offer an alternative to the conventional heat sources and in many ways the preferred media required in high temperature chemical processing systems. Use of thermal plasma based chemical reactors to provide better controlled thermo physical environment for material processing and to improve process efficiency has well been established not only at laboratory and R&D level but also in large-scale industrial applications. The extremely high enthalpies (MJ/kg), focused heat flux (MW/m²), high heat transfer potential (order of magnitude higher than conventional media) and abundance of atomic, ionic, free radical species ensure volume conversion, compact reactors and high specific yield. In typical systems of oxidation or reduction reactions, the availability of atomic and ionic species (H, O, OH, H⁺) ensures higher yields. Maintaining appropriate control of feed configuration and wall temperature, the temperature profile could be tailored to control specific chemical reactions. The present paper offers a numerical simulation study to analyze plasma chemical reactor system for possible direct reduction of UF$_6$ to UF$_4$, which takes place around 600-800K. The design approach is based on optimizing the plasma temperature and velocity profile in the reaction zone as functions of reactor geometry in terms of L/D sizing, wall temperature and wall heat loss. An analytical model is used to predict the effect of plasma power, cooling medium and size of tubular metallic reactor on the temperature profile inside the reactor. The model is based on solution of basic equations of conservation of mass, momentum and energy for reactors running on argon and hydrogen as plasma gas. The results are significant.

Introduction

U F$_6$ is the only known compound of Uranium that is highly volatile at ordinary temperature. UF$_6$ is used as a feed material in enrichment processes like gas diffusion, gas centrifuge etc. The enriched UF$_6$ as well as tails of UF$_6$ cannot be stored in cylinder for a longer duration of time because of their toxic & corrosive nature. Hence they should be converted to more stable compounds like UF$_4$/U$_3$O$_8$ for storage. These compounds are very much part of nuclear cycle as UF$_6$ on metalothermic reduction produces U metal that is used as fuel in research reactors & U$_3$O$_8$ is reduced to UO$_2$ to be used as ceramic fuel in power reactors. Conventionally UF$_6$ is reduced to UF$_4$ by hydrogen at about 600ºC. Thermal plasma process offers a clear, faster and advanced technology for processing waste UF$_6$ without needing any additional chemical and hence significantly reducing the waste

generated. Among the numerous applications of plasma jets, industrial applications of plasma jet as a heat sourse is well established as a material processing technology with growing importance. In order to achieve near optimal conversion, the reactor design to be used in the present investigation had to provide means of heating the reactant gas to a reaction temperature between 600-800K. In the present paper a computational model has been used to predict the effect of throughput, plasma power, and size of the tubular metallic reactor on the temperature profile inside the reactor.

Thermal Plasma Reactor

Thermal plasma reactors are used for the commercial production of a number of different ceramic powders. Peak temperatures are of the order of 15,000K for DC plasma torches & pressures are typically 1 – 10 atm. Typical residence time of reactors in plasma fireball

environment is of the order of 1 – 10 ms. Reactants passing through these regions are broken into their more active components like atoms, ions etc. and produces a better thermo chemical environment inside the plasma reactor. Typical elements of plasma reactor are as following (Fig.1):

1. D C Plasma source
2. Mixing of the plasma with reactants.
3. Reaction chamber
4. Rapid quenching zone
5. Chemical Scrubb

UF_6 is reduced to UF_4 by Hydrogen that is used in excess. Role of Hydrogen is to facilitate the Hydrogen atom/ion for reduction and act as a heat carrier as well. The unutilized H_2 is sent to scrubber along with HF that is produced after the reaction. The overall process may be subdivided into four stages.
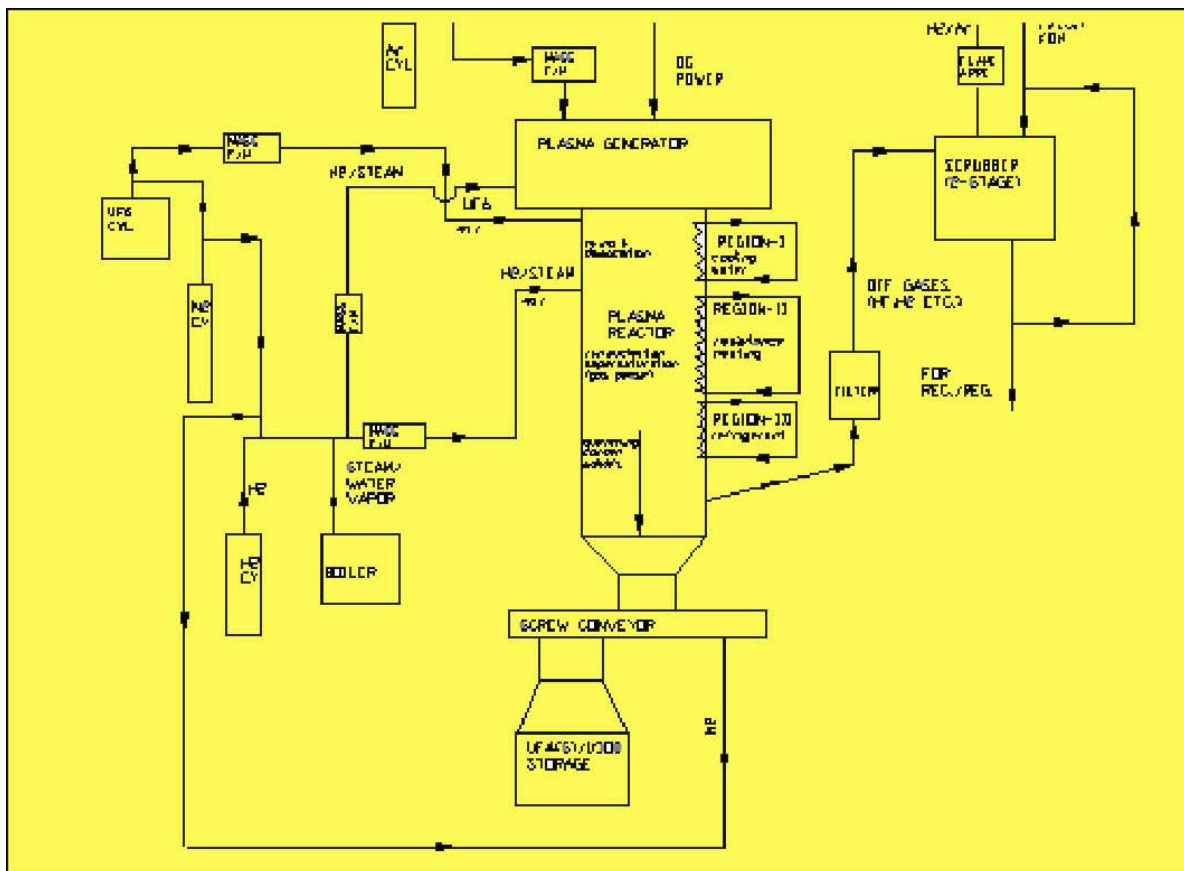

Fig.1. Elements of plasma reactor

1. Generation of Hydrogen plasma.
2. Interaction of the gaseousUF_6 with Hydrogen plasma flow resulting in formation of two principal products UF_4 and HF.
3. Nucleation, growth and Condensation of UF4 particles.
4. Scrubbing of outlet gases mainly consisting of HF and H_2.

HF can be recovered and may be utilized for the electrolytic production of pure gaseous Fluorine. It is necessary to emphasize another advantage of the approach described above is the absence of any harmful byproduct.
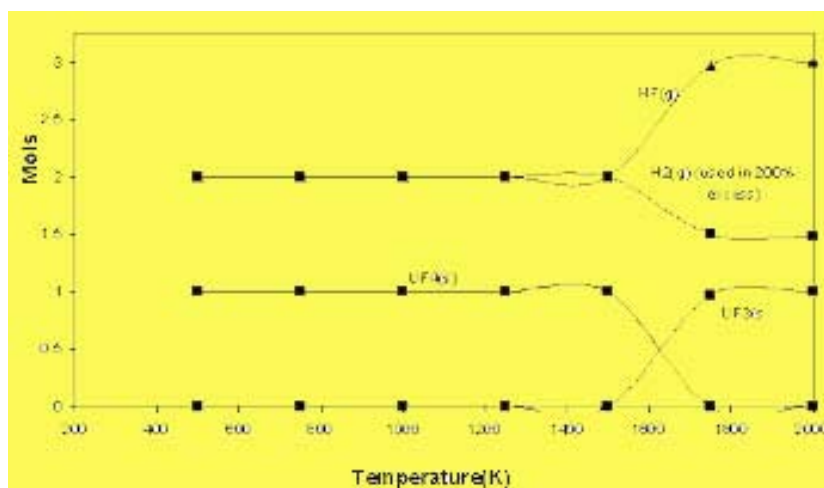

Fig.2 Gibbs free energy minimization plot for the system UF_6H_2.

The free energy minimization plots (Fig.2) for the system $UF_6 - UF_4$ indicate that plasma reactor temperatures in the range of 600 –1400 K will maximize the yield of the desired product. Thermodynamically the following reaction is favored in the temperature range of 600-1400 K in the reaction chamber (pressure inside being near atmospheric).

$$UF_6 (g) + H_2 (g) \rightarrow UF_4 (g) + 2 \, HF (g)$$
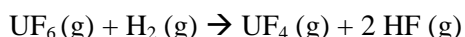
However, the operating range is preferred to be in the range of 600-800 K as at higher temperature the decomposition of UF_6 takes place. Moreover it is safer to operate the reactor at lower levels of temperature ranges.

Presence of more active species like atoms, ions etc provide more Gibbs free energy available for the reaction to take place. This enhances the rate of reaction. It is known that the reaction is diffusion controlled as the feed is injected into the hot plasma where the viscosity of the gases are very high; hence mixing of gases becomes an important criteria. The reactants should get sufficient residence time to react and give a higher rate of conversion. The reactor volume requirement depends not only on the residence time requirement for reacting species but also on the kind of temperature pattern desired in the reactor arena. The feed material if exposed to higher temperature undergoes decomposition giving several other unwanted products. This reduces the yield of product as well as the extent of conversion. On the other hand a minimum temperature is required for the reaction to take place. The quality of the powder being formed too largely depends on temperatures in the reaction chamber. The wall temperature should not fall below 150 ^{0}C so that to avoid any scale formation and deposition on the wall which affects the rate of heat transfer. At the same time the upper limit of the wall temperature should not exceed 500 ^{0}C such that the wall material is protected from any deformation. To obtain a flatter profile in the desired range of 600-800 K inside the reaction chamber; it is necessary to study the effect of several parameters like plasma power, length of the reactor, size of the reactor, wall temperature and throughput on the temperature profile inside the reactor and suggest an optimum value for different parameters for effective operation.

Design of a plasma reactor is an extremely complex task since complete model of the

processes in the reactor chamber would require hundreds of chemical reactions to be described. The designed technological scheme for reduction of UF6 to UF$_4$ starts with sublimation of UF$_6$ from storage cylinder followed by reduction of UF$_6$ with H$_2$ to UF4 and HF. Plasma reactors, owing to high enthalpy of plasma, to efficiently increases yield through maintenance of optimum temperature profile inside the reactor to achieve desired product composition. Heat flux imposed by the plasma jet is strongly dependent upon plasma power, thermophysical properties of plasma gas, gas flow rate, nozzle diameter, arc current.   The design approach is based on optimizing the plasma temperature profile in terms of L/D sizing, wall temperature & wall heat loss. The other primary variables are taken as plasma power and gas flow rate. The model is based on solutions of basic equations of conservation of mass, momentum and energy for reactors running on argon & hydrogen as plasma gas. The energy absorbed by the reactants has been suitably replaced by source term in the energy balance equation. For different combination of plasma power & reactor size, heat flux to wall and temperature profile has been is reported.

Numerical Simulation of Plasma Reactor

Simulated version of the experimental system and its various components are shown in Fig. 3. The plasma torch powered by a current regulated DC power source consists of a thoriated tungsten cathode located coaxially inside a copper anode in the form of a nozzle. Mixtures of argon with hydrogen at various proportions are used as plasma generating gas. The torch is encased in a SS pipe with a heat shield against the hot gases reflected. Nozzle diameter is 10 mm. All the thermally stressed elements of the torch are intensively water-cooled. Plasma generated by the torch is injected into the reactor chamber as shown in Figure 1. Chamber pressure remains near to atmospheric. The plasma torch operates

with a constant current power supply. Depending on set current of the arc, various plasma powers are realized by the system. Distribution of temperature inside the reactor depends on plasma power as well as diameter and length of the reactor. The system is simulated theoretically employing steady state governing equations of the system to study effect of reactor dimension, plasma power and reactor environment.
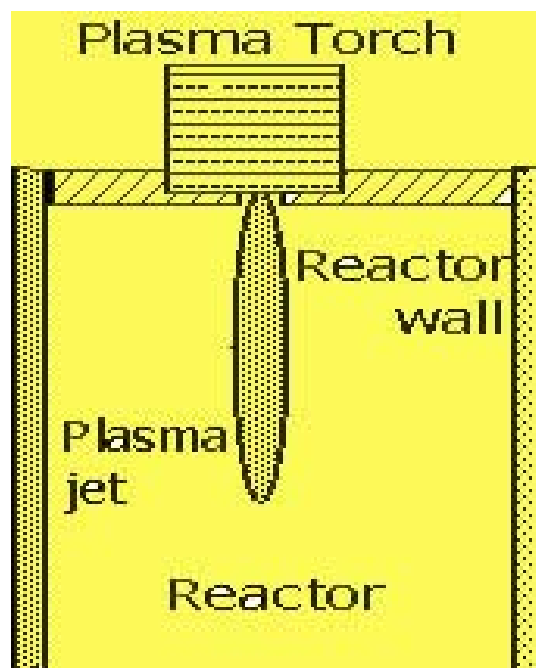
Fig.3. Simulated reactor system

Table 1 :Torch operating parameters

Parameters	Typical magnitude
Arc current	100A-400A
Arc Voltage	100V-250 V
Plasmagen gas flow rate	Argon: 0 to 30 LPM Hidrogen: 0 to 30 LPM Net flow: 20LPM-60 LPM
Torch efficiency	40%

Temperature, velocity and enthalpy profile inside the chamber is computed through solution of associated conservation equations using finite volume technique. The following simplifying assumptions are physically justifiable and used in the computation:

(i)   The non-transferred DC plasma torch generates a stabilized plasma jet inside the plasma reactor emanating from the nozzle.
(ii) The fluid flow is laminar.
(iii) The flow is fully developed at the nozzle exit so that the profiles for axial velocity and enthalpy can be assumed to be parabolic at the nozzle exit.
(iv) The operating arc is in steady state so that all the governing equations are independent of time.
(v)   The plasma jet inside the chamber is free from electric and magnetic field. Hence Joule heating and effect of magnetic and electric fields are not considered in the energy conservation equation.
(vi) The arc jet has cylindrical symmetry. This reduces the actual three-dimensional problem to an effective two-dimensional problem.
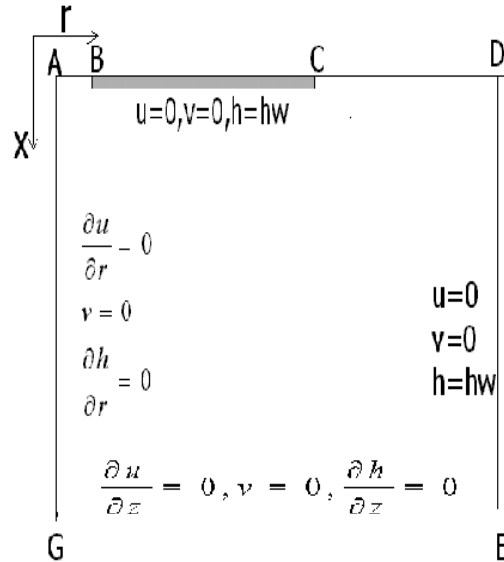
Various conservation equations for mass momentum and energy inside the reactor can be written in cylindrical co-ordinates as follows:

Mass Continuity:

$$\frac{\partial}{\partial x}(\rho u) + \frac{1}{r}\frac{\partial}{\partial r}(\rho rv) = 0 \qquad (1)$$

Axial momentum:

$$\rho u \frac{\partial u}{\partial x} + \rho v \frac{\partial u}{\partial r} = -\frac{\partial p}{\partial x} + 2\frac{\partial}{\partial x}(\mu \frac{\partial u}{\partial x}) + \frac{1}{r}\frac{\partial}{\partial r}(\mu r \frac{\partial u}{\partial r}) + \frac{1}{r}\frac{\partial}{\partial r}(\mu r \frac{\partial v}{\partial x}) \qquad (2)$$

Radial momentum:

$$\rho u \frac{\partial v}{\partial x} + \rho v \frac{\partial v}{\partial r} = -\frac{\partial p}{\partial r} + \frac{\partial}{\partial x}(\mu \frac{\partial v}{\partial x}) + \frac{2}{r}\frac{\partial}{\partial r}(\mu r \frac{\partial v}{\partial r}) + \frac{\partial}{\partial x}(\mu \frac{\partial u}{\partial r}) - \frac{2\mu v}{r^2} \qquad (3)$$

Energy:

$$\rho u \frac{\partial h}{\partial x} + \rho v \frac{\partial h}{\partial r} = \frac{\partial}{\partial x}(\frac{\kappa}{C_p}\frac{\partial h}{\partial x}) + \frac{1}{r}\frac{\partial}{\partial r}(\frac{\kappa r}{C_p}\frac{\partial h}{\partial r}) - 4\pi\varepsilon_N \qquad (4)$$

Here x and r are the axial and radial coordinates. u and v are the axial and radial velocity components. H is specific enthalpy and p is local pressure. μ, ρ, σ, κ and C_p are the viscosity, density, electrical conductivity, thermal conductivity and specific heat respectively. ε_N is the net emission coefficient of the generated plasma. Thermodynamic property data for

simulation are compiled from literature [1]. Data published by Menart[2] are used for radiation property of plasma.

Fig. 4 Computational domain

The above equations are solved in two dimension for the computational domain shown in Fig.4 using SIMPLE algorithm of Patankar [3]. AB is the nozzle exit, BC and CD are the heat shield and the space between heat shield and reactor wall. AG and GF are the axis of symmetry and radius of the window. Velocity and enthalpy profile of plasma generating (plasmagen) gas at AB is computed through mass flow and energy balance. With this profile the plasma jet enters the reactor chamber and propagates downstream. Radial velocity of gas is assumed to be zero at AB. Temperature along BCD is assumed to be 500K and assumed to be constant. No slip wall boundary condition is put along BCD and DE. Radial velocity, gradient of axial velocity and gradient of enthalpy is assumed to be zero on GE. Axis of symmetry boundary condition is put along AG.
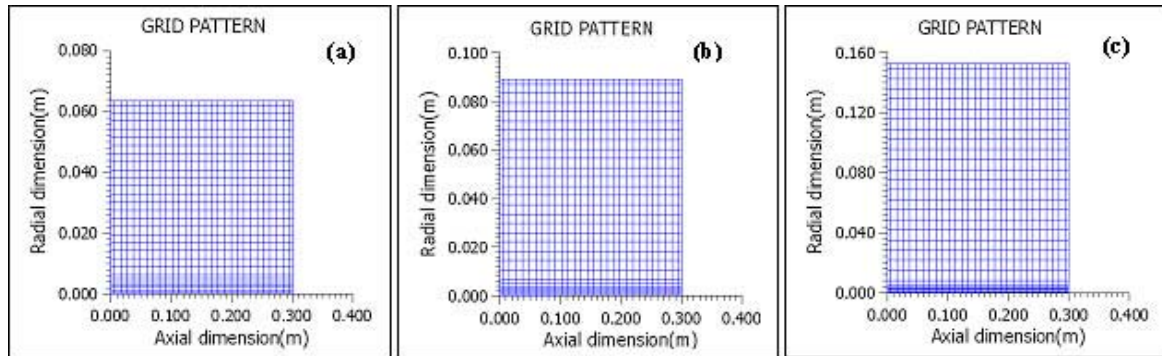
Fig.5(a) Grid for case(a) (b) Grid for case(b) (c) Grid for case(c).

Results

Temperature distribution inside the plasma chamber has been computed for two different input powers (20kW and 40 kW) of plasma torch. Dissociation energy loss is assumed to be 1.79 kJ per second and subtracted from the input power from the torch to get the temperature distribution. For each power three different chamber radii are considered to understand the influence of camber size on the effective reaction volume that remains within temperature range around 800K and below. It is assumed that the chamber surface stays at a temperature 600K. Various grid types used for the simulation in the three cases are shown in Fig.5.(a), (b) and (c) respectively. Finer grid is used in the central region to capture more details in the central region.

In the first case simulation is carried out for plasma power (P)=20 kW, flow rate=40 lpm Ar; torch efficiency 40%, dissociation loss (DL)=1.79kW and chamber radii (CR): (a) 3"(76.2 mm) (b) 4"(102 mm) (c) 6"(152.4 mm). Temperature distribution at various zones for respective chamber sizes are displayed in Fig. 6(a),(b) and (c) respectively. Various zones of interest are shown in different colors. Fig7(a) shows approximate volumes of reaction zones within temperature range 800-600 K and 1400-800 K for various chamber dimensions (CR: 2.5", 3.5", 6"). In the simulation temperature of the wall of the reactor is kept fixed at 600K. This can be realized easily in practice through adjustment of flow rate of cooling water in the wall. It is observed that as radius of the reactor increases, total volume in both the temperature range increases. However, volume fraction of such zones shows behavior typical to that shown in Fig5(b). While volume fraction in the range 800-600K increases with increase in dimension, that in the range 1400-800K decreases.
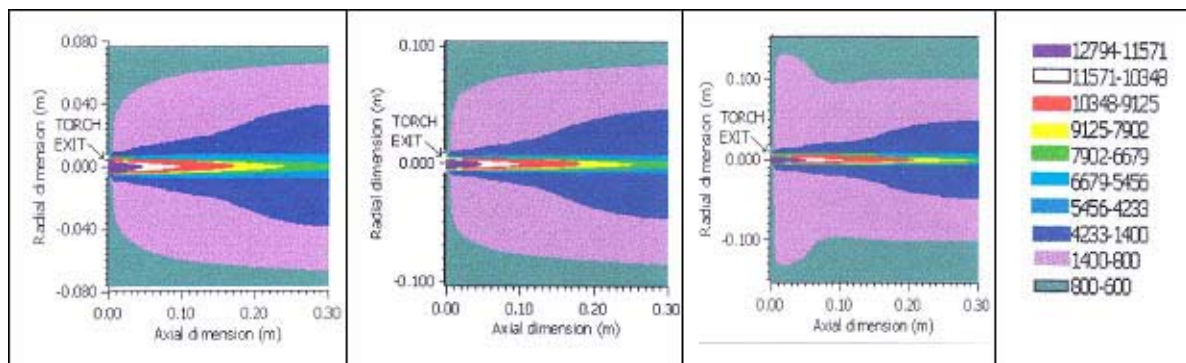
Fig 6. Temperature distributions for chamber radii: (a)3 inch (b) 4 inch (c) 6 inch. [P=20kW]
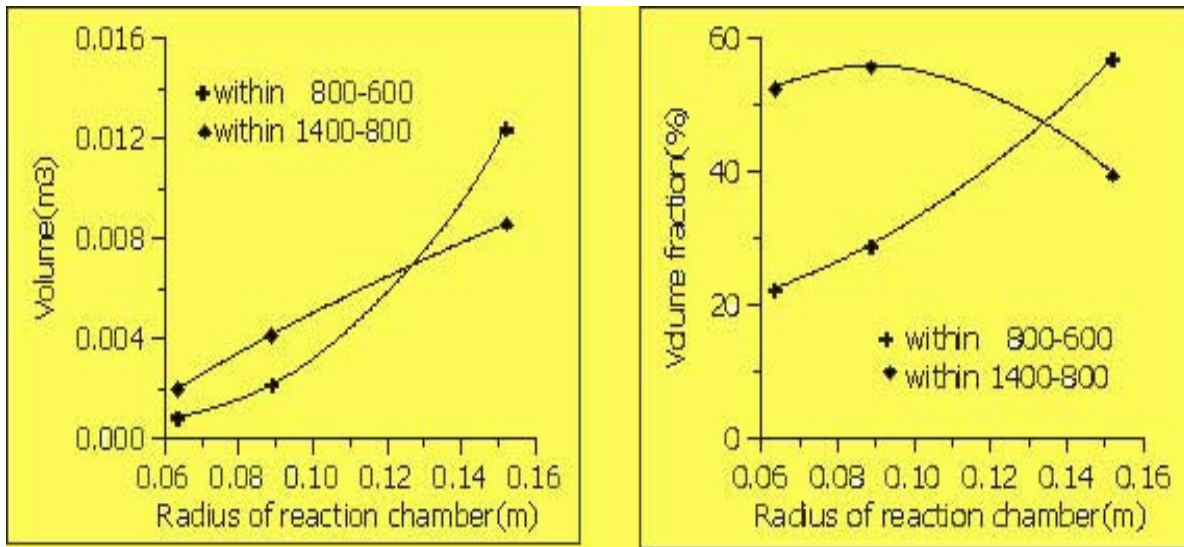
Fig.7. Dependence of (a) volume of reaction zone and (b) volume fraction of reaction zones on radius of chamber at temperature ranges of interest (r=2.5",3.5",6").
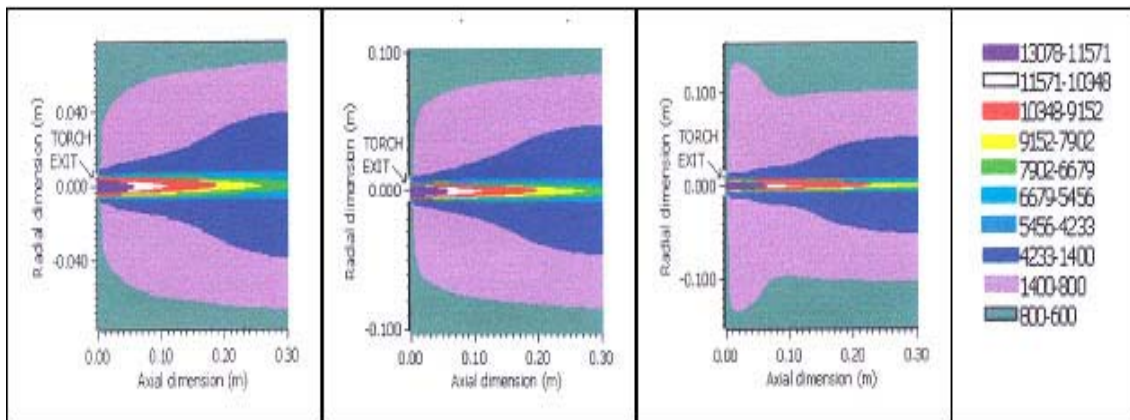
Fig 8. Temperature distributions for chamber radii: (a)3 inch (b) 4 inch (c) 6 inch. Torch power 40kW.

Table 2 : Plasma power statistics dissipated through various channels in the process

Torch power	Effici-ency	Power in plasma	Dissociation Loss	Power in plasma after dissociation	Power going out with exiting hot gas	Power absorbed by walls	Wall heat flux (W/cm^2)
40 kW	40%	16kW	8.95kW	7.05kW	(a)2.8 kW	4.25 kW	2.62
					(b)3.1 kW	3.95 kW	1.75
					(c)3.7 kW	3.35 kW	0.93
20 kW	40%	8kW	1.79kW	6.21kW	(a)2.6 kW	3.61 kW	2.23
					(b)2.9 kW	3.31 kW	1.47
					(c)3.5 kW	2.71 kW	0.75
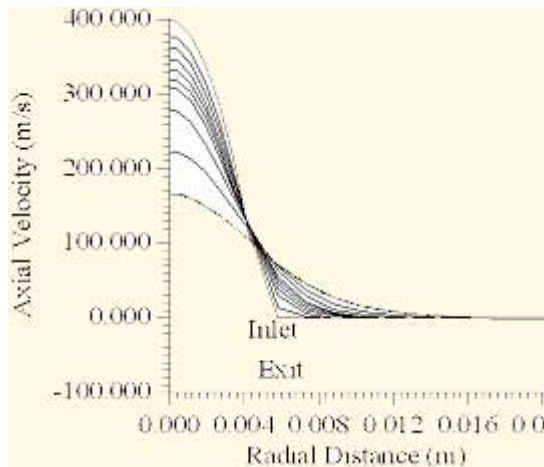
Fig.9 Typical axial velocity distribution in the reactor

In the second case simulation is carried out with parameters: Power=40 kW; Flow rate=40 lpm Ar; Efficiency 40%, Dissociation loss=5x1.79 kW. Chamber radii: (a) 3"(76.2 mm) (b) 4"(102 mm) (c) 6"(152.4 mm). Distribution of temperature in the reaction chamber for various chamber sizes are isplayed in Fig.8. Distribution is similar to that as observed in case-I except for higher maximum temperatures realized in this case. Behavior of reaction zone sizes, at different temperature ranges, is found to be similar to that as discussed in case-I. Typical profile of axial velocity, obtained in the simulation, looks as shown in Fig.9. Dissipations of plasma power through various channels are shown in Table-2. This may help in determining required flow rate of cooling water to carry out the dumped heat at the wall.

Summary and Conclusion

Design of plasma chemical reactor is an extremely complex task. Owing to advantages of high enthalpies in plasma reactors, yield of specific reactions can be increased efficiently though maintaining optimum temperature and velocity profiles inside the reactor. So far, the design of such reactors for plasma chemical processing applications are strictly application specific and more empirical than analytical. Information available in literature are rare. The present paper targets the problem analytically and presents a detail thermal analysis of a plasma chemical reactor for UF_6 to UF_4 reduction through numerical simulation. Effect of cooling medium, plasma power and size of metallic reactor on the desired reaction has been studied. Obtained results may be very much useful for design of such reactors.

Results presented above are obtained through standard finite volume simulation technique for simplified geometry of the system as mentioned with argon as plasma forming gas. Since the problem is basically a fluid dynamic problem with some specified heat sources, solution of Navier-Stokes equation is bound to give correct information on velocity and temperature distribution inside the system. However, in the present problem specific arrangements for introducing reacting gases into the system and their influences on the momentum balance equation has not been taken into account. Employed code for the simulation is two-dimensional (2D). To account for such specific arrangements three-dimensional (3D) code is necessary. Dissociation energy loss (DL) has been taken into account. However, employed value of DL is only a rough estimate. Radiation loss from the plasma is a complex phenomenon. Net emission coefficient for argon plasma available in literature has been employed to account this. Concept of net emission coefficient takes into account of emission and absorption but does not account for reflected heat from the wall if any. Reflected heat and its absorption are problem specific. Latest available thermodynamic property data has been used in the simulation. However, it may have maximum error up to 15%. Best available emission coefficient data in literature that are used in the simulation are obtained through theoretical computation assuming isothermal cylinder model of plasma. Validity of such isothermal model is very much limited in the present problem due to existence of steep temperature gradient in plasma jet emanated from any plasma

torch. Therefore, results presented in the paper shows only trends of behavior of such systems under the mentioned conditions. Numerical figures in actual systems may well vary to some extent. To employ the plasma simulation code for close prediction of actual system behavior, experiments need to be performed to fix relevant parameters employed in the code.

References

1. M. Boulos, P. Fuchais and E. Pfender, "Thermal plasmas, fundamentals and applications", Vol-1, Plenum press NY, 1994.

2. J. Menart, J. Heberlein and E. Pfender, "Line by line method of calculating emission coefficients for thermal plasmas consisting of monatomic species",J. Quant. Spectrosc. Radiat. Transfer, 56,(3), 1996.

3. S.V. Patankar, " Numerical heat transfer and fluid flow", Hemisphere publishing corporation,1980.

> ### This paper was adjudged as the Best Paper at the 18th National Symposium on Plasma Science & Technology Plasma-2003, held at BIT, Mesra, during December 8-11, 2003

About the authors ...

Mr A. K. Tiwari completed his B.E. in Chemical Engineering from Pt. Ravishankar Shukla University, Raipur, Chhattisgarh. After graduating from 44th batch of BARC Training School, he joined Chemical Technology Division in 2001. He is the recipient of Homi Bhabha Award. Currently, he has been working on the design and development of process technologies for fluorine-based compounds.

Mr C.S.R. Prasad is the Head of Materials Development Section of Chemical Technology Division, BARC. He completed B.Tech and M.Tech. in Chemical Engineering in 1971 and 1980 respectively from Andhra University, Visakha-patnam. He joined Chemical Engineering Division, BARC, through 17th batch of Training School in 1974. He has been involved in indigenous development of Fluorine Technology. His current research interests include design and development of chemical reactors processing energetic high temperature systems.

Mr V.K. Kansal graduated in Chemical Engineering from IIT, Roorkee in 1969. He joined 13th batch of BARC Training School the same year and was subsequently posted in Chemical Engineering Division in 1970. In the last 34 years of his career, he has been associated with R & D activities as well as project engineering in the field of uranium processing and fluorine and fluorine-based compounds of nuclear and non-nuclear interest. Presently, he is Head, Chemical Technology Division.

Mr S. Ghorui obtained his Master's degree in Physics with specialization in radio physics and electronics from the University of Burdwan in 1995. He graduated from BARC Training School in 1997. He is presently involved in research and development work in Laser and Plasma Technology Division, BARC. His current research interest is non-linear plasma dynamics, heat transfer and fluid flow.

Dr A. K. Das is a Life Member of the Plasma Science Society of India and ICTP Indian chapter. He joined Plasma Physics Division, BARC, in 1973 after graduating from the BARC Training School. He received his Ph. D. degree on "Thermal MHD generator grade plasmas" from University of Bombay in 1979. Currently, he heads the Power Plasma Device Section at BARC and is a Ph. D. guide in Plasma Physics at the Mumbai University. His research interests include basic plasma science, computational plasma physics, development of high power plasma sources and non-linear plasma dynamics.

CHARACTERIZATION OF MATERIAL PROPERTIES BY ULTRASONICS

P.P. Nanekar and B. K. Shah
Atomic Fuels Division
Bhabha Atomic Research Centre

Abstract

Non-destructive testing techniques are most commonly employed for detection and characterization of flaws in the component. Apart from flaw characteristics, another parameter which is equally important to assess the structural integrity of engineering components is the material property. Non-destructive testing techniques offer several advantages over the conventional coupon-based techniques. Ultrasonic Testing is one of the widely used NDT techniques for material characterization. In the past few decades, researchers all over the world have carried out extensive study to characterize, both microstructural and mechanical properties of materials by ultrasonic testing. This paper highlights the ultrasonic testing parameters useful for material characterization studies and also investigations carried out in various laboratories including authors' laboratory on characterization of microstructural and mechanical properties of materials, qualification of processing treatments during fabrication and assessment of damage during service due to various degradation mechanisms.

Introduction

One of the prime objectives of Non-Destructive Testing (NDT) is to certify that the component being examined is fit for the intended service. The most common way of doing it is by examination of the component with one or combination of various Non-Destructive Testing Techniques to determine the presence or absence of flaws in the component. If the flaw exists, then it is characterized with respect to location, size, orientation, shape, nature, etc. to determine its acceptability under the operating conditions. Apart from flaw characteristics, another parameter which is equally important to assess the structural integrity of a component is the material property. Ultrasonic Testing is the most preferred NDT technique for characterization of material properties. Ultrasonic testing parameters are significantly affected by changes in microstructural or mechanical properties of materials. With the advancement in electronics,

these parameters can be measured very accurately to correlate them with various material properties with a reasonable confidence level. Some of the important metallurgical properties that have been correlated with ultrasonic testing parameters are grain size, inclusion content, elastic modulus, hardness, fracture toughness, yield strength, tensile strength, etc. Ultrasonic material characterization has also been used to qualify various processing treatments during fabrication and to assess the damage due to various degradation mechanisms like fatigue, creep, corrosion, hydrogen damage, etc. The scope of material characterization by Ultrasonics is widened by development of Acoustic Microscopes, which produces images similar to the one obtained by optical microscopes. This paper briefly describes the importance of material characterization by non-destructive testing and the affect of material properties on various ultrasonic testing parameters. Ultrasonic characterization studies carried out in various

laboratories including authors' laboratory on determination of microstructural and mechanical properties of materials, qualification of various processing treatments and assessment of damage during service due to various degradation mechanisms are also discussed.

Importance of Non-destructive Characterization of Material Properties

There are four metallurgical characteristics, which controls all the material properties. These are chemical composition, microstructure, crystal structure and dislocation density. Material properties can broadly be classified as microstructural properties and mechanical properties. Conventionally, determination of microstructural properties is done by metallography which involves cutting, polishing, grinding and etching, while mechanical properties are determined by mechanical tests like tension tests, Charpy test, Drop weight test, etc. These tests being destructive in nature are done on coupons with an assumption that the coupon is the true representative of the component that will go into service. During fabrication of any component, processes like solidification, mechanical working and heat treatment governs the above four characteristics and thereby material properties. The conventional 'coupon based' approach of determining material properties may not be good enough as there may be variation in the thermo-mechanical treatment seen by the coupon and the component itself. Hence the results of destructive tests on coupons may not truly apply to the component to be used in service. During service, there are many factors, which adversely affect the designed life of a component leading to its premature retirement. Such factors include unanticipated stresses (residual and system), operation outside designed limits (excessive temperature and load cycling), operation and environmental effects, degradation of material properties in service, etc. It is difficult to predict the affect of these factors on the service life of

the component during the design stage itself. Moreover, it may not be possible to draw a coupon from a component to determine its health for continued service. Non-destructive characterization of material properties therefore assumes a great significance during fabrication as well as service life of the component. Some of the non-destructive testing techniques that have been used to characterize material properties are ultrasonic testing, eddy current testing, magnetic methods, Barkhaussen noise, radiometry, Mossabuer spectroscopy, positron annihilation, etc. [1 – 11, 40]

Material Characterization by Ultrasonic Testing

Ultrasonic Testing is the most preferred NDT technique for characterization of material properties. Being volumetric in nature, ultrasonic examination can give an idea about the bulk material properties. Moreover, ultrasonic testing parameters are significantly affected by changes in microstructural or mechanical properties of materials. With the advancement in electronics, these parameters can be measured very accurately to correlate them with various material properties with a reasonable confidence level. Some of the important metallurgical properties that have been correlated with ultrasonic testing parameters are grain size, inclusion content, elastic modulus, hardness, fracture toughness, yield strength, tensile strength, etc. Ultrasonic material characterization has also been used to qualify various processing treatments like precipitation hardening, case hardening, etc. and to assess the damage due to various degradation mechanisms like fatigue, creep, corrosion, hydrogen damage, etc. Following are some of the commonly measured ultrasonic testing parameters for material characterization studies:

Velocity

Ultrasonic velocity in longitudinal and shear modes can be correlated to various material

properties. The measurement involves determination of time of travel between the first and the second backsurface reflection and dividing it by the distance traveled by ultrasound. The accuracy of these measurements depends on the accuracy with which time of travel and the thickness of the component are measured. In cases, where there is access to only surface of the component (in-situ applications), velocity ratio (longitudinal to shear) serves as a useful parameter. Unlike velocity determination, which needs thickness of the component as input, velocity ratio can be found out from time of travel data alone for longitudinal and shear waves. Some of the techniques used for velocity determination are pulse echo overlap technique, pulse superposition method, sing around method and phase comparison method [40]. With the advancement in electronics and digital technology, velocity can be measured with an accuracy of less than 1m/sec, making it a very reliable parameter for material property characterization.

Attenuation

Attenuation refers to the loss of sound energy as the ultrasonic beam passes through the material. Attenuation has two components, absorption and scattering. Energy loss due to absorption is a result of mechanisms such as dislocation damping, hysterisis losses, thermoelastic effects, etc. Loss due to scattering in polycrystalline materials depend on the ratio of grain size (D) and wavelength (λ). There are three distinct regimes of scattering, each having different attenuation coefficient depending on grain size (D), wavelength (λ) and frequency (f). Attenuation co-efficient is measured by finding the amplitude difference (dB) between the two backsurface signals and then dividing it by the total path traveled. It is expressed in terms of dB/mm. In more advanced techniques, the frequency spectrum (frequency vs. amplitude plot) of two successive backsurface signals are obtained. From these spectra, attenuation co-efficient at different frequencies is found out

[12]. Attenuation measurement technique is widely used in material property characterization for determination of grain size, distribution of second phase participles like inclusions and porosity, distribution of diffuse discontinuities like micro-cracks, etc.

Backscatter amplitude

Backscattering signals (often referred to as noise) from grain boundaries or second phase particles create lots of problems during ultrasonic examination for flaw detection. However, the scatter signals carry information about the size and the nature of scatter. Techniques have been established to quantitatively determine backscatter amplitude for assessment of grain size and distribution of second phase particles [13]. Backscatter measurement also finds applications in determination of diffuse discontinuities like micro-cracks that appear in components due to various degradation mechanisms.

Spectral analysis

The ultrasonic wave traveling inside material consists of many frequency components. The energy distribution (amplitude) at different frequencies (frequency spectrum) can be obtained by taking the Fast Fourier Transform of the back surface reflection. Two parameters that can be useful from frequency spectrum for material characterization studies are peak frequency and the bandwidth. Due to changes in material properties some of the frequency components are preferentially attenuated as compared to others. This causes change in the spectrum, which can be correlated with the change in material properties.

Critical angles

When the longitudinal wave traveling in one medium is incident at an angle on the interface with the other medium, it undergoes refraction and mode conversion. The refracted angle of longitudinal and shear wave in other medium depends on the incident angle as well as the ratio

of sound velocities in the two media (Snell's Law). Increase in the incidence angle results in increase in refracted angles of longitudinal and shear wave. At the first critical angle the refracted longitudinal wave travels along the surface leaving only shear wave in the other medium. At the second critical angle the refracted shear starts traveling along the surface. The values of these critical angles are very sensitive to the surface property of the material. These can be measured very precisely by using Goniometer for studying the surface property variation and case depth measurements in components.

Acoustic microscopy

Acoustic Microscopy refers to high resolution, high frequency ultrasonic inspection techniques that produce images of features beneath the surface of the sample. Unlike optical microscopy, where one can get information only about the surface features, acoustic microscopes give information about the bulk or volumetric features. In conventional ultrasonic testing the frequency of examination varies from 1 to 10 MHz. In Acoustic Microscopy, the frequencies used are up to 1 GHz or even more. At these frequencies the wavelength in most of the engineering materials is of the order of few microns. Hence, resolution of the order obtained with optical microscopes is achieved with acoustic microscopes.

Characterization of Microstructural and Mechanical Properties by Ultrasonic Testing

Studies have been carried out in various laboratories to determine various microstructural properties like grain size, inclusion rating, etc. and also mechanical properties like Young's modulus, hardness, yield strength, tensile strength and fracture toughness. These properties have been determined by measurement of one or the combination of the above ultrasonic testing parameters. Following are the some of the studies carried out in various laboratories for measurement of metallurgical properties:

Measurement of grain size

Grain size is one of the important microstructural properties, which controls mechanical properties like strength and fracture toughness. Measurement of grain size by ultrasonic testing is based on measurement of scattering co-efficient [13-16]. Scattering co-efficient α_s is given by:

$$\alpha_s = C_r . D^3 . f^4 \tag{1}$$

C_r is the scattering parameter depending on the type of wave used and the material anisotropy
D is the mean grain size.

f is the frequency

The above equation is valid in Rayleigh Scattering range, where wavelength is greater than the grain size. This is the region in which majority of ultrasonic examination is carried out. The scattering co-efficient varies with the frequency as well as the grain size. To begin with, calibration curves between the scattering co-efficient and known grain sizes at different frequencies are obtained. Then scattering co-efficient for an unknown grain size is obtained at a particular frequency. From the calibration curves the grain size is estimated.

Estimation of nom-metallic inclusions in steel

Non-metallic inclusions in steel can be in the form of sulphides, alumina, silicates and oxides. These inclusions adversely affect mechanical properties like fatigue limit and often act as an initiation site for pitting corrosion. They are also responsible for poor surface finish, which cannot be tolerated for components used for sealing applications. Conventionally, metallographic examination is carried out as per ASTM E 45 to rate the severity of these inclusions. These inclusions can be rated by ultrasonic examination as well. There exists an ASTM standard E 588 titled 'Detection of large

inclusions in bearing quality steel by ultrasonic method'. The advantage of this technique is that it can detect inclusions in the entire volume. However, this technique is not very sensitive to all types and sizes of inclusions. Ultrasonic examination involves immersion scanning of the component using 5 to 10 MHz transducer. Reflected signals from inclusions of various sizes and different depths are categorized into different groups. The severity rating S is given by the following formula:

$$S = \{A\,(N_L) + B\,(N_M) + C\,(N_H)\}\,/\,V \qquad (2)$$

A, B, C are weighting factors
N_L, N_M & N_H are number of low, medium & high level indications counted
V is the volume of material tested

Measurement of degree of recrystallization

In the Rayleigh scattering region, the attenuation co-efficient is given by the Equation 1. In the Stochastic scattering region, where the grain size is of the order of wavelength, the attenuation coefficient is given by

$$\alpha_s = C_s.\,D.f^{\,2} \qquad (3)$$

C_s is the scattering parameter
D is the mean grain size
f is the frequency

Equation 1 & 3 indicate that with the increase in grain size relative to the wavelength, there is the change in the exponent of ultrasonic frequency dependence on attenuation (from 4 to 2). This factor has been found to be a key variable relating ultrasonic attenuation to the thermal kinetics of recrystallization process. Study was carried out on cold worked Nickel 200 rod to correlate ultrasonic parameter with different stages of recrystallization process [17]. The exponent of frequency dependence (N) is found out from the frequency vs. attenuation curves ($\alpha_s = C.f^{\,N}$). At a constant frequency, the attenuation coefficient shows a non-monotonic behavior with the increase in annealing temperature. When recrystallization starts, small nucleated

crystallites form, which act as Rayleigh scatters, yielding to higher value of N. With increase in temperature, more number of crystallites nucleates and few of them grow to a region of stochastic scattering. At this stage the value of N drops.   The onset, degree and the end of recrystallization are monitored from the transition in the attenuation vs. temperature and exponent of frequency vs. temperature plots.

Determination of elastic modulus

Elastic Modulus is related to the inter-atomic forces and hence indicates maximum attainable strength. There exists a direct mathematical relationship between elastic modulus and ultrasonic longitudinal and shear velocity. These relationships are as follows:

Young's Modulus $E = \rho.\,V_T^{\,2}.\,(3V_L^{\,2} - 4V_T^{\,2})\,/$
$$(V_L^{\,2} - V_T^{\,2}) \qquad (4a)$$
Shear Modulus $G \quad = \rho.\,V_T^{\,2} \qquad\qquad (4b)$
Bulk Modulus $B \quad = \rho.\,(V_L^{\,2} - 4.\,(V_T^{\,2})\,/\,3)\;(4c)$
Poisson's Ratio $\upsilon \quad = (V_L^{\,2} - 2.\,V_T^{\,2})\,/$
$$(2.\,V_L^{\,2} - 2.\,V_T^{\,2}) \qquad (4d)$$

One of the major applications of modulus determination by ultrasonic velocity measurements is for brittle materials since other methods like tensile test produce poor results. Young's and Shear Modulus have been determined in authors' laboratory for several grades glass and resins. The values obtained are in good agreement with the ones reported in the literature.

Estimation of hardness

Hardness refers to the resistance of material to plastic deformation. It is measured in terms of resistance to indentation by using Brinell, Vickers and Rockwell hardness testers [18]. Ultrasonic hardness testers are also used in many applications, especially for in-situ measure-ments. In this technique a Vickers diamond is attached to one end of the magneto-strictive rod. The diamond tipped rod is excited to its natural frequency by a piezo-electric converter. The resonant frequency of the rod changes as the free

end of the rod is brought into contact with the surface of a solid body. The change is frequency depends upon the area of contact between the diamond tip and the test surface, which is inversely proportional to hardness of the test specimen. Studies have also been carried out to measure velocity and attenuation for determining the hardness. It has been observed that the velocity varies parabolicaly and attenuation varies linearly and inversely with the hardness.

Estimation of strength

Strength of metals is estimated by subjecting the specimen to tension test. However, for non-metallic materials like concrete and ceramics, tension test cannot be used. Ultrasonic velocity measurement is an established and widely used technique to estimate the strength of concrete and ceramics. The following table gives the relationship between velocity and the strength of concrete structure:

Table 1: Condition of concrete structure vis-à-vis ultrasonic velocity

Velocity (m/sec)	Structure Condition
4575 and above	Excellent
3600 to 4575	Good
3050 to 3600	Questionable
2135 to 3150	Poor
Below 2135	Very Poor

Ceramic materials are also characterized by ultrasonic velocity and attenuation measurements. Ultrasonic characterization of Alumina-Zirconia-Silica ceramic was carried out in authors' laboratory [19]. This ceramic material is used as refractory lining in glass melting industry. The objective of this study was to correlate ultrasonic velocity and attenuation with the soundness of refractory. Ultrasonic measurements on the samples indicated that the velocity is found to be higher ((6800m/sec as against 6400m/sec) and attenuation is found to be lower in the sound material as compared to the region where there exists a shrinkage cavity.

Monitoring ductile to brittle transition temperature

Ductile to brittle transition temperature (DBTT) is related to the toughness of the material. It represents the temperature below which the component is likely to fail by catastrophic brittle fracture. In order to avoid this, it must always be ensured that the service temperature of a component is well above DBTT. Conventionally DBTT is determined by Drop Weight Test (destructive) on coupons during the fabrication stage. However during service, there can be factors like neutron irradiation, which increase DBTT and may take it beyond the service temperature. One of the important factors, which control DBTT, is the grain size. For a fixed composition, DBTT increases with the grain size. Since increase in grain size also results in increase in attenuation, attenuation measure-ments can be used to monitor DBTT. A study was carried out to monitor DBTT in Fe-C alloys [20]. In these alloys DBTT increases with the increase in carbon content. For a fixed grain size, attenuation measurements were taken with varying carbon content. It was observed that attenuation decreases with increase in carbon content (i.e. with increase in DBTT). The reduction in attenuation is due to decrease in dislocation damping in high carbon steel, which is one of the predominant mechanisms of absorption. For this alloy system it was observed that although increase in grain size and carbon content increase DBTT, their influence on attenuation variation is contradictory.

Estimation of fracture toughness

Fracture toughness is an intrinsic property that characterizes fracture behavior of a material. It corresponds to the critical stress intensity factor at which crack propagates catastrophically. Fracture toughness K_C is given by:

$$K_C = \sqrt{E'} . G_c \qquad (5)$$

E' is the Young's Modulus
G_c is the strain energy release factor

E' is related to ultrasonic velocity and K_C is related to the microstructure, which in turn affects ultrasonic attenuation. Hence correlation exists between fracture toughness and ultrasonic propagation properties via ultrasonic velocity and attenuation. A Vary demonstrated the feasibility of ultrasonic measurement of plane strain fracture toughness K_{IC} for two grades of Maraging steels and a Titanium alloy [21]. The following empirical correlation was found between ultrasonic attenuation slope β_δ and K_{IC}:

$$(K_{IC}/\sigma_Y)^2 = M (V_l . \beta_\delta / m)^{\frac{1}{2}} \qquad (6)$$

V_l is the longitudinal velocity

β_δ is $d\alpha/df$ (α is attenuation coefficient and f is the frequency) evaluated at a particular frequency, which is based on mean grain size δ

M is the empirical constant

Qualification of Processing Treatments

During fabrication the components are subjected to various processing treatments in order to achieve required material properties. Studies have been carried out in various laboratories to establish the feasibility of using ultrasonic testing parameters to qualify these processing treatments. Some of these studies are discussed below:

Nodularity of cast iron

Cast irons are classified based on the morphology of graphite. Carbon in cast iron can be forced to agglomerate into spheroidal form or nodules during solidification of iron by the addition of magnesium ferrosilicon to the melt. Lack of this treatment results in gray cast iron in which carbon is present in the form of flakes. Graphite morphology in cast irons affects their

mechanical properties. Nodular cast irons are superior in strength and toughness as compared to gray cast iron. Relationship between ultrasonic velocity and strength is used to many industries to assure the strength of components made of nodular cast iron. The increase in degree of nodularity increases the strength which in turn results in increase in the ultrasonic velocity [22, 23, 40].

Qualification of β heat treatment of uranium rods

Uranium rods are used as fuel in nuclear research reactors. One of the critical steps in the fabrication route of fuel elements is the β heat treatment of uranium rods after hot rolling. The β heat treatment randomizes the preferential texture that gets developed during hot rolling operation. The presence of texture leads to non-uniform elongation during irradiation in the reactor. Conventionally, β heat treatment of uranium rods is qualified by thermal cycling test, during which the sample is subjected to 1000 thermal cycles from 0^oC to 550^oC and back. The acceptance criteria demands that the total elongation after the test should not exceed 15%. The thermal cycling test is very time consuming and by the time the results are obtained the rod is already loaded in the reactor. Hence, there was a need to develop an NDT technique by means of which β heat treatment can be qualified quickly. Ultrasonic testing technique based on velocity measurement was developed in authors' laboratory [24]. The following table gives the variation in axial and radial velocity in uranium rod for rolled and rolled & β heat treated conditions:

Table 2: Ultrasonic longitudinal velocity in uranium rods for different conditions

Condition	Long. Velocity Radial (m/sec)	Long. Velocity Axial (m/sec)
Hot Rolled	3434	3242
Rolled, β heat treated and water quenched	3365	3360

This technique has now been incorporated as a quality control step to qualify the β heat treatment of uranium rods.

Qualification of heat treatment of precipitation hardenable 17-4 PH stainless steel

17-4 PH Stainless Steel exhibits high strength and corrosion resistance. It is procured in solution annealed condition (Condition A), machined to desired shape and then subjected to low temperature heat treatment (900 -1000°F) to achieve desired strength. Strength increases during heat treatment due to precipitation of copper. Ultrasonic testing technique based on velocity and attenuation measurement was developed in authors' laboratory to qualify the heat treatment of these steels [25]. The following table shows the variation in velocity and attenuation with heat treatment:

Table 3 : Variation in ultrasonic velocity and attenuation with heat treatment for 17-4 PH SS

Heat treatment Condition	Hardness Rc	Longitudinal Velocity m/s	Attenuation dB/mm
Soln. Annealed	27	5776	0.120
900°F/ 1hr	47	5878	0.159
1025°F / 4 hr	37	5839	0.160
1100°F / 4 hr	36	5877	0.173

The table indicates that following the heat treatment, the hardness increases and so does the velocity as compared to the solution annealed condition. There is also an increase in attenuation after heat treatment.

Measurement of case depth

Many applications demand that the surface of component to be hard retaining its core in soft and tough condition. In such cases, the components are subjected to surface hardening treatments like carburizing, nitriding carbo-nitriding, flame hardening, etc. One of the important parameters that needs to be controlled in these processing treatments is the depth up to which hardening is carried out, referred to as case depth Conventionally, case depth measurement is carried out on coupon basis by cutting the sample at a particular location and observing it under microscope. Weston – Bartholomew successfully carried out study to measure case depth of carburized layer by ultrasonic testing. Measurement employed surface waves and was based on finding the critical angle at which Rayleigh waves are generated in the material. Rayleigh waves are confined to the surface (for a depth of one wavelength). The critical angle for generation of Rayleigh wave is given by:

$$\theta_R = Sin^{-1} (C_w/ C_r) \tag{7}$$

C_w is the velocity of longitudinal waves in water
C_r is the velocity of Rayleigh waves in the material

Precise measurement of critical angle was carried out by using a goniometer. It was observed that θ_R increases with the case depth. A calibration curve was first obtained between case depth and θ_R, by taking measurements on the samples of known case depth at a particular frequency. Then the precise critical angle for the unknown case depth was found out by using a goniometer. From the calibration curve the case depth was estimated. This technique was able to measure the case depth from 400 to 1200 micron with an accuracy of 50microns [26].

Ultrasonic Characterization of Material Degradation during Service

Any engineering component when put in service, is designed to last for a definite amount of time, which is referred to as useful life or designed life of the component. There are many factors, which adversely affect the designed life of the component and lead to its premature retirement from service. Such factors include, unanticipated stresses (residual and system), operation outside

designed limits (excessive temperature and load cycling), operation and environmental effects, degradation of material properties in service, etc. Some of the most common types of degradation mechanisms observed in engineering components include fatigue, creep, uniform and localized corrosion, age hardening, hydrogen damage, neutron irradiation, etc. It is difficult to predict the extent of their damage on the serviceability of the component at the designed stage. It is also not possible to take out a coupon from the component to assess its microstructural and mechanical properties for continued service by destructive tests. Non-destructive evaluation of material properties play a crucial role to assess the damage caused by various degradation mechanisms in components during service. Ultrasonic testing is widely used in many industries for this purpose. Following are some of the investigations carried out to characterize the material degradation during service by ultrasonic testing:

Detection of fatigue damage

Two techniques have been used for ultrasonic detection of fatigue damage, one based on reflection and the other on attenuation measurement. Acoustic emission (AE) technique is also used, but the background noise during fatigue tests causes problems during AE. For reflection based ultrasonic examination techniques, either using bulk waves or surface waves, the fatigue crack has to be sufficiently deep to record a measurable signal. Hence, these techniques are not suitable for detection of early fatigue damage. However, these are best suited for accurate sizing of cracks once they grow deeper. Attenuation measurement has been observed to be very sensitive to detect early stages of fatigue damage [27]. Since dislocation motion is prerequisite to any kind of plastic deformation and ultrasonic attenuation is sensitive to dislocation motion or dislocation damping, very precise attenuation measurement during fatigue tests gives very useful information about the initiation of fatigue

damage. Attenuation changes because of interaction of ultrasonic waves with physically deformed region or micro-crack that forms at an early stage of fatigue damage. Study was carried out by Joshi and Green [28] on aluminum and steel samples by employing attenuation measurement as well as reflection based technique. The results indicate that change in attenuation during the fatigue test is observed much earlier during the fatigue test than the appearance of reflected signal in reflection based technique.

Early detection of creep damage

Creep refers to the time dependent plastic deformation at constant load at high temperature. Creep damage is characterized by three stages viz. micro-pore formation at grain boundaries, pore growth & pore coalescence and micro-crack formation and crack growth. Density of the material depends on pore concentration. The elastic and shear modulus is also affected by the pore fraction. Since ultrasonic longitudinal and shear wave velocity is mathematically related to modulus of elasticity and density, their measurement forms the basis of detection of early creep damage. Dobmann observed that longitudinal, shear as well as Rayleigh wave velocity decreases with increase in the pore fraction [29]. The measurements were sensitive to detect the density change of the order of 0.8% due to pore formation. Presence of pores also affects the attenuation and very precise measurement of this parameter gives useful information about the creep damage.

Hydrogen attack in low alloy steel

Hydrogen attack in low alloy steel has been observed in components which are exposed to high pressure hydrogen at high temperatures. The chemical reaction between hydrogen and steel produces methane gas, which bubbles at grain boundaries, grow and interlink to form fissures and micro-cracks. These cracks are responsible for lowering of fracture toughness of the material. It is important to detect this damage

non-destructively in pressure vessel and piping which are prone to such attack. Ultrasonic testing parameters viz. velocity, attenuation and backscattering have been observed to be very sensitive to detect hydrogen damage in low alloy steel [30, 31]. It is observed that the velocity in the affected samples decreases (from 5800m/sec to 5280 m/sec) due to overall decrease in bulk modulus of elasticity caused by micro-cracks. This parameter is useful to monitor extensive damage. Attenuation, as expected is found to increase with the damage due to increase in scattering form the micro-cracks. Backscatter is found to increase in the affected sample due to impedance mismatch at the grain boundary. It is a useful parameter for monitoring low level of hydrogen attack. Its primary advantage is that this parameter is unaffected by the condition of inside surface of the component when the measurements are being made from the outside surface.

Hydrogen damage in zircaloy – 2

Zircaloy – 2 (Zr-2.5%Sn. 0.1%Fe, 0.1%Cr and 0.1%Ni) is used as pressure tube material in pressurized heavy water reactors. The corrosion reaction during service between pressure tube and high temperature heavy water coolant results in evolution of hydrogen, a part of which is absorbed in pressure tube material. In zircaloy – 2 pressure tubes, damage due to hydrogen manifests itself in two forms, delayed hydride cracking and hydride blister formation. In the former case, hydrogen migrates to a region of high localized stress like flaw tip, resulting in precipitation of hydride platelets, their growth and cracking. This cycle continues as the crack initiates and grows in the pressure tube. In the case of blister, hydrogen migrates down the temperature gradient at a localized cold spot, which can form if the pressure tube comes in contact with the surrounding (cold) calandria tube during service. The hydride blister grows and cracks after attaining the critical size. There are threshold limits of hydrogen for initiation of DHC and blister, but these are too low

(25-70ppm) to be measured reliably by ultrasonic techniques. P.K. De, et. al. [32] used ultrasonic velocity, attenuation and electrical conductivity measurements to assess the hydrogen in the level of few hundred ppm. It is mandatory to carry out periodic in-service inspection of pressure tubes in the reactors to assure their structural integrity during operation. While detection of DHC is based on conventional ultrasonic flaw detection techniques, these are not useful for detection of hydride blisters. This is because the interface between the zircaloy-2 pressure tube and the zirconium hydride blister is a poor reflector of ultrasound. In order detect zirconium hydride blister, two techniques were standardized in the authors' laboratory [33-36]. Detection of zirconium hydride blister is based on difference in longitudinal and shear wave velocity in zircaloy – 2 and zirconium hydride. It has been observed that the velocity ratio (longitudinal to shear) for zircaloy-2 is 2.0 as against 2.8 for zirconium hydride. The velocity ratio at the blister location is between these two limits depending on the depth of blister. The change in time of travel at blister location due to difference in velocity was utilized to get the B-scan images.

Intergranular Corrosion attack in Austenitic Stainless Steel

Intergranular Corrosion (IGC) attack refers to localized corrosion along the grain boundary. Sensitized steels (due to chromium depletion along grain boundaries) are prone to this attack when exposed to corrosive environment. Conventionally, IGC tests are performed as per ASTM A262 Practice A to E. The severity of IGC is expressed as depth of IGC attack. Ultrasonic velocity and attenuation are very useful parameters to monitor the depth of IGC attack [37]. Velocity is reduced in attacked region as the acoustic property of corrosion products filling IGC affected micro-cracks are different than that of grain matrix. Attenuation increases in IGC affected region due to increased scattering by micro-cracks at grain boundaries.

Study carried in authors' laboratory indicates that with the depth of attack in excess of 200 micron, there is a significant change in the velocity and attenuation.

Thermal Embitterment of Duplex Stainless Steel

The microstructure of duplex stainless steel consists of austenite and ferrite. They offer high corrosion resistance, high strength & toughness and good weldability. They find extensive use in chemical plants and marine construction. One of the degradation mechanism observed in duplex stainless steel is the embrittlement during exposure to $600^{o}C$ to $800^{o}C$, due to precipitation of sigma phase As a result the fracture toughness comes down. E. Ikuta, et.al. carried out study on ultrasonic evaluation for thermal embrittlement of duplex stainless steels. The test samples were annealed at $800^{o}C$ for up to 10 hours to produce sigma phase. Ultrasonic measurements and destructive tests were performed on these samples. Ultrasonic evaluation involved measurement of ultrasonic velocity, attenuation and the central frequency of the received ultrasonic pulse. Destructive tests like Charpy Impact Test and Vicker's Test were carried out to correlate ultrasonic parameters with the degree of embrittlement. It was observed that while the attenuation decreases, the velocity and the central frequency increase with the embrittlement [38].

Ageing degradation in Alloy 625

Alloy 625 (Ni based) is extensively used in chemical industry for its high temperature strength and corrosion resistance. Ageing degradation during long term exposure at high temperature due to precipitation of Ni_3Nb/Ni_2Mo phase causes reduction in ductility and toughness. Study was carried out in authors' laboratory to correlate ultrasonic testing parameters viz. velocity and attenuation with the degree of age hardening in Alloy 625 [39]. The study was carried out on samples with high temperature service exposures (approx. $500^{o}C$ to

$600^{o}C$) for 25,000, 50,000 and 1,00,000 hrs. Study indicated that in the service aged samples, both velocity and attenuation was higher as compared to virgin sample. No significant difference was observed in these two parameters in samples exposed for different times. The samples were then subjected to heat treatment ($700^{o}C$, 6 hrs.) in order to regain the mechanical properties. Consequent to this heat treatment the velocity and attenuation reduces and approaches that of the virgin sample. The study established that the onset of age hardening in this alloy as well as the recovery of its mechanical properties after heat treatment can be detected by monitoring ultrasonic velocity and attenuation.

Conclusion

Ultrasonic testing is traditionally used for flaw detection and characterization. The spectrum of ultrasonic testing applications is widened by its use for material characterization. With the advancement in electronics and digital technology, ultrasonic testing parameters, which are affected by changes in material properties, can be measured with high accuracy to provide a reasonable confidence level. Ultrasonic testing for material characterization can not play a vital role in quality assurance during in-manufacture inspection but can serve as a powerful tool for life prediction technology during in-service inspection, residual life assessment and plant life extension. There are however few difficulties which are encountered during ultrasonic testing for material characterization. There is no one to one mapping between ultrasonic parameters and microstructural / mechanical properties. Microstructural properties, which control the mechanical properties, affect the ultrasonic propagation factors differently. In order to establish any correlation between mechanical properties and ultrasonic parameters the effects of various microstructural properties on ultrasonic testing parameters must be separated. For quantitative material characterization, empirical correlations and calibration must be

established for each material. It is important to have a mechanistic understanding of relationship between ultrasonic testing parameters and individual microstructural properties for effective non-destructive characterization of material properties and their performance.

References

1. Analytical ultrasonics in material research and testing, NASA CP 2383, 1984

2. S. Banerjee & BK Shah, 'Characterization of Industrial Materials', Material Characterization Techniques – Principals and Applications, Ed. G. Sridhar, S. Ghosh Chowdhary and N.G. Goswami, 1999, pp 1- 15

3. G. Dobmann, et.al., 'Non-destructive characterization of materials: A growing demand for describing damage and service-life relevant ageing process in plant components', Nuclear Engineering and Design, Vol. 171, 1997, pp-95-112

4. R.B. Thomson, 'Laboratory Non-Destructive Evaluation technology material characterization', Journal of Non-Destructive Evaluation, Vol. 15, Nos. 3&4, 1996

5. Baldev Raj, et. al., 'NDE methodologies for characterization of defects, stresses and microstructure in pressure vessels and pipes', International Journal on Pressure Vessel and Piping, Vol. 73, Issue 2, Sept. 1997, pp 133 – 146

6. Proc. Workshop on 'Testing and characterization of materials', Convener D.N. Sah, IIM, Mumbai Chapter, 1990

7. Proc. Seminar on 'Advances in NDT techniques for flaw and materials characterization', Convener B.K. Shah, IIM, Mumbai Chapter, 1992

8. Proc. Workshop on 'Recent trends in non-destructive evaluation of materials', Ed. A. Mitra, et.al., 1997

9. D.K. Bhattacharya, 'Characterization of microstructure in steels by magnetic techniques – An overview', ISNT Journal of Non-Destructive Evaluation, Vol. 17, No. 1, 1997

10. G. Dobmann, et., al., 'Ageing material evaluation and studies by non-destructive techniques (AMES-NDT), A European Network Project', Nuclear Engineering and Design, Vol. 206, 2001, pp 363-374

11. WA Theiner, et., al., 'Non-destructive analysis of the structure of pressure vessel steels by micromagnetic testing techniques', Nuclear Engineering and Design, Vol. 76, Issue 3, December 1983, pp 251-260

12. A.Vary , 'Quantitative ultrasonic evaluation of mechanical properties of engineering materials', NASA TM – 78905, 1978

13. H. Willems and K. Gobbeles, 'Characterization of microstructure by backscatter ultrasonic waves', Material Science, Vol. 15, Nov. Dec. 1981, pp 549-553

14. D.K. Mak, 'Determination of grain size, hysterisis constant and scattering factor of polycrystalline material using ultrasonic attenuation', Canadian Metallurgical Quarterly, Vol. 25, No.3, pp 253-255

15. R.D. Diamand, 'Development of instrument for on-line measurement of grain size in copper alloys and stainless steels', 21st Annual British Conference on Non-Destructive Testing NDT 0 86, pp 225-242

16. A. Badidi Bouda, et. al., 'Grain size influence on ultrasonic velocities and attenuation', NDT & E International, Vol. 36, Issue 1, Jan 2003, pp 1-5

17. E.R. Generazio, 'Ultrasonic attenuation measurements to determine onset, degree and completion of recrystallization', Materials Evaluation, Vo. 46, August 1998, pp 1198-1203

18. Metals Handbook, 9th Edition, Vol. 8, Mechanical Testing

19. P.P. Nanekar, et.al. 'Non-destructive characterization of ceramics and concrete structure', Testing and Quality Control,

conducted by ASM India Section, May 2001, Mumbai.

20. RL Smith, et.al., 'Ultrasonic attenuation, microstructure and ductile to brittle transition temperature in Fe-C alloys', Materials Evaluation, Vol. 41, Feb. 1983, pp 219-222

21. A. Vary, 'Concepts for interrelating ultrasonic attenuation, microstructure and fracture toughness in polycrystalline solids', Materials Evaluation, Vol. 46, April 1988, pp 642-649

22. Metals Handbook, Ninth Edition, Volume 17, Non-Destructive Evaluation and Quality Control, p- 532

23. Jean F. Bussiere, et.al., 'Analysis of the effect of graphite morphology on the elastic properties of cast iron', Proc. of 3rd Symposium on Non-Destructive Characterization of Materials, Saarbrucken, FRG, Oct. 3-6, 1988, pp 353-660

24. B.K. Shah, et.al., 'Qualification of beta heat treatment of uranium fuel rods by ultrasonics', Insight, Journal of British Institute of Non-destructive Testing, Vol. 41, No. 11, Nov. 1999, pp. 707-709

25. PP Nanekar, et.al., 'Ultrasonic characterization of Precipitation Hardenable 17-4 PH Stainless Steel', Proc. of 47th Annual technical meeting of Indian Institute of Metals, Hyderabad, Nov. 93

26. W. Weston-Bartholomew, 'Use of ultrasonic goniometer to measure depth of case hardening', International Advances in Nondestructive Testing, 1979, Vol. 6, pp 111-123

27. Robert E. Green, et.al., 'Ultrasonic and Acoustic Emission detection of fatigue damage', International Advances in Nondestructive Testing, 1979, Vo. 6, pp 125-177

28. N.R. Joshi and R.E. Green, 'Ultrasonic detection of fatigue damage', Fract. Mech. 4, 1972, 577-583

29. Gerd Dobmann, et.al., 'Nondestructive characterization of materials (ultrasonic and magnetic techniques) for strength and toughness prediction and the detection of early creep damage', Nuclear Engineering and Design, 157, 1992, pp. 137-158

30. A.S. Birring, et.al., 'Ultrasonic detection of hydrogen attack in steels', Corrosion, Vol. 45, No. 3, pp. 259-263

31. S.E. Kruger, et.al., 'Hydrogen damage detection by ultrasonic spectral analysis', NDT & E International, Vol. 32, 1999, pp 275-281

32. P.K. De, et.al., 'Assessment of hydrogen levels in zircaloy-2 by non-destructive testing', Journal of Nuclear Materials, Volume 252, 1998, pp 43-54

33. PP Nanekar, et.al. 'Detection of zirconium hydride blister in pressure tubes of pressurized heavy water reactors', INSIGHT – The Journal of British Society of Non-Destructive Testing, Vol. 40, No.10, Oct. 1998, pp. 722 – 723.

34. PG Kulkarni, M Bandyopadhyay, PP Nanekar, MD Mangsulikar, BK Shah, R Ramanathan, SV Paibhale and DSC Purushotham, 'Development towards NDT techniques for detection of hydride blisters in pressure tubes of PHWRs', International Atomic Energy Agency (IAEA) Technical Meeting, Vienna, July 94.

35. PP Nanekar, M Bandyopadhyay, MD Mangsulikar and BK Shah, 'Ultrasonic characterization of service induced flaws in zirconium alloy pressure tubes of pressurized heavy water reactors', ZIRC – 2002, September 2002, BARC, Mumbai.

36. PP Nanekar, BK Gaur, AK Sinha, Arbind Kumar, PR Vaidya, BK Shah and PG Kulkarni, 'Non-Destructive Evaluation of Corrosion and Hydriding in Zirconium Alloys', Global 2000 Corrosion Meet, NACE India Section, Nov. 2000, Mumbai

37. B.K. Shah, M. Tech Thesis, 'Monitoring of intergranular corrosion in austenitic stainless steels AISI 304 by non-destructive testing methods', IIT, Bombay, 1984

38. E.Ikuta, et.al. 'Ultrasonic evaluation of thermal embrittlement', Proc. Of the 13th International Conference in the Nuclear and Pressure Vessel Industries, Kyoto, Japan, 1985, pp 285-289

39. BK Shah, et.al., 'Ultrasonic characterization of aging degradation during long term high temperature exposure in Nickel base alloy 625', Proc. of 14th World Conference on NDT, pp 2235 – 2238, New Delhi, Dec. 96

40. E.P. Papadakis, 'Ultrasonic velocity and attenuation measurement methods with scientific and industrial applications', Physical Acoustics, Vol. 12, 1976, pp 277-374

This paper received the 'Best Paper Award' during the National Seminar on Non-Destructive Evaluation, NDE 2003, conducted by Indian Society for Non-Destructive Testing, held at Trivandrum during December 2003

About the authors ...

Mr P.P. Nanekar is a metallurgical engineer from VNIT, Nagpur. He joined BARC in the year 1992 (35th batch of BARC Training School) and is working in the field of Non-Destructive Testing. He holds a Level III certificate in ultrasonic testing and Level II certificate in eddy current testing and liquid penetrant testing. His field of work includes:

- *Development of techniques for in-service inspection of nuclear reactors*
- *Quality assurance during fabrication of nuclear reactor components*
- *Flaw characterization by advanced ultrasonic testing techniques*
- *Material characterization studies on nuclear fuel, zirconium alloys and stainless steel*

He has published over 30 technical papers in the field of NDT. Three of his papers, including the two presented during 14th World Conference on NDT, received 'Best Paper Award'.

Mr B.K. Shah did his B.Sc. Engg. (Metallurgy) from Regional Institute of Technology (RIT), Jamshedpur and M.Tech. (Corrosion Science & Engg.) from Indian Institute of Technology (IIT), Bombay. He joined BARC in 1973(17th batch of BARC Training School). Presently, he is Head, NDT & Quality Evaluation Section, Atomic Fuels Division, BARC. His field of work includes :

- *Quality assurance in the manufacture of nuclear fuel & reactor core components*
- *Material characterization by NDT*
- *Metallurgical failure analysis*
- *In-service inspection*
- *Corrosion studies on reactor materials*

He has published more than 160 technical papers in various National & International journals and Conference proceedings. He has received best paper awards for four technical papers, including the two presented during 14th World Conference on NDT. In recognition of his contributions to the Research & Development in the area of Non-destructive Testing & Evaluation, he has been awarded NDT National Award 1998 and ISNT Mumbai Chapter NDT Achievement Award 2001.

He is a Life Fellow of Indian Society for NDT and Regional Controller of Examination (Western Region), National Certification Board on NDT. He is Life Member of IIM, INS, IVS, & NAARRI.

DETERMINATION OF BURN-UP OF IRRADIATED THORIA USING TIMS

S.K. Aggarwal, R. Govindan, P.G. Jaison, P.S. Khodade, A.R. Parab,
V.L. Sant, P.M. Shah and V. Venugopal
Fuel Chemistry Division
Bhabha Atomic Research Centre

Introduction

The Indian nuclear fuel cycle aims at the large scale utilization of thorium for the sustained growth of nuclear energy in the country. This implementation of Th fuel cycle requires development of new technologies including post-irradiation studies. Burn-up is one such important parameter and it is defined as the atom percent fission of heavy elements (mass >225) during the life of the fuel in a reactor. The experimental data with high accuracy on burn-up is essential to develop the computer codes for thoria-based fuels as well as it helps in evaluating the performance of the fuel in the reactor. The procedure for the experimental determination of burn-up involves the determination of the total heavy-element composition after irradiation and the concentration of a fission product in the irradiated fuel that can be related to the total number of fissions in the fuel [1]. Isotope Dilution Mass Spectrometry (IDMS), being a very accurate and sensitive method, was utilised for carrying out these measurements. The advantages of this method such as low limits of detection and non-essentiality of quantitative recovery reduce the problems associated with handling of radioactive samples. Stable fission product ^{148}Nd was chosen as the monitor for determining the burn-up of thoria-based fuel [2].

Experimental

Dissolution of irradiated thoria sample (~500mg) was carried out in (Con. HNO_3 + HF) mixture behind the shielding of a lead cell set up in glove box. Aliquots were drawn from this solution for mixing with respective spikes and also for the isotopic composition determination of Nd, Th and U. ^{142}Nd, ^{229}Th and SRM 950a U were used as the spikes for the concentration determination of Nd, Th and U, respectively. The spike solutions of Nd and Th were calibrated against chemical assay standards: ^{142}Nd against high purity natural Nd_2O_3 and ^{229}Th spike against high purity ThO_2. Spiked aliquots were treated with redox reagents for the proper chemical exchange between the spike and the sample isotopes.

Uranium and thorium fractions were purified by anion exchange (Dowex 1x8) separation in 10M HCl and in 7M HNO_3 media, respectively. The non-retained fission products were collected and Nd fraction was purified by loading on Bio-Rad 1x2 anion exchange column in a mixed solvent medium of (HNO_3 + MeOH) [3]. Purified fractions were loaded on to the vaporization filament of double rhenium filament assembly. Uranium, thorium and neodymium fractions from spiked as well as from the unspiked samples were analysed for the determination of concentration and isotopic compositions respectively. Concentration of Th was also determined by EDTA titration using xylenol orange indicator.

A Thermal Ionisation Mass Spectrometer (MAT 261) with multi-collector system was employed for carrying out the mass spectrometric analyses. The isotope ratio measurements were made at

filament temperatures of 2.0–2.5A and 6.0–6.2A for vaporizing and ionizing filaments, respectively.

Results and Discussion

Dissolution: Dissolution of irradiated thoria was initially carried out in (Conc.HNO₃+HF) mixture. But the process of dissolution being very slow, HF was replaced with NaF (0.05M) and the sample could be dissolved within 20 hrs [4].

Mass Spectrometric Analysis: Extreme care was taken during the isotopic composition determination of U to minimise natural contamination.

Table 1 : Isotopic composition of U in the irradiated ThO₂ sample

Nuclide	Atom % abundance	Avg. At. Wt. of U
232*	0.0489	
233	88.91	233.171
234	9.58	
235	0.94	
236	0.078	
238	0.44	

* Determined by alpha spectrometry

Table 2 : Isotopic composition of Nd in the irradiated ThO₂ sample

Isotope	Atom % abundance	Avg. At. Wt. of Nd
142	0.4038	
143	23.3314	144.6029
144	33.7325	
145	17.4141	
146	15.0729	
148	7.2814	
150	2.7639	

The isotopic composition data of U and Nd are given in Tables 1 and 2, respectively. Since ^{232}U content in the sample was too less to give any appreciable signal on TIMS, alpha spectrometry was used for this purpose. Purified fractions of the spiked mixture were analysed for the ratios 142/148 for Nd and 233/238 for U. (^{142}Nd/^{148}Nd) ratio was also corrected for the natural contamination. The method for the mass spectrometric analysis of thorium was standardized by loading natural Th(NO₃)₄ sample and monitoring ^{229}ThO$^+$(m/z 245)/ ^{232}ThO$^+$(m/z 248) for the determination of isotopic composition and concentration. The thorium concentration value obtained by IDMS was 9.87mg/g. The thorium concentration value obtained by EDTA titration was higher and the bias is attributed to the interference from the non-separated fission products in the dissolver solution used for titration.

Using the concentration and the isotopic composition data of uranium, thorium and neodymium and the fission yield of ^{148}Nd, burn-up was calculated using the equation:

$$\text{Atom \% fission} = \frac{(N_{FM}/Y_{FM}) \times 100}{[N_U + N_{Th} + (N_{FM}/Y_{FM})]}$$

where,
N_{FM} = Number of atoms of burn-up monitor
N_U = Number of atoms of U
N_{Th} = Number of atoms of Th
Y_{FM} = Fission yield of burn-up monitor

The burn-up calculated using ^{148}Nd as the burn-up monitor was found to be 1.251%.

Conclusion

Isotope dilution Mass Spectrometry provides a reliable method for the experimental determination burn-up of Thoria based fuels. Experiments are underway for determining the burn-up using ^{139}La also as the burn-up monitor.

References

1. R.M. Cassidy, S. Elchuk, L.W. Green, C.H. Knight, F.C. Miller and B.M. Recoskie, J. Radioanal. Nucl. Chem. **130** (1990) 55.
2. M.E. Meek and B.F. Rider, Compilation of fission product yields, General Electric, NEDO-12154-1 (1974) p 37,42.
3. K.L.Ramakumar, S.K. Aggarwal, V.D. Kavimandan, V.A. Raman, P.S. Khodade, H.C .Jain and C.K. Mathews, Separation Sci. Technol. **15** (1980) 1471.
4. G.K. Mallik, R.K. Malik, K. Raju and H.S. Kamath, Proceedings of Nuclear and Radiochemistry Symposium held at University of Pune, Pune from Feb. 7-10, 2001, p. 260.

This paper received the 1ˢᵗ Prize in the category of "Nuclear Technology (NT-9)" presented during ISMAS Silver Jubilee Symposium on Mass Spectrometry (ISMAS-SJS-2003) held at National Institute of Oceanography, Goa, during January 27-31, 2003

About the authors ...

Dr S.K. Aggarwal is currently Head, Mass Spectrometry Section of the Fuel Chemistry Division, BARC. He received his B.Sc. (Hons.) from Guru Nanak Dev University, Amritsar, in 1972 with two Gold Medals. He joined the 16ᵗʰ batch of BARC Training School in 1972 and received the Homi Bhabha Award. He did his Ph.D. from Mumbai University in 1980. He is a coauthor of 300 scientific publications, which include 100 articles published in reputed journals. Dr. Aggarwal has participated in several international and national conferences and in different international intercomparison experiments. He is a specialist in the field of atomic mass spectrometry and alpha spectrometry and is interested in various mass spectrometric techniques. His other areas of interest include electrochemistry and solvent extraction. He represents India in the Executive Committee of International Mass Spectrometric Conferences. He has visited several countries in America, Europe and Australia as an expert as well as for delivering lectures. He is a recognized Ph.D. Guide of the Mumbai University.

Mr R. Govindan obtained his M.Sc. in Chemistry from Annamalai University. He joined Mass Spectrometry Section of Fuel Chemistry Division, BARC, during November 2001 after working in Advanced Fuel Fabrication Facility, BARC, Tarapur for a period of 14 years. He is currently working in the field of inorganic Mass Spectrometry for precise isotopic analysis and concentration determination of elements which are important in nuclear technology. He has actively participated in the chemical characterisation of mixed oxide fuel for BWR, Tarapur. His other areas of interest include Potentiometry and Electro-analytical chemistry involving ion selective electrodes.

Mr P.G. Jaison joined Fuel Chemistry Division after graduating from 41ˢᵗ batch of BARC Training School in 1998. He has been actively working on the development of HPLC methods for the separation of lanthanide and actinide elements. His other fields of interest are mass spectrometry and microwave assisted digestion.

Mr P.S. Khodade *is working in Mass Spectrometry Section of the Fuel Chemistry Division, BARC, since 1975 in the field of inorganic Mass Spectrometry and Alpha Spectrometry for precise isotopic analysis and concentration determination of elements which are important in nuclear technology. He is a coauthor of 50 scientific publications in various journals and symposia.*

Mr A.R. Parab *is working in the Mass Spectrometry Section of Fuel Chemistry Division, BARC. His scientific interest is in the area of thermal ionisation Mass Spectrometry for precise isotopic analysis of elements which are important in nuclear technology. He has more than 60 research publications in various journals and symposia.*

Mr V. L. Sant *is presently working in Fuel Chemistry Division, BARC. He is specialised in the field of solid state mass spectrometry and actively involved in chemical quality control (CQC) of nuclear fuels and other high purity nuclear grade materials for the last 28 years. Utilising expertise in Spark Source Mass Spectrometry (SSMS) in particular, he has developed and standardised different quantification and spectral interference correction methodologies for the critical trace constituents of the variety of matrices specified in the nuclear technology. His other sphere of activity comprises determination of burn-up of uranium and thorium based reactor fuels and recovery of plutonium from different types of nuclear wastes. He has more than 50 publications in international journals and symposia.*

Dr P.M. Shah *is presently working in the Mass Spectrometry Section of Fuel Chemistry Division, BARC. He has been working in the area of Thermal Ionisation Mass Spectrometry since 1970 and has been involved in determining the isotopic composition and concentrations of various elements using isotope dilution thermal ionisation mass spectrometry. His other research interests include microwave digestion and alpha spectrometry.*

Dr V. Venugopal *is currently the Associate Director, Radiochemistry & Isotope Group and Head, Fuel Chemistry Division, BARC. He has authored more than 120 scientific papers in international journals of repute and the research work carried under his guidance has resulted in 13 Ph.D. theses in the field of Thermal and Thermodynamic Science. His research interest includes solid state reaction mechanism, synthesis of advanced materials, material characterization and calculation of phase diagrams.*

DETERMINATION OF Th CONCENTRATION USING ID-TIMS

S.K. Aggarwal, D. Alamelu, R. Govindan, P.G. Jaison, P.S. Khodade, A.R. Parab, V.L. Sant and P.M. Shah
Fuel Chemistry Division
Bhabha Atomic Research Centre

Introduction

Thorium-based reactors (AHWRs) have been proposed to extend the nuclear energy reserves in the country. This implementation of thorium fuel cycle requires development of new analytical methods for nuclear material management. Accurate data on the concentration of thorium content is essential for the experimental determination of burn-up of irradiated thoria-based fuels. Various analytical methods are in use for measuring the thorium content in reactor related materials [1,2]. However, most of these techniques are applicable to samples containing purified thorium and thus require prior separation of thorium from the interfering elements [3]. Isotope Dilution Mass Spectrometry (IDMS) is an accurate and sensitive method and application of this technique for the concentration determination of thorium in irradiated thoria is the objective of the present work. IDMS is well established to obtain reliable data on concentration determination since it does not demand quantitative recovery and is free from matrix effects [4]. ^{229}Th was used as the spike for ID-TIMS analysis of thorium in the dissolver solution of irradiated thoria.

Experimental

Approximately 500mg of irradiated thoria sample was treated with a mixture of (Conc.HNO$_3$+HF) behind a lead cell set up in a glove-box. Since the process of dissolution was observed to be extremely slow, HF was replaced

with NaF (0.05M) and the sample could be dissolved within 20 hrs. The isotopic composition of ^{229}Th spike, milked from aged ^{233}U, was determined using TIMS. The spike solution was then calibrated against a chemical assay standard of Th, prepared by the quantitative microwave assisted digestion of high purity thoria in Conc. HNO$_3$. Concentration of Th in this standard solution was cross-checked by EDTA complexometric titration method. Aliquots of the dissolver solution were mixed with known amounts of the ^{229}Th spike solutions. Spiked aliquots were treated with Conc. HNO$_3$ for ensuring proper chemical exchange between the spike and the sample isotopes. The mixture was later on loaded onto the vaporization filament of a double rhenium filament assembly. A Thermal Ionisation Mass Spectrometer (MAT 261) with multi-collector system was employed for carrying out the mass spectrometric analyses. The ionization filament was kept at 6.2A whereas vaporization filament current was varied from 0 to 5A in steps of 0.2A while monitoring the relative intensities of Th$^+$ and ThO$^+$ signals.

Results and Discussion

The method for the mass spectrometric analysis of thorium was standardized by loading a solution of natural Th(NO$_3$)$_4$ sample on the vaporization filament and monitoring the intensities of the metal (Th$^+$) and oxide (ThO$^+$) peaks. These intensities of the metal and the oxide peaks were monitored as a function of the

vaporization filament temperature. It was observed that at a vaporization filament current of about 2.5 to 3.0A $^{232}ThO^+$ (m/z 248) started to appear whereas $^{232}Th^+$ starts appearing only after 3.5A. Metal oxide to metal ion ($^{232}ThO^+/^{232}Th^+$) intensity ratio at vaporization filament current of 4.0 to 4.5A was about 50. At these temperatures, $^{232}Th^+$ ion intensity was about 50 mV only. $^{232}ThO_2^+$ (m/z 264) signal was not detected even at a vaporization filament current of 5.0A. These observations suggested that for the analysis of Th by TIMS, ThO^+ ion would give the best possible results on isotope ratio measurements. Thus the spiked samples were analysed for oxide ratio $^{229}ThO^+$(m/z 245)/$^{232}ThO^+$(m/z 248) required for the determination of isotopic composition and concentration. Data on the isotopic composition of ^{229}Th are given in Table 1.

Table 1 : Isotopic composition of Th in the ^{229}Th Spike

Nuclide	Atom % abundance	Avg. At. Wt. of Th
229	97.764	
230	0.324	229.0581
232	1.912	

Table 2: Data on the concentration of Th in the irradiated ThO_2 sample by ID-TIMS

Sl. No.	Concentration (mg/g)
1	9.938
2	9.803
Mean	9.870

Table 2 gives the data on the concentration of Th in the dissolver solution determined by ID-TIMS. EDTA titration method was also tried after purification of thorium from uranium and fission products. This method led to a higher value for thorium concentration with respect to ID-TIMS results. This could be attributed only due to the presence of some interfering elements in the purified thorium fraction. This type of discrepancy demonstrates the useful of ID-TIMS as a reference method.

Conclusion

Isotope Dilution-Thermal Ionization Mass Spectrometry (ID-TIMS) offers precise and accurate results on Th concentration without using any pre-separation procedures. We have used ^{229}Th spike in the present work. It would be worthwhile using ^{230}Th as a spike, in view of its long half-life compared to that of ^{229}Th.

References

1. G.R. Relan and V. Venugopal, Proceedings of Nuclear and Radiochemistry Symposium held at BARC, Mumbai from Jan. 19–22, 1999, p.367.

2. Keshav Chander, S.P. Hasilkar, A.V. Jadhav and H.C. Jain, Proceedings of International symposium on Radiochemistry (Plutonium – 50 Years) held at BARC, Mumbai from Feb. 4 – 7, 1991, Paper No. AC-11.

3. J.J. Fritz and J.J. Ford, Anal. Chem. 25 (1) (1953) 1640.

4. S.K. Aggarwal and H.C. Jain, Introduction to Mass Spectrometry, ISMAS publication, (Editors S.K. Aggarwal & H.C. Jain) Mumbai, (1997) Chapter 17, p 371.

This paper received the 1ˢᵗ Prize in the category of "Isotopic Composition and Concentration(ICC-13)" presented during ISMAS Silver Jubilee Symposium on Mass Spectrometry (ISMAS-SJS-2003) held at National Institute of Oceanography, Goa, during January 27-31, 2003

About the authors ...

Dr S.K. Aggarwal *is currently Head, Mass Spectrometry Section of the Fuel Chemistry Division, BARC. He received his B.Sc. (Hons.) from Guru Nanak Dev University, Amritsar, in 1972 with two Gold Medals. He joined the 16ᵗʰ batch of BARC Training School in 1972 and received the Homi Bhabha Award. He did his Ph.D. from Mumbai University in 1980. He is a coauthor of 300 scientific publications, which include 100 articles published in reputed journals. Dr. Aggarwal has participated in several international and national conferences and in different international intercomparison experiments. He is a specialist in the field of atomic mass spectrometry and alpha spectrometry and is interested in various mass spectrometric techniques. His other areas of interest include electrochemistry and solvent extraction. He represents India in the Executive Committee of International Mass Spectrometric Conferences. He has visited several countries in America, Europe and Australia as an expert as well as for delivering lectures. He is a recognized Ph.D. Guide of the Mumbai University.*

Ms D. Alamelu *obtained her M.Sc. Degree in Physics from Annamalai University. After graduating from 38ᵗʰ batch of Training School, BARC, she joined Mass Spectrometry Section of the Fuel Chemistry Division in 1995. Since then, she has been actively involved in the indigenous development of Time of Flight Mass Spectrometer. Her other areas of interest include thermal ionisation mass spectrometry and alpha spectrometry.*

Mr R. Govindan *obtained his M.Sc. in Chemistry from Annamalai University.   He joined Mass Spectrometry Section of Fuel Chemistry Division, BARC, during November 2001 after working in Advanced Fuel Fabrication Facility, BARC, Tarapur for a period of 14 years. He is currently working in the field of inorganic Mass Spectrometry for precise isotopic analysis and concentration determination of elements which are important in nuclear technology. He has actively participated in the chemical characterisation of mixed oxide fuel for BWR, Tarapur. His other areas of interest include Potentiometry and Electro-analytical chemistry involving ion selective electrodes.*

Mr P.G. Jaison *joined Fuel Chemistry Division after graduating from 41ˢᵗ batch of BARC Training School in 1998.   He has been actively working on the development of HPLC methods for the separation of lanthanide and actinide elements. His other fields of interest are mass spectrometry and microwave assisted digestion.*

Mr P.S. Khodade *is working in Mass Spectrometry Section of the Fuel Chemistry Division, BARC, since 1975 in the field of inorganic Mass Spectrometry and Alpha Spectrometry for precise isotopic analysis and concentration determination of elements which are important in nuclear technology. He is a coauthor of 50 scientific publications in various journals and symposia.*

Mr A.R. Parab *is working in the Mass Spectrometry Section of Fuel Chemistry Division, BARC. His scientific interest is in the area of thermal ionisation Mass Spectrometry for precise isotopic analysis of elements which are important in nuclear technology. He has more than 60 research publications in various journals and symposia.*

Mr V. L. Sant *is presently working in Fuel Chemistry Division, BARC. He is specialised in the field of solid state mass spectrometry and actively involved in chemical quality control (CQC) of nuclear fuels and other high purity nuclear grade materials for the last 28 years. Utilising expertise in Spark Source Mass Spectrometry (SSMS) in particular, he has developed and standardised different quantification and spectral interference correction methodologies for the critical trace constituents of the variety of matrices specified in the nuclear technology. His other sphere of activity comprises determination of burn-up of uranium and thorium based reactor fuels and recovery of plutonium from different types of nuclear wastes. He has more than 50 publications in international journals and symposia.*

Dr P.M. Shah *is presently working in the Mass Spectrometry Section of Fuel Chemistry Division, BARC. He has been working in the area of Thermal Ionisation Mass Spectrometry since 1970 and has been involved in determining the isotopic composition and concentrations of various elements using isotope dilution thermal ionisation mass spectrometry. His other research interests include microwave digestion and alpha spectrometry.*

ION SOURCE CHEMISTRY DURING SIMULTANEOUS ANALYSIS OF THORIUM AND URANIUM BY THERMAL IONISATION MASS SPECTROMETRY (TIMS)

S.K. Aggarwal, D. Alamelu, R. Govindan, P.G. Jaison,
P.S. Khodade, A.R. Parab and P.M. Shah
Fuel Chemistry Division
Bhabha Atomic Research Centre

Introduction

Thermal ionisation mass spectrometry (TIMS) is conventionally a single element analysis technique and requires the element to be present in the purest chemical form to achieve the ultimate in terms of precision and accuracy in isotope ratios determination. However, in many practical situations, such a condition cannot be satisfied. For example, when Th is irradiated in a nuclear reactor, ^{233}U is produced along with other isotopes of U viz. ^{232}U, ^{234}U, ^{235}U, ^{236}U and ^{238}U. Inspite of the separation and purification of this U from bulk of Th, there would always be small amounts of Th associated with purified fraction of U. Depending upon the separation efficiency, U/Th amount ratio in the purified U fraction would vary and this would alter the ion source chemistry occurring in the thermal ionisation source of the mass spectrometer compared to when the pure forms of U or Th are analysed by TIMS. Hence, it was of interest to study the ion source chemistry of Th and U during their simultaneous analysis by TIMS. This was also considered interesting for developing a TIMS method for determination of ppm levels of ^{232}U in ^{233}U sample obtained by irradiation of ^{232}Th and also for understanding the behaviour of Th during TIMS analysis. This paper presents the results of the studies carried out for the ion source chemistry of U and Th during their simultaneous mass spectrometric analysis by TIMS.

Experimental

Different synthetic mixtures were prepared by mixing solutions of thorium nitrate and uranyl nitrate (both natural). The samples were loaded onto the sample filament of a high purity double rhenium filament assembly from the dilute HNO_3 medium and were subjected to TIMS analysis.

The temperature (heating current) of the ionisation filament was fixed (about 6A) by monitoring the $^{187}Re^+$ signal and was maintained constant throughout the analysis. The vaporisation filament was heated manually in steps upto about 5A. The various ions monitored at different temperatures of the vaporization (sample) filament were U^+, UO^+, UO_2^+, Th^+, ThO^+ and ThO_2^+ and the corresponding m/z values were 238, 254, 270, 232, 248 and 264, respectively.

Results and Discussion

Figs. 1, 2 and 3 present the results obtained on ion source chemistry of U and Th when present together on the sample filament of a double rhenium filament assembly. It may be noted that the intensity ratios plotted in these Figures are normalized w.r.t. the amount ratio of U/Th in the

mixture. Among the various ions monitored, only U^+, UO^+, ThO^+ were observed to have sufficient intensity and hence these were only used to compare the ion source chemistry.
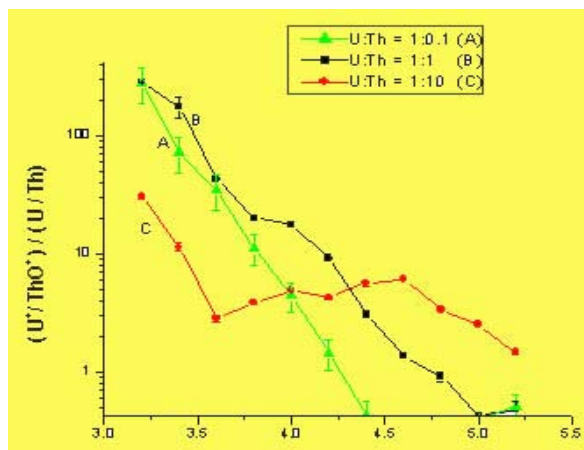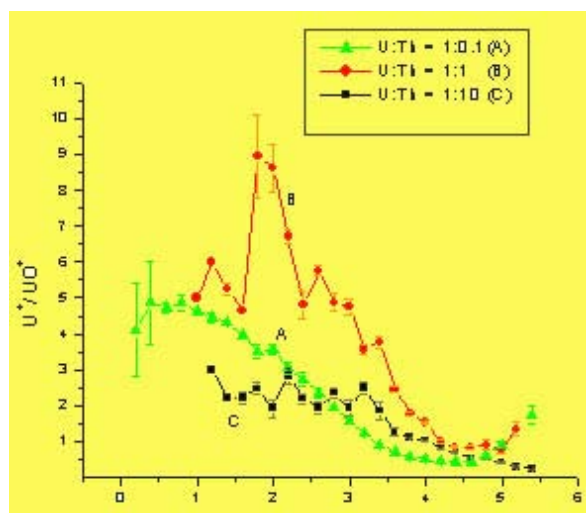

Fig. 1 Vaporisation filament current (Amp.)

Fig. 1 shows the change in U^+/ThO^+ intensity ratio as a function of vaporization filament heating current. It is obvious that the intensity of U^+ ion current is significantly higher than that of ThO^+ in all the synthetic mixtures upto the vaporization filament heating current of about 3.5 A. Further, it is seen that when the amount of Th in the mixture increases, the intensity of U^+ decreases significantly (curve C). This means that in the presence of Th, one will have to load relatively large amount of U on the filament to get sufficient ion current of U^+ for precise and accurate analysis.

Fig. 2 presents the change in UO^+/ThO^+ intensity ratio as a function of vaporization filament heating current. In above cases, there is a decrease in the UO^+/ThO^+ intensity ratio with increasing vaporization filament heating current. Further, it is observed that UO^+ intensity is quite appreciable even at vaporization filament heating current upto about 3.5A. This suggests that the presence of Th along with U on the filament enhances the stability of UO^+ compared to when pure uranium sample is used for TIMS analysis.
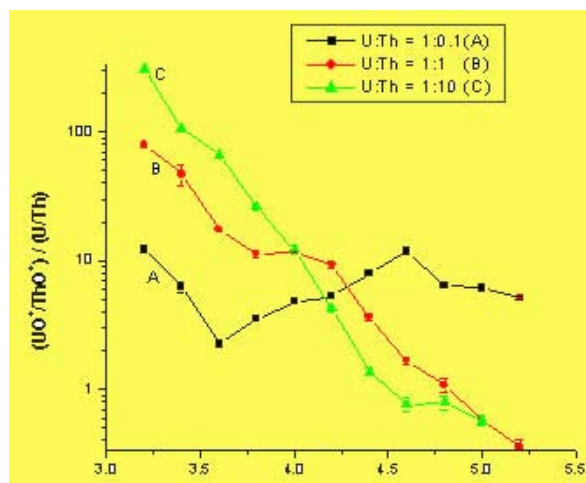
Fig. 2 Vaporisation filament current (Amp.)

Fig. 3   Vaporisation filament current (Amp.)

Fig. 3 shows the U^+/UO^+ intensity ratio as a function of vaporization filament heating current. In all the cases studied, the intensities of U^+ and UO^+ are comparable which again shows that the presence of Th on the filament leads to stabilization of UO^+ ion.

These studies indicate that the presence of large amount of Th (Th/U > 10) on the filament will degrade the precision of U isotopic analysis by monitoring U^+ ions due to their poor yield. Further for Th isotopic analysis, ThO^+ should be preferred to Th^+ ion due to higher intensity of the oxide species. Also during the determination of ^{232}U in ^{233}U by TIMS, it would be interesting

to carry out the analysis using U^+ as well UO^+ ions and this would be helpful to verify the presence/absence of isobaric interference of ^{232}Th at ^{232}U.

Acknowledgements

This paper received the 2nd Prize in the category of "Isotopic Composition and Concentration(ICC-13)" presented during ISMAS Silver Jubilee Symposium on Mass Spectrometry (ISMAS-SJS-2003) held at National Institute of Oceanography, Goa, during January 27-31, 2003

About the authors ...

Dr S.K. Aggarwal *is currently Head, Mass Spectrometry Section of the Fuel Chemistry Division, BARC. He received his B.Sc. (Hons.) from Guru Nanak Dev University, Amritsar, in 1972 with two Gold Medals. He joined the 16th batch of BARC Training School in 1972 and received the Homi Bhabha Award. He did his Ph.D. from Mumbai University in 1980. He is a coauthor of 300 scientific publications, which include 100 articles published in reputed journals. Dr. Aggarwal has participated in several international and national conferences and in different international intercomparison experiments. He is a specialist in the field of atomic mass spectrometry and alpha spectrometry and is interested in various mass spectrometric techniques. His other areas of interest include electrochemistry and solvent extraction. He represents India in the Executive Committee of International Mass Spectrometric Conferences. He has visited several countries in America, Europe and Australia as an expert as well as for delivering lectures. He is a recognized Ph.D. Guide of the Mumbai University.*

Ms D. Alamelu *obtained her M.Sc. Degree in Physics from Annamalai University. After graduating from 38th batch of Training School, BARC, she joined Mass Spectrometry Section of the Fuel Chemistry Division in 1995. Since then, she has been actively involved in the indigenous development of Time of Flight Mass Spectrometer. Her other areas of interest include thermal ionisation mass spectrometry and alpha spectrometry.*

Mr R. Govindan *obtained his M.Sc. in Chemistry from Annamalai University. He joined Mass Spectrometry Section of Fuel Chemistry Division, BARC, during November 2001 after working in Advanced Fuel Fabrication Facility, BARC, Tarapur for a period of 14 years. He is currently working in the field of inorganic Mass Spectrometry for precise isotopic analysis and concentration determination of elements which are important in nuclear technology. He has actively participated in the chemical characterisation of mixed oxide fuel for BWR, Tarapur. His other areas of interest include Potentiometry and Electro-analytical chemistry involving ion selective electrodes.*

Mr P.G. Jaison *joined Fuel Chemistry Division after graduating from 41st batch of BARC Training School in 1998. He has been actively working on the development of HPLC methods for the separation of lanthanide and actinide elements. His other fields of interest are mass spectrometry and microwave assisted digestion.*

Mr P.S. Khodade *is working in Mass Spectrometry Section of the Fuel Chemistry Division, BARC, since 1975 in the field of inorganic Mass Spectrometry and Alpha Spectrometry for precise isotopic analysis and concentration determination of elements which are important in nuclear technology. He is a coauthor of 50 scientific publications in various journals and symposia.*

Mr A.R. Parab *is working in the Mass Spectrometry Section of Fuel Chemistry Division, BARC. His scientific interest is in the area of thermal ionisation Mass Spectrometry for precise isotopic analysis of elements which are important in nuclear technology. He has more than 60 research publications in various journals and symposia.*

Dr P.M. Shah *is presently working in the Mass Spectrometry Section of Fuel Chemistry Division, BARC. He has been working in the area of Thermal Ionisation Mass Spectrometry since 1970 and has been involved in determining the isotopic composition and concentrations of various elements using isotope dilution thermal ionisation mass spectrometry. His other research interests include microwave digestion and alpha spectrometry.*

ROOM TEMPERATURE OPERATING NH₃ GAS SENSOR BASED ON TELLURIUM THIN FILM

Shashwati Sen, K. P. Muthe, Niraj Joshi, S. C. Gadkari, S. K. Gupta, Jagannath and J. V. Yakhmi
Technical Physics and Prototype Engineering Division
Bhabha Atomic Research Centre

M. Roy
Novel Material and Structural Chemistry Division
Bhabha Atomic Research Centre

and

S. K. Deshpande
Inter University Consortium, Mumbai Center, BARC

Abstract

Tellurium thin films were studied for use as ammonia gas sensors operable at room temperature. The films showed a reversible increase in resistance when exposed to ammonia and the response was found to be linear in the range of 0-100 ppm. The interaction of ammonia with tellurium film was investigated using Raman, X-ray photoelectron and impedance spectroscopy techniques. The results of Raman and XPS spectroscopy showed that ammonia reduces tellurium oxide present on the surface and grain boundary region of the film to tellurium. Results of impedance spectroscopy revealed that the change in resistance of the film after exposure to NH₃ is mainly contributed by intragrain region. On interaction with NH₃ the electrons trapped by adsorbed oxygen in the grain boundary are released which decreases in the majority carriers and thus increasing the resistance of the Te film.

Introduction

Ammonia (NH₃) is a toxic gas with threshold limit value of 25 ppm for long-term exposure (8 hrs). Therefore, gas sensors for detecting ammonia (NH₃) are required for environmental monitoring in chemical plants and research laboratories. Semiconductor oxides such as SnO_2 and WO_3 have been reported for detection of NH₃ [1]. The operation of these sensors is based on the reversible change of electrical conductance (resistance) on exposure to NH₃. The main disadvantage of semiconductor oxide sensors is their high operating temperature (350-450ºC) [1,2]. Maintenance of sensor at high temperature increases power consumption, reduces sensor life and complicates the design of the sensor due

to need for integration of heater and temperature sensor with gas sensing film [3]. Thus there is a need for ammonia sensors, which are operable at room temperature and have long operating life.

Recently Tsinlyamu et al. [4,5] have shown sensors operable at room temperature based on tellurium thin films to detect NO_2, CO and $C_3H_7NH_2$. However, no report about the detection of ammonia gas by tellurium films is available in the literature. Further, mechanism of detection of different gases by tellurium films has not been investigated. In the present study, ammonia sensors based on Te film are reported and detection mechanism has been investigated in detail.

Te films were prepared by thermal evaporation. These films were characterized for

microstructure and ammonia sensing properties. The gas sensing mechanism was studied using X-ray photoelectron, Raman and impedance spectroscopy techniques. The results showed that sensitivity of tellurium films reduces with increase of temperature and they have optimum response at room temperature. Detection of NH_3 is seen to take place via interaction of the gas with adsorbed oxygen at grain boundaries. Adsorbed oxygen acts as hole dopant for p-type tellurium and its removal leads to increase in resistance of the film.

Experimental

Tellurium films of ~200 nm thickness were deposited on polycrystalline and single crystal Al_2O_3 substrates by thermal evaporation using Ta boat, at a substrate temperature of 150°C and a background pressure of 10^{-6} mbar. Contacts were made by evaporating indium [4,6] and resistivity measurements were made using two probes.

Response of sensors to NH_3 was measured by mounting them in a housing having a volume of 250 cm^3. A glass ampoule containing known amount of NH_3 (with ±5% accuracy) was broken inside the housing so as to yield the desired concentration of NH_3 in air and resistance of the sensor as a function of time was measured. After steady state was achieved, recovery in response was studied by removing the sensor from housing and exposing it to air. The measurements were carried out at different temperatures to determine optimum operating temperature.

Mechanism of gas detection by tellurium films was investigated using Raman, x-ray photoelectron (XPS) and impedance spectroscopy techniques. Raman spectra of the films before and immediately after exposure to ammonia were recorded in a back scattering geometry with a spectral resolution of 2 cm^{-1}. The 514.5 nm line of an Ar^+ laser, focused to a spot size of ~1 μm (using optical microscope

with 100 X objective) was used for excitation. The Raman scattered light was analyzed using an optically aligned triple monochromator Raman spectrometer (Dilor-XY) equipped with a charge coupled device (CCD) camera for multi channel detection. XPS measurements were performed in a M/s RIBER make XPS system comprising of an Al-K_α (1486.6 eV) x-ray source (Model CX700) and a MAC-2 electron analyzer. The binding energy scale for XPS was calibrated using Au-4$f_{7/2}$ line of 83.95 eV. For charge referencing adventitious C-1s peak set at 285 eV was used. The data was fitted with Gaussian function to find the peak positions. Impedance measurements were carried out in frequency range of 100 Hz to 40 MHz using HP make (model 4192-A) impedance analyzer. The measurements were carried out at room temperature.

Results and Discussion

Gas sensitivity

Resistance of the Te films was seen to increase on exposure to NH_3. The sensitivity of films to ammonia was calculated using the relation:

$$S = (R_g - R_a) \times 100 / R_a$$

where, S is the sensitivity, R_a the resistance of the film in air and R_g the resistance in presence of gas. Typical data on sensitivity of the film as function of ammonia concentration obtained at room temperature is shown in Fig.1. Response of the films was found to be linear in 10-100 ppm range and the film resistance was seen to saturate at higher concentrations. To determine the optimum operating temperature, sensitivity of a film was measured as a function of temperature at a fixed concentration of NH_3 (100 ppm) and the results are shown in figure 2. Optimum sensitivity was found at room temperature and had a value of 150-200% for different films.
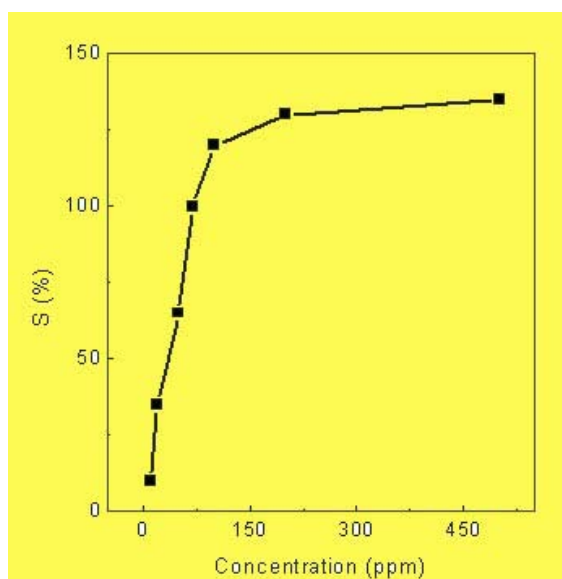
Fig. 1 Sensitivity (S) of tellurium films (measured at room temperature) as a function of ammonia concentration.
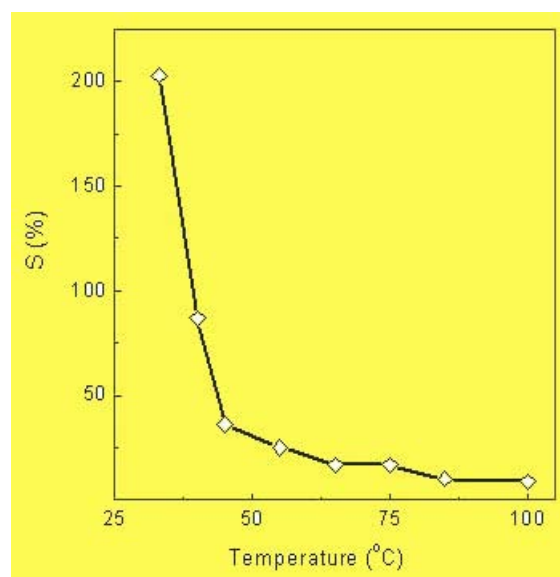

Fig. 2 Sensitivity of Te films measured after exposure to 100 ppm of NH_3 as a function of temperature.

Raman Spectroscopy

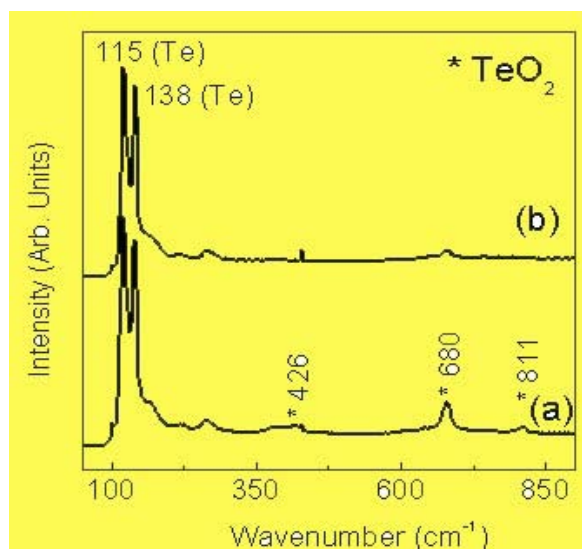Raman spectra of a film recorded before and after exposure to NH_3 gas is shown in figure 3.

Fig. 3 Raman Spectra of (a) as prepared and (b) NH_3 exposed Te film. Peaks marked (*) are due to TeO_2.

The Raman spectra for unexposed film showed peaks at 115 and 138 cm^{-1} corresponding to elemental Te and at 426, 680 and 811 cm^{-1} corresponding to TeO_2 [6]. Spectra of film obtained after exposure to NH_3 showed absence of TeO_2 indicating conversion of tellurium oxide to Tellurium on exposure. No peaks corresponding to nitrogen or nitrogen containing compounds was seen in exposed films (these could be expected due to interaction with NH_3).

XPS studies

XPS spectra were recorded for unexposed and NH_3 exposed Te films. The results obtained for Te-3d and O-1s peaks are shown in Fig. 4. Spectra of as prepared films showed Te-3d$_{5/2}$ peaks at 574.8 eV and 577.8 eV that may be attributed to TeO_2 and TeO_3 respectively [7,8]. This indicates surface (and possibly grain boundary) oxidation of Te films in agreement with results of Raman spectroscopy. No peak corresponding to Te metal was seen for unexposed films. This shows that top surface (few nm) of unexposed film is predominantly covered with TeO_2 and TeO_3 formed by the reaction of atmospheric oxygen and Te. On exposure to ~100 ppm of NH_3 at room temperature, two peaks in Te-3d$_{5/2}$ region were observed at 571.7 eV and 575 eV. These peaks correspond to Te metal and TeO_2 respectively.
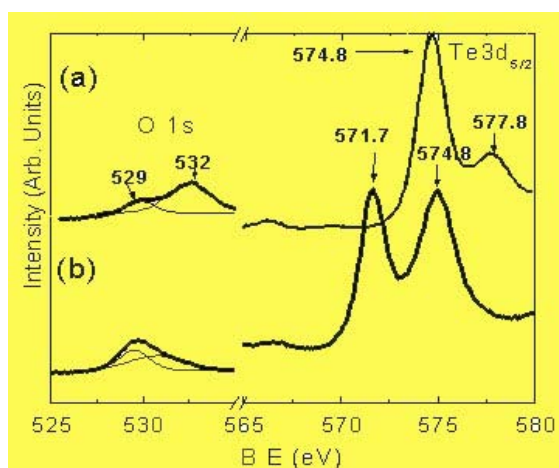
Fig. 4. XPS spectra in O-1s and Te-3d$_{5/2}$ region for (a) unexposed and (b) NH$_3$ exposed Te film

No peak corresponding to TeO$_3$ was seen here. Similarly, O-1s spectrum of an unexposed film was seen to be composed of two peaks at 529 eV (attributed to physically adsorbed oxygen) and 532 eV, which indicates chemisorbed oxygen in the form of TeO$_3$ and TeO$_2$ [7,8]. The intensity of the physisorbed oxygen peak was seen to be less than that of chemisorbed oxygen. On exposure to NH$_3$, the relative intensity of two peaks was seen to change with physisorbed oxygen peak having higher intensity, indicating reduction of tellurium oxides. A small amount of adsorbed oxygen in this case could arise while transferring the sample to analysis chamber after exposure to ammonia. Results show that NH$_3$ reacts with the oxygen present on the surface of the film and reduces Tellurium oxide to Tellurium metal as also seen by Raman spectroscopy. As observed in Raman spectroscopy, XPS data also did not indicate the formation of any new compound containing nitrogen.

Impedance spectroscopy studies

Impedance measurements were performed on a Te film before and after exposure to NH$_3$. The results are shown in fig. 5 in the form of cole-cole plot. The impedance spectra were analyzed using equivalent circuit shown in fig 6 [9]. Here R$_0$ is dc resistance, which is independent of

frequency and is attributed to the bulk and surface contributions to the total resistance. R$_b$ and C$_b$ are resistance and capacitance of intra-grain region while R$_g$ and C$_g$ are resistance and capacitance of grain boundary region. Curves obtained by fitting of experimental data to the equivalent circuit are also shown in Fig. 5. A good agreement of the data with theoretical curve is observed. Values of various parameters of the equivalent circuit obtained by curve fitting are given in table-1. It is seen that on exposure to ammonia the bulk resistance R$_b$ of the film increases more then three times while the grain boundary resistance R$_g$ doubles indicating that both grain boundary and intragrain regions contribute to gas sensitivity.
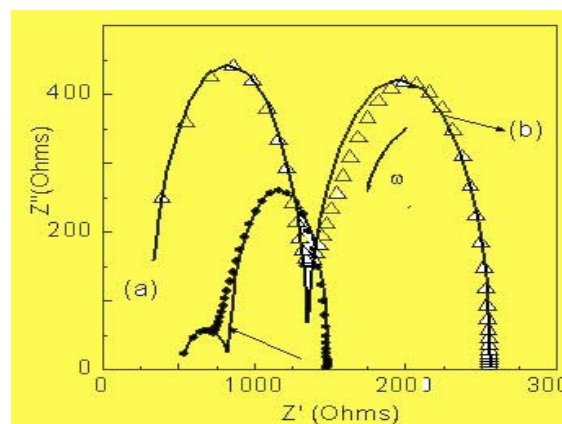
Fig. 5 Impedance spectra of Tellurium film before (solid circle) and after (open triangle) exposure to NH$_3$. Curves (a) and (b) have been obtained by fitting of the data to equivalent circuit of Fig. 6.
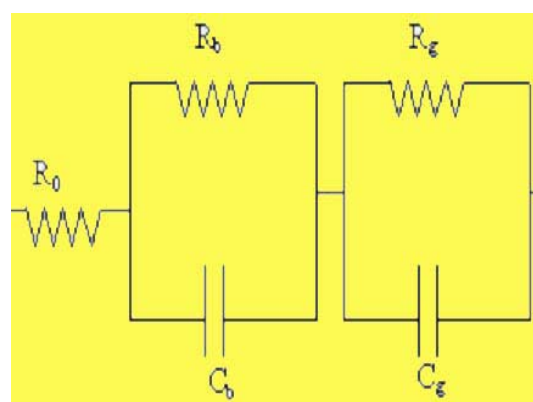

Fig. 6 Equivalent circuit used to interpret the impedance spectroscopy data obtained for polycrystalline Te films.

Table 1 : **Parameters obtained by fitting experimental curve of impedance spectroscopy to equivalent circuit**

	R_0	R_b	C_b	R_g	C_g
Unexposed	525 Ω	307Ω	3.6 pF	659Ω	6.4 nF
Exposed to 100 ppm NH_3	300Ω	1053Ω	8.21 pF	1209Ω	2.4 nF

We have semiconducting Te (p-type) grains separated by intergrain region having significant fraction of TeO_2, adsorbed oxygen and defects. Adsorbed oxygen atoms trap electrons and thereby act as acceptors increasing the hole density in the grain boundary and intragrain regions. Increase in hole density in the intragrain region is more significant near the interface. This increases the conductivity in both regions. The removal of adsorbed oxygen (acceptors) by ammonia leads to decrease in the majority carrier density and thus increasing the resistivity of the film.

Conclusions

Properties of Te thin films for ammonia gas sensing were investigated. The films were found to be sensitive to ammonia with optimum response observed at room temperature. Response of films to ammonia was seen to arise from reduction of Tellurium oxides present on the surface and intergrain regions of the film to tellurium metal on interaction with ammonia. Adsorbed oxygen atoms trap electrons and thereby act as acceptors, increasing hole density and conductivity. On removal of adsorbed oxygen, hole density and conductivity are reduced. Due to simplicity of fabrication and room temperature operation, tellurium metal film based gas sensors are promising for various applications.

References

1. G. Sberveglieri, L. Depero, S. Groppelli, P. Nelli, Sensors and Actuators B 26-27, 89 (1995) .
2. B. T. Marquis, J. F. Vetelino, Sensors and Actuators B 77, 100 (2001).
3. C. L. Johnson, J. W. Schwank, K. D. Wise, Sensors and Actuators B 20, 55 (1994).
4. D. Tsiulyanu, S. Marian, V. Miron, H. D. Liess, Sensors and Actuators B 73, 35 (2001).
5. D. Tsiulyanu, S. Marian, H. D. Liess, Sensors and Actuatore B 85, 232 (2002).
6. J. C. Chambarnaud-Mesjard, S. Blanchandin, P. Thomas, A. Mirgorodsky, T. Merle-Mejean, B. Frit, J. Phys. Chem of solids 61, 501 (2000).
7. C.D. Wagner, W.M. Riggs, L.E. Davis, J.F. Moulder, J.E. Millenberg, *Handbook of the X-ray Photoelectron Spectroscopy* (Perkin-Elmer Corporation, Eden Draivie, MN, 1979).
8. D. Briggs and M.P. Seah, *Practical Surface Analysis by Auger and X-ray Photoelectron Spectroscopy* (John Wiley, New York, 1983).
9. J. R. Macdonald, *Impedance Spectroscopy* (Wiley, New York, 1987).

This paper received the "Shri C. Ambasankaran Best Paper Award" at National Symposium on "Vacuum Science and Technology and Vacuum Metallurgy – IVSNS 2003" organised by Indian Vacuum Society in collaboration with BARC during October 15-17, 2003

About the authors ...

Dr Shashwati Sen joined TPPED through 40th batch of Training School. She obtained Ph.D. degree from University of Mumbai for her work on "Dissipation mechanisms in high temperature super-conductors". Currently, she is working on gas sensors based on elemental and metal oxide semiconductor thin films.

Mr K.P. Muthe has been working in the field of thin film growth and characterization for the last 17 years. He has studied the growth behavior of HTSC films using MBE. The reference value of this work has fetched him a place in Marquis' "Who's Who of the World (1997)". His current interests include development of Toxic gas sensors for Heavy Water Plants and, synthesis of advanced radiation sensors for Personal Dosimetry.

Mr Niraj Joshi joined TPPED as Ph.D. Research Fellow under BARC-Mumbai University collaboration program. He is carrying out his Ph.D. work on "Growth, characterization and studies of thin films of metal and metal oxides".

Dr Sanjay C. Gadkari joined BARC through 24th batch of Training School. At present, he is Head of Synchrotron & Surface Analytical Instrumentation Section in TP&PED. He has been working on the development of technology for material synthesis, single crystals; thin/thick films based gas sensors and electronic instruments. Areas of his current interest include development of beamlines on synchrotron radiation sources INDUS-I and INDUS-II at CAT, Indore, and development of ultra high vacuum based analytical instruments. He is a member of the National Academy of Sciences, Institute of Smart Structures & Systems, and Indian Vacuum Society.

Dr S.K. Gupta joined BARC in 1975 and is presently Head of Thin Films Devices Section in TPPED. Over the years, he has worked on space quality silicon solar cells,

high temperature superconductor thin films and single crystals, gas sensors and thermoelectric materials. He is a member of the National Academy of Sciences, India.

Mr Jagannath received his M.Sc. degree in Physics from University of Gorakhpur and M.Tech. in Applied Optics from IIT Delhi. He joined Technical Physics and Prototype Engineering Division in 1997 through 6th batch of OCPGE. He has been working in the development of Angle Resolved Photoelectron Spectrometer for Indus-1 and Photoelectron Spectroscopy Beamline for Indus-2. His other areas of interest include XPS and Auger studies, beamline instrumentation and control software.

Dr J.V. Yakhmi, Head, Technical Physics and Prototype Engineering Division, BARC, has worked in BARC for the past 37 years on diverse areas of research in materials science, such as high Tc systems, magnetic alloys, molecular materials, etc. His contributions to the field of molecular electronics and bio-sensors are internationally recognized.

Mr M. Roy joined Novel Materials & Structural Chemistry Division, BARC, in 1999 after completing his M.Sc. (Chemistry) from the Burdwan University and graduating from the 42nd batch of the BARC Training School. His research interests include thin films of diamond and diamond-like materials and their spectroscopic characterization.

Dr S.K. Deshpande obtained Ph.D in Physics from University of Pune in 1994 and worked at the Institute for Plasma Research, Gandhinagar, on Tokamak plasma spectroscopic diagnostics. Later, he was a Lecturer at the Department of Physics, University of Pune. Currently, he is working as Scientist at the Mumbai Centre of Inter University Consortium for DAE Facilities (IUC-DAEF). His activities include research and developmental work in neutron and X-ray diffraction, and dielectric studies.

IN-SITU CHELATION AND EXTRACTION OF HEAVY METAL OXIDES USING MODIFIED SUPERCRITICAL CARBON DIOXIDE

Tessy Vincent and P.K. Wattal
Nuclear Recycle Group
Bhabha Atomic Research Centre

and

Mamata Mukhopadhay
Department of Chemical Engineering, IIT Bombay

A b s t r a c t

Conventional processes used in nuclear facilities, engaged in the extraction of heavy metals, generate considerable quantity of radioactive liquid wastes that requires further treatment. Use of SFE significantly reduces the waste volumes. It, additionally, avoids the dissolution step prior to extraction. A method of extracting metals directly from metal oxides by exposing the oxide to a SC solvent containing a chelating agent is described. Cerium oxide has been considered as a candidate material to carry out feasibility studies along with TTA as the chelating agent for extraction. Solubility of Ce $(TTA)_3$-chelate has been investigated in the pressure range of 150-350 bar at 40^0C. A linear relationship between the solubility and SC CO_2 density is observed. TG-DTA and IR spectra of the chelate and TTA are discussed. Feasibility of in-situ conversion of cerium oxide to Ce $(TTA)_3$-chelate in SC CO_2 with TTA and water followed by its recovery by SC CO_2 extraction has been experimentally demonstrated. Both static as well as dynamic extraction studies were performed at 350 bar and $50^0 C$ in a stainless steel extractor of 500 ml capacity without the use of nitric acid. The samples collected in n-dodecane were analysed for Ce by ICP-AES. ESR as well as IR spectra of the chelate collected during dynamic extraction are discussed. X-ray powder pattern of both Cerium oxide fed to the extractor and the residue after the extraction have been brought out. This study illustrates the potential of SC CO_2 modified with organic ligands to process heavy metals directly from irradiated spent fuel.

Introduction

Uranium and plutonium are recovered from irradiated nuclear fuel through the widely practiced Purex process [1]. Fuel cladding encasing the fuel is removed either chemically or mechanically and the fuel is dissolved in nitric acid. Pu and U are co-extracted using TBP/n-dodecane leaving the fission products in the raffinate stream. The loaded organic is contacted with the reductant to separate Pu from U. Finally U is stripped into dilute nitric acid solution from TBP. Additional extraction strip cycles are performed with the separated uranium and plutonium streams in order to complete the purification from fission products. Spent fuel reprocessing flow diagram is given in Fig. 1.

The Purex process generates considerable volumes of several kinds of nuclear wastes which require different treatment steps before the liquid wastes could be released to the environment safely. The use of SFE in place of Purex would significantly reduce the reprocessing cost by improving the waste management and process simplification [2].

The unique ability to fine tune the solvent properties by adjusting its temperature and pressure and the excellent transport properties makes SCF a favourable solvent for extraction. Since CO_2 is inert, odourless, tasteless,
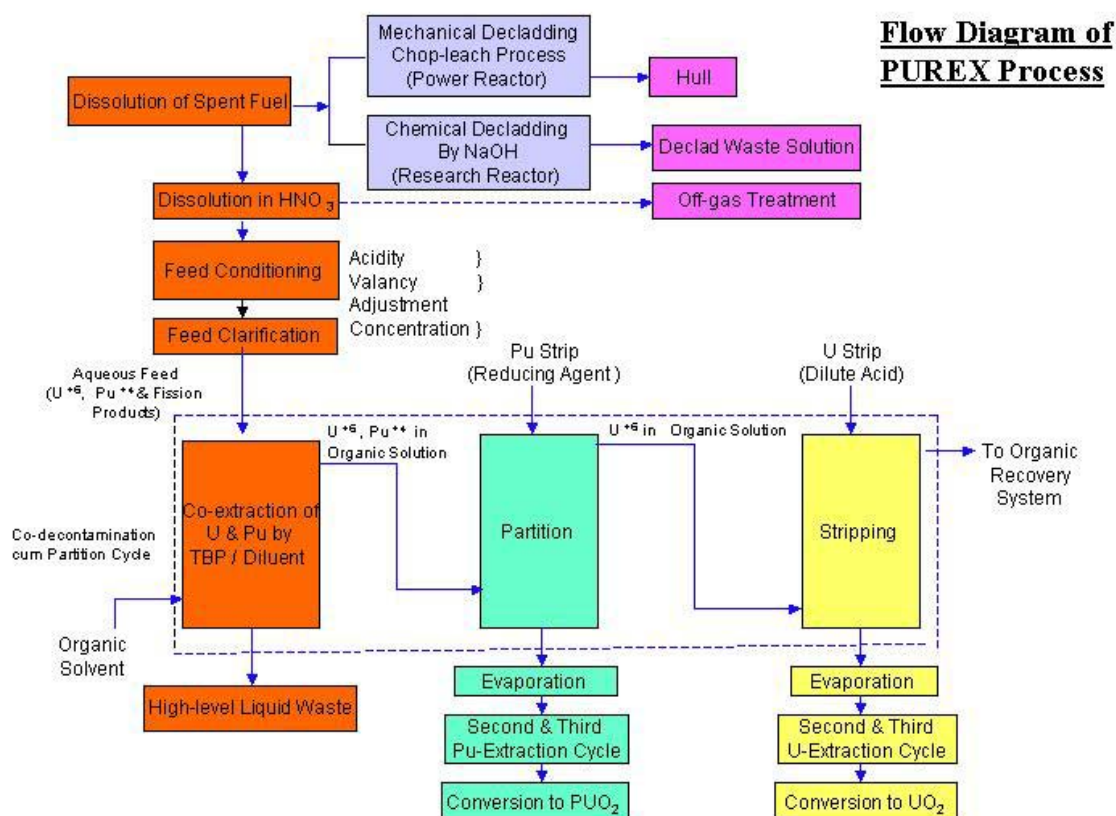
Fig. 1 Block diagram of purex process

environment–friendly, inexpensive and is easily available, it has been regarded as a safe and viable SCF solvent. Further, radiation stability of SC CO_2 is high. Since solubility of metal oxides in SC CO_2 is poor, it needs to be associated with organic ligands in order to enhance the capacity of SC CO_2 for metal extraction. It has been reported that β-diketones, can be used as the chelating agents for the extraction of f-block elements using SCF[3].

The objective of the work is to explore the potential of SC CO_2 for the extraction of valuable heavy metal ions from the spent fuel without dissolution step For the present study TTA which is a solid at atmospheric conditions has been selected as the chelating agent. Use of TTA leads to better safety control, absence of phosphorous aerosols and lesser corrosion as compared to HNO_3/TBPsystem. Since the chemistry of Pu and Ce is similar and yield of

Ce is also high compared to other lanthanides in the spent nuclear fuel, Ce was selected as candidate metal.

Experimental

Solubility studies

SFE depends on number of factors including i) stability and solubility of ligand, ii) solubility of the metal–chelate iii) water and pH iv) temperature and pressure v) chemical form of the metal species and vi) matrix. Since the solubility of the metal–chelate provides the limit of extractability, solubility studies were performed prior to extraction studies.

For experimental measurements of the neat solubility in SC CO_2, TTA (99.0% purity, Aldrich make) and Ce $(NO_3)_3.6H_2O$ (99.9% purity, M/s. Indian Rare Earths) were used. Ce $(TTA)_3$-chelate was prepared by dissolving TTA

in acetone followed by addition of required quantity of cerium nitrate. Upon evaporation, the solution was made into solid Ce (TTA)$_3$-chelate.

The chelate was subjected to DTA/TG in nitrogen atmosphere at a heating rate of 2^0C/min from room temperature to 200^0C and is given in Fig. 2. Thermographs show that the chelate starts melting at 48^0C and then volatilizing. The chelate was found to be stable till 118^0C without any decomposition as seen from DSC curve shown in Fig. 3.

Fig. 4: TG-DTA of chelating agent TTA

Fig. 2: TG-DTA of prepared Ce-TTA   chelate
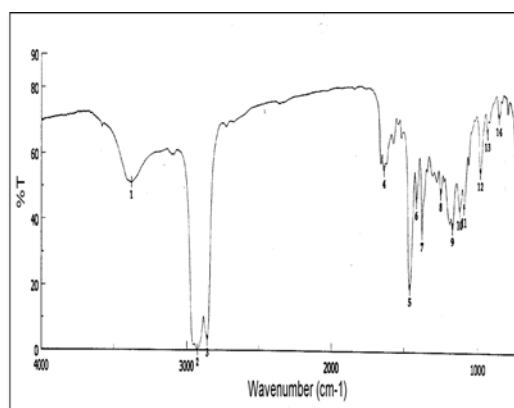
Fig. 5 : IR Spectra of prepared chelate

*Fig. 3: DSC Analysis of prepared Ce- TTA
chelate*

IR spectra of TTA as well as prepared chelate are represented in Fig. 5 and Fig. 6 respectively.
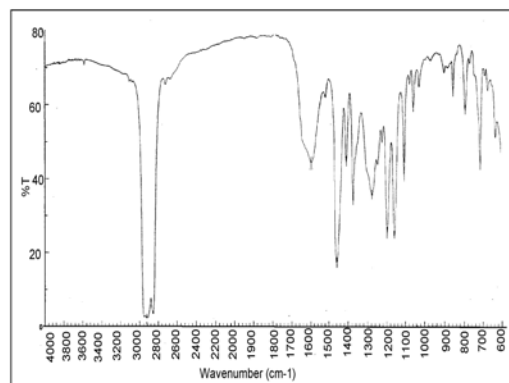
Fig. 6 : IR Spectra of TTA

The spectra indicate the presence of free TTA and water in the prepared chelate.

A schematic diagram of the experimental setup is given in Fig. 7. The internal capacity of the stainless steel extractor was 500 ml. Before starting the studies, each part of the system was
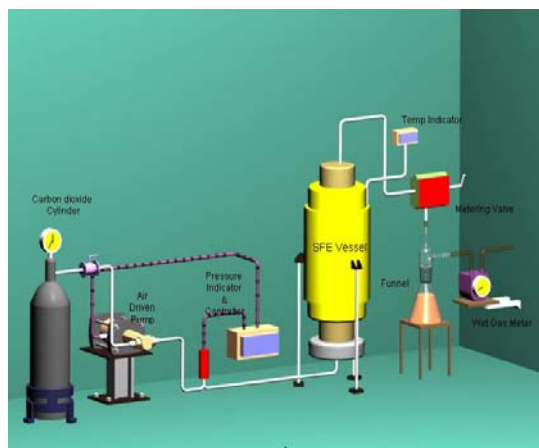
Fig. 7: Schematic of experimental set up

cleaned with acetone and lines were flushed with liquid CO_2. About 40g of the prepared chelate was charged into the extractor and the remaining portion was packed with glass beads. Stainless steel filters were used to prevent any carryover of the solute. Set point of the pressure was kept at 180bar. After closing the metering valve completely, the chelate in the cell was pressurized to the liquid CO_2 pressure. When the pressure indicated was 58.5 bar, corresponding to the CO_2 cylinder pressure, air driven pump was put on to reach the pressure to the set value. The pressure was maintained within ± 20bar through an on/off control system. Skin temperature was maintained around 44-45°C and was monitored with temperature indicator. The whole system was kept under static conditions for 2 hrs. In order to prevent plugging, the restrictor was warmed electrically. Then the metering valve was opened slowly to release 1/3rd volume of the extractor. The chelate was collected in dodecane. Solubility studies were also conducted for 250 & 350 bar at 40^{0}C in the same manner. After that the whole system was depressurized from 350bar to atom-spheric condition.

The samples collected in n- doecane were analysed for Ce by ICP-AES. The solubility data is given in Table 1.

Table 1: Solubility of Ce (TTA)$_3$ - chelate in supercritical CO_2 at 40°C

Pressure (bar)	Solubility of Ce (TTA)$_3$ - chelate (ppm)
180	57
250	69
350	79

Solubility data has been plotted against sc-CO_2 density. A linear relationship is observed in Fig. 8.
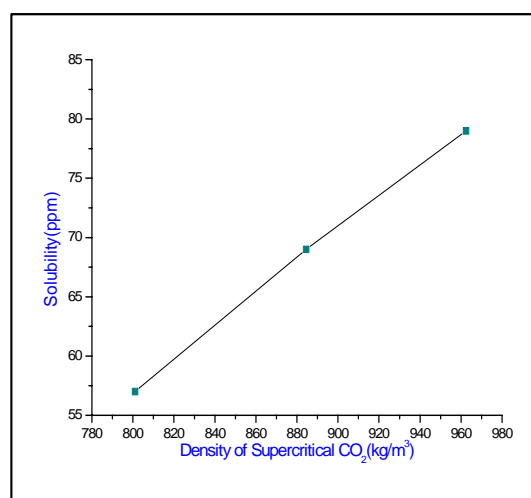
Fig. 8: Chelate solubility v/s SC CO_2 density

Extraction Studies

The same experimental set up given in Fig. 7 was used. Bottom portion of the extractor was packed with glass beads. CeO_2, TTA and distilled water were made into paste and added to the extraction vessel. Based on the solubility studies, pressure and temperature conditions for the extraction studies were chosen as 350 bar and 50°C. The entire system was kept in static condition for 45 minutes to reach equilibrium at 350bar and 50^{0}C. Dynamic extraction was achieved by slowly opening the metering valve and continued for 1 ½ hours by maintaining the same temperature and pressure values with average CO_2 flow rate of 6.35lpm. Flow rate was controlled manually to achieve smooth flow of

the chelate. The chelate was collected in dodecane through a restrictor. After that the whole system was depressurized from 350 bar to atmospheric conditions. The collected chelate in dodecane was analysed for cerium by ICP-AES and results are given in Table 2.

Table 2: Recovery of cerium from cerium oxide (350 bar, 50^0C)

CeO_2 (g)	TTA (g)	Water added (ml)	% extraction
1	10	10	1.25

%extraction =

$$\frac{\text{concn. of metal in SC phase}}{\text{concn. of metal in feed before extraction}}$$

Results and Discussion

From the results of the solubility studies, it is noted that Ce $(TTA)_3$-chelate is quite soluble in SC CO_2. Since the percentage extraction obtained is low and the solubility observed is quite high, it is inferred that the kinetics of chelation is the rate controlling step rather than the mass transfer. IR spectra of the chelate collected during dynamic extraction is represented by Fig. 9. It confirms the presence of water molecules which can be replaced by neutral ligands to enhance the solubility. To confirm the valency state of Ce, ESR spectrometry was done. It can be seen from Fig. 10 that peak exists in the ESR spectra taken at low temperature.
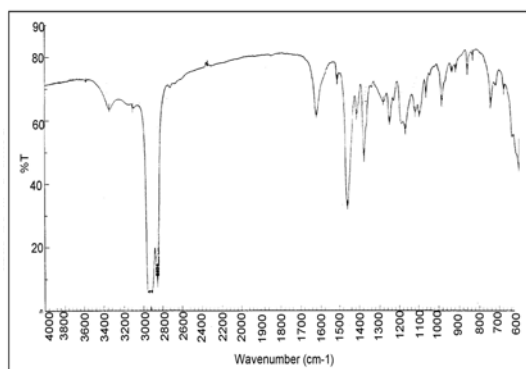
Fig. 9: IR spectra of collected chelate
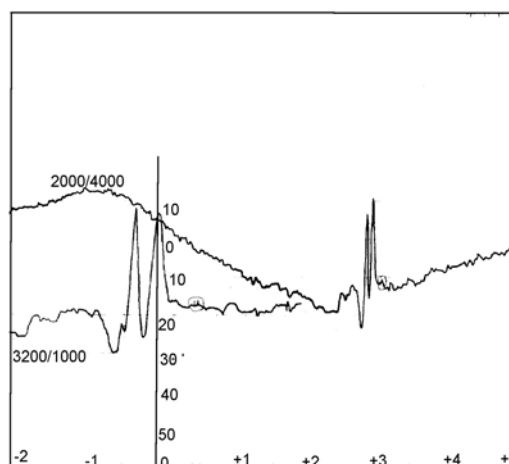
Fig. 10: ESR spectra of Cerium in Ce-TTA chelate collected in methanol taken at liquid nitrogen temperature
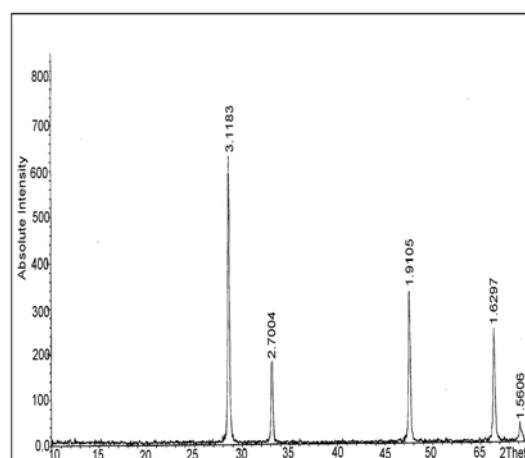

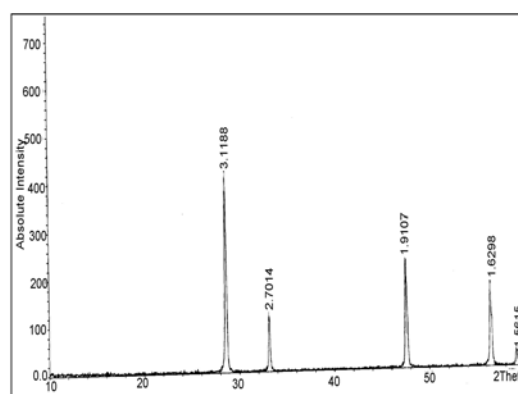Fig. 11: X-ray powder pattern of CeO_2 residue

Fig. 12: X-ray powder pattern of Ce O_2 fed to the extractor

This ensures that the Ce remains in +3 state in the supercritical phase. The material left in the extractor was washed with dodecane and the X-ray powder pattern of the residue is represented by Fig. 11. It matches with that of CeO_2 fed to the extractor as shown in Fig. 12. Since there is no variation in the line intensities, it indicates that unconverted CeO_2 has not undergone any structural changes even after 2 hours of extraction process.

Conclusion

1. A mixed ligand approach can be tried to increase the percentage extraction since the chelate collected during dynamic extraction contains water molecules.
2. As the kinetics is controlling, parametric studies have been planned to investigate the effects of the temperature, pressure, residence time for chelation and relative ratios of CeO_2-TTA-H_2O.
3. It can be concluded from this study that SC CO_2 modified with TTA and water has the capacity for recovering Ce directly from oxides.

References

1. Glasstone S. and Sesonske A., Nuclear Reactor Engineering, CBS Publishers, New Delhi (1986).
2. Shimda T. et al., *Super Green 1st International Symposium on Supercritical Fluid Technology for Energy and Environment Applications* (2002).
3. Wai, C.M., *Anl. Chem.*, 66 (13), 1971 (1994).

Nomenclature

Ce	Cerium
DSC	Differential Scanning Calorimeter
ESR	Electron Spin Resonance
HNO_3	Nitric acid
IR	Infra Red
Pu	Plutonium
Purex	Plutonium uranium extraction
SC CO_2	Supercritical Carbon dioxide
SCF	Supercritical Fluid
SFE	Supercritical Fluid Extraction
TBP	Tributyl Phosphate
TG-DTA	Thermo-Gravimetry & Differential Thermal Analysis
TTA	Thenoyl Trifluoro Acetone
U	Uranium

This paper has been adjudged as the Best Presentation paper in Indian Chemical Engineering Congress-2003 (CHEMCON-2003) at Regional Research Laboratory, Bhubaneswar, Orissa, during December 19-22, 2003

About the authors ...

Ms Tessy Vincent is from 35th batch of BARC Training School and is presently working in Back-End Technology Development Division of Nuclear Recycle Group, BARC. She did her post graduation in Chemical Engineering from Bharathiar University, Coimbatore. She is currently working on application oriented process and equipment development for fuel reprocessing plants. Additionally, she is perusing her Ph.D. programme in supercritical fluid extraction with specific reference to nuclear fuel reprocessing and waste management.

Prof. Mamata Mukhopadhyay is a professor in Chemical Engineering Department of Indian Institute of Technology, Bombay. She holds a Ph.D. from Ohio State University, U.S.A. and has been a Visiting Professor to a number of Universities in U.S.A. in the area of Supercritical Fluid Technology. She is a recipient of many awards including prestigious Suman Sharma Design award by Institute of Engineers (India); Dr P.K. Patwardhan award for Technology Development & Transfer, etc. She has authored a number of books notably on Natural Extracts using Supercritical Carbon Dioxide, Phase Equilibrium in Solid Supercritical Fluid Systems, etc.

LASER CLADDING OF NICKEL BASED HARDFACING MATERIALS AS AN ALTERNATIVE OF STELLITE

G. L. Goswami and Santosh Kumar
Laser Processing & Advanced Welding Section
Bhabha Atomic Research Centre

and

R. Galun and B. L. Mordike
Institut fur Wekstoffkunde and Werkstofftechnik
Technical University of Clausthal, Germany

Abstract

Stellites, the cobalt based alloys, are most common hardfacing materials used to enhance wear resistance of a relatively softer material like mild steel. Unfortunately cobalt and boron are not preferable in nuclear industry. Therefore there is a need to develop hardfacing materials free of cobalt and boron. This work is aimed at exploring the possibility of producing nickel-based claddings for hardfacing applications as an alternative of stellite by blown powder laser cladding process

Cladding of three nickel based materials, one metallic system (Ni-15Cr-32Mo) and two composite systems ((Ni-20Cr)-40Cr$_2$C$_3$ and (Ni-20Cr)-40WC) has been done on mild steel plate by blown powder laser cladding process. The process parameters were optimized to obtain defect free claddings. The cladded samples were characterized by visual examination, optical microscopy and microhardness measurements. Wear testing of these claddings was done by the pin on disc method against 600-grit size abrasive paper. The results were compared with those of stellite-6 claddings produced on same substrate by same method. The Ni-15Cr-32Mo claddings showed better hardness and wear resistance while (Ni-20Cr)-40Cr$_2$C$_3$ / WC claddings showed lower hardness but still much better wear resistance as compared to stellite-6 claddings. Therefore, nickel-based claddings process appear as promising alternative of stellite-6 claddings for hardfacing applications.

Introduction

Cladding of a hard material onto relatively softer materials for enhancing its wear resistance is a common industrial practice. Most commonly, the alloys of the stellite family (Co-Cr-W/Mo-C) are used as hardfacing material [1] and their application as hardfacing material is well established. Borides are also being developed as hardfacing material [2]. In many other cases, boron is added in the hard facing alloys to enhance self-fluxing characteristic. But unfortunately, these materials (i. e. Co and B) are not preferred in nuclear industry.

Cobalt, the matrix material of stellite family of alloys becomes radioactive (Co^{60}) by (n,γ) reaction in radioactive environment. This is hard γ-emitter, therefore a component hardfaced with stellite family of alloys will become radioactive source after service in radioactive environment, and its further handling, repair and decommissioning will cause extra dose of radiation to the personnel. In fact Co^{60} is the largest contributor to occupational radiation

exposure of plant maintenance personnel [3]. Boron has high absorption cross-section σ_a) for thermal neutrons and therefore a component hardfaced with borides will act as neutron sink. Due to these reasons, Co or B based hardfacing material is not preferred in the nuclear industry and there is sustained effort to develop Co and B free hardfacing material. Also because of high and highly varying price of cobalt [3], there is incentive to use hardfacing materials based on less costly materials like iron and nickel in other industries as well.

The current approach is to replace Co-matrix with Ni-matrix and design alloy chemistry together with a processing route that will yield a hard and wear resistant microstructure. Iron based systems e.g. Iron - Manganese and Iron - Chromium based alloys are also being developed [4,5]. Uniform dispersion of hard and fine particles in a ductile matrix results in considerable improvement in wear resistance [6]. Such a composite microstructure combines advantages of both the hard but brittle ceramic particles and the soft but ductile metallic matrix. This microstructure if produced onto a surface layer of a component enhances wear life of that component. Hard particles can be ceramic particles like carbides, borides, nitrides etc. and the ductile matrix can be a ductile metallic system like nickel alloy.

Laser cladding is a process in which a directed high power laser beam is used to melt the cladding material and very thin layer of the substrate, which then solidifies together as shown in Fig. 1. The cladding material can be either in the form of a pre placed coating or it can be in the form of powder, which is blown to the spot where the laser beam is directed. The laser cladding process with the blown cladding powder (Fig. 1) is preferred, because it is fast (as the pre placing of powder is done away). In laser cladding process due to directed and localised heat input thermal distortion of the substrate, thermal damage of the substrate microstructure and dilution of the clad layer by the substrate

material is negligible. In this blown powder laser cladding process, one can optimise the laser energy density, powder feed rate, speed of the substrate (as the substrate is mounted on a CNC) and the laser beam scan rate to ensure that minimum substrate layer is melted. Thus the sound interfacial bond can be obtained with minimum dilution of the clad layer.
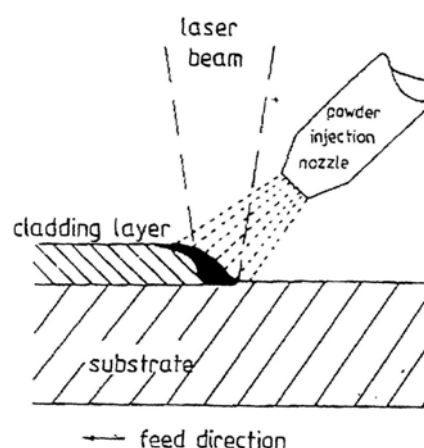

Fig 1: Schematic diagram of laser cladding by blown powder technique

In these experiments three compositions of nickel-based system were explored for hardfacing purpose by blown powder laser cladding process. Three compositions - one metallic (Ni-15Cr-32Mo) and two composites ((Ni-20Cr)-40Cr_2C_3 and (Ni-20Cr)-40WC) were cladded onto 10 mm plate of 0.15%C-steel plate by blown powder laser cladding process. Stellite - 6 was also cladded on same substrate by same process for comparison. Process parameters were optimised to obtain a defect - free cladding. The cladded samples were characterised by visual examination, optical microscopy and microhardness measurements and pin on disc wear testing. The Ni-15Cr-32Mo claddings show comparable hardness and wear resistance with stellite - 6 claddings. In case of composite claddings the Ni-12Cr-40Cr_2C_3 claddings show comparable hardness and much better wear resistance than that of stellite-6 claddings. The

(Ni-20Cr)-40WC claddings need further process parameter optimisation to produce a defect free cladding. In these experiments the (Ni-20Cr)-40WC claddings have shown 25% lower hardness but much better wear resistance when compared with the stellite-6 cladding.

Experimental

Laser cladding of the metallic hardfacing alloy (Ni-15Cr-32Mo) powder and the composite powder mix of nickel - chromium alloy powder and chromium / tungsten carbide powder was performed using Roffin_Sinar continuous wave CO_2 laser (fig. 2) with 10 kW maximum power as heat source. Exact composition and particle size of the cladding powders and other experimental details are described elsewhere [7,8].
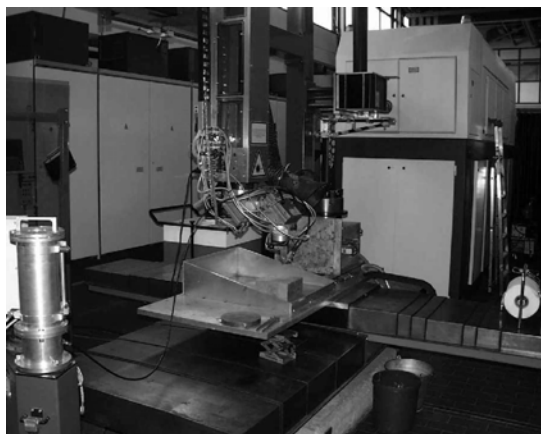
Fig. 2: The set up used for cladding

The laser cladded samples were prepared for metallographic examination. These samples were examined at lower magnification cladding defects and at higher magnification for microstructural characterization. Microhardness measurements across the substrate – clad interface, at varying distance from the interface, were performed using Vickers indenter on as polished cross-section. For metallic cladding 50 gf and for composite claddings 500 gf loads were used. This difference of the load used was on account of difference in the scale of homogeneity of microstructure of the metallic

and the composite cladding. Wear samples (pins of 4 mm diameter) were made of the cladded samples for comparative study of wear resistance of the four clad layers. Wear test wascarried by the pin on disc method. Dry wear resistance of the four clad layers was measured against 600-grit size polishing paper at 1.5kg load and various relative speeds.

Results & Discussion

Cladding operation was smooth for stellite-6 powder and also for Ni-15Cr-32Mo powder and all the samples appeared good under visual examination. But the story was not so simple with composite hardfacing materials. Burning of carbide was observed during cladding of (Ni-20Cr)-40WC mix and this led to choking of powder feeding nozzle and blackening of the clad layer. In such cases porosity were also observed in the clad layer. Similarly, during cladding of (Ni-20Cr)-40Cr$_2$C$_3$ sparks were observed due to oxidation of chromium. These problems were more pronounced at higher feed rate and higher laser power. Therefore, powder feed rate and laser power and correspondingly substrate speed was reduced and defect free cladding was produced. Figures 3 through 5 show claddings free of defects and also those with cracks and porosity.
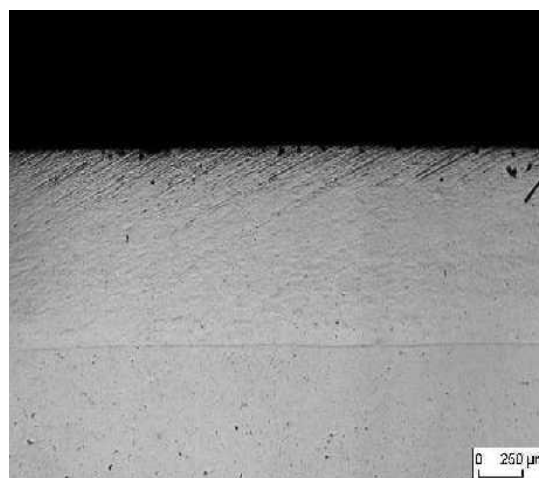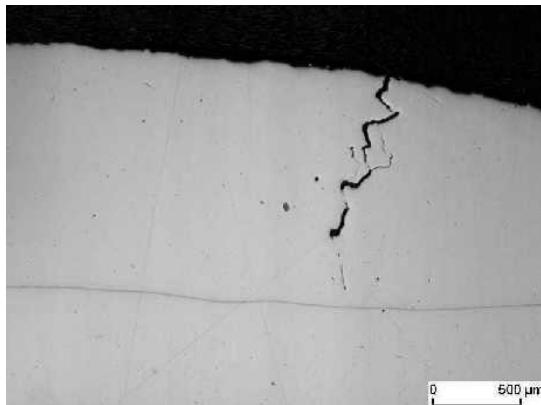

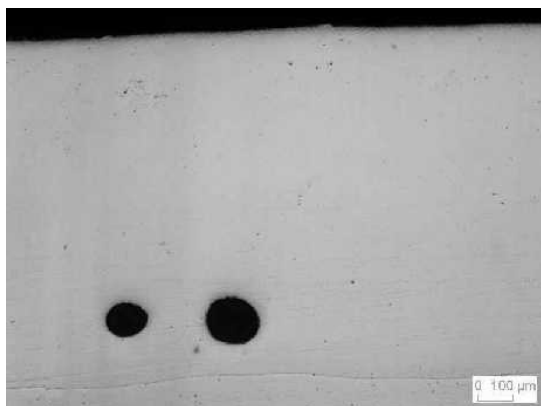*Fig. 3: Defect-free cladding*

Fig. 4: Crack in the clad layer

Fig. 5: Porosity in the clad layer

The microstructure of Ni-15Cr-32Mo clad layer is very fine (Fig. 6). This microstructure can be grossly divided into three zones from the substrate side towards the surface of the clad layer. Near substrate side is very fine-grained structure followed by relatively coarser dendritic structure and finally near the surface of the clad layer again the microstructure is fine grained.
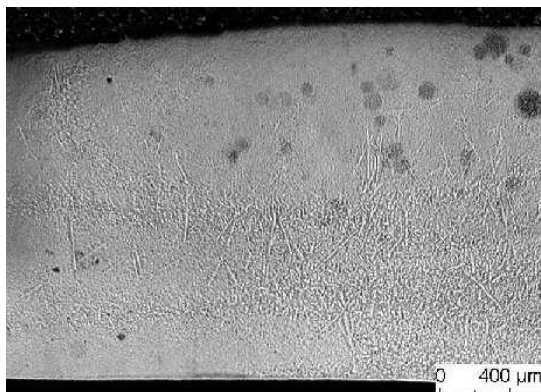

Fig. 6: Microstructure of Ni-15Cr-32Mo cladding

Near surface region dark circular features can also be noticed. Upon closer examination it is flower like structure and this region shows increased hardness (~ 770 $HVN_{0.05}$) compared to the surrounding region (~ 680 $HVN_{0.05}$). This must be some intermetallic cluster.
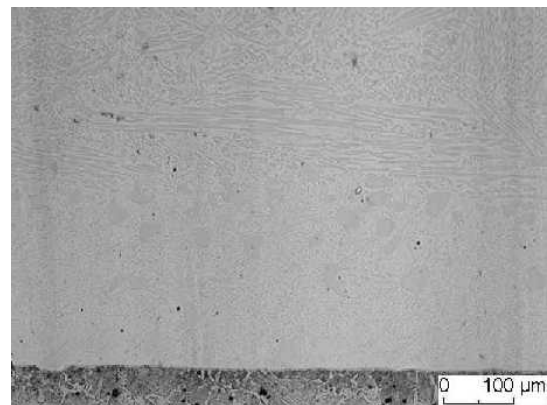

Fig. 7: Microstructure of (Ni-20Cr)-40Cr$_2$C$_3$ cladding

Microstructure of the (Ni-20Cr)-40Cr$_2$C$_3$ clad layer (Fig. 7) can be grossly divided in two zones from the substrate side towards surface of the clad layer. Approximately 300 μm wide zone near the substrate consists of bulky carbides in metallic matrix. Upon closer examination these appear to be the original unmelted carbide particles. In this region volume fraction of reprecipitated carbides is very less. Beyond this zone towards the surface side we have acicular carbides uniformly distributed in metallic matrix. Reprecipitated carbides gradually grow in size as we move away from the substrate side towards surface of the clad layer to become very long needles near the surface. This gradual variation in size of the reprecipitated carbides is indicative of variation in solidification rate as we move away from the interface towards surface of the clad layer.

Microstructure of (Ni-20Cr)-40WC (Fig. 8) can be grossly divided in two zones from the substrate side towards the surface of the clad layer. Near the substrate microstructure consists of very fine dendritic carbides indicative of rapid solidification. Carbide volume fraction is less in
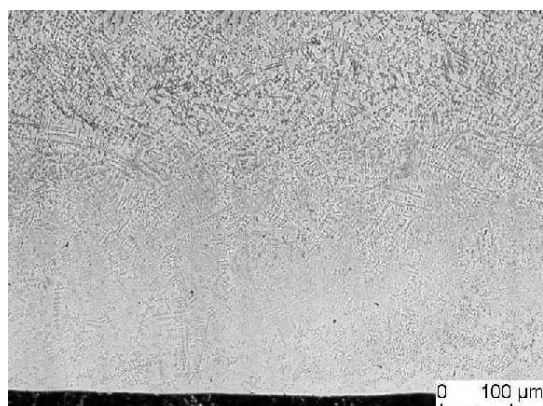
Fig. 8: Microstructure of (Ni-20Cr)-40WC cladding

this zone compared to surface side micro-structure. Towards the surface side the dendritic carbides are gradually grow in size and also their volume fraction is increasing. One can also notice the plate shaped carbide particles, which are essentially the original unmelted particles.
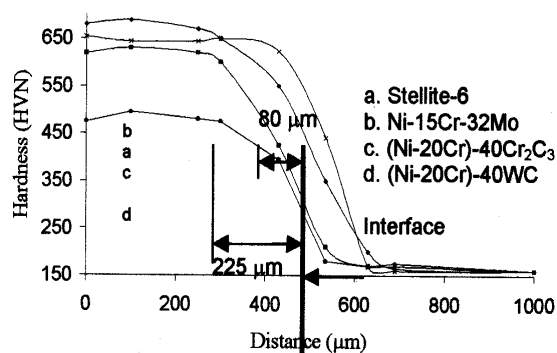

Fig. 9: Hardness profile across the interface 0.15C steel and four different claddings

Hardness profile across the interface is shown in Fig. 9 for stellite-6, Ni-15Cr-32Mo, (Ni-20Cr)-40Cr$_2$C$_3$ and (Ni-20Cr)-40WC claddings. The Ni-15Cr-32Mo and (Ni-20Cr)-40Cr$_2$C$_3$ claddings show comparable hardness (~680 & 630 HVN$_{0.50}$) with that of stellite-6 cladding (~640 HVN$_{0.050}$). Therefore, these materials can be considered as potential alternatives of stellite-6 for hardfacing application. The (Ni-20Cr)-40WC clad layer does not show much improvement in hardness. This can be due to loss of carbon by burning of powder, which was

observed during cladding process, thereby reducing the actual WC content in the microstructure of the clad layer. Hardness of the clad layer with 40% WC is around 480 HVN$_{0.50}$, which is not sufficient for hardfacing applications.

Dilution zone, as shown by loss of hardness, is approximately 225 μm for Ni-15Cr-32Mo, (Ni-20Cr)-40Cr$_2$C$_3$ and (Ni-20Cr)-40WC claddings which is only 80 μm in case of stellite-6 cladding. This difference can be due to higher specific heat input (36-40 J/gm) in case of cobalt-boron free claddings than that (~20 J/gm) in case of stellite-6 cladding. This dilution is mainly due to mixing and diffusion of iron into cladding material from the mild steel substrate and diffusion of chromium and carbon from the clad layer to the substrate material. In case of composite claddings lower hardness near the interface can be explained by less reprecipitation of chromium/ tungsten carbides, that can be seen in the microstructure (Figs. 7 & 8). This is because kinetics of carbide precipitation is not favourable near the interface due to rapid solidification.
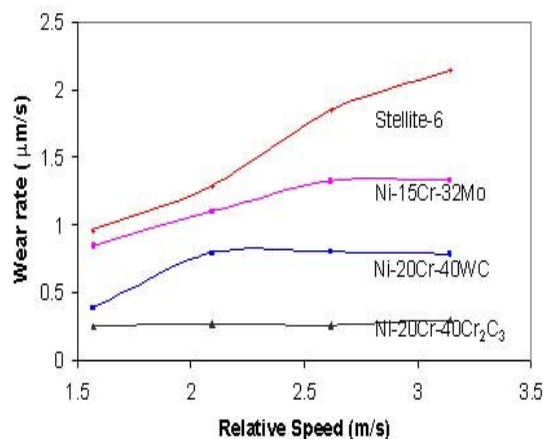

Fig. 10 : Variation of abrassive wear rate of various hardfacings with relaative speed

Wear resistance of Ni-15Cr-32Mo cladding is slightly higher while that of composite claddings is much higher than that of stellite-6 cladding [Fig. 10]. Higher wear resistance of Ni-15Cr-Mo

cladding can be due to presence of Mo rich intermetallics and that of composite claddings is due to presence of hard carbide particles in the microstructure. These particles are distributed uniformly in the microstructure.

Conclusions

- Laser cladding of nickel based hardfacing materials has been done to produce defect free claddings, by optimising the process parameters.
- Ni-15Cr-32Mo claddings have better hardness & wear resistance compared to stellite-6 claddings.
- (Ni-20Cr)-40Cr_2C_3 claddings show comparable hardness and much higher wear resistance than that of stellite-6 clad layer.
- (Ni-20Cr)-40WC clad layers show lower hardness and much higher wear resistance than that of stellite-6 clad layer.
- Nickel based hardfacing materials emerge as potential alternative of stellite-6.

References

1. K. C. Antony, J. Metals 35 (1983) p 52-60.
2. "Cobalt and cobalt alloys", Metals Handbook, 9th edition, Vol. 6, ASM International, Ohio, USA.
3. H. Ocken, Surface and Coating Technology 76-77 (1995) 456-461.
4. J. Mazumder and J. Singh, Proceedings of the Nato Advanced Study Institute on laser Surface Treatment of Metals, 1986, p 297.
5. J. Mazumder, Proceedings of the Nato Advanced Study Institute on laser Surface Treatment of Metals, 1996, p 47.
6. K. P. Cooper, ASM Metals Handbook on Surface Treatment and Coatings for Friction and Wear Control, 9th Edition, p861.
7. G. L. Goswami, Santosh Kumar et al, "Cobalt-boron free nickel based hardfacing alloy for laser cladding", Heat Treat Show & Int. Symposium on Thermal Spray, May 2-4, 2002, Mumbai, India.
8. G. L. Goswami, Santosh Kumar et al, "Laser cladding of dispersion alloy for hardfacing application", Heat Treat Show & Int. Symposium on Thermal Spray, May 2-4, 2002, Mumbai, India.
9. G. L. Goswami, Santosh Kumar et al, "Laser cladding of nickel-based hardfacing materials for nuclear applications", to be submitted to Lasers in Engineering, Ed. B. L. Mordike, Germany.

This Paper received the Panthaki Award as the Best paper on ''Welding of Non-Ferrous Metals'' at National Welding Seminar, 2002 held at Kolkata during January 23-25, 2003.

About the authors ...

Mr Gyanottam Lal Goswami is B. E. in Metallurgy from University of Roorkee, 1970. He had graduated from 14th batch of BARC Training School with Metallurgy discipline. He has made important contributions in nuclear fuel fabrication, thermodynamics of nuclear materials and laser materials processing. He is currently Head of Laser Processing & Advanced Welding Section of the Nuclear Fuels Group, BARC.

Mr Santosh Kumar is B. Tech in Metallurgical Engg. from IT-BHU, 1998. After working for one year with Tata Steel, he joined BARC Training School Orientation Course - 43rd batch as Trainee Scientific Officer and currently working with Laser Processing and Advanced Welding section of Nuclear Fuels Group, BARC for last four years. He is working in the field of laser materials processing.

Dr Ing. Rolf Galun is the Leader of Laser Processing Group in the Institüt für Workstöfftechnik and Workstöffkunde at the Technical University of Clausthal, Germany. His fields of interest are laser materials processing and magnesium technology.

Prof. B. L. Mordike has retired recently as the Director of the School of Materials Science and Technology at The Technical University of Clausthal, Germany. During his tenure of more than 25 years here, he established himself in Magnesium technology and laser material processing. He has several patents and publications in these fields. He is the Editor of the international journal, "Lasers in Engineering".

RESIDUAL STRESS ESTIMATION IN THE INELASTIC RANGE WITH NON-LINEAR FINITE ELEMENT AND ARTIFICAL NEURAL NETWORK ANALYSIS

Kamal Sharma, R.K. Singh, K.K. Vaze and H.S. Kushwaha
Reactor Safety Division
Bhabha Atomic Research Centre

A b s t r a c t

A combined residual stress simulation methodology with non-linear finite element analysis and ANN (Artificial Neural Network) analysis is evolved to evaluate the residual stresses for the welded pipes. The experimental strain data obtained with the hole drilling technique is converted into meaningful residual stresses in the inelastic range. The hole drilling technique (ASTM Standard Test Method E837) is the most simple and reliable methodology to predict the residual stresses in the structures and components. But this method in the present form can be used to predict the residual stresses within the elastic range. The inherent assumption of constant stress field around the hole in the standard ASTM method is present in this case also, but this limitation can be overcome with more data on variation of the strain field near the narrow gap weld zone and refined analysis is possible. ANN database is generated with the help of non-linear finite element analysis by numerically simulating the hole drilling operation for various magnitudes of residual stresses with a range of biaxiality ratios. For the present problem 1/16" hole diameter with a gauge length of 1/8" around the hole is used to sense the numerical strain field around the hole. The gauge location is at r/a = 3.08, where r is the distance of hole center to gauge mid point and a is the hole radius [1]. This analysis approach assumes that stress field is constant for a small region of strain gauge (~ 3mm) as has also been used in the residual stress estimation in the standard ASTM method. Further, this database after network training is used to analyze measured strain data on a 6-inch diameter welded pipe. The ANN predictions are reconfirmed with non-linear finite element analysis. The methodology evolved in this work can be extended to predict residual stresses in the inelastic range for complex geometries such as elbows and tee joints.

Introduction

The effect of residual stresses may be either beneficial or detrimental depending on its magnitude, sign and distribution with respect to load-induced stresses. Very commonly, the residual stresses are detrimental and there are many documented cases in which these stresses have been a predominant factor contributing to fatigue, brittle fracture, stress corrosion cracking leading to structural failures when the service stresses are superimposed on the in-situ exiting residual stresses. In particular, the insidious aspect of residual stress is that its presence generally goes unrecognized until after malfunction or failure occurs. Apart form the complete knowledge of failure mode it is also necessary to determine effectiveness of post weld stress relieving by thermal and mechanical methods and hence the detail information of residual stresses is important.

High tensile stress regions near weld may promote brittle fracture, fatigue or stress corrosion cracking. Compressive residual stress and initial distortion may lead to reduction in buckling strength. The presence of residual stresses is more detrimental in case of dynamic loading. During welding, the weldment

undergoes complex temperature changes and resulting transient thermal stresses, due to incompatible strains near the weld is often in the inelastic range. After welding is completed, the residual stresses remain locked as a result of these strains. In the weldment the maximum stress is as high as the yield stress of weld metal and often beyond the yield stress (*Masubuchi-1980*)[4].

The hole drilling technique (ASTM Standard Test Method E837)[2] is the most simple and reliable methodology to predict the residual stresses in the structures and components. But this method in the present form can be used to predict the residual stresses within the elastic range. The present work is useful in the prediction of the residual stresses in the inelastic range and overcomes the limitations of the standard ASTM method. The estimation of residual stresses in the conventional elastic range as per the ASTM standard is based on the superimposition of two constant stress fields in a plate – the constant stress field in a plate with hole and the stress field around a hole. The strain relaxation due to the hole drilling is converted into constant elastic stress field that exited before the hole drilling operation. Here the basic assumption is that the stress field is constant and the material behaviour is elastic. To overcome the limitation of elastic behaviour the present non-linear finite element simulation is used to obtain the strain field developed due to the residual stress field in the inelastic range for a range of stress biaxiality ratios. The numerical strain field around the hole is used to train ANN with the known values of residual stresses at the hole drilling point. The experimental strain data obtained on a 6-inch diameter pipe around the narrow gap weld zone is converted to residual stresses with the ANN. The stress predictions from the trained ANN are again reconfirmed with inelastic finite element analysis and accuracy of ANN prediction in the range of ~ 2% to 3% is noted. This analysis approach assumes that stress field is constant for a small

region of strain gauge (~ 3mm) as has also been used in the residual stress estimation in the standard ASTM method. However influence of varying stress field and complex geometry can also be accounted with the present methodology.

Numerical Model and Analysis Procedure

For the present study, stainless steel 304-L material properties are used, which is the 6-inch diameter pipe specimen material on which the experiment has been performed and the strain data is available. The measurement location is simulated with a 20mm×20mm plate model as the curvature effects are very small within this region and finite element simulation is carried out. The finite element model is shown in figure 1. The simulation of residual stresses in the component is carried out by loading the plate with a large stress range varying form 0.1 of the yield stress to 1.6 times of the yield stress in both compression and tension regimes. The simulation includes the complete range of the biaxiality ratio (β) varying from -1 to +1.
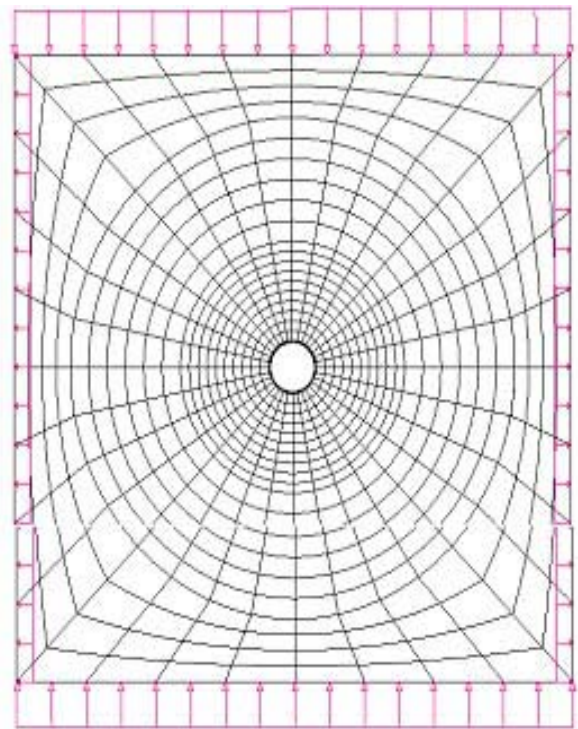

Fig. 1: Mesh configuration after the drilling operation

The drilling process was simulated in the numerical model with element death option by killing the respective surface near the hole location at the onset of drilling operation. For the present problem 1/16" hole diameter with a gauge length of 1/8" around the hole is used to sense the numerical strain field around the hole. The gauge location is at *r/a = 3.08,* where *r* is the distance of hole center to gauge mid point and *a* is the hole radius. This data is consistent with the strain rosettes used for the experiment. Refined mesh is used near the gauge location to compute the strain field accurately. The strain responses of the three gauges in the rosette, which are located at 0 degree, 90 degrees and 225 degrees location are obtained. As the strain field varies along the gauge length the representative average value is obtained with area integration using 8th degree polynomial of curve fitting for the numerical strain values after ensuring the desired accuracy. These strain and stress databases are used to train the ANN, since it is the most powerful tool for such inverse problems. The trained ANN is rechecked for the strain response prediction for a few combinations of stresses and it is found that the predictions are quite satisfactory both in the elastic and the inelastic range. Further, the experimental strain data obtained on the narrow gap welded pipe specimen is fed to the ANN to obtain the residual stresses. The stress response is again checked by simulation of the elastic and inelastic residual stresses on the plate component and the difference between the computed strain response and experimental strain values is .

ensured to be within the accepted range of experimental/numerical error (~ 2% to 3%). Following is the material data used in the analysis.

Material Data of Stainless Steel 304L

Yield limit (σ_y) = 326MPa; Ultimate limit (σ_{ult}) = 637MPa;
Young's modulus (*E*) = 200GPa; Percentage elongation = 49%;
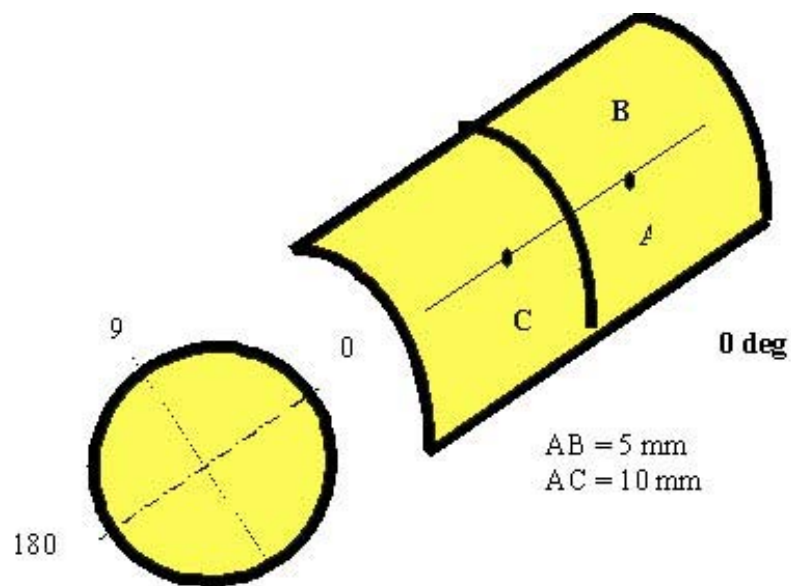Poisson Ratio (υ) = 0.3

Fig. 2 : Welded pipe configuration

Analysis Results

The configuration of 6-inch diameter stainless steel 304L welded pipe with strain measurement points A (at the weld line), B (5mm from the weld line) and C (10 mm from weld line) at reference zero degree location is shown in the Figure 2. Three circumferential positions (0 degree, 90 degrees and 180 degrees) are covered in the experiment with total number of 12 strain rosettes as shown in Table 1. The stress combination applied in the simulation and the strain responses used for training the ANN are presented in the plots of Figures 3-11.
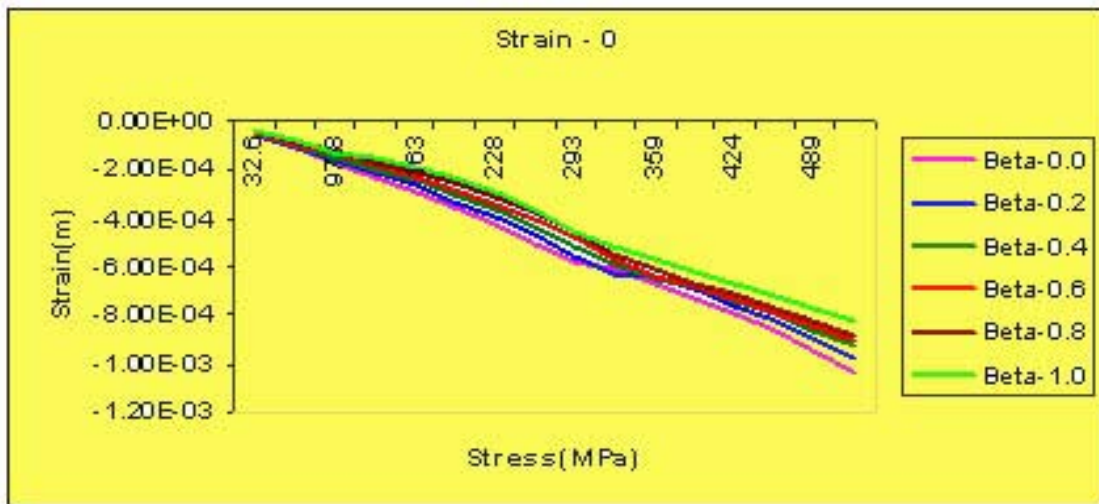
Fig. 3 : Gauge location 0 Deg. & β = 0 to 1.0

Fig 4 : Gauge location 90 Deg. & β = 0 to 1.0

Fig 5 : Gauge location 225 Deg. & β = 0 to 1.0

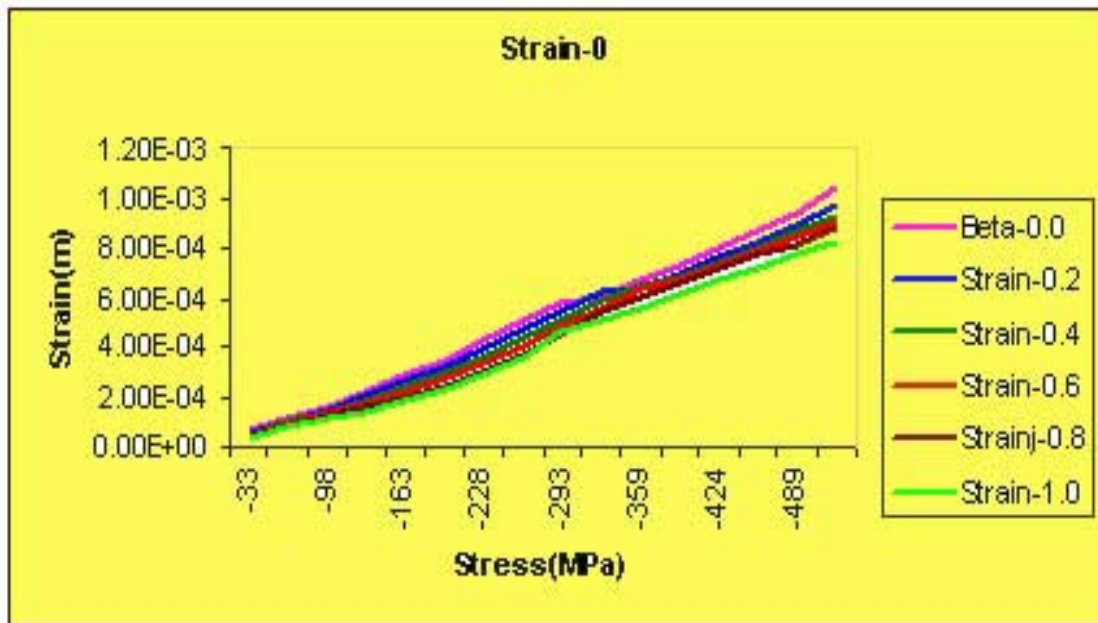*Fig. 6 : Gauge location 0 Deg. & β = 0 to 1.0*

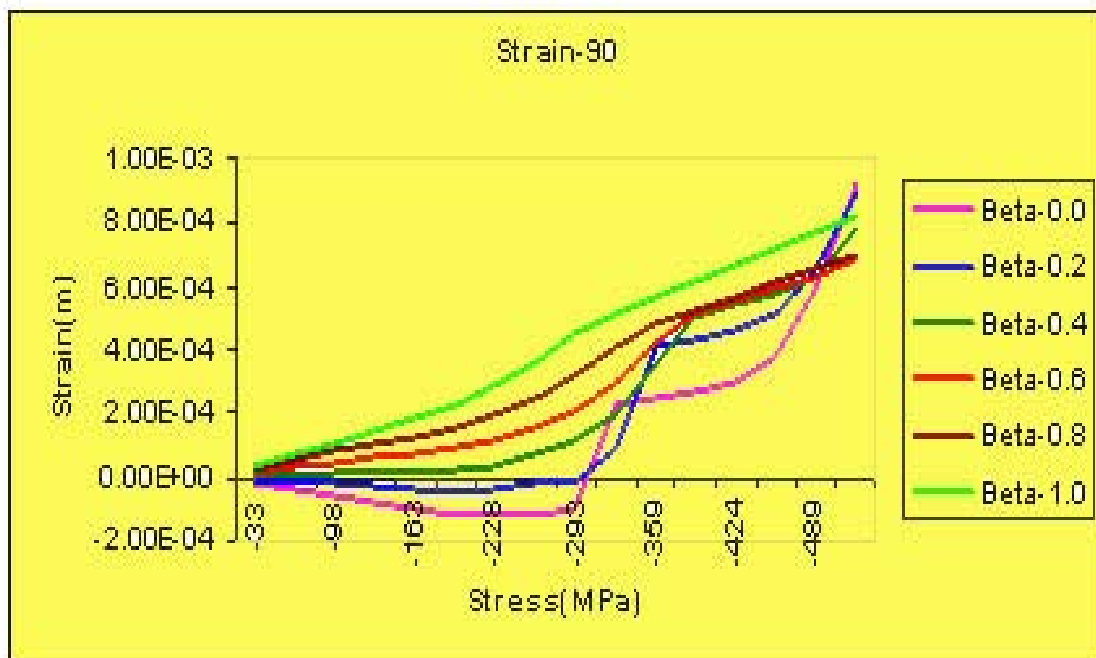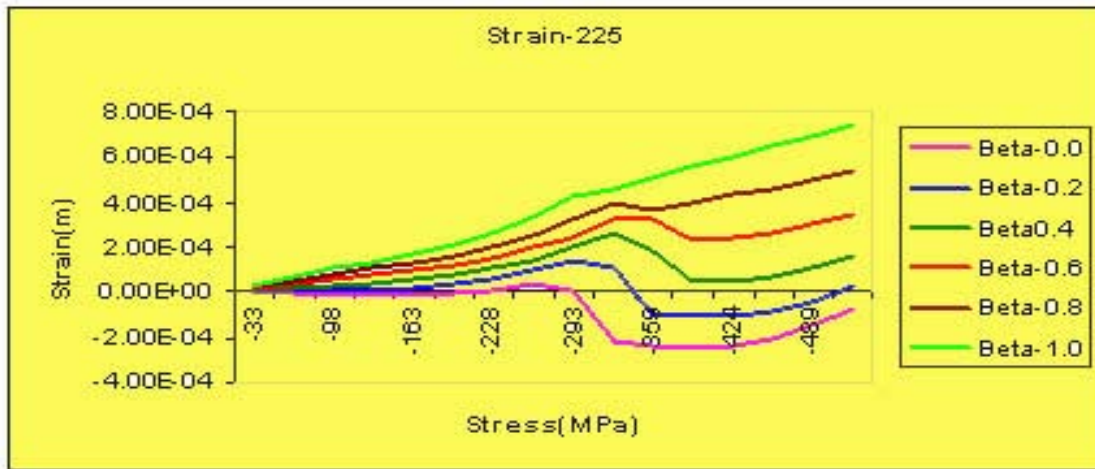*Fig. 7 : Gauge location 90 Deg. & β = 0 to 1.0*
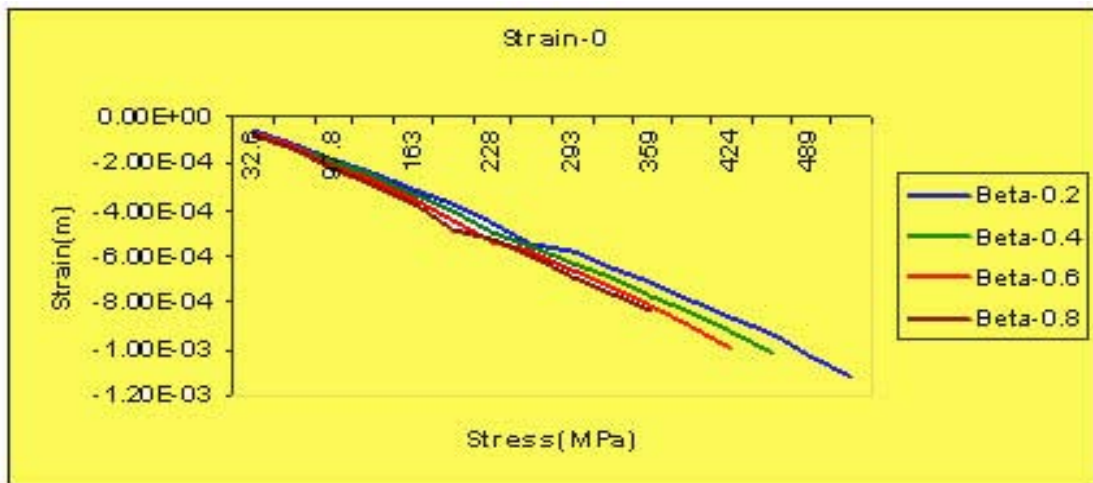
Fig. 8 : Gauge location 225 Deg. & β = 0 to 1.0
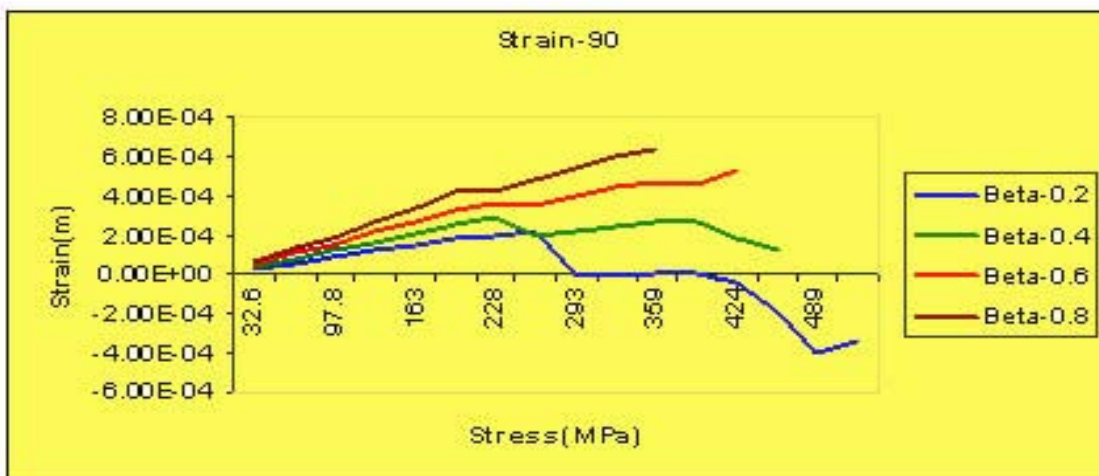

Fig. 9 : Gauge location 0 Deg. & β = -0.2 to -0.8

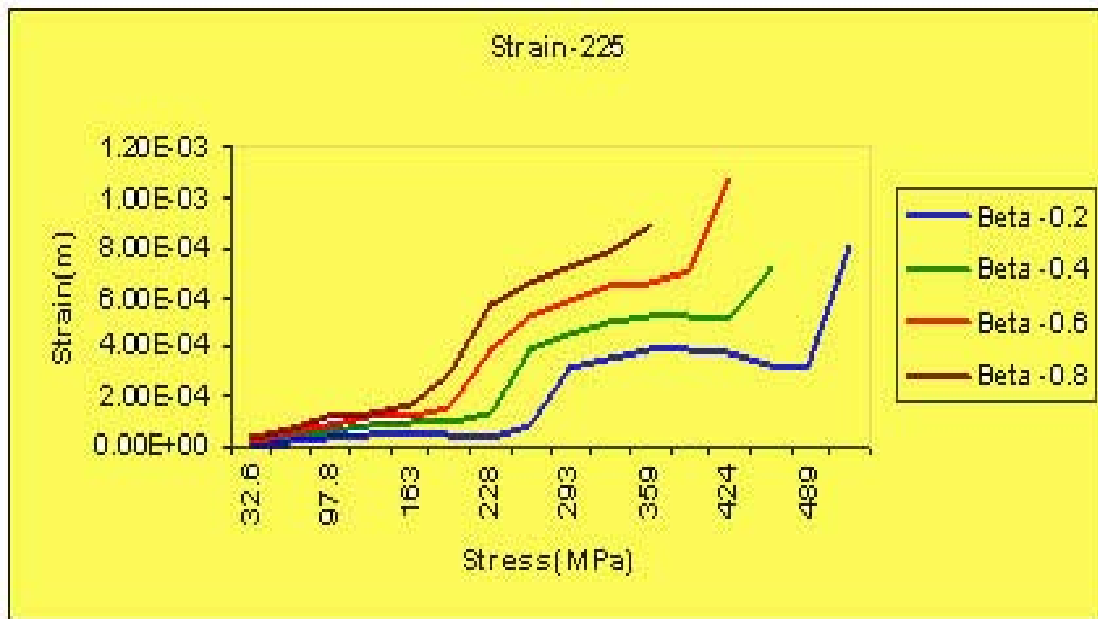*Fig. 10 : Gauge location 90 Deg. & β = -0.2 to -0.8*

Fig. 11 : Gauge location 225 Deg. & β = -0.2 to -0.8

Table 1 : Residual stresses for 6" NB SS welded pipe from ANN

S. No.	Location	Dist. form the weld center line	Strain 1	Strain 2	Strain 3	Stress 1	Stress 2	Angle θ
			μ m			MPa		
1	0 Deg.	At weld line	-97	-325	-313	234.84	118.57	-24.00
2	0 Deg.	5 mm	-311	-180	-194	237.73	171.53	-25.55
3	0 Deg.	10 mm	-191	-186	-166	170.77	166.25	15.48
4	90 Deg.	At weld line	-512	-496	-332	322.37	208.31	19.71
5	90 Deg.	15 mm	-93	-94	-59	90.054	52.673	23.31
6	90 Deg.	20 mm	-154	-182	-190	168.53	158.28	-14.52
7	180 Deg.	At weld line	-436	-359	-289	282.78	220.69	-1.363
8	180 Deg.	5 mm	-484	-502	-404	319.87	248.56	27.70
9	180 Deg.	10 mm	-283	-280	-147	219.19	155.59	21.85
10	180 Deg.	30 mm	-115	-193	-319	223.55	150.88	6.620
11	0 Deg.	At weld line	-270	-189	-127	203.15	158.07	-3.784
12	0 Deg.	5 mm	-169	-156	-280	222.31	163.02	25.49

Table 2 : Error calculation of measured strain values and computed strain values for non-linear finite element analysis

S N	Measured Strain Value (μm)				Computed Strain Value (μm)			(%) Error		
	0	90	225	θ	0	90	225	0	90	225
1	-311	-194	-180	-25.5	-306.61	-196.84	-177.92	1.41	-1.46	-1.51
2	-154	-190	-182	-14.5	-158.3	-193.92	-179.59	-2.79	-2.06	-1.32
3	-436	-289	-359	-1.36	-433.14	-292.43	-352.39	0.65	-1.18	1.84
4	-115	-319	-193	6.62	-117.03	-316.42	-189.47	-1.76	0.808	1.82
5	-169	-280	-156	25.4	-166.25	-284.98	-152.85	1.627	-1.77	2.019

Experimenal Data on a six inches Stainless Steel 304 L Pipe

Table 1 also shows the strain data collected at various rosette locations in the experiment. First of all the measured strain responses are converted into principal strains and the orientation of the principal strains with respect to the first gauge axis is evaluated at each point. The strain data of the third rosette (225 degrees) is converted by strain transformation in this principal system of strains. This reorientation is needed as the ANN is trained for the database of two principal stresses and the two principal strains are aligned with the principal stress direction. These residual stresses obtained form ANN along with the principal angles are shown in Table 1. Now for reconfirming the ANN predictions, the residual stress field is again applied on the finite element model and the strain data are obtained at 0 degree, 90 degrees and 225 degrees. The two strain values (0 degree and 90 degrees) are aligned with the principal axis; hence they are again transformed to the experimental rosette system. In Table 2, the comparison of measured strain and the computed strain are presented and ANN prediction is in the range of ~2% to 3 %. Thus the accuracy of the present prediction is ensured

in the inelastic range. It is observed from the Table 1 that the residual stresses in all the cases are realistic and within the yield stress of stainless steel 304L material, which cannot be obtained by direct application of standard ASTM elastic formula.

Conclusions

The conventional ASTM procedure for the residual stress estimation with elastic formula gives very high unrealistic stress values in the inelastic range. This method is valid only if the residual stress field is up to 0.5 of yield stress of the material. In the present study, the stress field from 0.1 of the yield stress to 1.6 times of the yield limit with different biaxiality ratios along with resulting strain field around the hole have been used to train the ANN. This process of evaluation of the residual stress in the narrow gap welding pipe joints overcomes the limitation of the existing ASTM method and the computed strain field is in very good agreement with the experimental results as has been reconfirmed with finite element analysis. The inherent assumption of constant stress field around the hole in the standard ASTM method is present in this case also, but this limitation can be overcome with more data on variation of the strain field near the narrow gap weld zone and

refined analysis is possible. However it may be noted that for a hole of 1/16 inch (1.58 mm) if the stress field is constant for a length of 2.5 times the hole diameter (~4 mm) from the hole edge the present approach is valid as the gauge length in the rosette is ~ 3 mm. The experimental data also generates strain/stress at a point, which the representative value averaged over the gauge length.

References

1. Measurements Group, Inc., Tech Note TN-503 " *Measurement of Residual Stresses By The Blind Hole Drilling Method*".

2. ASTM Standard E837, " *Determining Residual Stresses by the Hole Drilling Strain Gage Method*".

3. M T Flaman and B H Manning, 1985, "*Determination of Residual Stress Variation with Depth by the Hole Drilling Method*", *Experimental Mechanics,* 205-207

4. Koichi Masubuchi, "*Analysis of welded structures*" Volume 33, Pergamon Press

> *This paper received the Best oral presentation paper award from Indian Society of Mechanical Engineers (ISME) at its 13th National Conference held at Indian Institute of Technology, Roorkee, during December 30-31, 2003.*

About the authors ...

Kamal Sharma is a Mechanical Engineer from 2nd batch of DAE/IITK training programme course 2002. He received his Master's Diploma from IIT Delhi in 2000. He completed his M.Tech (Nuclear Engg &Technology) from IIT Kanpur (2002) and secured the first position in the discipline and joined Reactor Safety Division, BARC. He is currently engaged in FEM simulation for stress analysis and artificial neural network.

Dr R K Singh is a Mechanical Engineer from 21st batch of BARC Training School. He has been involved with in-house finite element code development for structural, fluid and thermal computational problems, fluid-structure interaction problems, nuclear containment safety studies related to Pressurised Heavy Water Reactor and Boiling Water Reactor. His other research interests include problems of rock dynamics, seismic wave propagation analysis and experimental stress analysis.

Mr K.K. Vaze got his B.Tech. degree in Mechanical Engineering from IIT, Bombay in 1973. He is graduate of the BARC Training School, 17th batch. After working in the areas of structural design and analysis of fast reactor components in Nuclear Systems Division, IGCAR, Kalpakkam from 1974 till 1989, he joined Reactor Structures Section of Reactor Engineering Division of BARC in 1989. Currently, he is heading that section, which is part of Reactor Safety Division. He has 30 years of experience in the following areas : Structural Analysis and Design,

Seismic Analysis, Fatigue, Fracture Mechanics, Residual Life Estimation, Failure Analysis, Experimental Stress Analysis, Analytaical and Experimental Evaluation of Structural Integrity of Flawed Components. He has published over 50 papers in National and International Conferences.

Mr H.S. Kushwaha *has made significant and important contributions in the design and analysis of Nuclear Structures, Components and Piping of the Indian Pressurised Heavy Water Reactors. He has done pioneering work in the area of seismic design and analysis of 500 MW(e) PHWR being built at Tarapur, Maharastra. He has successfully applied leak-before-break criteria in 500 MW(e) Primary Heat Transport Piping.*

Mr Kushwaha has developed several finite element computer programmes in the field of structural mechanics, heat transfer and fluid mechanics. His contributions in the area of failure analysis of Madras Atomic Power Inlet Manifold, life assessment and extension of nuclear and heavy water plant components are highly noteworthy. He has played a major role in the seismic reassessment and plant life management of Boiling Water Reactor at Tarapur and PHWRs at Madras and Rajasthan. He is a member of Project Design Safety Committee of PHWRs/PFBR and Civil Engineering Safety Committee constituted by Atomic Energy Regulatory Board, Mumbai. Mr Kushwaha is an active member of Safety Review Committee for Operating Plants (SARCOP) constituted by the Atomic Energy Regulatory Board. He has published around 400 papers/ reports in national and international journals.

Xanthomonas PROGRAMMED CELL DEATH HAS SIMILARITIES WITH EUKARYOTIC APOPTOSIS

Satyendra Gautam and Arun Sharma
Food Technology Division
Bhabha Atomic Research Centre

S u m m a r y

Xanthomonas bacterium *exhibited post-exponential programmed cell death (PCD) under certain nutritional conditions especially in a protein rich medium. PCD was not displayed by* Xanthomonas *cells while growing in minimal medium like starch minimal medium or M9 medium. While undergoing PCD, the organism was found to transform to spherical membranous apoptotic body like structures. The transformation was confirmed by scanning electron microscopy. The membranous bodies were found to contain DNA, which was devoid of the indigenous plasmids of the organism. These bodies were also found to bind annexin V indicative of the externalization of membrane phosphatidyl serine. Nicking of DNA was also detected using a Tunnel assay in* Xanthomonas campestris pv. glycines *(Xcg) cultures undergoing PCD in LB medium. The PCD in* Xanthomonas *was found to be associated with the synthesis of an endogenous enzyme similar to human caspase-3, a known marker of apoptosis in eukaryotes. Caspase-3 like protein was detected only in the cells growing in proteinous medium and not in those growing in minimal medium. It was found that starch or its hydrolytic product acted as the repressor of biosynthesis for the* Xanthomonas *caspase, thereby, preventing the organism from undergoing PCD, upon its addition. Caspase negative mutants of Xcg strain AM2 did not display PCD. The importance of PCD in* Xanthomonas *life-cycle needs to be elucidated as the system appears to have significant similarities with the eukaryotic apoptosis.*

Introduction

*X*anthomonas campestris pv. *glycines* strain AM2 (XcgAM2), the etiological agent of the bacterial pustule disease of soybean, was isolated in this laboratory from the field grown soybean in Maharashtra and biochemically characterised (Sharma *et al*., 1993; 1994; Sharma, 1999). During the course of our studies on XcgAM2 it was found that the survival of the organism in protein rich medium as Luria-Bertani (LB), nutrient broth (NB), or casein medium was found to be very poor compared to that in minimal medium like starch minimal medium or M9 medium. In a protein rich medium like LB XcgAM2 was found to undergo post-exponential programmed cell death (PCD). PCD was found to be associated with the

production of an endogenous enzyme similar to human caspase-3. Caspases, the cysteinyl aspartate-specific proteinases, were first implicated in programmed cell death in the nematode *Caenorhabditis elegans* (Yuan et al., 1993). The product of ced-*3* gene in this organism was found to be related to a family of caspases in mammalian systems. These proteases are important components of the programmed cell death pathway and appear to be conserved throughout the evolution (Nicholson et al., 1995; Nicholson and Thornberry, 1997; Hengartner, 2000). Programmed cell death or apoptosis is a fundamental process in the development and maintenance of multi-cellular organisms. It may be initiated by many physiological, pathological or environmental stimuli and all cells under apoptosis are reported

to undergo similar sequence of morphological and biochemical events (Raff, 1992; Collotta et al., 1992; Hockenbery et al., 1993; Rudel and Bokoch, 1997). The existence of programmed cell death in bacteria was suggested in several studies earlier (Gerdes et al., 1986; Zambrano *et al.*, 1993; Jensen and Gerdes, 1995; Naito *et al.*, 1995; Snyder, 1995; Yarmolinsky, 1995; Aizenman *et al.*, 1996; Naito *et al.*, 1998; Nakayama and Kobayashi, 1998). However, none of these studies provided evidence for the existence of mechanisms in prokaryotes similar to eukaryotic organisms. The present study describes the identification of a caspase like protein, and other markers of apoptosis associated with a nutritionally regulated programmed cell death in *Xanthomonas*.

Experimental Procedures

Light microscopy. The cell suspension was spread on a glass slide, allowed to dry in air, heat fixed and stained negatively with India ink. Stained slides were visualised under a light microscope (Carl Zeiss, Germany) using 100 X oil immersion objective. The image was transferred to a TV screen using a CCD camera attached to the microscope and photographed.

Scanning electron microscopy : The cells and membranous apoptotic body suspension was fixed with equal volume of glutaraldehyde (25%) diluted 4 fold in sodium phosphate buffer (0.1 M, pH 7.4). Fixed sample was mounted on a metal stub, air dried, and desiccated in $CaCl_2$ desiccator. Gold sputtering (100 nm thick) was performed and the sample visualised under SEM (SEM-S-240, Cambridge Instruments, UK).

Apoptotic body isolation : For obtaining apoptotic body preparation the post-exponential phase culture of the LB medium grown XcgAM2 was centrifuged at 25,000g for 10 min twice to remove the cell debris. The resultant cell-free supernatant was re-centrifuged at 100,000g for 2 h to obtain a pellet containing membranous bodies. The pellet was suspended in sodium phosphate buffer (0.1 M, pH 7.4).

Caspase-3 assay : Overnight grown cells were centrifuged, washed, and lysed using 10-volume lysis buffer [Tris-HCl (10 mM), NaH_2PO_4/ $NaHPO_4$ (10 mM, pH 7.5), NaCl (130 mM), triton X- 100 (1%) and sodium pyrophosphate (10 mM)]. A 50 µl aliquot of the cell lysate (10^8 CFU/ ml) was reacted with 10 µl (1 µg/µl) of synthetic fluorogenic substrate, Ac-DEVD-AMC (PharMingen, USA) at 37 °C for 1h in I ml reaction buffer [HEPES (20 mM, pH 7.5), glycerol (10 %), and DTT (2 mM)]. In the control set the reaction was inhibited by 10 µl (0.1 µg/µl) of the synthetic inhibitor of caspase-3 (Ac-DEVD-CHO) per reaction. After incubation the fluorescence intensity was measured using a spectroflourophotometer (EX_λ 380 nm, EM_λ 440 nm).

SDS-PAGE and Western Hybridisation : SDS-PAGE was performed as per the standard method. After completion of the electrophoresis electro-blotting was done using a Hybond–P membrane (Amersham-Pharmacia) in a transfer buffer [25 mM Tris, 192 mM glycine (pH 8.3); 20 % methanol] employing 50 mA constant current at 4^oC overnight. The blotted membrane was hybridized with the affinity purified biotin-conjugated, polyclonal rabbit anti-active human caspase-3 antibody (10 µl, 0.5 mg/ml) (PharMingen, USA) in 100 ml of the antibody buffer (TBS having 0.05%Tween-20 and 1% gelatin) for 20 h and then incubated in the antibody buffer having streptavidin–horseradish peroxidase conjugate (PharMingen, USA) for 1.5 h. Lastly, the blot was detected using the colour reagent solution [4-chloro-1-naphthol (Sigma) / H_2O_2].

Annexin V-FITC labelling assay : An aliquot (50 µl) of the apoptotic body preparation was mixed with 900 µl Annexin V-FITC binding buffer [10 mM HEPES, pH 7.4; 140 mM NaCl and 2.5 mM $CaCl_2$], 5 µl Annexin V-FITC (PharMingen, USA) and incubated for 30 min at ambient temperature (26±2°C). The fluorescence intensity was measured using a spectro-

flourophotometer [EX$_\lambda$ 488 nm, EM$_\lambda$ 520 nm]. Similarly, Annexin V-FITC labelling was also done with the membrane preparation obtained from starch minimal medium grown XcgAM2 cells.

TUNEL assay : DNA from XcgAM2 cells and those under going PCD was isolated, purified, and subjected to nick end labelling using fluorescein isothiocyanate (FITC) labelled dUTP and terminal deoxynucleotidyl transferase (TDT) (PharMingen, USA), and incubated for 60 min at 37°C. The fluorescence intensity was measured using a spectroflourophotometer [EX$_\lambda$ 488 nm, EM$_\lambda$ 520 nm].

Mutagenesis of XcgAM2 : XcgAM2 cells were subjected to N-methyl-N'-nitro-N-nitrosoguanidine (MNNG) (0.5-1 mg/ml) mutagenesis. The plates were incubated at 26±2°C for 72 h. The colonies from these plates were picked, numbered, and transferred to LB-gelatin (1%) -agar plates in duplicate and incubated at 26±2°C for 72 h. One of the two plates was treated with tichloroacetic acid (TCA, 25%) to check the level of extracellular proteolytic activity. Complete loss or significant reduction in extracellular proteolytic activity was used as a marker to screen out the putative mutants.

Results

Rapid cell death in *Xanthomonas campestris* pv. *glycines* AM2. *Xanthomonas campestris* pv. *glycines* AM2 (XcgAM2) cells displayed a typical exponential phase followed by a stationary phase in starch minimal medium (Fig. 1). However, in Luria-Bertani (LB) medium, instead of entering the normal stationary phase at the end of exponential phase,
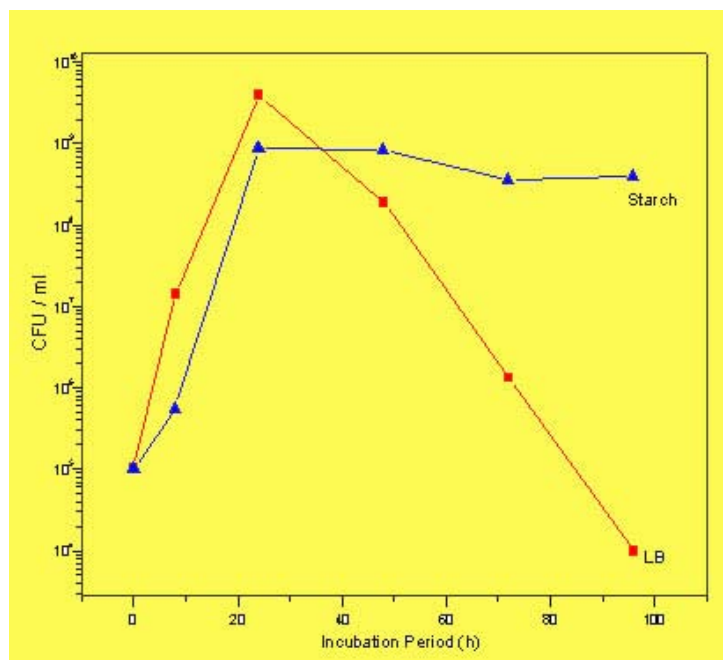

Fig.1 Growth profile of XcgAM2 culture in LB and starch minimal media
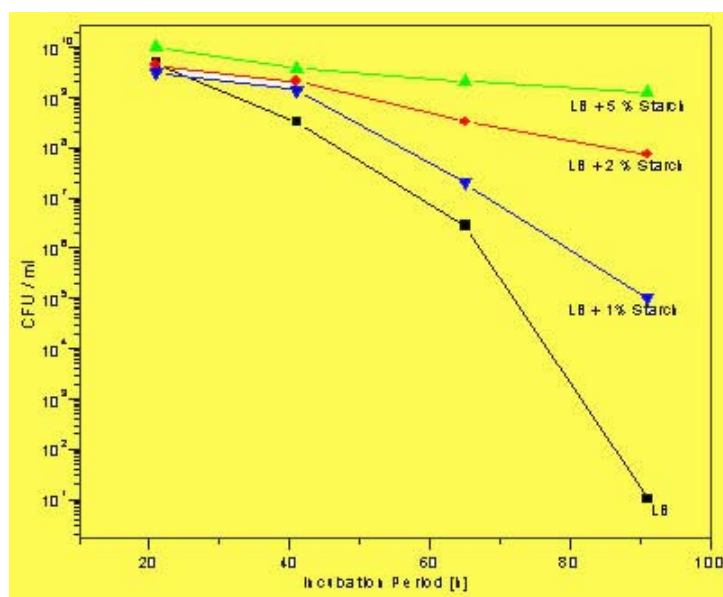

Fig. 2   Viable cell number of XcgAM2 in post-exponential phase when the organism was grown in LB medium with different concentrations of starch.

the culture was found to undergo rapid cell death (RCD) (Fig. 1). Other pathovars of *Xanthomonas*, *X. campestris* pv. *malvacearum* NCIM 2310 and *X. campestris* NCIM 2961 also showed RCD in stationary phase, though less

Table 1 : Determination of the period within which addition of starch was effective in arresting RCD in LB growing cultures of XcgAM2. The RCD was inhibited only if the starch was added within 15 h of the start of incubation.

Time (h) of incubation at which 5% starch was added to LB growing Xcg cells	Viable cell number at the end of incubation period (96 h) (CFU/ ml)
0	7.3×10^9
3	3.1×10^9
6	3.3×10^9
10	3.5×10^9
15	1.3×10^9
24	1.2×10^6

* CFU = Colony forming units.
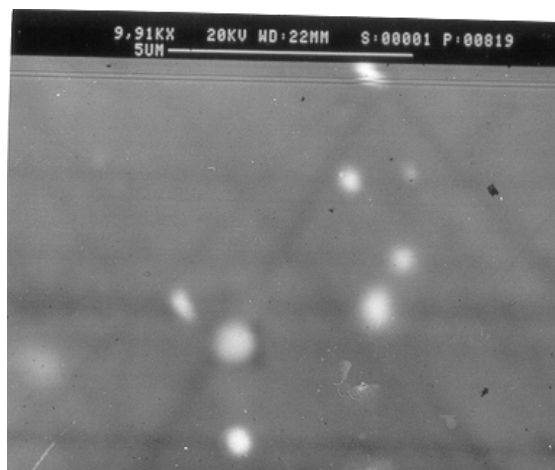
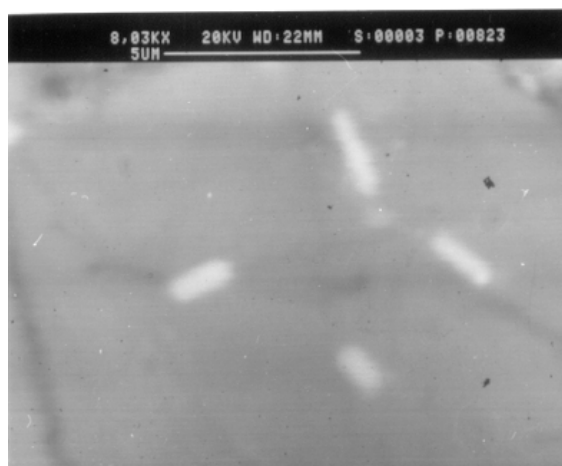*Fig.3. SEM photomicrograph showing image of (A) normal Xanthomonas cells, (B) morphological transformation of Xanthomonas cells to apoptotic body like structures.*

pronounced than XcgAM2 (data not shown). RCD in LB medium was not displayed by *Escherichia coli* (data not shown). Incubating the LB grown post-exponential phase culture of XcgAM2 at 4°C was found to arrest RCD (data not shown). In starch minimal medium all the *Xanthomonas* strains tested did not display RCD (data not shown). Addition of starch to LB growing cultures of XcgAM2 could arrest RCD as shown in Fig.2. The concentration and time of addition of starch to LB cultures determined the extent of RCD. As shown in Fig. 2 addition of starch at 5% level to LB medium was found to prevent RCD. The RCD was inhibited only if starch was added within 15 h of the start of the incubation in LB medium (Table 1).

Microscopy. The formation of membrane bound bodies was confirmed by the change in the cell morphology of the stationary phase cultures of LB and starch minimal medium grown Xcg under a light microscope with the help of

negative staining using India ink. The typical rod shaped Xcg cells were found to transform to spherical bodies in LB but not in starch minimal medium The membrane bodies of Xcg could be concentrated by centrifuging the cell-free culture supernatant of Xcg at 100,000g for 2 h. The normal Xcg cells and the transformed cells (membrane bodies) are seen in the scanning electron micrographs (Fig. 3, A and B). The Xcg cells generally measure between 0.4-1 μm x 1.2-3 μm. The size of the spherical membrane body of Xcg was found to range between 0.4-0.7 μm.

Presence of caspase-3 like activity :
While looking for endogenous proteases in XcgAM2, we found the presence of caspase-3 like activity in the XcgAM2 cells from LB grown cultures. The presence of endogenous caspase-3 like activity was assayed using a fluorogenic substrate of caspase-3, Ac-DEVD-AMC [N-acetyl-Asp-Glu-Val-Asp-AMC (7-amino-4-methylcoumarin)] and an aldehyde inhibitor of the enzyme, Ac-DEVD-CHO [N-acetyl-Asp-Glu-Val-Asp-CHO] (Thornberry *et al*., 1992; Li *et al*., 1995a; Nicholson and Thornberry, 1997). XcgAM2 was found to possess caspase-3 like activity. This is evident from the fact that the relative fluorescence intensity produced by the action of caspase-3 like enzyme from LB grown XcgAM2 on the fluorogenic substrate was almost four fold higher (~940 units) compared to the intensity in the experimental controls, the reaction mixture containing the inhibitor of caspase-3 (~250 units). The reaction mixture with the enzyme from starch grown XcgAM2 cells showed fluorescence intensity values similar to controls (~250 units). It was therefore clear that this activity was not induced in the cells grown in the starch minimal medium.

Western blot analysis of Xanthomonas caspase:
Fig. 4 shows the western blot analysis of the

Xanthomonas caspase protein using human caspase-3 antibody. As is evident from the blot a strong hybridisation signal was obtained with the *Xanthomonas* caspase in LB grown cultures of all the three *Xanthomonas* strains tested. Interestingly, the hybridisation signal was obtained only with the LB grown cells and not with the starch minimal medium grown cells of the three strains (Fig.4).The caspase protein was not detected in LB grown *E. coli* cells (Fig. 4).
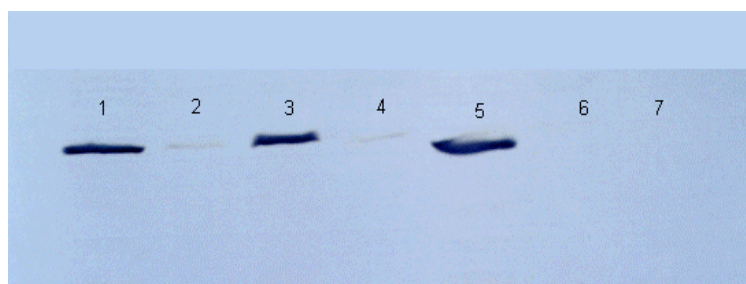

Fig.4 Western blot hybridization showing caspase-3 protein in different strains of Xanthomonas. *The protein was observed only in LB medium growing cells but not in starch minimal medium growing cells (1,3,5-LB grown* Xanthomonas *strains, 2,4,6-starch minimal medium grown Xanthomnas strains, 7-LB grown* E.coli*).*

Changes in plasma membrane : The fluorescence intensity resulting from the binding of annexin V-FITC to the membrane preparation from the post-exponential phase XcgAM2 cultures grown in LB was very high compared to that of starch minimal medium grown cells (data not shown).

Characterisation of DNA : The agarose gel electrophoresis of genomic DNA from LB grown cells and DNA isolated from the supernatant of post-exponential phase LB cultures of XcgAM2 showed reduced mobility compared to the genomic DNA of the starch minimal medium grown cells (data not shown). However, the DNA from the supernatant of culture under RCD was found to possess nicks as confirmed by the end labelling or TUNEL (terminal deoxynucleotidyl transferase dUTP nick end labelling) assay (Li *et al*., 1995b). The DNA of the post-exponential phase LB grown XcgAM2 cultures under RCD showed significantly higher fluorescence intensity

compared to the genomic DNA of starch minimal medium grown XcgAM2 cells (data not shown).

Characterisation of caspase mutants : XcgAM2 cells were subjected to N-methyl-N'- nitro-N-nitrosoguanidine (MNNG) treatment and screened for extracelluar proteolytic activity on LB-gelatin agar. The MNNG treatment of XcgAM2 cells resulted in 2-3 log cycle reduction in cell numbers and resulted in some putative mutants showing reduced extracellular proteolytic activity. Amongst these, four mutants (M-11, M-20, M-24, M-42) were found to show poor hybridization signal with human caspase-3 antibody during western blot hybridization, indicative of lack of or reduced caspase protein presence (data not shown). All these four mutants were found to synthesize some amount of caspase-3 like protein, however no significant caspase enzyme activity was observed compared to the wild type XcgAM2 (data not shown). This showed that whatever caspase-3 like protein observed to be produced by these mutants in the western blot analysis, was largely inactive.
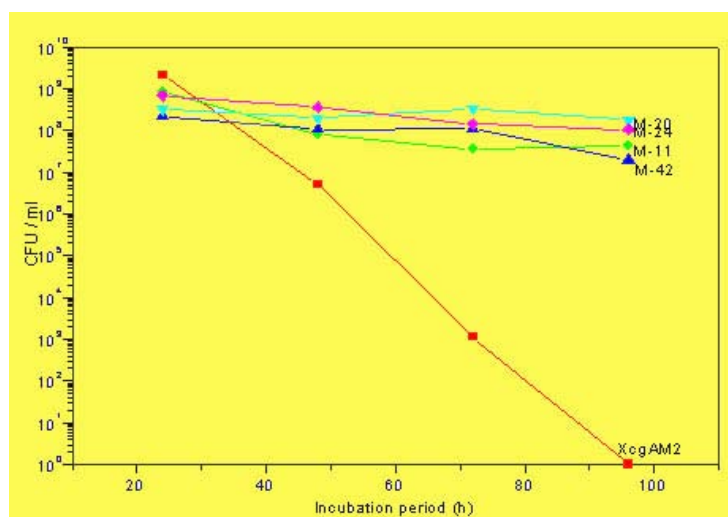

Fig. 5. Viable cell number of XcgAM2 and its mutants (M 11, M 20, M 24, and M 42) in post-exponential phase when the organisms were grown in LB medium.

The caspase mutants of XcgAM2 were found to retain the other characteristics of the wild type XcgAM2, including the amylase activity, pigment production, SDS-PAGE protein profile

and the two indigenous plasmids (data not shown) (Sharma et al., 1994). However, the characteristic post-exponential RCD observed in the wild type XcgAM2 was not displayed by all these four caspase mutants (Fig. 5).

Discussion

All the three *Xanthomonas* strains tested in this study were found to undergo post-exponential rapid cell death (RCD) in LB medium. None of the strains showed RCD in starch minimal medium. A control *E. coli* culture used in the study neither exhibited RCD, nor the presence of caspase protein. Addition of starch to LB culture of XcgAM2, at any point of incubation during the exponential growth, was found to arrest the onset of the RCD. LB grown post-exponential phase XcgAM2 culture was incubated at 4°C to check if the low temperature could arrest RCD. Many of the enzyme activities are reduced at low temperature, and if the process is genetically regulated, the RCD will be affected. Interestingly, at 4°C RCD was found to be inhibited indicating the possible involvement of enzymes. The onset of RCD could be correlated with the synthesis of an endogenous caspase-3 like enzyme activity in XcgAM2 cells. The protein from XcgAM2 that gave a strong hybridisation signal with the human caspase-3 antibody could be called *Xanthomonas* caspase (Gautam & Sharma, 2002a; 2002b). Caspase mutants of XcgAM2 obtained through MNNG mutagenesis did not display the characteristic post–exponential RCD observed in the wild type XcgAM2 (Gautam & Sharma, 2002a; 2002b). The caspase protein synthesized by these mutants was found to be enzymatically inactive. This clearly indicates the association of caspase activity with the RCD in XcgAM2. This also suggested that the observed RCD in XcgAM2 was indeed a

programmed cell death (PCD). Besides the presence of caspase activity the PCD in *Xanthomonas* was also found to be associated with the additional features of eukaryotic apoptosis. Annexin V binding to the membrane preparation of the post-exponential phase LB cultures of XcgAM2 indicated externalisation of phosphatidyl serine moieties in the transformed cultures. Annexin V is a 35-36kDa Ca^{2+} dependent phospholipid-binding protein that has a high affinity to phosphatidyl serine, and therefore, it binds to membranes with exposed phosphatidyl serine. Changes in plasma membrane are reported to be one of the earliest features of apoptotic transformation in eukaryotes (Raynal and Pollard, 1994; Martin *et al*., 1995; Vermes *et al*., 1995). The DNA in the post-exponential phase LB cultures of XcgAM2 was found to be nicked. However, no ladder pattern, characteristic of DNA fragmentation in eukaryotic apoptosis, was observed (Wyllie, 1980; Wyllie, 1993; Walker and Sikorska, 1994; Enari *et al*., 1998). DNA fragmentation has not been detected in several examples of apoptosis in higher organisms, and need not be an absolute requirement for apoptotic cell death (Barres *et al*., 1992; Ucker *et al*., 1992; Oberhammer *et al*., 1993).

Conclusion

These studies show that the RCD in *Xanthomonas* has similarities with the programmed cell death of eukaryotes. The possibility of existence of programmed cell death in prokaryotes has been suggested by many earlier studies (Gerdes et al., 1986; Zambrano *et al*., 1993; Jensen and Gerdes, 1995; Naito *et al*., 1995; Snyder, 1995; Yarmolinsky, 1995; Aizenman *et al*., 1996; Naito *et al*., 1998; Nakayama and Kobayashi, 1998). Programmed cell death was also reported to be an altruistic effort under the conditions of starvation, allowing survival of some cells at the expense of others, in a bacterial culture (Zambrano and Kolter, 1996). Further investigations are necessary to confirm the potential role of the observed programmed cell death in XcgAM2. These studies strongly suggested that the programmed cell death in *Xanthomonas* probably has the mechanism similar to eukaryotic apoptosis (Gautam & Sharma, 2002a; 2002b; Gautam, 2003; Gautam & Sharma, 2004). It is believed that apoptosis is an essential part of life for any multi-cellular organism and that the way in which most cell die is conserved from worm to mammal (Meier *et al*., 2000). This is the first report showing the presence of the main markers of eukaryotic apoptosis in a bacterial cell and may provide important clues to the evolution of PCD in higher life forms (Bayles, 2003; Rice & Bayles, 2003).

References

1. Aizenman, E., Engelberg- Kulka, H., and Glaser, G. (1996) An *Escherichia coli* chromosomal "addiction module" regulated by 3', 5'- bispyrophosphate: A model for programmed bacterial cell death. *PNAS (USA)* 93: 6059-6063.
2. Barres, B. A ., Hart, I. K., Coles, H. S. R., Burne, J. F., Voyvodic, J. T., Richardson, W. D., and Raff. M. C. (1992) Cell death and control of cell survival in the oligodendrocyte lineage. *Cell* 70: 31-46.
3. Bayles, K. W. (2000) Are the molecular strategies that control apoptosis conserved in bacteria? *Trends microbiol*., 11: 306-311.
4. Colotta, F., Polentarutti, N., Sironi, M., and Mantovani, A. (1992) Expression and involvement of c-fos and c-jun proto-

oncogenes in programmed cell death induced by growth factor deprivation in lymphoid cell lines. *J Biol Chem* 267:18278-83.

5. Enari, M., Sakahira, H., Yokoyama, H., Okawa, K., Iwamatsu , A., and Nagata, S. (1998) A Caspase- activated DNase that degrades DNA during apoptosis, and inhibitor ICAD. *Nature* 391: 43-50.

6. Gautam, S. and Sharma, A. (2002a) Involvement of caspase-3 like protein in rapid cell death of *Xanthomonas*. *Mol. Microbiol*., 44(2), 393-401.

7. Gautam, S. and Sharma, A. (2002b) Rapid Cell Death in *Xanthomonas campestris* pv. *glycines*. *J. Gen. and Appl. Microbiol.,* 48, 67-76.

8. Gautam, S. (2003) Ph. D. (Science) Thesis, University of Mumbai. Studies on *Xanthomonas campestris* pv. *glycines* with special reference to its programmed cell death.

9. Gautam, S., and Sharma, A. (2004) Programmed Cell Death: An Overview. *In: Advances in Biochemistry and Biotechnology*, Ed. Chakraborty, C. (Daya Publishing House, New Delhi, INDIA), (in press).

10. Gerdes, K., Rasmussen, P. S., and Molin, S. (1986) Unique type of plasmid maintenance function: Postsegregational killing of plasmid-free cells. *PNAS (USA)* 83: 3116-3120.

11. Hengartner, M. O. (2000) The biochemistry of apoptosis. *Nature* 407: 770-776.

12. Hockenbery, D. M., Oltvai, Z. N., Yin, X. M., Milliman, C. L., and Korsmeyer, S. J. (1993) Bcl-2 functions in an antioxidant pathway to prevent apoptosis. *Cell* 75: 241-251.

13. Jensen, R. B., and Gerdes, K. (1995) Programmed cell death in bacteria: proteic plasmid stabilization systems. *Mol Microbiol* 17: 205-210.

14. Li, P., Allen, H., Banerje, S., Franklin, S., Herzog, L., Johnston, C *et al.* (1995a) Mice deficient in IL-1β-converting enzyme are defective in production of mature IL-1β and resistant to endotoxic shock. *Cell* 80:401-411.

15. Li, X., Traganos, F., Melamed, M. R., and Darzynkiewicz, Z.(1995b) Single- step procedure for labelling DNA strand breaks with fluorescein- or BODIPY- conjugated deoxynucleotides: Detection of apoptosis and bromodeoxyuridine incorporation. *Cytometry* 20: 172-180.

16. Martin, S. J., Reutelingsperger, C. P., McGahon, A. J., Rader, J. A., van Schie, R. C., LaFace, D. M., and Green. D. R. (1995) Early redistribution of plasma membrane phosphatidylserine is a general feature of apoptosis regardless of the initiating stimulus: Inhibition by over expression of Bcl-2 and Abl. *J Exp Med* 182: 1545-1556.

17. Meier, P., Finch, A., and Evan, G. (2000) Apoptosis in development. *Nature* 407: 796-801.

18. Naito, T., Kusano, K., and Kobayashi, I. (1995) Selfish behaviour of restriction-modification systems. *Science* 267: 897-899.

19. Naito, Y., Naito, T, and Kobayashi, I. (1998) Selfish restriction modification genes: Resistance of a resident R/M plasmid to displacement by an incompatible plasmid mediated by host killing. *Biol Chem* 379: 429-436.

20. Nakayama, Y., and Kobayashi, I. (1998) Restriction- modification gene complexes as selfish gene entities: Roles of a regulatory system in their establishment, maintenance, and apoptotic mutual exclusion. *PNAS (USA)* 95: 6442-6447.

21. Nicholson, D. W., and Thornberry N. A. (1997) Caspases: Killer proteases. *Trends Biochem Sci* 22: 299-306.

22. Nicholson, D. W., Ali, A., Thornberry N. A., Vaillancourt, J. P., Ding, C. K., Gallant, M.

et al., (1995) Identification and inhibition of the ICE/CED-3 protease necessary for mammalian apotosis. *Nature* 376: 37-43.

23. Oberhammer, F., Fritsch, G., Schmied, M., Pavelka, M., Printz, D. Purchio, T *et al*., (1993) Condensation of the chromatin at the membrane of an apoptotic nucleus is not associated with activation of an endonuclease. *J Cell Sci* 104: 317-326.

24. Raff, M. C. (1992) Social controls on cell survival and cell death. *Nature* 356: 397-400.

25. Raynal, P., and Pollard, H. B. (1994) Annexins: The problem of assessing the biological role for a gene family of multifunctional calcium and phospholipid-binding proteins. *Biochim Biophys Acta* 1197: 63-93.

26. Rice, K. C., and Bayles, K. W. (2003) Death's toolbox: examining the molecular components of bacterial programmed cell death. *Mol. Microbiol*., 50(3): 729-738.

27. Rudel, T., and Bokoch, G. M. (1997) Membrane and morphological changes in apoptotic cells regulated by caspase-mediated activation of PAK2. *Science* 276: 1571-1574.

28. Sharma, A., Nair, P. M., and Pawar, S. E. (1993) Identification of soybean strains resistant to *Xanthomonas campestris* pv. *glycines*. *Euphytica* 67: 95-99.

29. Sharma, A., Syed, A. N., and Nair, P. M. (1994) Characterisation and plasmid profile of *Xanthomonas campestris* pv. *glycines*. *J Phytopathol* 141: 53-58.

30. Sharma, A. (1999) *Xanthomonas*. Encyclopedia of Food Microbiology. London: Academic Press, pp.2323-2329.

31. Snyder, L. (1995) Phage-exclusion enzymes: a bonanza of biochemical and cell biology reagents? *Mol Microbiol* 15: 415-420.

32. Thornberry, N. A ., Bull, H. G., Calaycay, J. R., Chapman, K. T., Howard, A. D., Kostura, M. J *et al*. (1992) A novel heterodimeric cysteine protease is required for interleukin-1-beta processing in monocytes. *Nature* 356: 768-776.

33. Ucker, D. S., Obermiller, P. S., Eckhart, W., Apgar, J. R., Berger, N. A., and Meyers, J. (1992) Genome digestion is a dispensable consequence of physiological cell death mediated by cytotoxic T lymphocytes. *Mol Cell Biol* 12: 3060-3069.

34. Vermes, I., Haanen, C., Steffens, N. H., and Reutelingsperger, C. (1995) A novel assay for apoptosis. Flow cytometric detection of phosphatidylserine expression on early apoptotic cells using fluorescein labelled Annexin V. *J Immunol Method* 184: 39-51.

35. Walker, P. R., and Sikorska, M. (1994) Endonuclease activities, chromatin structure, and DNA degradation in apoptosis. *Biochem Cell Biol* 72: 615-623.

36. Wyllie, A. H. (1980) Glucocorticoid-induced thymocyte apoptosis is associated with endogenous endonuclease activation. *Nature* 284: 555-556.

37. Wyllie, A. H. (1993) Apoptosis. *Br J Cancer* 67: 205-208.

38. Yarmolinsky, M. B. (1995) Programmed cell death in bacterial populations. *Science* 267: 836-837

39. Yuan, J., Shaham, S., Ledoux, S., Ellis, H. M., and Horvitz, H. R. (1993) The *C.elegans* cell death gene *ced-3* encodes a protein similar to mammalian interleukin-1β-converting enzyme. *Cell* 75: 641-652.

40. Zambrano, M. M., Siegele, D. A., Almiron, M., Tormo, A., and Kolter, R. (1993) Microbial competition: *Escherichia coli* mutants that take over stationary phase cultures. *Science* 259: 1757-1760.

41. Zambrano, M. M., and Kolter, R.(1996) Gasping for life in stationary phase. *Cell* 86: 181-184.

This paper received the young scientist award for the Best Paper presentation at the National Conference on Environmental Biology held at Saurashtra University, Rajkot, during October 17-18, 2002. This research work was also one of the twenty-five selected presentations at Humboldt Kolleg symposium (sponsored by Alexander von Humboldt Foundation, Germany) on Genetics & Human Health, held at Manipal during October 29-31, 2003 by young doctorates/researchers working in the area related to genetics and human health from all over the country.

About the authors ...

Dr Satyendra Gautam joined the Food Technology Division in 1995 after graduating from the 38th batch of Training School as a biology-radiobiology trainee. Dr Gautam was awarded Ph.D. degree in Biochemistry by University of Mumbai under the guidance of Dr A. K. Sharma, Head, Food Technology Division. The topic of his doctoral research was "Studies on Xanthomonas campestris pv. glycines with special reference to its programmed cell death". His current research interests include mechanism and regulation of bacterial programmed cell death, and radiation preservation of foods using gamma radiation.

Dr Arun Sharma joined the 19th batch of BARC Training School in 1975 after a Master's Degree in Microbiology from National Dairy Research Institute, Karnal. He was awarded Ph.D. degree in Biochemistry by University of Mumbai. Dr Sharma was a post-doctoral fellow at the University of California, USA. At present, Dr Sharma is Head, Food Technology Division, and Project Manager, Food Irradiator Project. He has made substantial contribution in the field of food irradiation with special reference to microbiological safety of irradiated foods, irradiation of spices and food biotechnology. Besides, Dr Sharma has also immensely contributed in the research areas of mycotoxins control in foods, host-pathogen interaction in plant pathology, and bacterial programmed cell death.

A RAPID PLATE SCREENING TECHNIQUE FOR EXTRACELLULAR RIBONUCLEASE PRODUCING STRAINS

R.C. Hole   and R.S. Singhal
Food and Fermentation Technology Department,
Institute of Chemical Technology, University of Mumbai

and

J.S. Melo and S.F. D'Souza
Nuclear Agriculture & Biotechnology Division
Bhabha Atomic Research Centre

Abstract

A plate assay is described to detect extracellular RNase producing strains. RNA is used in the Petri dish assay for the determination of RNase activity. After growth of the organisms, the agar plate is flooded with a RNA precipitant and enzyme activity is shown by clear zones (halos) around the colonies. The simultaneous use of specific RNase inhibitor like diethyl pyrocarbonate allow the specificity of enzyme to be determined. Besides the efficiency of this technique has also been tested to select mutants during strain improvement.

Introduction

Ribonuclease has gained importance in recent times due to their therapeutic effects (Newton *et al*., 1992). Besides, RNase finds extensive applications as an analytical enzyme, for the determination of structure, nearest neighbor sequence and sequence of RNA (Sambrook and Russell, 2001). It has been used in molecular biology for the isolation of DNA, RNase protection assays and for mapping single base mutations in RNA. RNase has also been used for the synthesis of oligonucleotides and in the manufacture of nucleotides 2',5'-cyclic phosphates (Rowe and Smith, 1972; Chacko and Shankar, 1998).

Screening of microorganisms for selecting suitable strains is an important preliminary step in the production of desired metabolites. Besides, a good plate screening method essentially plays a vital role in the selection of appropriate mutants during strain improvement. (Rowlands, 1984).   In view of the numerous applications of RNase, the work presented, addresses the development of an appropriate selection procedure for extracellular RNase producing strains and mutants.

Materials And Methods

Commercial yeast RNA was purchased from Sisco Research Laboratories, Mumbai, India. Ribonuclease-A Type (I-A) and diethyl pyrocarbonate were procured from Sigma Chemical Co, St. Louis, MO, USA. Uranyl acetate was a product of Loba Chemie, Mumbai, India. Pre-sterile disposable Petri plates, potato dextrose agar [PDA] and nutrient agar [NA] were purchased from Hi Media Laboratories Pvt. Ltd, Mumbai, India, and 0.22 μm sterile disposable filters were procured from Millipore Corporation, USA All other chemicals used were of analytical grade.

Strains

The microbial strains (fungi and bacteria) used for screening, some of which were known

RNase producers, were procured from culture collections. The fungal strains were routinely maintained on 2 % potato dextrose agar slants and bacterial strains on 2 % nutrient agar slants.

Preparation of media for screening

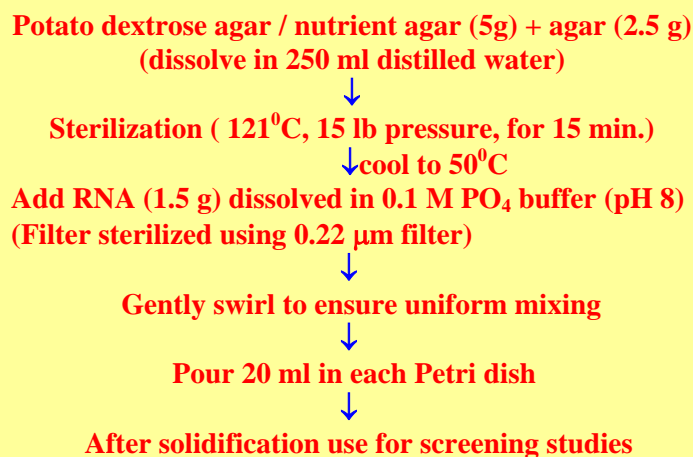Media was modified for use, as shown in the following schematic representation (Fig. 1)

Potato dextrose agar / nutrient agar (5g) + agar (2.5 g) (dissolve in 250 ml distilled water)
↓
Sterilization (121^{0}C, 15 lb pressure, for 15 min.)
↓cool to 50^{0}C
Add RNA (1.5 g) dissolved in 0.1 M PO$_4$ buffer (pH 8) (Filter sterilized using 0.22 μm filter)
↓
Gently swirl to ensure uniform mixing
↓
Pour 20 ml in each Petri dish
↓
After solidification use for screening studies

Fig.1 Scheme for preparing screening medium for RNase

Test procedure / Selection of mutants

Different cultures (fungi, bacteria and mutants) were screened for producing extracellualr RNase, by point inoculating onto respective plates containing modified agar medium as indicated above. The plates were than incubated at required temperatures until growth was clearly visible. After incubation the plates were flooded with 3 ml of the precipitant (perchloric acid) and left to stand for 5 min. The plates were then visualized for transparent halos formed around the grown colonies, against an opaque background.

Optimization of parameters

a) *Linearity*: A stock solution of RNase-A (5 mg/ml) was prepared in 0.1 M acetate buffer (pH 5) which was then diluted to obtain concentrations in the range of 1–5 mg/ ml. With the help of cork borer, 6 wells were punched into the solidified medium in the plates. Each of the RNase-A dilutions (0.1 ml) was dispensed into the wells with 0.1 ml of buffer in one well as a control. Three such identical plates were then incubated at 37^0 C for different time intervals; 30 min, 60 min and 90 min respectively. The plates were overlaid with 3 ml of 1 M perchloric acid for 5 min. Subsequently, the precipitant is poured off and then the zone diameters were measured and plotted as a function of RNase-A concentration.

b) *Selectivity*: Diethyl pyrocarbonate (0.2 ml) a known inhibitor of RNase (Rangarajan et al., 1999) was incorporated aseptically into the plate by spreading it on the surface of solidified medium. The strains showing good RNA zone clearance in screening experiment mentioned above, were point inoculated on this plate and observed for the appearance of zone of clearance.

Mutagenesis using gamma radiation

Rhizopus stolonifer-880 a known producer of RNase was attempted for overproduction of enzyme by induced mutagenesis. Spore suspension (10 ml) of the parent strain whose spore count was adjusted to 10^6 CFU/ml, was dispensed in 6 sterile test tubes. It was then incubated at 50^{0}C for 10 min and exposed to γ radiation (Co^{60}) in a Gamma 220 Cell for different time intervals corresponding to 0.5 to 2.5 KGy. After exposure, the tubes were immediately kept in dark to prevent photo-reactivation. Exposed spores (0.1 ml) were serially diluted and the respective dilution (0.1 ml) were plated on 2% potato dextrose agar plates. The plates were incubated at 30^{0}C for 20 h. Percentage survivors were calculated by considering the colonies developed on control plates as 100 per cent. Spores unexposed to radiation were considered as control.

Fermentation conditions

An amount of 1.0 ml of the spore suspension containing 4 x 10^6 CFU/ml was added to 500 ml Erlenmeyer flasks containing 100 ml of the optimized production medium for RNase (Chacko *et al.*, 1996). The flasks were incubated at 30^{0}C on a rotary shaker at 150 rpm for 6 days. Aliquots were withdrawn every 24 h. and monitored for enzyme activity. The wild strain grown in a similar manner was considered as control. The mutant was sub cultured every week for five weeks to ascertain its stability.. After each subculture the mutant was checked for its fermentation profile.

Ribonuclease assay

RNase activity was assayed by the method of Tomoyeda et al. (1969).

Results and discussion

Plate assays for screening of strains producing proteases, lipases and polysaccharases have been reported (Hagerman *et al.*, 1985; Mala *et al.*, 2001; Ruijssenaars and Hartmans, 2001). Wilson (1969) described the use of toluedine blue for detection of RNase after polyacrylamide gel electrophoresis. However, the requirement for thorough destaining with 5 % acetic acid repeatedly, makes its use unsuitable for the screening of RNase producing strains. A technique providing a rapid assay would be more useful. The use of RNA followed by its precipitation serves as an indicator for RNase production in an agar medium and provides the basis for a rapid and sensitive test in the present study. RNA in the plate media is present in soluble form and can be precipitated by flooding the plate with a precipitant. The method has been adapted from the liquid

enzyme assay described by Tomoyeda *et al.* (1969). As seen in Fig. 2. strains like *Rhizopus stolonifer* 880, *Aspegillus niger* 660 and *Escherichia coli* JA-200 which are known producers of RNase and an unknown producer *Bacillus megaterium* developed halos, as precipitation of undegraded RNA gives the plate an opaque milky white appearance, whereas degradation zones are visible as clear haloes.
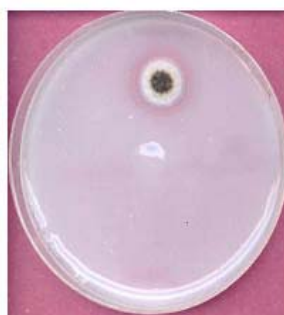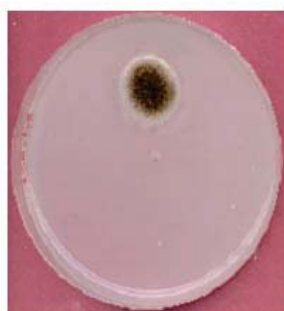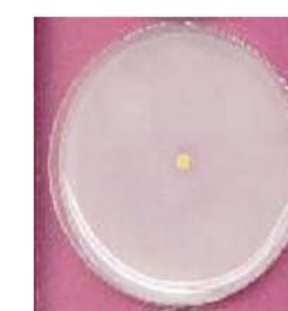

Aspergillus niger 660   *E. coli* JA 200

Rhizopus stolonifer 880   *Bacillus megaterium*

Rhizopus oryzae   *Streptococcus sp.*

Fig. 2 Plate assay for screening RNase producing strains

The diameter of the halos provides a preliminary quantification of the enzyme activity produced. Such studies carried out by Breccia et al. (1995) reported that the diameter of the transparent halos around colonies, plotted against the xylanolytic activity of two different xylanases showed a rectangular hyperbole. Further, they have suggested plotting a double reciprocal graph for better estimation of enzyme activity. However, more quantitative results can be obtained by using liquid samples of enzyme placed in wells in an agar plate containing the substrate. Using the method there is direct relation between log enzyme concentration and the diameter of cleared zone (Teather and Wood, 1982). In our studies as seen in figure 3, a linear relationship exists between the cleared zone diameter and concentration of enzyme within the range of enzyme concentration studied and also with respect to the time of assay, thus validating the plate technique for estimating enzyme activity.
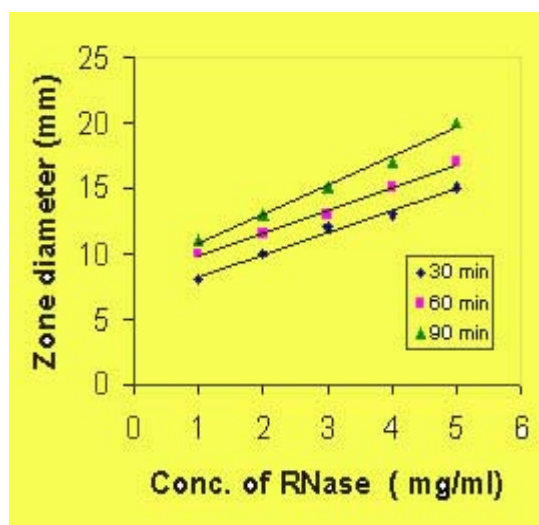

Fig. 3: Linearity curve for RNase plate assay

The validation of analytical method with respect to selectivity or specificity is also an important criteria. Some of the authors have carried out studies with respect to the specificity of the substrate being acted upon by the enzyme as in the case of cellulase and alginate lyases (Hankin and Anagnostakis, 1977; Gacesa and Wusteman,

1990). Also studies have been reported regarding the specificity of the precipitant. Ethanol is generally used for precipitation of the polysaccharides, however not all polysaccharides precipitate equally efficiently. Alternatively more efficient precipitants such as cetyltrimethylammoniumbromide or the use of dyes that show strong interaction with polysaccharides containing contiguous β-$(1\rightarrow4)$ or β $(1\rightarrow3)$ D-glucans have been reported (Hankin et al., 1971; Teather and Wood, 1982). To confirm that the zone of clearence, in the present study is specifically due to the action of RNase, diethyl pyrocarbonate (DEP), a potent irreversible inhibitor of RNase was incorporated into the RNA plate. The plate technique is specific for RNase as all the strains which showed clear zone of hydrolysis in the test medium, failed to produce the halo around the colonies, in the presence of DEP.

The technique has also been extended to screen for mutant strains. Strain improvement of microorganisms is an important requisite for enzyme production because the production levels of these enzymes could be quite low (Mala *et al*., 2001). Even with the advent of newer techniques, the traditional method of strain improvement by mutagenesis and selection on basis of direct measurement, the so called "random screening" still plays a central role as a reliable and cost effective procedure (Rowlands, 1984). Several successful attempts have been reported with the use of physical mutagens such as radiation like γ-rays, X-rays, UV rays etc. and chemical mutagens such as nitrous acids, alkylating agents and nitrosoguanidine. Since *Rhizopus stolonifer* is reported to be resistant to radiation with a D_{10} of 1 KGy (Chang and Lee 1980) and that the combination of heat and radiation reduces the D_{10} value to approximately half (Robbertse et al. 1983), the protocol for mutagenesis of *Rhizopus stolinfer* 880 incorporated heat treatment at 50^0C for 10 min followed by irradiation at various doses. Higher irradiation dose decreased the

percent survival. The D_{10} value was found to be 0.5 KGy which is in agreement with the report of Robbertse *et al*., (1983). Mutant selection was performed using the plate technique based on the increased zone size (Fig. 4). In order to confirm the characteristics of the mutant, the fermentation profile was examined (Fig.5).
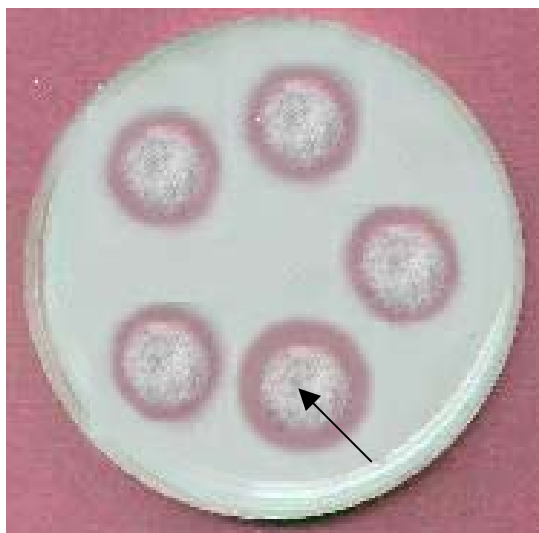

Fig.*4 Plate assay for screening mutants. Fungal colony indicated by arrow represents the mutant of Rhizopus stolonifer 880*
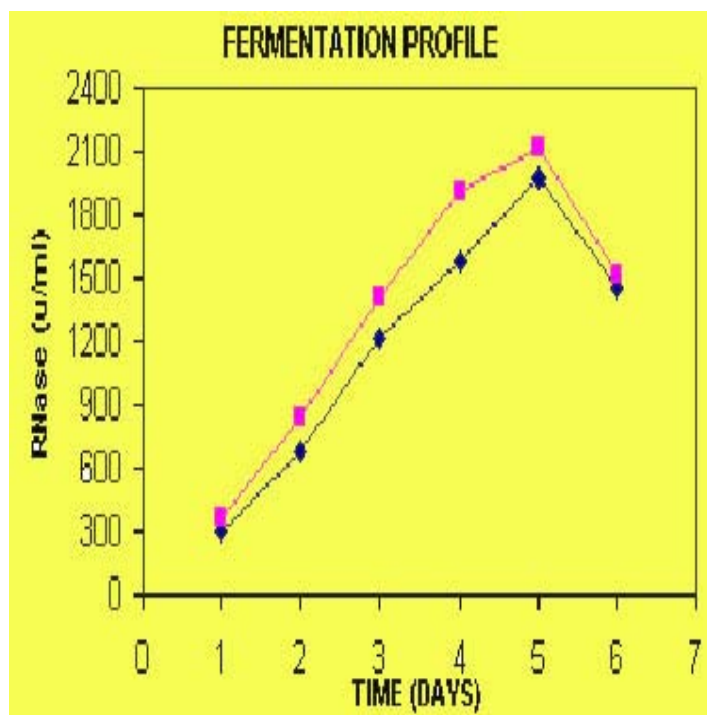

Fig.5 *Fermentation profile of parent (♦) and mutant (■) strain of R. stolonifer*

From studies carried under identical conditions, it is evident that the mutant gave an increased enzyme activity from the first day and showed an activity of 1907 U/ml on the fourth day. In comparison the parent strain could produce the corresponding amount of enzyme only on the fifth day, thus reducing the fermentation time by 20 percent. Stability of the strain was also confirmed as fermentation profile did not change to any significant extent over the five week study period. This study thus confirms the ability of this technique to screen for strains and isolate mutants producing extracellular RNase.

Conclusion

The plate technique described herein for screening RNase producing strains is simple and rapid. Besides the method is specific and can be used for both qualitative and quantitative screening. It has also been extended to select mutants.

References

1. Breccia, J.D., Castr, G.R., Balgori, M.D. and Sineriz, F. (1995) Screening of xylanolytic bacteria using a color plate method. *J. Appl. Bacteriol*. **79**, 469-472.

2. Chacko, R., Deshpande, M., Shankar, V. (1996). Extracellular ribonuclease production by *Rhizopus stolonifer*: influence of metal ions. *Current Microbiol.*, **32**, 246 – 251.

3. Chacko, R. and Shankar, V. (1988) Extracellular ribonuclease from *Rhizopus stolonifer*: characteristics of an atypical guanylic acid preferential enzyme from ribonuclease T_2 family. *Biochim. Biophys. Acta*. **1379**, 262-272.

4. Chang, H.G. and Lee, B.H. (1980) Radiation sensitivity of food decay fungi. *Kor. J. Microbiol*. **18(1)**, 1-6.

5. Gacesa, P. and Wusteman, F.S. (1990). Plate assay for simultaneous detection of alginate lyases and determination of substrate specificity. Appl. Environ. Microbiol. **56(7)**, 2265-2267.

6. Hagerman, A.E., Blau, D.M. and McClure, A.L. (1985) Plate assay for determining the time of production of proteases, cellulases and pectinases by germinating fungal spores. Anal. Biochem. **151(2)**, 334-342.

7. Hankin, L., Zucker, M. and Sands, D.C. (1971). Improved solid medium for the detection and enumeration of pectolytic bacteria. Appl. Microbiol. **22(2)**, 205-209.

8. Hankin, L. and Anagnostakis, S.L. (1977). Solid media containing carboxymethylcellulose to detect C_x cellulase activity of micro-organisms. J. Gen. Microbiol. **98**, 109-115.

9. Mala, J.G.S., Kamini, N.R. and Puvanakrishnan, R. (2001). Strain improvement of Aspergillus niger for enhanced lipase production. J. Gen. Appl. Microbiol. **47**,181-186.

10. Newton, D., Ilercil, O., Laske, D., Odefield, E., Rybak, S. and Youle, R. (1992) Cytotoxic ribonuclease chimeras: targeted tumoricidal activity in vitro and in vivo, J. Biol. Chem., **267**, 1972-1978.

11. Rangarajan, S. Chacko, R. and Shankar, V. (1999). Active site characterization of RNase Rs from Rhizopus stolonifer: involvement of histidine and lysine in catalysis and carboxylate in substrate binding. Biochim. Biophys. Acta. **1428**, 372-380.

12. Robbertse, P.J., Du-Tolt, T.L.. Van-der-Merwe, L.J., Koekemoer, M.L. and Ellers, I.M.I. (1983) Radiation resistence of Rhizopus stolonifer. South African J. Sci. **79(5)**, 173-174.

13. Rowe, M. and Smith, M. (1972). Synthesis of oligonucleotides with ribonucleases-T_1, Biochim. Biophys. Acta, **281**, 338-343.

14. Rowlands, R. T. (1984). Industrial strain improvement: mutagenesis and random screening procedures, Enzyme Microb. Technol., **6**, 3 –10.

15. Ruijssenaars, H. and Hartmans, S. (2001) Plate screening methods for the detection of polysaccharase-producing microorganisms, Appl. Microbiol. Biotechnol., **55**, 143-149.

16. Sambrook, J. and Russell, D.W. (2001) Molecular cloning: A laboratory manual vol 1 3rd edition, Cold Spring Harbour Press, N.Y.

17. Teather, R.M. and Wood, P.J. (1982) Use of congo red-polysaccharide interactions in enumeration and characterization of cellulolytic bacteria from the bovine rumen. Appl. Environ. Microbiol. **43(4)**, 777-780.

18. Tomoyeda, M., Eto, Y., Yoshino, Y. (1969). Studies on ribonuclease produced by Rhizopus sp. 1. Crystallization and some properties of the ribonuclease. Arch. Biochem. Biophys., **131**, 191 – 202.

19. Wilson, C. W. (1969). A rapid staining technique for detection of RNase after polyacrylamide gel electrophoresis, Anal. Biochem.**, 31**, 506 – 511.

20. Zitomer, S. and Eveleigh, D. (1987) Cellulase screening by iodine staining: an artifact, Enzyme Microb. Technol., **9**, 214-216.

This paper was given the Best Poster Paper award at the 11th Annual Research Papers/Poster Presentation Competition, held at Bhavan's College, Mumbai, on February 1, 2003

About the authors ...

Mr. Rahul C. Hole obtained his M.Sc. (Tech.) degree in Bioprocess Technology and presently he is a Senior Research Fellow pursuing Ph.D. (Tech.) degree in Pharmacology in Department of Pharmaceutical Sciences & Technology, Institute of Chemical Technology, University of Mumbai

Dr Rekha S. Singhal *is a Senior Lecturer in the Department of Food & Fermentation Technology, Institute of Chemical Technology. She is a research guide for M.Tech and Ph.D. (Tech.) in Food Technology and Bioprocess Technology. Her research interests are in food quality, food chemistry, food processing, biopolymers, lipid chemistry, enzyme modifications and downstream processing. She has over 100 international research publications, 15 book chapters and over 10 reviews. She is editor for Bombay Technologist and UICT Patrika and is a referee for national and international journals.*

Dr S. Melo *joined BARC in 1984 and is posted in the Enzyme and Microbial Technology Section of Nuclear Agriculture & Biotechnology Division, BARC. He obtained his Ph.D. (Biochemistry) degree from Mumbai University in 1990. In the field of bioprocessing, he has developed a number of novel techniques for immobilization of enzymes and cells and preparation of coimmobilizates. His current field of interest is in bioremediation of inorganic and organic pollutants. He has also contributed to science education as an invited resource person at National workshops and as an invited guest faculty member at UICT and IIT. He has also guided students for their project work. He has to his credit several publications in International Journals, Symposiums and Workshops.*

Dr S.F. D'Souza *graduated from the 15th batch of the BARC Training School (Biology & Radiobiology) and is currently the Head of the Nuclear Agriculture and Biotechnology Division of BARC. His major research interest has been in the field of Enzyme and Microbial Technology with special reference to immobilized cells for use in bioprocessing, biosensors and bioremediation. He has to his credit over 150 scientific papers and invited reviews in reputed International / National journals / books. He is a member / expert at National Scientific committees, member of the editorial board of scientific journals and has been invited to deliver talks / key note lectures, chair scientific sessions at various scientific forums. He has also contributed significantly to science education as an invited resource person at National workshops and short term courses as well as UGC refresher courses as an invited guest faculty member, as a Ph.D., M.Sc. examiner (Univ. / IIT) and as a member of the board of studies and research advisory committees and has guided a number of students for Ph.D. and M.Sc. He was presented the prestigious AMI- Louis Pasteur award (2001) for his significant contribution to the field of Microbiology and has been honored as a Fellow of the National Academy of Science (1993), Fellow of the Association of Food Scientists & Technologists (1999) and Fellow of the Maharashtra Academy of Science (2001).*

RADIOPROTECTIVE PROPERTIES OF BAICALEIN

J.C. Tilak and T.P.A. Devasagayam
Radiation Biology & Health Sciences Division
Bhabha Atomic Research Centre

Abstract

Radiation is an important source of free radicals in living systems. Ionizing radiations such as γ-rays exert their biological effects through generation of reactive oxygen species and the resultant damage to DNA and cellular membranes. Several natural compounds, especially with antioxidant abilities are known to be radioprotective. Baicalein (5,6,7-trihydroxy-2-phenyl-4H-1-benzopyran-4-one), a naturally occurring flavone, present in some Indian and Chinese medicinal plants (such as Terminalia arjuna Scutellaria rivularis, Scutellariae radix and Scutelleria baicalensis) has antioxidant effects. We have examined the radioprotective effects of baicalein using plasmid pBR322 DNA, calf thymus DNA and rat liver mitochondria as model systems. The assays used are strand-break estimation and DNA binding for measuring DNA damage besides protein oxidation, protein hydroperoxide formation, glutathione peroxidase, glutathione reductase, superoxide dismutase, succinate dihydrogenase and lipid peroxidation for estimating membrane damage. For estimating lipid peroxidation different products were used. Significant membrane damage was observed with 450 Gy and strand break formation with 6 Gy. Our results indicate that baicalein is a potent radioprotector at micromolar (5-50) levels. The protective effect, at 5 μM, was 80% against formation of thiobarbituric acid reactive substances (TBARS) and 50% against lipid hydroperoxide. The protective ability against protein carbonyl formation was 50% and protein hydroperoxide formation 85% at the same concentration. Similar protective effects were also observed against damage to glutathione peroxidase and superoxide dismutase. A concentration dependent effect also was seen with most of the parameters examined. Single-strand break formation induced by radiation also was accentuated with baicalein. It also inhibited the DNA binding caused by radiation. In conclusion our studies reveal the potent radioprotective effect of the natural compound baicalein.

Introduction

The deleterious effects of ionizing radiation of low energy transfer (LET), in biological systems are mainly mediated through the generation of oxygen derived free radical intermediates (Von Sonntag, 1987). Besides the beneficial role of these free radicals in signal transduction, phagocytosis and apoptosis, it is established that excess generation of ROS is involved in structural alterations of cellular molecules leading to cytotoxicity and cell death. Oxidative damage to cellular components can have serious effects leading to

various diseases and ageing. This results in a variety of biological phenomena such as mutation, carcinogenesis, ageing, inflammation, ischemia-reperfusion injury, atherosclerosis, diabetes mellitus and neurodegenerative disorders (Packer and Ong, 1998). Hence in recent years much attention has been given to the subject especially in the field of clinical medicine. Oxidative damage to proteins as assessed by carbonyl and hydroperoxide formation has been implicated in the etiology of many physiological disorders and diseases (Stadtman and Berlett, 1997).

Among the subcellular organelles mitochondria are major sites of oxidative damage. It can lead to membrane permeability transition, cytochrome c release and dysfunction of mitochondria associated with decrease in membrane potential, respiratory control etc. (Yoshikawa et al, 2000). Hence the mechanistic study of membrane damage induced by ROS in relation to various human ailments and its prevention by antioxidants from natural dietary sources is very important.

There are several Indian medicinal plants known for their beneficial therapeutic effects, which also might have antioxidant properties (Tilak et al, in press). Several natural compounds from plants exhibit radioprotection mainly due to antioxidant properties (Goel et al, 1998). Hence we have focused our studies on baicalein (5,6,7-trihydroxy-2-phenyl-4H-1-benzopyran-4-one), a naturally occurring flavone, present in some Indian and Chinese medicinal plants such as *Scutellaria baicalensis*, *Scutellaria rivularis*, *Terminalia arjuna* etc. It has been attributed to have several therapeutic effects such as anti-allergic, anti-proliferative, antitumor, anti-genotoxic and antioxidant properties (Gao et al., 1996; Shieh et al., 2000). However, the radioprotective effects of baicalein and the mechanisms underlying its antioxidant ability are still not determined. In this regard, we have examined the radical scavenging activities and membrane protective abilities of baicalein. To this end we have chosen rat liver mitochondria comprising of lipid and proteins besides plasmid DNA (pBR322) for studying radiation-induced damage to these important biological molecules and its possible prevention by baicalein.

Materials and Methods

Materials

Catalase, butylated hydroxy toluene (BHT), 5,5'-dithio-bis(2-nitrobenzoic acid) (DTNB), dinitrophenyl dydrazine (DNPH), ethylene diamine tetra acetic acid (EDTA), ethanol, ethyl acetate, ferrous ammonium sulphate, Folin-Ciocalteu reagent, glutathione reductase, glutathione (oxidized and reduced), guanidine hydrochloride, nicotinamide adenine dinucleotide phosphate: reduced (NADPH), perchloric acid, potassium phosphate (monobasic and dibasic), sodium carbonate, 1,1,3,3-tetraethoxypropane, 2-thiobarbituric acid, tert butyl hydroxide, trichloroacetic acid, Triton X 100 and xylenol orange were purchased from Sigma Chemical Co. pBR 322 plasmid DNA was purchased from Banglore Genei Ltd. Baicalein was purchased from Aldrich Chemical Co. Other chemicals used in our studies were of the highest quality commercially available from local suppliers.

Methods

Isolation of mitochondrial fraction from rat liver: Three months old female Wistar rats (weighing about 250 ± 20 g) were used for the preparation of mitochondria. The mitochondrial pellet was washed thrice with 5 mM potassium phosphate buffer, pH 7.4, to remove sucrose (Devasagayam, 1986). Protein was estimated and pellets were suspended in the above buffer at the concentration of 10 mg protein/ml.

Exposure of rat liver mitochondria to radiation and agents for inducing oxidative stress: Oxidative damage was induced by exposure to γ-rays from a ^{60}Co source (dose rate 65 Gy/min, Bhabha Atomic Research Centre, Mumbai). The mitochondria (final conc. 2 mg/ml) were suspended in 5 mM phosphate buffer (pH 7.4) and exposed to radiation with and without extracts or baicalein. The dose selected was 450 Gy at which optimum damage is obtained. For treating plasmid DNA, 6 Gy dose was selected which gives the optimum damage. The unexposed samples served as controls.

Biochemical assays: After exposure of mitochondria to oxidative stress, the products of lipid peroxidation were measured as thiobarbituric acid reactive substances (TBARS)

and lipid hydroperoxides (LOOH). TBARS were measured immediately after the treatment. On addition of TBA reagent comprising of 0.5% thiobarbituric acid, 10% trichloroacetic acid, 2 mM EDTA, 0.63 M hydrochloric acid and the reaction mixtures were boiled for 20 min. The pink coloured TBARS formed were estimated spectroflurometrically using excitation at 532 nm and emission at 553 nm, after accounting for appropriate blanks. Malonaldehyde standard was prepared by the acid hydrolysis of tetramethoxypropane (Devasagayam, 1986). The lipid hydroperoxides were measured by using FOX (Ferrous Oxidation in Xylenol orange) II method (Sodergren et al, 1998). FOX II reagent contains 90% (v/v) methanol, which facilitates lipids to solubilize. Concentration of LOOH is then calculated with the help of standard graph using H_2O_2. FOX II gives ε for hydroperoxides as 4.46×10^4 $M^{-1}cm^{-1}$.

We have studied oxidative damage to proteins using protein carbonyl (Palamanda and Kehrer, 1992), protein hydroperoxide (Platt and Gieseg, 2002) and total protein thiol (Santos et al, 1998) assays. The superoxide dismutase (SOD) activity was also estimated (Das et al., 2001). We also examined succinate dehydrogenase acitivity (Caplan and Greenwalt, 1968), glutathione reductase and glutathione peroxidase activity (Smith and Levander, 2002). Data were presented as mean $\pm$ SE. Significance of inter-group differences was determined by Student's *t* test (two-tailed). A *p* value of p < 0.05 was considered statistically significant.

Results

Fig. 1 presents the data on the inhibition of γ-radiation-induced lipid peroxidation in rat liver mitochondria by baicalein. The enhanced concentration of LOOH and TBARS obtained at the optimum dose of 450 Gy was reduced when irradiation was carried out in presence of baicalein. Baicalein at a concentration of 5 μM shows 34 % protection against LOOH formation (Fig. 1a). However, in case of TBARS, it gives

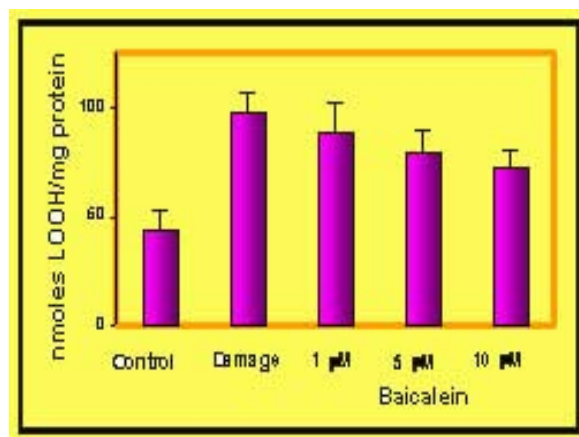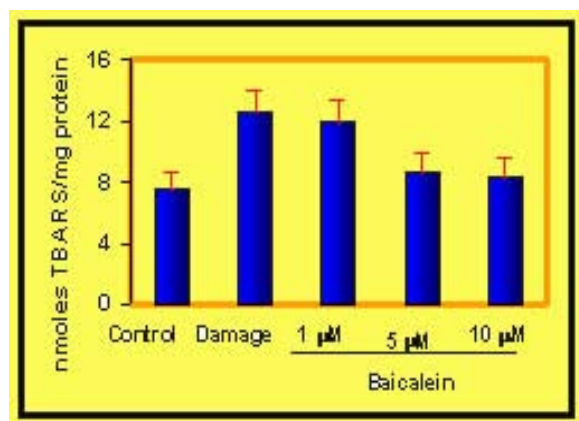74 % protection from radiation-induced damage (Fig. 1b).

Fig. 1a

Fig. 1b

The results on protein damage induced by γ-radiation and its inhibition by baicalein are shown in Fig. 2. Ionizing radiation at 450 Gy could increase the formation of protein carbonyls and protein hydroperoxides (Fig. 2a and 2b).

The inhibitions obtained by 5 μM baicalein were 56 % and 71 % in case of protein carbonyl and hydroperoxide formation, respectively. Decrease of total protein thiol was observed after an exposure to radiation (Fig. 2c). While the same irradiation experiment was carried out in presence of baicalein, protein thiol levels were restored to the control values as shown in Fig. 2c. Even presence of low concentrations of

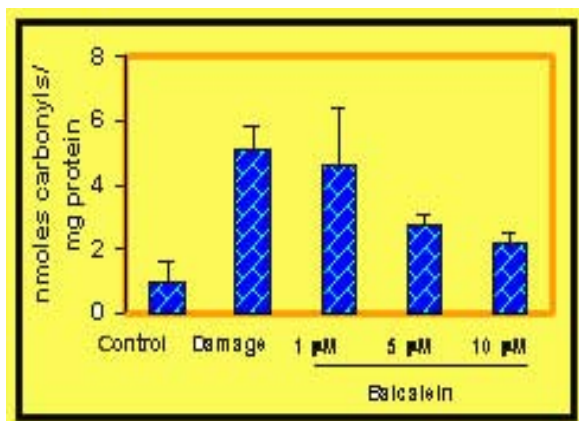baicalein (1 μM and 5 μM) protects against thiol damage to the extent of 26 % and 62 %, respectively.

Fig. 2a
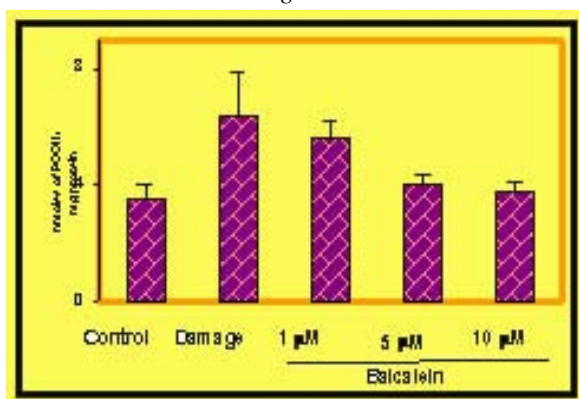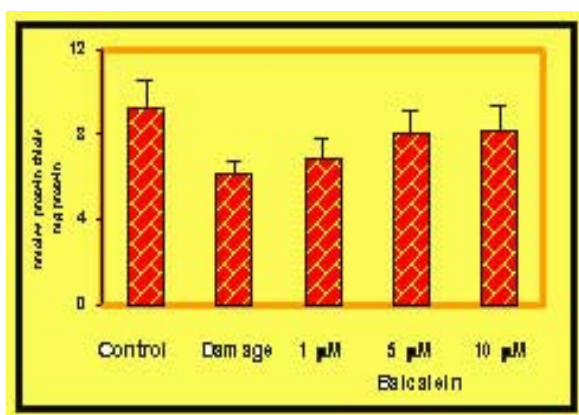

Fig. 2b

Fig. 2c

Fig. 2 Effect of different concentrations of baicalein on γ-raidation induced protein carbonyl formation (Fig. 2a), protein hydroperoxide (Fig.2b) and total protein thiol (Fig. 2c) in rat liver mitochondria at an optimum dose of 450 Gy.

Fig. 3 demonstrates the γ-radiation-induced depleted levels as well as protection by baicalein of enzymes in rat liver mitochondria.

These include antioxidant enzymes such as superoxide dismutase (SOD), glutathione peroxidase (GPx) and glutathione reductase (GR) besides the mitochondrial marker enzyme, succinate dehydrogenase (SDH). It can be seen from Fig. 3a, that there is a significant reduction of SOD actiivity following 450 Gy of γ-radiation dose. Baicalein, when present at the time of irradiation could effectively restore the depleted activity back to the control level, in a concentration dependent manner. The percentage protection obtained by baicalein at the concentration of 1, 5 and 10 μM were 32, 54 and 78 % respectively.
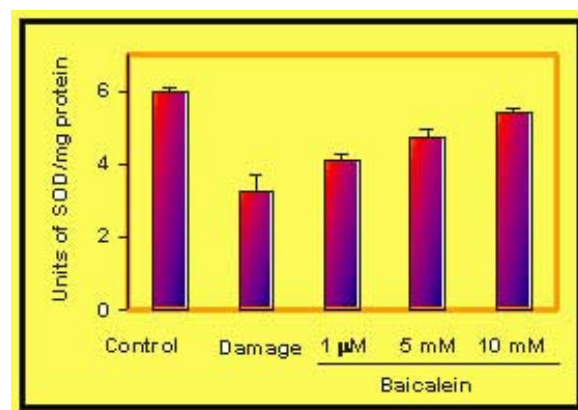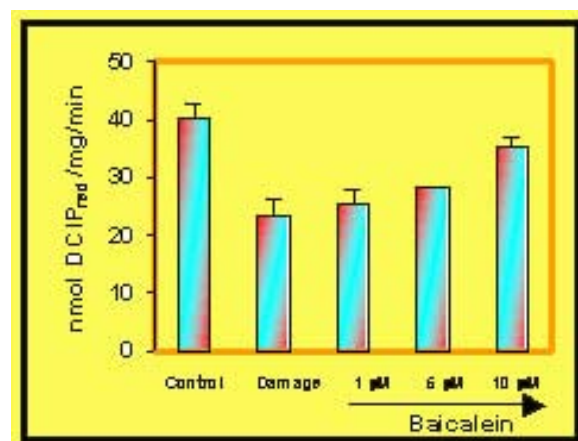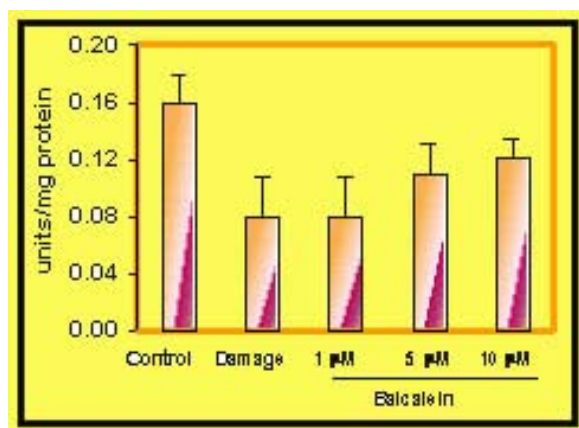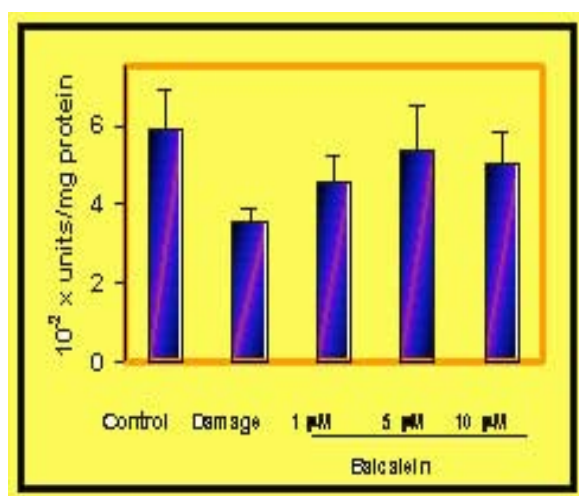

Fig. 3a

Fig. 3b

Fig. 3c

Fig. 3d

Fig. 3 *: Effect of different concentrations of baicalein on γ-raidation induced LOOH formation (Fig. 1a) and TBARS formation (Fig.1b) in rat liver mitochondria at an optimum dose of 450 Gy.*

The results on depletion of SDH activity and its restoration by baicalein are presented in Fig. 3b. The concentration of 10 µM baicalein could restore SDH activity by 70 %. In Fig. 3c, γ-radiation-induced depletion of glutathione peroxidase deactivation was shown. This was brought back to control levels by baicalein in a concentration dependent manner, 10 µM baicalein giving the protection of 57 %. The data on the activity of glutathione reductase is presented in Fig. 3d. At the concentration of 5 µM, baicalein afforded the highest recovery of GR by 77 %.
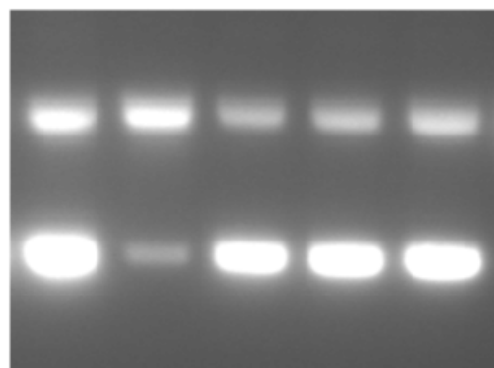

Fig. 4

1. Lane 1: Control (pBR 322)
2. Lane 2: After irradiation (6 Gy)
3. Lane 3: Radiation + 5 µM Baicalein
4. Lane 4: Radiation + 10 µM Baicalein
5. Lane 5: Radiation + 50 µM Baicalein

Fig. 4 shows the pattern of agarose gel electrophoresis of pBR322 DNA exposed to γ-radiation (dose = 6 Gy) in the presence and absence of baicalein at different concentrations. On exposure of plasmid to γ-radiation the intensity of the band corresponding to form II (lane 2) was increased. Addition of baicalein (1, 5 and 10 µM in lane 3, 4 and 5) reduced the increase in form II.

Discussion

In biological systems, oxidative stress can be generated using various physical/chemical agents. Among them, ionizing radiation such as γ-rays is an important source of reactive oxygen species. The exposure of biological systems to radiation results in radiolytic cleavage of water yielding $^{\cdot}OH$, $^{\cdot}H$, e^{-}_{aq} etc. In the presence of oxygen even $O_2^{\cdot-}$, H_2O_2, $^1O_2$ are also produced. These free radicals especially, $^{\cdot}OH$ and $LOO^{\cdot}$, can initiate lipid peroxidation. Ionizing radiation induces lipid peroxidation, protein damage, DNA damage and cell death (Leyko and Bartosz, 1986; Noda et al, 1993). Therefore any agent that can protect against such alterations can provide protection against radiation damage.

In this study, we have demonstrated that ROS induce significant lipid peroxidation in the model system i.e. rat liver mitochondria as measured by LOOH, an unstable intermediate, which further breaks down to stable aldehydes and react with thiobarbituric acid (TBA) to form thiobarbituric acid reactive substances (TBARS), the final stable end product (Girotti, 1990).

Our present investigations demonstrated radiation-induced lipid peroxidation in mitochondria by estimating two products of peroxidation namely LOOH, and TBARS. Our results have shown that baicalein when present during radiation exposure, can prevent damage to the cell membranes. Baicalein, a flavone and an active ingredient of *T. arjuna*, efficiently protects mitochondrial membrane against radiation damage. At concentration of 5 μM, it inhibits LOOH and TBARS formation due to radiation exposure by 34 and 74 %, respectively. Apart from enhancing lipid damage, radiation treatment leads to protein damage in terms of protein carbonyls, protein hydroperoxides and depletion of total protein thiols. Baicalein was also shown to protect against damage to various mitochondrial enzymes such as succinate dehydrogenase, superoxide dismutase, glutathione peroxidase and glutathione reductase. 5 μM baicalein was shown to protect against γ–radiation-induced single strand breaks in DNA.

Baicalein has been reported to possess lipid peroxidation inhibitory activity (Gao et al, 1996; Masataka and Keiko, 1998). It has also been reported to scavenge $^.$OH, DPPH$^{.+}$ and alkyl radicals (Gao, 1998) and $O_2^{.-}$ and H_2O_2 (Shao et al, 1999). Earlier, our studies have shown that baicalein effectively scavenges DPPH, ABTS and peroxyl radicals and also possesses ferric reducing activities. In our previous study, we evaluated the ability of baicalein to react with radiation derived reactive species such as $^.$OH, $CCl_3OO^.$, $LOO^.$ etc. This activity might contribute to the observed radioprotection in the present study. We observed significant reduction in lipid peroxidation and protein and enzyme damage in presence of 5-10 μM baicalein. The present observations suggest that baicalein is a potent radioprotector in biological systems.

References

1. Caplan, A.I., Greenwalt, J.W. The effects of osmotic lysis on the oxidative phosphorylation and compartmentation of rat liver mitochondria. *J. Cell Biol.* 36, 15-31, 1968.

2. Das, K., Samanta, L. and Chainy, G.B.N. A modified spectrophotometric assay of superoxide dismutase using nitrite formation by superoxide radicals. *Ind. J. Biochem. Biophys.* 237: 201-204, 2000.

3. Devasagayam TPA. 1986. Lipid peroxidation in rat uterus. *Biochim Biophys Acta* 876: 507-514.

4. Gao D, Sakurai K, Katoh M, Chen J, Ogiso T. Inhibition of microsomal lipid per oxidation by baicalein: A possible formation of an iron-baicalein complex. Biochem. Mol. Biol. Int. 1996, 39, 215-255.

5. Goel HC, Prasad J, Ashok S, Brahma S. Anti-tumour and radioprotective action of *Podophyllum hexandrum*. Indian J. Exp. Biol. 1998, 36, 583-587.

6. Palamanda, A.R., Kehrer, J.P. Inhibition of protein carbonyl formation and lipid peroxidation by glutathione in rat liver microsomes. *Arch. Biochem. Biophys.* 293, 103-109, 1992.

7. Platt, A.A., Gieseg, S.P. Inhibition of protein hydroperoxide formation by protein thiols. *Redox Rep*. 8, 81-86, 2002.

8. Santos, A.C., Uyemura, S.A., Lopes, J.L.C., Bazon, J.A., Mingatto, F.E., Curti, C. Effect of naturally occurring flavanoids on lipid peroxidation and membrane permeability transition in mitochondria. *Free Rad. Biol. Med.* 24, 1455-1461, 1998.

9. Shieh DE, Liu LT, Lin CC. Antioxidant and free radical scavenging effects of baicalein,

10. baicalin and wogonin. Anticancer Res. 2000, 20: 2861-2866.

11. Smith, A.D., Levander, O.A. High throughput 96-well microplate assay for determining specific activities of glutathione peroxidase and thioredoxin reductase. Meth Enzymol. 347, 113-121, 2002.

12. Sodergren, E., Nourooz-Zadeh, J., Berglund, L., Vessby, B. Re-evaluation of the ferrous oxidation in xylenol orange assay for the measurement of plasma lipid hydroperoxides. *J. Biochem. Biophys. Methods* 37, 137-146, 1998.

13. Tilak JC, Devasagayam TPA, Lele RD. Antioxidant activities from Indian medicinal plants: A review – Current status and future prospects. *Res Comm Pharmacol Toxicol* (invited paper, in press).

14. Von Sonnatag, 1987, The Chemical Basis of Radiation Biology, Taylor and Francis, London

15. Packer L, Ong ASH. Biological oxidants and Antioxidants: Molecular Mechanisms and Health Effects. AOCS Press, Champaign, Illinois, 1998

16. Stadtman FR, Berlett BS. Reactive oxygen mediated protein oxidation in ageing and disease. Chem. Res. Toxicol. 1997, 10, 485-494.

This paper won the Outstanding Paper award at the International Meeting of the Society for Free Radical Research (SFRR) – Asia, held at Seoul National University, Seoul, Korea during November 6-8, 2003

About the authors ...

Ms Jai C. Tilak received her M.Sc. degree in Biotechnology from Ruia College, Mumbai, in 2000. She was a topper during her Graduation and Post Graduation from the same college. At present, she is a DAE fellow attached with Radiation Biology and Health Sciences Division, BARC, pursuing her Ph.D. on a project entitled "Studies on the antioxidant effect of natural compounds from Indian medicinal plants."

Dr T.P.A. Devasagayam joined BARC in 1975 after completing BARC Training School in Biology and Radiobiology. At present he is with Radiation Biology and Health Sciences Division of BARC. He is deeply involved in research related to Human Health and Radiation Biology. He has done his Post-Doctoral work at the University of Dusseldorf, Germany and at Wayne State University, USA. He holds the post of Honorary Secretary General of SFRR-India Chapter and also Vice-President of EMSI-India.

ROLE OF MEMBRANE OXIDATIVE DAMAGE AND REACTIVE OXYGEN SPECIES IN RADIATION INDUCED APOPTOTIC DEATH IN MOUSE THYMOCYTES

B. N. Pandey and K. P. Mishra
Radiation Biology and Health Sciences Division
Bhabha Atomic Research Centre

A b s t r a c t

Involvement of membrane damage and reactive oxygen species (ROS) in mechanism of radiation induced apoptotic death were investigated in mouse thymocytes in presence of eugenol, a membrane specific antioxidant from plant sources. The membrane damage in thymocytes by γ-irradiation was determined by measurement of thiobarbituric acid reactive species (TBARS). Generation of reactive oxygen species and apoptosis in irradiated thymocytes was estimated by using fluorescence probes, 2,7-dichlorodihydrofluorescien diacetate (DCH-FDA) and annexin-V method, respectively. The radiation response of thymocytes for ROS generation was found to be dependent on radiation dose and dose rate. DCH-FDA fluorescence appears sensitive for detection of radiation exposures at low doses, and a dose of 0.5 cGy and 0.5 Gy was detected for the dose rate of 0.45 cGy / min. and 0.5 Gy / min, respectively. Lipid peroxidation was inhibited in irradiated (2 Gy) thymocytes with increasing concentrations of eugenol (10-200 μM) treated prior to irradiation. The concentration of eugenol required to inhibit half of the MDA formation (IC_{50}) in irradiated thymocytes was 100 μM. Percentage apoptosis in irradiated thymocytes was significantly inhibited by these antioxidants, which was however, more effective inhibited by lipophilic antioxidants. The results suggest the linkage of radiation generated membrane damage and ROS in the mechanism of apoptotic death in thymocytes.

Introduction

Involvement of plasma membrane and reactive oxygen species (ROS) generated by ionizing radiation in modification of radiation response has increasingly been investigated (1-4). The structural and functional properties of membrane lipids determine and control the transport of various molecules like proteins, enzymes and ions, and do regulate crucial signaling processes controlling the cellular fate. Moreover, the free radicals generated by radiation exposure caused damage to cellular membrane predominantly through indirect damage processes. Substantial evidences have been accummulated to demonstrate the active regulation of cellular radio-sensitivity by the oxidative signals generated on cell membrane. Damage to biomolecules such as proteins and lipids of membrane by radiation induced ROS has been shown to initiate cascade of biochemical reactions and signaling events resulting in loss of cellular functions and eventually cell death (5-8). Direct evidence has been reported to demonstrate the active involvement of gap junction communication in α-particle irradiated human normal fibroblast affecting the radiation induced bystander phenomenon (2). In addition, the magnitude of radiation damage and resultant redox state of

intracellular milieu govern the cell division and differentiation including apoptosis, necrosis or senescence (4). Apoptosis or programmed cell death has been known to contribute to organ development and tissue homeostasis (9). In addition, apoptotic mechanisms have been implicated in the radio-sensitivity to normal and tumor cells. Evidently, the modification of radiation induced poptotic death might have significant consequences in cellular radioprotection as well as in improvement of cancer radiotherapy (3, 10-11). Accumulated evidences suggest the active involvement of ROS as signaling molecule for the initiation and execution of apoptotic death (Fig. 1). It has been shown that decrease in pool of intracellular glutathione (GSH), either by its oxidation to GSSG or by active GSH extrusion, increased the

cellular ROS by lowering the cytoplasmic reducing capacity resulting in apoptosis. Cellular antioxidants, such as GSH and thioredoxin not only serve to regulate ROS level but also act as reversible redox modifiers of activity of proteins/enzymes involved in apoptotic machinery. Mitochondria, which are known as one of the major site of intracellular ROS generation, have been central in apoptotic phenomenon. It has been known that cytochrome c localized in inner mitochondrial space, was released into inter-membrane space under high mitochondrial oxidative stress. Moreover, increased ROS and depletion of cellular GSH were capable of stimulating Bax homodimerization responsible for release of cytochrome c from mitochondria (8,12).
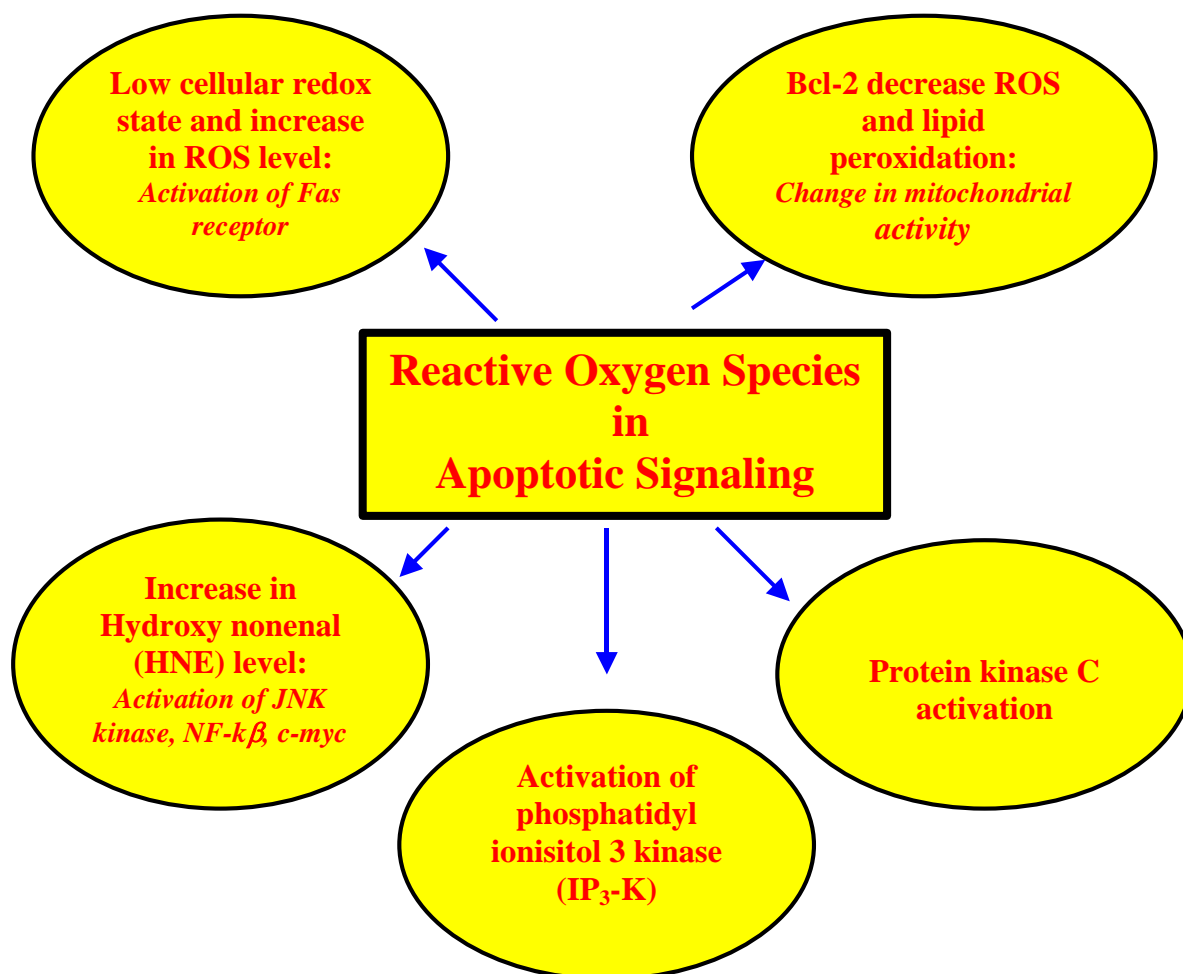

Fig. 1

Additionally, sensitivity of key death enzymes like PKC, p53 and calcineurin to oxidative stress suggest the cross talk of ROS and apoptosis (8, 13). Hence, the deeper insight in the molecular interaction between membrane damage and ROS in apoptotic pathway may have significant implication in understanding the mechanisms and modification of cellular radiation damage. Eugenol (4-allyl-2-methoxy phenol) is an active component of Indian medicinal plants, clove (*Syzygium aromaticum*) and tulsi (*Oscimum sanctum*), and been generally used as a food flavoring agent. In the present work, we have studied the modification of radiation induced membrane damage, ROS level and apoptotic death in mouse thymocytes by eugenol to understand the contribution of membrane damage and ROS in machinery of apoptosis.

Materials and Methods

Thymocytes cell suspension was prepared from thymus tissue dissected out from Swiss female mice (4-5 weeks old) in RPMI-1640 medium (10) at ice temperature adhering the guidelines from BARC Animal Ethics Committee. Cells suspensions (1×10^7 cells/ml) with FCS were treated with eugenol (100 μM prepared in PBS) for 30 min. at 25 ^{0}C followed by irradiation by ^{60}Co γ -rays (dose rate: 0.5 Gy/min or 0.46 cGy/min). Lipid peroxidation in control and irradiated samples was quantified as described in Ref. (14–15). The generation of intracellular ROS after radiation exposure in control and eugenol treated thymocytes was determined by using DCH-FDA as fluorescence probe (6). This was probably first approach to optimize the experimental condition and to use this fluorescent dye to detect/quantify sensitively the intracellular ROS generated by ionizing radiation (Fig. 2A). The ROS generation in control and irradiated samples was quantified using the protocol mentioned in Ref. (6). Briefly, cell suspension (1×10^7 cells) prepared in PBS was incubated with DCH-FDA (10 μM in ethanol, 0.001 % v/v) at 25 ^{0}C for 20 min.
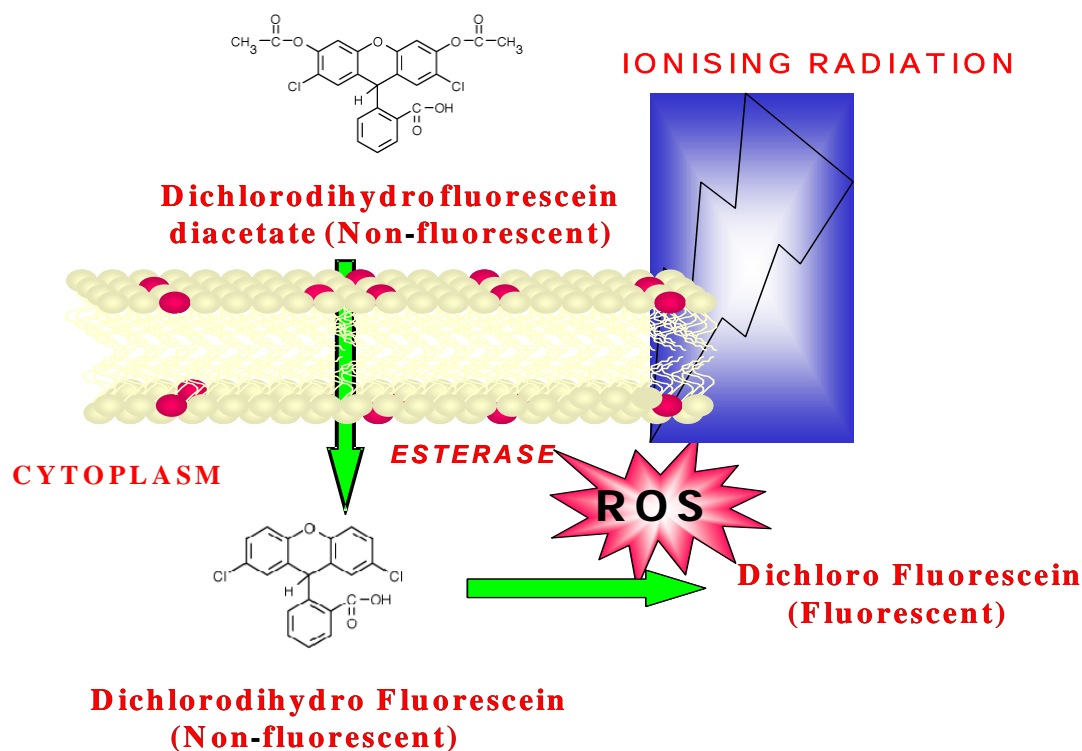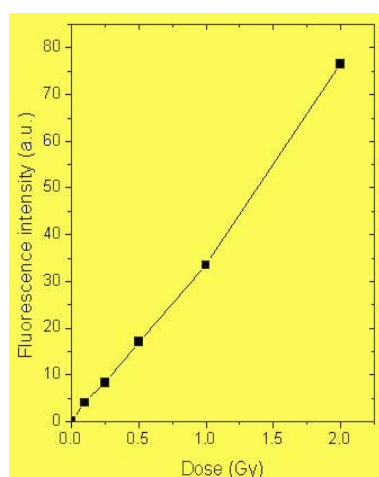

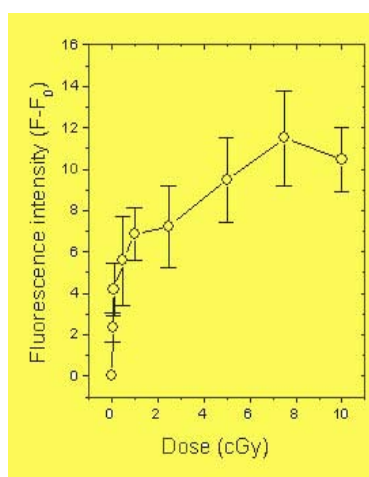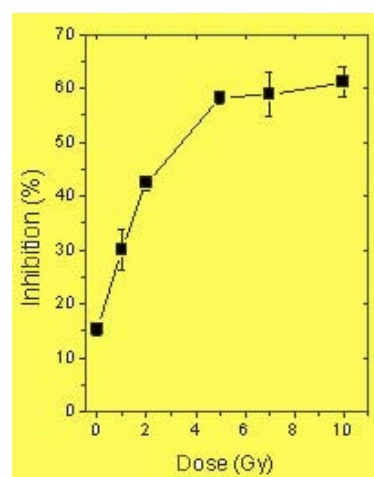Fig. 2a

Fig. 2b   *Fig. 2c*   *Fig. 2d*

Fig. 2   Generation of ROS in irradiated thymocytes. (A) Schematic representation of quantification of intracellular ROS generated after radiation exposure using DCH-FDA as fluorescent probe. DCH-FDA is a non-fluorescent ester derivative of florescein. Being a non-polar molecule it can pass through membrane. In side the cytoplasm, esterase enzymes cleave off the acetate groups. Moreover, the two chlorine groups improve the retention of dye inside the cell. ROS produced either endogenously or by exogenous factors oxidize the probe molecule resulting a strong fluorescence. (B) Thymocytes were labeled by DCH-FDA followed by irradiation with increasing doses of γ-radiation with 0.5 Gy/min. a.u.: arbitrary units. (C) Similar experiment was performed at dose rate: 0.46 cGy/min. Relative fluorescence is fluorescence intensity of unirradiated control (F_0) was subtracted from intensity of irradiated samples (F). (D) Thymocytes pre-treated with eugenol (100 μM) were irradiated with increasing doses of radiation. The fluorescence intensity was expressed in terms of percentage inhibition compared to untreated samples irradiated at same dose.
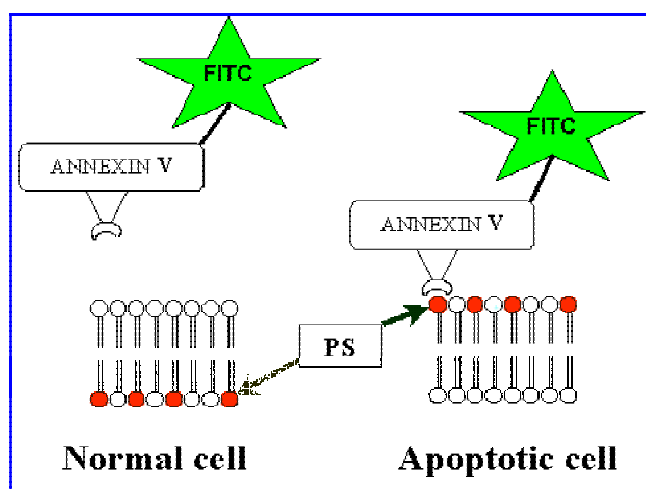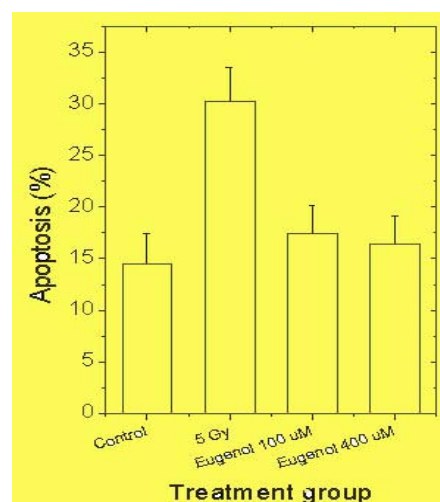

Fig. 3a   *Fig. 3b*

Fig. 3   Radiation induced apoptotic death in thymocytes. (A) Membrane asymmetry caused by flipping of phosphatidyl serine (PS) to outer leaflet of membrane, which otherwise remain localized to inner leaflet of bilayer in normal cells, is considered as one of the early hallmark feature of induction of cellular apoptosis. Annexin-V, a glycoprotein tagged with fluorescein, having specificity with PS binds only to apoptotic cells giving green fluorescence. The probe is added with propidium iodide (PI), which is permeable to necrotic or late apoptotic cells, binds to DNA and gives red fluorescence. Hence, the using this method apoptotic and necrotic cells could be distinguished. Fig. 2A. shows the schematic representation of PS externalization in apoptotic cells and its quantification by annexin-V method. (B) Percentage apoptotic (annexin positive) thymocytes after radiation (5 Gy) and after treatment with eugenol 100 and 400 μM.

TABLE 1 : Modification of radiation induced lipid peroxidation in thymocytes after eugenol treatment. Cell suspensions of thymocytes in RPMI-1640 were treated with 100 μM eugenol at 25 ^{0}C for 30 min. prepared in PBS followed by γ-irradiation (5 Gy). Lipid peroxidation was expressed in terms of malondialdehyde (MDA).

Treatment Group	Lipid Peroxidation (MDA nmoles/mg protein)
Control	0.18 ± 0.01
5 Gy	0.39 ± 0.02
Eugenol + 5 Gy	0.19 ± 0.01

These labeled samples were irradiated with desired radiation doses at 25 ^{0}C followed by measurement of fluorescence intensity by fluorimeter (LS50B, Perkin Elmer). Percentage apoptosis in control and irradiated thymocytes was determined by annexin-V-fluos staining kit (Boehringer Mannheim GmbH, Germany) following the protocol provided along with kit (Fig. 3A). From the labeled thymocytes suspension green and red cells were counted out of 400 randomly selected cell population using fluorescence microscope (Optiphot 2, Nikon, Japan). The cells showing both green and red fluorescence were considered as necrotic.

Results And Discussion

In present investigation, radiation induced membrane damage, ROS generation and apoptotic death and its modification by eugenol were studied in mouse thymocytes. The activity of eugenol and its derivatives have been shown with several reactive oxidizing species including hydroxyl radicals (16). Radiation triggers the lipid peroxidation by initiating radical mechanism (5) and the activity of eugenol seems to render its antioxidant property by scavenging the radicals by transferring its electron. This interpretation is further supported by our observation that there was increased lipid peroxidation in irradiated thymocytes, as measured in terms of malondialdehyde (MDA), which was significantly decreased in thymocytes pre-treated with eugenol (Table 1). The level of intracellular reactive oxygen species generated

during aerobic metabolic pathways through mitochondria and peroxysomes could be elevated by external stimuli like radiation and cytotoxic drugs resulting in the cellular oxidative stress. Dose dependent increase in ROS level was observed in γ-irradiated thymocytes as measured by DCH-FDA fluorescence method. A dose of 0.5 cGy and 0.5 Gy was sensitively detected in thymocytes for the applied dose rate of 0.46 cGy/ min and 0.5 Gy/min (Fig. 2B and C). However, a significant decrease in ROS generation was observed when cells were treated with eugenol before irradiation (Fig. 2D). Increased level of ROS may be associated with the activation of signaling molecules like PKC, transcription factors like NF-κB and destabilized mitochondrial membrane (4) inducing the release of apoptosis inducing agents like cytochrome C (Fig.1) The generation of ROS and damage to membrane seems interrelated in the induction of apoptosis. The radical species generated inside the cytoplasm or membrane may directly or indirectly initiate radical mediated lipid chain reaction in membrane responsible for the alterations in their structural and functional features (5,7-8), and, therefore, the cellular signaling mechanism leading to apoptotic death (6,10,13). In further experiments, thymocytes treated with eugenol showed significant inhibition in annexin positive cells compared to untreated irradiated controls (Fig. 3 B). Results have shown that presence of eugenol interfered with the generation of ROS and membrane lipid

peroxidation induced by radiation. In summary, our results suggest active involvement of ROS and membrane damage in apoptosis induced by radiation in mouse thymocytes, which was significantly modified by eugenol.

References

1. Ramakrishnan N, McClain DE, Catravas GN. Membrane as a sensitive target in thymocyte apoptosis. Int J Radiat Biol 1993; 63:693-701.

2. Azzam EI, de Toledo SM, Little JB. Direct evidence for participation of gap junction mediated intracellular communication in the transmission of damage signals from α-particle irradiated to non-irradiated cells. Proc Natl Acad Sci USA 2001; 98: 473-478.

3. Pandey B N, Mishra K P. Radiation biology for cancer radiotherapy. Adv Radiat Biol & Peace, Uttar Prades J Zool Soc, 1999; Suppl. 2: 45-51.

4. Carmody RJ, Cotter TG. Signalling apoptosis: a radical approach. Redox Rep 2001; 6: 77-90.

5. Stark G. The effect of ionizing radiation on lipid membranes. Biochim Biophys Acta 1991; 1071:103-122.

6. Pandey BN, Mishra KP. *In vitro* studies on radiation induced membrane oxidative damage in apoptotic death of mouse thymocytes. Intl J Low Radiat 2003; 1:113-119.

7. Pandey BN, Mishra KP. Radiation induced oxidative damage modification by cholesterol in liposomal membrane. Radiat Phys Chem 1999; 54:481-489.

8. Pandey BN, Mishra KP. Fluorescence and ESR studies on membrane oxidative damage by gamma radiation. Appl Magn Res 2000; 18:483-492.

9. Kerr JFR, Wyllei AH, Currie AR. Apoptosis: A basic biological phenomenon with wide ranging implications in tissue kinetics. Br J Cancer 1972; 26:239-257.

10. Pandey BN, Mishra KP. Oxidative membrane damage and its involvement in radiation induced apoptotic cell death. Iran J Radiat Res 2003, 1, 17-22.

11. Thulsidas S, Mishra KP. Radiation oxidative membrane damage and apoptosis with relevance to cancer therapy. Natl Acad Sci Lett 2002; 25:327-338.

12. Hockenbery DM, Oltvai ZN, Yin XM, Milliman CL, Korsmeyer SJ. Bcl-2 functions in an antioxidant pathway to prevent apoptosis. Cell 1993; 75: 241-251.

13. Mates, J.M. Effects of antioxidant enzymes in the molecular control of reactive oxygen species toxicology. Toxicology 2000; 153: 83-104.

14. Konings AWT, Drijver EB. Radiation effects on membrane. 1. Vitamin E deficiency and lipid peroxidation. Radiat Res 1979; 80: 494-501.

15. Plummer DT. Introduction to practical biochemistry. 3rd Ed, New Delhi: Tata McGraw Hill Press, 1988: 159-160.

16. Priyadarshini KI, Guha SN, Rao MNA. Physico-chemical properties and antioxidant activities of methoxy phenols. Free Rad Biol Med 1998; 24:933-941.

This paper received the Best Oral Presentation award at the International Conference on "Role of Free Radicals and Antioxidants in Health and Disease," C.S.M. Medical University, Lucknow, during Feburary 10-12, 2003

About the authors ...

Dr Badri Narain Pandey *is a young investigator in mammalian and cancer Radiobiology at Radiation Biology and Health Sciences Division, BARC. He has completed his Ph.D. in Life Sciences from Mumbai University in 2003. Currently he is working as Post-Doctoral Fellow in Department of Radiology, New Jersey Medical School, USA, to study the involvement of membrane and oxidative stress in radiation induced bystander effect. His major research interest involves membrane damage and generation of Reactive Oxygen Specie by high and low LET radiation with relevance to modification of cellular radio-response. Employing fluorescence and cell culture methods, he has made significant contribution in understanding the role of reactive oxygen species (ROS) in cellular and membrane damage resulting apoptotic death in normal as well as in cancer cells induced by ionizing radiation.*

Dr Kaushala Prasad Mishra *joined BARC in 1969 through 12th batch Training School in Chemistry and is internationally known for his contributions in the area of Free Radical Biology and Radiation Biology. His major research interests concern the mechanism of radiation damage to normal and tumor cells and its modification by chemical and physical agents. More recently, focus of his research has been concerning the role of ROS in oxidative stress induced apoptotic cell death relevant to radioprotection and cancer radiotherapy. Currently, Dr Mishra is the Head, Radiation Biology and Health Sciences Division of BARC. He has edited a book titled* **Radiobiology and Biomedical Research**. *Together with his colleagues, Dr Mishra has designed and developed a Cell Electroporator for biomedical research and applications, which is under Technology Transfer from this Centre. He has received several professional recognitions for his significant research contributions in the area of Radiation Biology and Life Science. Dr Mishra is a Fellow of National Academy of Sciences, India, Vice President of Bioelectrochemical Society of India, Past President of Section of New Biology, 88th Indian Science Congress, a Member of the Executive Council of Asia Pacific ESR/EPR Society, General Secretary, Indian Biophysical Society, Vice President of Society of Free Radical Research of India, Council Member, International Association of Radiation Research. He was invited as Visiting Scientist to several Universities/Institutions in India and abroad.*

INSIGHT INTO THE ONE-ELECTRON REDOX CHEMISTRY OF SUBSTITUTED INDOLES

G. H. Naik, K. I. Priyadarsini and Hari Mohan
Radiation Chemistry & Chemical Dynamics Division
Bhabha Atomic Research Centre

A b s t r a c t

Pulse radiolysis technique has been employed to study the redox chemistry of tryptophol, tryptophanol and 5-hydroxy tryptophol. The redox chemistry of tryptophol and tryptophanol is not different suggesting that modification of side chain at 3-position of the indole ring has very little effect. However the redox chemistry of tryptophol is different from that of 5-hydroxy tryptophol. Based on these studies it is concluded that the presence of 5-hydroxyl group plays a significant role on the redox chemistry of substituted indoles.

Introduction

The redox chemistry of substituted indoles has been the subject of great interest due to their role in processes such as melanoma, antioxidant activity and neurotransmission [1]. Tryptophol and 5-hydroxy tryptophol are the metabolites of indolic neurotransmitter serotonin, while tryptophanol is the reduced derivative of essential aromatic amino acid tryptophan [2]. There are some reports which suggest that tryoptophol induce necrosis by causing scission in DNA while its 5-hydroxy analogue is involved in the regulation of body temperature, sleep, pituitary function [3]. In the present study we employed pulse radiolysis technique to study the reaction of different oxidizing ($^{\bullet}$OH, $^{\bullet}$N$_3$, Br$_2^{\bullet-}$) and reducing radicals (e$^-_{aq}$, $^{\bullet}$H) with these compounds. The emphasis is given to the understanding of the transient behavior, identifying the reaction mechanism, effect of pH, oxygen and functional group on the free radical induced redox chemistry of indoles.

Experimental

Freshly prepared aqueous solutions of tryptophol (TP), 5-hydroxy tryptophol (HTP) and tryptophanol (TPN) [scheme 1] were used for each experiment.

Scheme : 1
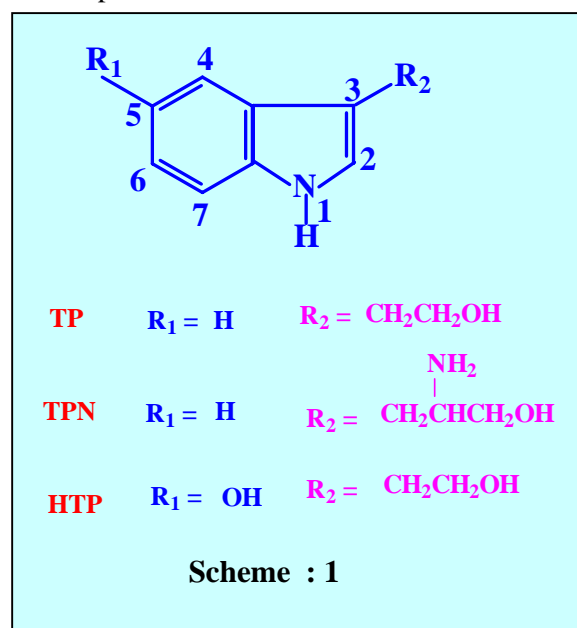
Pulse radiolysis experiments were carried out with high energy electron pulses (7 MeV, 50 ns) obtained from a linear electron accelerator and the transient species were detected by optical absorption detection technique whose details are given elsewhere [2]. Radiolysis of N$_2$-saturated neutral aqueous solution leads to the formation

of three highly reactive species (•H, •OH, e_{aq}^-) [4]. The reaction of •OH radicals was carried out in N_2O-saturated solutions. The reaction of e_{aq}^- (pH 7) and H• (pH 1) was carried out in N_2-saturated conditions containing tert-butyl alcohol to scavenge •OH radicals. The details regarding the generation of different oxidizing and reducing radicals are given in the literature [4, 5].

Results and Discussion

Reaction with specific one-electron oxidant

The one-electron oxidation of TP by Br_2^- was observed to depend on pH of the solution (Fig 1) and the pK value of the indolyl radical was determined to be 4.9. The reaction of Br_2^- with TPN also showed the formation of a transient species, similar to that of TP, with radical pK_a of 3.6. The transient species of TP and TPN showed no reactivity towards oxygen.
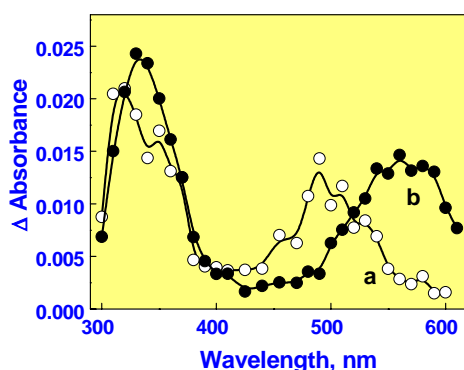

Fig. 1   Difference transient absorption spectra obtained during the reaction of TP with Br_2^- at (a) pH 9 and (b) pH 3.

One electron oxidation of HTP produced indoloxyl radical absorbing at 420 nm without any pK_a in the studied pH range (Fig 2). Like the indolyl radicals, the indoloxyl radical also showed no reaction with oxygen. The indoloxyl radical was found to react with HTP to give a dimer radical absorbing in 405 - 420 nm region (Fig 2). The association constant for the

dimerisation process was determined to be 6.7 ± 0.4 x10^4 M^{-1}. The dimer radical was found to decay by first order kinetics (k = 7 s^{-1}). The probable site of dimerisation is either C(4) position or through oxygen atom of indoloxyl radical. This dimerisation reaction was not seen in indolyl radicals of TP and TPN. Thus showing that 5-hydroxy substitution plays an important role in oxidative dimerisation of substituted indoles.
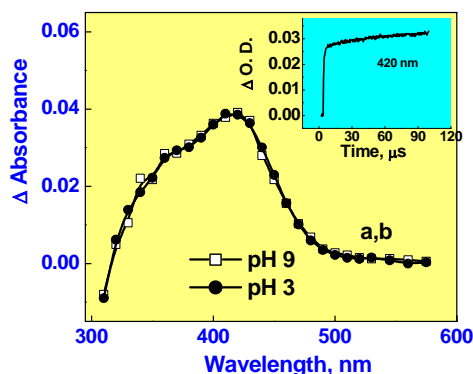

Fig. 2   Difference transient absorption spectra obtained on reaction of Br_2^- with HTP (a) at (☐) pH 9 and at (●) pH 3. Inset (c) shows absorption-time plot at 420 nm.

Reaction with hydroxyl radical

The reaction of hydroxyl radical with TP, TPN and HTP was studied in the pH range of 3 - 9. The transient spectra were different from those produced by specific one-electron oxidants. However the contribution of oxidized species of TP, TPN and HTP were seen at corresponding wavelength. The time resolved spectra for the •OH radical reactions with TP, TPN and HTP showed that the initially formed hydroxyl radical adduct undergo dehydration to form one-electron oxidized species. Rate of dehydration has been catalysed in acidic and alkaline medium. The change in parent concentration from 25 μM to 500 μM was found to have no effect on the absorbance of one-electron oxidized species of TP and TPN. However in the case of HTP, the

absorbance at 420 nm increased with increasing parent concentration suggesting that dimerisation is possible with HTP and not with TP and TPN.

Reaction with e_{aq}^- and $\cdot$H atom

The reaction of e_{aq}^- with TP, TPN and HTP produced a transient species absorbing at 345 - 350 nm. The bimolecular rate constant for the reaction was determined by following the decay of hydrated electron at 700 nm in presence of different indole concentrations. It was found to be $2 \pm 0.5 \times 10^8$ M^{-1} s^{-1}, $4.2 \pm 0.3 \times 10^8$ M^{-1} s^{-1} and $3.7 \pm 0.4 \times 10^8$ M^{-1} s^{-1} for TP, TPN and HTP respectively.

The spectra of transient species obtained on reaction of e_{aq}^- with TP and TPN did not change significantly with pH where as the transient species of HTP showed a broad red shift with pK$_a$ value 9.

The transient species of TP, TPN and HTP decayed by second order kinetics. In aerated solutions, the indolyl radicals of TP, TPN and HTP decayed by pseudo-first order kinetics by reaction with oxygen. The reaction of HTP with oxygen produced strongly absorbing radical with maximum absorption at 400–410 nm (Fig. 3). Similar absorption changes were not seen with TP and TPN.

The reaction of $\cdot$H atom (pH = 1) with TP, TPN and HTP showed formation of transient species, absorbing in 300 – 350 nm region. The nature of the transient spectrum was similar to that of produced on reaction of e_{aq}^- with TP,
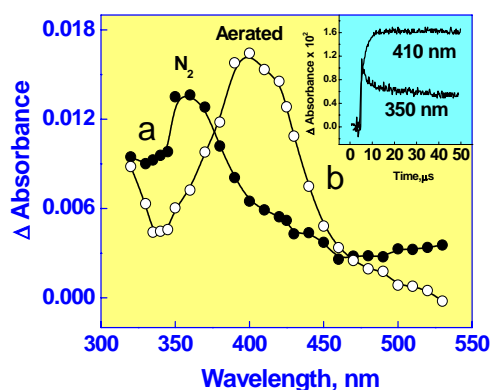
Fig. 3 Time resolved absorption spectra obtained on reaction of e_{aq}^- with HTP (a) 1.1 µs and (b) 12 µs after the pulse. Inset show absorption–time plots at 345 nm and 400 nm.

TPN and HTP indicating that formation of indolyl radical (scheme 2). The bimolecular rate constants for the formation of indolyl radical was determined to be $3.9 \pm 0.2 \times 10^9$ M^{-1} s^{-1}, $4.2 \pm 0.3 \times 10^9$ and $4.6 \pm 0.3 \times 10^9$ M^{-1} s^{-1} for TP, TPN and HTP respectively. The indolyl radical was observed to reduce MV^{2+}.
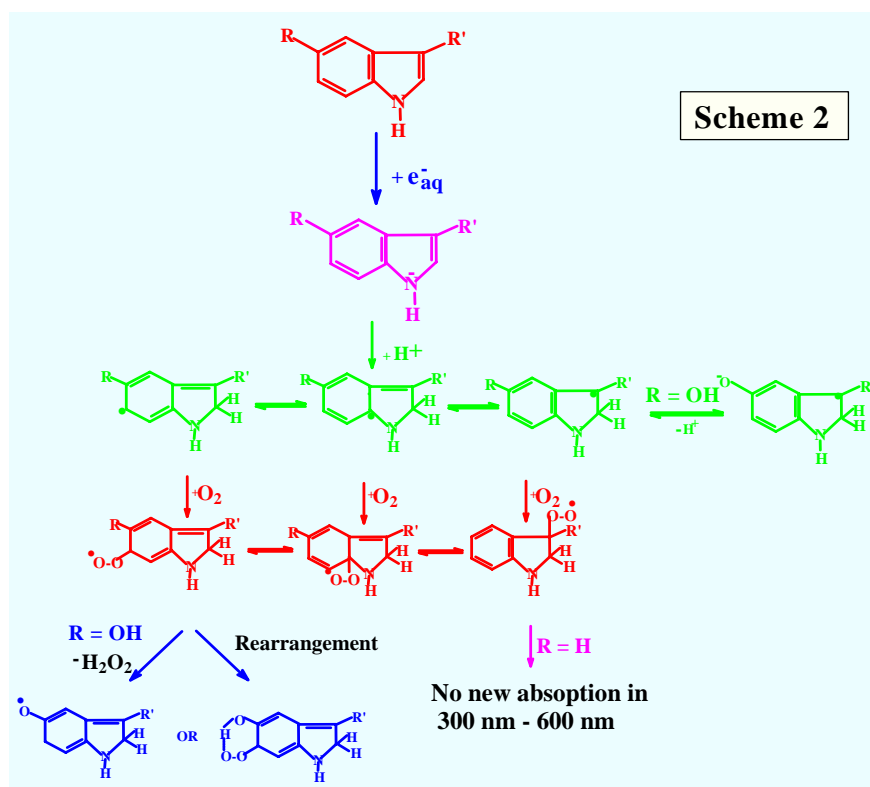
Conclusions

The one-electron redox chemistry of TP and TPN was found to be same. They both produced N-centred (scheme 3) and C–centred indolyl radicals (scheme 2) during their oxidation and reduction studies respectively at physiological pH.

Scheme 3

Radical cation

R = H -H+

R = OH -H+

HTP

──→ Dime

Indolyl radical　　**Indoloxyl radical**
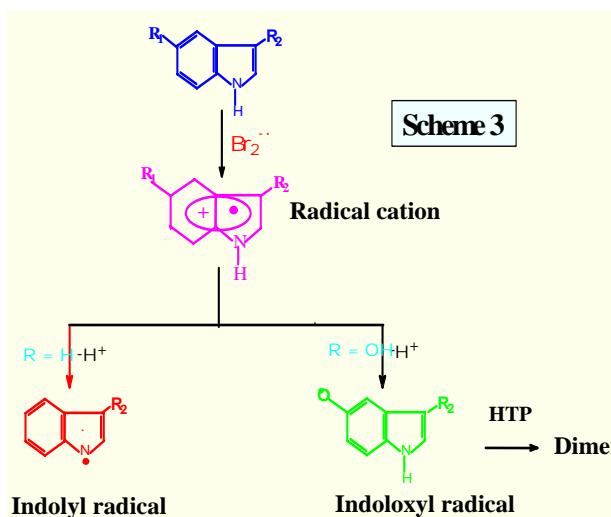
The redox chemistry of HTP was found to be different from that of TP and TPN. During oxidation and reduction studies it produced O–centred indoloxyl radical (scheme 3) and C-centered indolyl radical (scheme 2) respectively. at physiological pH. The indoloxyl radical was found to react with parent to form dimers. This dimerisation reaction was not seen in case of TP and TPN.

References

1. R. J. Sundberg, Chemistry of Indoles, Academic Press, New York, 1970.
2. G. H. Naik, K. I. Priyadarsini, H. Mohan, Phys. Chem. Chem. Phys., 4, 5872 2002.
3. G. Dryhurst, Chem. Rev., 90, 795, 1990.
4. J. W. T. Spinks, and R. J. Woods, An Introduction to Radiation, John Wiley, New York 243, 1991.
5. C. von Sonntag, The Chemical Basis of Radiation Biology, Taylor and Francis, New York, 1987.

This paper received the "Prof. S. R. Palit Award" in Physical Chemistry Section at 40th Annual Convention of Chemists, held at Bundelkhand University, Jhansi, during December 23 – 27, 2003.

About the authors ...

Mr Ganesh Naik received his M.Sc degree in Organic Chemistry from Somaiya College, Mumbai University in 2000. He is a DAE fellow working in Radiation Chemistry and Chemical Dynamics Divison, BARC. He is persuing his Ph.D degree in the subject entitled, 'Study of Free Radicals and Excited States of Some Important Biomolecules'.

Dr Indira Priyadarsini joined BARC in 1983. She obtained her Ph. D. in Radiation and Photochemistry in 1990. She has co-authored more than 70 papers in international journals on radiation chemistry, photo-chemistry and radiation biology.

Employing fast reaction techniques, she has been studying the free radical reactions involving antioxidants, radio protectors and radio sensitizers in model systems. She is currently working on the elucidation of mechanism of antioxidant action involving natural products and herbal extracts.

Dr Hari Mohan joined BARC in 1967. Since then, he is actively involved in the study of fast reaction kinetics using accelerators and lasers. His current research interests include free radical reactions of halogenated and sulfur compounds and biomolecules of natural origin. He has co-authored more than 150 research papers in international journals. Presently, he is the Head, Radiation Chemistry Section of Radiation Chemistry & Chemical Dynamics Division, BARC.

DEVELOPMENT OF AUTOMATIC REMOTELY OPERABLE LASER CUTTING SYSTEM FOR DISASSEMBLY OF PHWR SPENT FUEL BUNDLES

G. L. Goswami and Anjan Chatterjee
Laser Processing & Advanced Welding Section, Nuclear Fuels Group
Bhabha Atomic Research Centre

Munish Chandra, H.B. Kulkarni and K.K. Prasad
Nuclear Recycle Group
Bhabha Atomic Research Centre

K. Jayarajan and J.K. Mishra
Division of Remote Handling & Robotics
Bhabha Atomic Research Centre

Shailesh Kumar
Laser & Plasma Technology Division
Bhabha Atomic Research Centre

S. Gangotra and K.C. Sahoo
Post Irradiation Examination Division
Bhabha Atomic Research Centre

and

T. P. S. Nathan
Solid State Laser Division
CAT, Indore

A b s t r a c t

PHWR fuel bundles are required to be dismantled for inspection the individual pins under highly radioactive environment of the hot cell. PHWR fuel bundle consists of 19 tubular pins, spot-welded to two end plates (tie plates) on each side. It is of about 14.5mm diameter and 495mm long. It is proposed to carry out the disassembly operation by laser cutting of both the tie plates. Accordingly the experiments were conducted at LPAW Section, BARC to study the feasibility of the scheme, which gave the encouraging results. A dummy end plate was successfully cut to separate spot weld location using laser on a 3-Axis CNC workstation. Based on the feasibility studies, a design for totally automatic and remotely operable system has been made and is proposed to be used for dismantling of PHWR fuels inside the hot cell.

The system has to perform operations like moving the bundle to laser cell from charging cask, cutting both the end plates using laser to separate out 19 pins for examinations and finally chopping of each pin for dissolution of the fuel for further processing.

Introduction

The Laser Cutting processes, involving laser energy to cut the sample, are sufficiently attractive and unique to explain the great breadth of applications. The mechanisms involved in laser cutting are (a) vapourisation, (b) fusion cutting- i.e melting & blowing, (c) reactive fusion cutting, (d) controlled fracture and (e) scribing. The choice of a mechanism depends on the materials to be cut. The laser cutting process provides a certain advantages as (a) Sharp corners can be cut since it is almost a point source cutting, (b) there is minimum distortion and a very narrow heat affected zone, (c) it produces a very narrow kerf, (d) this being a non contact process there is no tool wear during the process and (e) cutting can be done to some inaccessible location with the help of a fiber optics.

PHWR fuel bundle consists of 19 tubular pins, spot-welded to two end plates on each side. It is of about 14.5mm diameter and 495mm long. For the purpose of fuel reprocessing these bundles are presently being chopped by a heavy duty 20T shear machine inside the hot cell for dissolution of oxides. There are certain problems in mechanical chopping specially when the entire bundle is sheared at a very high pressure. Cutting of the Tie plate provides a better alternative where the bundle can be dismantled to individual pins and these pins can be sheared individually at lower pressure. PHWR fuel bundles are also required to be disassembled for inspection the individual pins under highly radioactive environment of the hot cell. It was proposed to carry out the disassembly of PHWR fuel bundles by laser cutting of both the tie plates. Accordingly, the experiments were conducted at LPAW Section, NFG, BARC to study the feasibility of the scheme, which gave the encouraging results. A dummy end plate was successfully cut to separate spot weld location using existing laser on a 3-Axis CNC workstation. Based on the feasibility studies, a design for totally automatic and remotely

operable system has been made and is proposed to be used for dismantling of PHWR fuels inside the hot cell for both reprocessing purpose and Post Irradiation Examination.

A separate Nd-YAG laser-cutting system with fiber optics beam delivery system has been assembled and tested for disassembly of the PHWR fuel bundles. The system has to perform operations like moving the bundle to laser cell from charging cask, cutting both the end plates using laser to separate out 19 pins for further processing.

Major sub-systems of the system are as follows:

- Bundle Lifting Tool
- Laser Cutting Tool
- Bundle Handling Tools
- Laser Source and Beam Delivery Systems
- Controller and Operating Console

Laser focusing tool is mounted on a 3-axis CNC table. The fuel bundle with tie end plate is brought to a fixed location and the focusing tool is moved through a predetermined path to cut the end plate. After cutting one end plate, the bundle is rotated and cut is given to the opposite end plate. In the scheme, the bundle disassembly is performed in two stages in hot cells. In the hot cell, both the end plates are cut into pieces by laser to separate the fuel pins. It involves tools for handling of bundle, CNC station for laser movements and beam delivery system. A 150W Nd-YAG laser is used for cutting. All these operations are performed remotely and automatically.

Feasibility Studies & Concept Design

Experiments were conducted to study the feasibility of the scheme. The experiments were conducted inside a simulated hot Cell made by PVC material creating the actual experimental conditions. A dummy end plate was successfully cut to separate spot weld location using laser on a 3-Axis CNC workstation. The total path covered by the laser head was about 600mm, out

of which about 300mm was the ON time for the laser. It was found that cutting of the tie plate is very convenient by laser.

Experiments were conducted to study the feasibility of decladding of fuel pins by laser cutting. Fuel pin clad was given helical and circumferential cuts using laser to separate it from the fuel pellets inside. Helical path was taken such that it does not pass through bearing pads and spacer pads. So this method of decladding requires precise positioning of pins and also needs complex mechanical systems to be placed inside the more active cell. It was observed that about 20 metres (0.5 m per linear cut ie length of the tube X 2 cuts per pin X19 pins + end plug removal) of cutting required to remove the pellets. It was observed that with the present level of cutting rate, it would need much more than an hour to achieve this. Moreover, laser cut marks of up to 100 μm on the pellets were also seen as PHWR fuel pins are made up of collapsible zircaloy tubes and pellets are in the intimate contact with the tube. These marks are difficult to avoid and would lead to evaporation of radioactive material and would result in high level of contaminations[1,2]. In view of such long processing time and also observation of 100 μm cuts on the pallets due to laser, the option of cutting single pin by laser was not considered appropriate and multiple shear device (hydraulic press) for chopping was studied.

To see the performance of fuel chopping, fuel pins were cut into pieces in a hydraulic press. The cut section was found to be clean with no generation of Zr fines[3]. No pinching or closing of chopping face was observed. Also, the chopping force per pin was found to be about 100kg, which is very low compared to the present method of chopping.

Effect of nuclear radiation on various optical components and Optical fiber used for beam delivery inside the hot cell were studied and systematic experiments have been carried out for various dose rates and exposure times. The change in optical properties like transmission, coloration and refractive index were recorded before and exposure[4]. It is concluded that low impurity pure crystalline quartz optics is usable in harsh radiation environment up to one mrad exposure. Likewise low impurity silica fiber like TECS-393M is also usable inside Hot cell with proper protection. This data was used for design of laser beam delivery system for the machine.

Special Features for Radioactive Operation

The special care was taken to find out the suitability of different parts of the machine to be used in the radioactive area before going for the design aspect of the machine. Accordingly following aspects were considered in designing the machine[5].

- Laser is delivered by fiber optics beam delivery system.

- Main parts of the machine are outside the radioactive compartment. Only cutting head is inside the hot-cell.

- Modular system design to allow easy removal of defective parts.

- Easy plug in type electrical connectivity to facilitate easy disconnection/connection through manipulators.

- Special quartz lenses to sustain the radioactive environment.

- All the lenses & the fiber optics have been radiation tested in the hot cells against their damages.

- All the critical components inside the cell are tested for radiation resistance.

- Additional sensors are included in the system.

- Complete system can be operated through a computer by a single button. Display indicates the status of the operation graphically.

The System

Laser is a coherent, monochromatic and a very high intensity light source, which is being used for several material processing applications. our system consists of a laser source of Nd-YAG laser of 1.06 μ wavelength and 150 watts average power with pulse mode operation. The other parts consist of the bundle lifting system to lift the fuel bundle to the height of the CNC stage to enable the manual pushing to the gripper stage. The gripper assembly then grips the bundle in the proper alignment and then the CNC system starts the movement of the proximity sensor to find out the alignment of the centre and the other locations of the tie plate. Accordingly, laser nozzle takes the predetermined path automatically for cutting. After cutting the first tie plate the bundle rotates automatically by 180° and completes the cutting of the tie plate on the other side, after sensing again. The laser system delivered by CAT, Indore was interfaced with the CNC system and a number of dummy subassemblies were cut using the laser to test the functioning of the machine. Two such systems are being made. One of them will be integrated with other mechanical shear system for fuel reprocessing while the other system shall be used for post irradiation examination activities.

A fully automatic remotely operable system has been designed and fabricated to carry out Nd-YAG laser cutting of the tie-plates followed by mechanical shear of individual pins (15 cuts at a time). The mechanical shear of each pin, carried out in AFD, BARC indicated that around 100-150 Kg load is needed to chop the individual pin. Additionally it has a conveyer system to carry the dismantled pins to the chopping bed and then the single stroke chopping action is done by the system and then fuels are taken out for dissolution works.

The requirement of the post irradiation examination division is only cutting of the tie plates to dismantle the individual fuel pins inside the hot cell for the post irradiation examination of the individual pins. For this purpose additionally a motorised bundle lifting system is provided to lift the bundle to the height of the CNC stage to enable the manual pushing of the bundle to the gripper stage.

Commissioning & Testing

The system has been designed fabricated assembled and tested in the laser Lab, Laser Processing & Advanced Welding Section, Nuclear Fuels Group, BARC. The Mechanical handling system was designed by special task force and fabricated by the local outside party while the laser system was supplied by CAT, Indore. The system have been integrated and tested in the Laser Lab, LPAW Section, Nuclear Fuels Group, South Site, BARC, as shown in figs. 1-3. Satisfactory cutting trials have been performed using the system automatically and remotely.
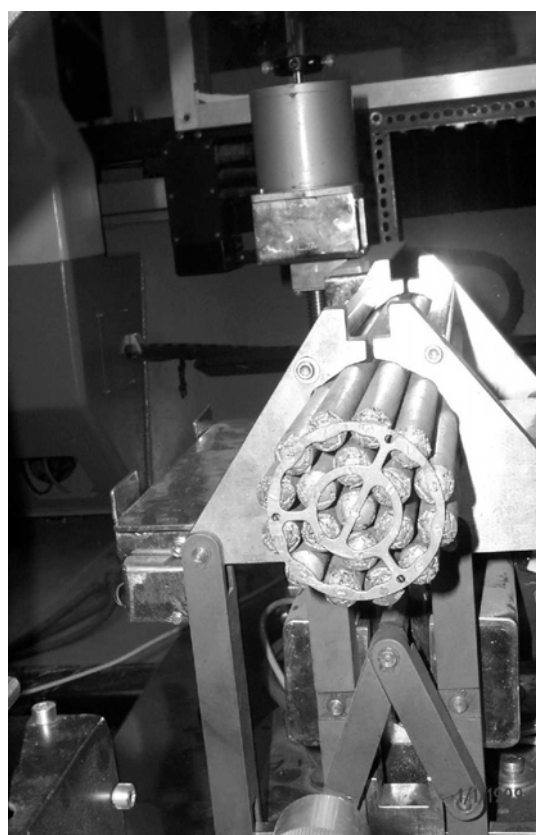

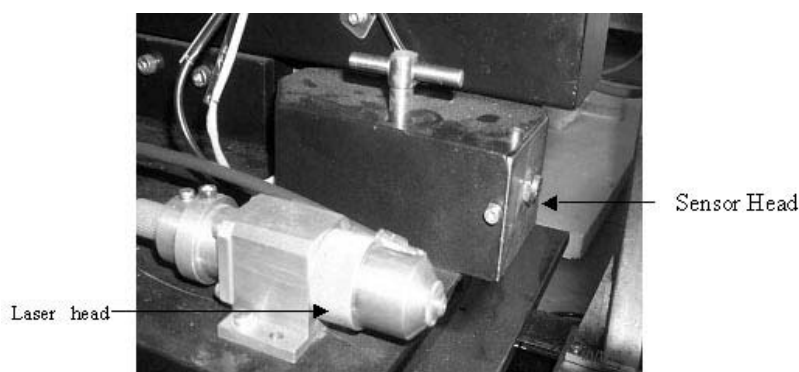*Fig. 1 : Gripper assembly with fuel bundle*

Fig. 2 Laser head and sensor head

Fig. 3 Overall view of the machine

Conclusion

The tie plate cutting operation by laser was a very clean operation. It was found that after cutting both the tie plates pins separate easily as soon as the gripper is released. Laser cutting also avoids opening up of the pins from the welds as no pressure is exerted on the pins during the cutting process. It should also be mentioned that the dissolution time would be low in the proposed scheme, because of the clean edge of cut and no cut piece will be blind. The generation of Zr fines will be low in single pin chopper. Since the cutting force is very low in the proposed method of chopping, maintenance and downtime is expected to be low. Based on the feasibility studies, a design for totally automatic and remotely operable system has been made & the machine has been fabricated and tested for its satisfactory performance.

References

1. Laser cutting for dismantling of PHWR fuel bundle- Dilip Kr, B.P. Badgujar, G.L Goswami - National Welding Seminar, IIW-CAT Indore Jan-94

2. Automated laser cutting system for disassembly of PHWR fuel bundle - A report on laser cutting trial - Sanjiv K. Jha AFD, BARC, Oct 1999.

3. Single Pin shear for development of laser based disassembly system - A report - G.L. Goswami & Munish Chandra, 2000

4. A Technical report on radiation effect on optical components and optical fibres. Life of such system under sustained radiation. Results of the experiments and literature survey - G.L. Goswami et al.

5. Development of laser based disassembly and single shear system for reprocessing Thoria fuels - G.L. Goswami et al. Proceedings symposium on Thoria Technology, Indian Nuclear Society, Mumbai 2000

This paper received the KCP award at National Welding Seminar 2002 held at Kolkata during January 23-25, 2003.

About the authors ...

Mr Gyanottam Lal Goswami is B. E. in Metallurgy from University of Roorkee, 1970. He had graduated from 14th batch of BARC Training school with Metallurgy discipline. He has made important contributions in nuclear fuel fabrication, thermodynamics of nuclear materials and laser materials processing. He is currently Head of Laser Processing & Advanced Welding Section of the Nuclear Fuels Group, BARC.

Mr Anjan Chatterjee obtained his B.E. in Metallurgy from Jadavpur University, Kolkata in 1981. He had graduated from 25th batch of BARC Training School with Metallurgy discipline in 1981-1982 He has made important contributions in nuclear fuel fabrication and laser materials processing. He is currently working in Laser Processing & Advanced Welding Section of the Nuclear Fuels Group, BARC.

Mr Munish Chandra is a Machanical Engineer from 14th batch of BARC Training School. He has extensive experience in the field of nuclear fuel reprocessing. Presently, he is with the Nuclear Recycle Group, BARC.

Mr H. B. Kulkarni is currently a Chief Design Engineer (Mech.) at NRG projects. He graduated from the 14th batch of the BARC Training School. He has a wide experience in nuclear fuel recycling activities.

Mr K. K. Prasad is currently Head, Back End Technology Development Division, BARC. He graduated from the 13th batch of the BARC Training School. He has a wide experience in the activities of back end of the nuclear fuel cycle.

Mr K. Jayarajan is heading the Tele-manipulator Section of Division of Remote Handling and Robotics, BARC. His area of work is the design and development of remote handling systems such as Mechanical Master Slave Manipulators, Servo Manipulators, Robots, Automation Systems and Hotcell Equipment. He has also developed many remote handling systems for medical and defence applications. His research activities in robotics include Gait Generation of Walking Machines, Obstacle Avoidance Algorithm and Robot Dynamics.

Mr J. K. Mishra, after graduating from University College of Engineering, Burla, Orissa, joined the 33rd batch of BARC Training School in 1989. Subsequently, he joined Division of Remote Handling & Robotics, and is working on the control of robots and specialized remote handling equipment. Presently, he is working on the magnetic measurement and testing of the superconducting magnet for the Large Hadron Collider project in CERN, Switzerland.

Dr Shailesh Kumar obtained his M.Sc (Hons) in Physics from Punjab University, Chandigarh in 1981. After graduating from 25th batch of BARC Training School, he joined Laser Section in 1982. Since then, he has worked on the development of various aspects of High Power Carbondioxide Lasers and laser material processing. In 1992, he was deputed to AEC, Syria. In 1993, he was awarded Ph.D. and is a receipt of ILA best thesis award.

Mr Suresh Gangotra *is a gold medalist in Metallurgical Engineering from M.S. University for the year 1983. After completing training from the 27th batch of BARC Training School, he joined Radiometallurgy Division, BARC. His areas of interest are Laser applications for hot cells and Non-destructive testing of irradiated nuclear fuels and reactor components.*

Mr K.C. Sahoo *is a graduate in Metallurgy from Sambalpur University. He joined the 14th batch of BARC Training School in 1970. He worked at the Hot Cells Facility of Risø National Laboratory of Denmark under IAEA fellowship programme during 1976-1977. He is a specialist in the field of irradiation behaviour of nuclear fuels and reactor core components. His field of interest is non-destructive testing and metallurgy of nuclear materials. He is an Outstanding Scientist and currently Head of Post Irradiation Examination Division of BARC.*

Mr T.P.S. Nathan *is Head, Solid State Laser Division of CAT, Indore. He has wide experience in development of different solid state lasers.*

PREPARATION AND STUDIES OF STRUCTURAL AND THERMO-MECHANICAL ASPECTS OF SOME SPECIAL GLASSES AND GLASS-CERAMICS

G.P. Kothiyal
Technical Physics and Prototype Engineering Division
Bhabha Atomic Research Centre

A b s t r a c t

Glasses and glass-ceramics (GCs) used for sealing, coating and high voltage applications belong to a special class of materials in which among other requirements, matching of thermal expansion coefficient with that of metal as closely as possible up to set temperature is an important consideration. In this paper I shall concentrate on some indigenous efforts carried out in my laboratory on the preparation and studies related to structural and thermo-mechanical aspects of glasses such as lead silicate, borosilicate, sodium aluminium phosphate (NAP) and glass-ceramics such as magnesium aluminium silicate(MAS) and lithium zinc silicate(LZS). Glasses have been prepared by melt quench technique while bulk nucleation method has been followed for the preparation of glass ceramics. Structural aspects of lead silicate glasses having alkali- and alkaline earth metal oxides, and B_2O_3 have been studied using MAS-NMR, XRD and optical transmission and have been found to affect both micro-hardness and thermal expansion coefficients. As regards, MAS glass- ceramics a systematic study to find out the effect of MgF_2 content and processing temperatures on the crystallisation process and thermo-mechanical properties was carried out. Some results related to structural and optical studies of NAP and LZS have been discussed. Finally high quality machinable MAS glass ceramic has been developed which has been found suitable for high voltage applications in ultra high vacuum at relatively high temperatures. Both lead silicate, borosilicate glasses and lithium zinc silicate glass-ceramics have been employed in special types of glass to metal and glass-ceramics to metal seals.

Introduction

Need for joining glass-to-metal, and ceramic-to-metal etc arises in many vacuum devices especially where ceramic/glass forms the part of envelope and vacuum tight seals are needed to leads connecting active structure inside the envelope. In addition, this is a novel way of providing access from one atmosphere to another even in presence of very high voltage, reasonably high temperature and quite high-pressure difference. These glass-to-metal (GM), ceramic-to-metal (CM) and glass-ceramics-to-metal (GCM) seals and coatings find numerous applications in various disciplines of science and technology

[1-6]. The main requirement for the formation of a high quality seal or coating is to achieve ideal bonding structure at the interfaces. Further, the thermal expansion coefficients of both, the metal and ceramic should match as closely as possible to minimize the stresses. There is another method of forming the seal in which metal should only exert the compression stresses on glass/ceramic. Glass-ceramics are also used as a bonding media (like a thin glue layer) between bulk materials.

While electrical conductivity, machinability, outgassing properties are important for applications involving high voltage and ultra high vacuum, the knowledge of thermal and

mechanical properties of glass-ceramic is needed for the applications in the field of CGM seals. Generally the glass-ceramics exhibit a wide range of thermal expansion coefficients depending upon the composition and the presence of relative proportions of the crystalline phases. Some studies to see the effect of nucleating agent on the crystalline-phases developed and on thermal properties of magnesium aluminium silicate(MAS), Li_2O-MgO-Al_2O_3-SiO_2 , etc glass and glass-ceramics are reported[7, 8]. Donald *et al* [9] and Demirkesen *et al* [10] have reported similar studies on lithium zinc silicate glass-ceramics. Donald *et al* [9] discussed the effect of composition including the influence of nucleating agent on crystallization behaviour and on the thermal and mechanical properties of resultant glass ceramics. Metcalfe et al [4] have studied expansion behaviour with and with out Cu / Ni in lithium zinc silicate (LZS). Different glass and glass ceramic compositions based on silicates, borates, phosphates etc have been considered suitable for sealing applications [6, 11-13].

Glass-ceramics are remarkable materials for providing the wide range of thermal expansion coefficients. At one extreme, materials having negative coefficients of thermal expansion are available while for other compositions very high positive TEC are observed. We also have GC with zero TEC. The thermal expansion coefficients of GC can be remarkably different from the parent glass and are basically controlled by the crystallization process. It has been shown to a first approximation [6] that expansion coefficient (α_{gc}) of a glass-ceramic material is an additive function of thermal expansions of various phases present, and can be represented by following relationship :

$$\alpha_{gc} = \{(\alpha_1 k_1 w_1/\rho 1 + \alpha_2 k_2 w_2/\rho_2 + --) / k_1 w_1/\rho_1 + k_2 w_2/\rho_2 + --)\} \qquad (1)$$

Where, α_1, α_2,---, are the expansion coefficients of various phases, k_1, k_2, --, the bulk modulii,

w_1, w_2,-- the weight fractions, and ρ_1, ρ_2, --- the densities. Therefore, by proper selection of glass composition and processing parameters, one can engineer the material of desired expansion coefficient that is, in principle we can match the thermal expansion characteristics of GC material to those of special alloys. However, this is seldom achieved in practice over the entire range of interest because of the presence of various phases, their relative content and different temperature dependencies. Chemical reaction within the glass-ceramic close to metal interface may change the microstructure relative to bulk. Consequently the quality of the seal/coating gets affected.

In this paper, I shall concentrate on some indigenous efforts carried out in my laboratory on the preparation and studies related to structural and thermo-mechanical aspects of glasses such as lead silicate, borosilicate, sodium aluminium phosphate (NAP) and glass-ceramics such as magnesium aluminium silicate and lithium zinc silicate. Glasses have been prepared by melt quench technique while bulk nucleation method has been followed for the preparation of glass ceramics. Various characterization techniques such as XRD, MAS-NMR, SEM, FTIR, DTA, TMA, microhardness etc were used to study different aspects in these materials.

Some Investigations

We have carried out studies on lead silicate glass(LS), boron oxide substituted LS glass, borosilicate glass, sodium aluminium phosphate(NAP) glass, MAS and LZS glass ceramics. The glass samples were prepared by melt quench technique [14] while for transforming the glass into glass ceramics controlled crystallization was carried out[15,16]. Glass nature as well as phase formation were ascertained by XRD. MAS-NMR and FTIR measurements provided structural information while DTA/TG gave information about the crystallization temperature and glass transition temperature. The thermal expansion coefficient

measurements were carried out in a Dilatometer (model - TMA / 92 Setaram, France) using silica probe. Microhardness was measured on LEICO microhardness tester using Vicker's indentor while scanning electron microscopy revealed the microstructure.

Glasses

Lead silicate and borosilicate : We have studied $(PbO)_{0.5-x}$ - $(SiO_2)_{0.5}$ $(B_2O_3)_x$ and $(PbO)_{0.5}$ - $(SiO_2)_{0.5-y}$ $(B_2O_3)_y$ with $0.0< x<0.4$, $0.0< y<0.5$ glasses. Dependence of TEC as function of $[B_2O_3]$ concentration is shown in Fig.1. When SiO_2 was partially substituted by B_2O_3, it was found to gradually decrease to 9.18×10^{-6} /^{o}C with increase in B_2O_3 content up to 20mole%.

The marginal decrease in TEC, when SiO_2 is substituted by B_2O_3, may be due to less structural changes in SiO_2 network, as B_2O_3 is also a network former. This may be attributed to the formation of somewhat more rigid network due to incorporation of B_2O_3. In the case of glass, formed by partially substituting PbO by B_2O_3. TCE was found to substantially decrease from 10.114×10^{-6} /^{o}C to 6.507×10^{-6} /^{o}C. This is thought to be due to the formation of rigid silica network containing more number of bridging oxygen ions. This is borne out from ^{11}B and ^{29}Si MAS NMR studies on these glasses reported elsewhere [17]. Variation of average TEC and Tg as a function of mole fraction of Q4 structural units of Si(derived from Si MAS NMR) for $(PbO)_{0.5-x}$ - $(SiO_2)_{0.5}$ $(B_2O_3)_x$,$0.0< x<0.4$ is shown in Fig. 2. As replacement of PbO by B_2O_3 leads to an increased number of Q4 structural units and better cross-linking through the formation of covalent Si-O-B bonds, thereby leading to a more rigid structure. The enhanced rigidity of glass structure leads to decrease in TEC and increase in Tg. Fig.3 shows compression type seals fabricated using in-house developed lead silicate glass.
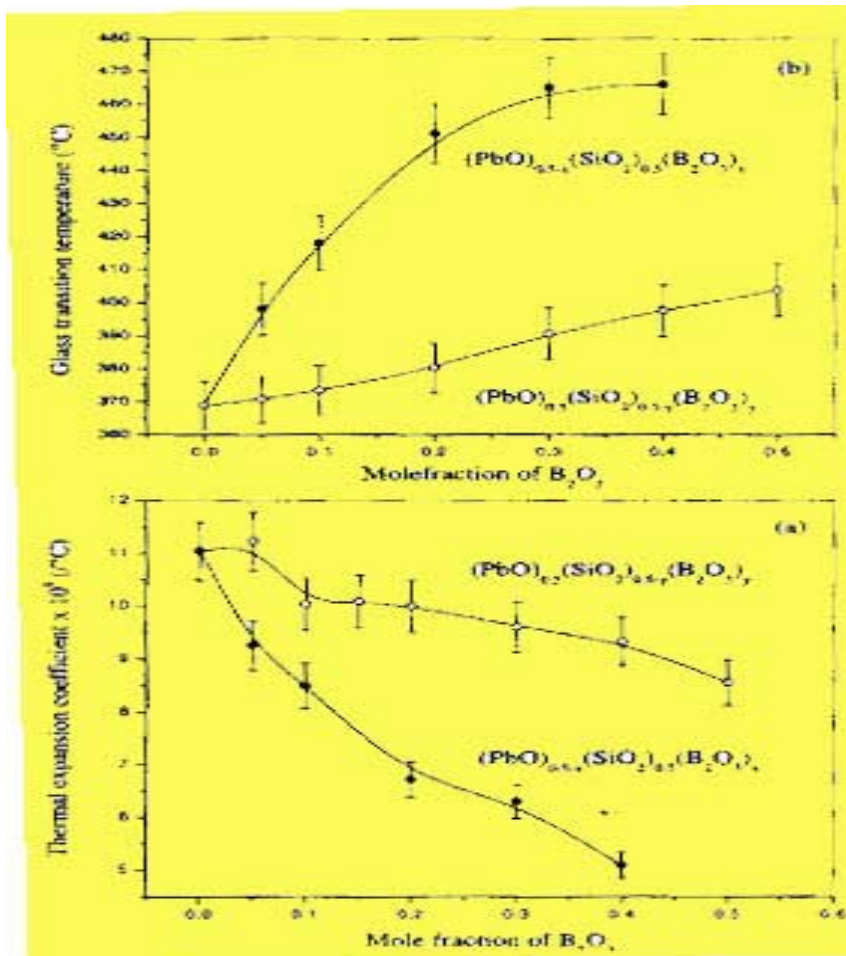

Fig. 1. Dependence of TEC and Tg as function of $[B_2O_3]$ concentration

Phosphate glass : Sodium alumino-phosphate glass system in particular is important not only because
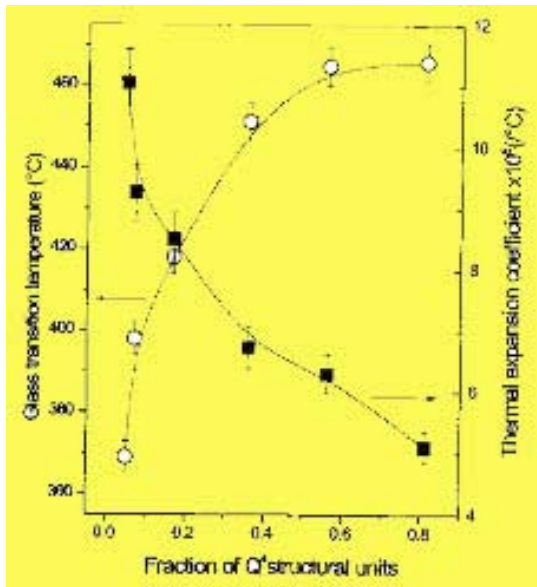
Fig.2. Variation of average TEC and Tg as a function of mole fraction of Q4 structural units of Si (derived from Si MAS NMR data)

Fig 3. Photograph of 7-pin seal fabricated used indigenously developed lead silicate glass withstands a pressure of 12,000 psi and used in HWPS)

of its improved chemical durability but also because of its potential use in fabrication of glass-to-metal seals with high expansion coefficient metals like Cu and Al[12,18-19] at relatively low temperatures. Sodium alumino-phosphate glasses having compositions of x Al_2O_3. (1-x) $NaPO_3$ (x=0.05-0.2) were prepared using conventional melt-quench technique. Density, glass transition temperature, microhardness, thermal expansion coefficient and transmission characteristics were measured

as a function of alumina content for different samples (Table-1). They were found to depend on O/P ratio with pronounced changes taking place for O/P ratio greater than equal to 3.5 and average Al co-ordination number[20,21]. A typical Vickers impression obtained on the surface of glass sample is shown in Fig.4. Density, glass transition temperature, microhardness were found to increase up to 15mol% of alumina and then they showed the decreasing trend. Thermal expansion coefficient decreased continuously with alumina content as seen in Fig. 5.
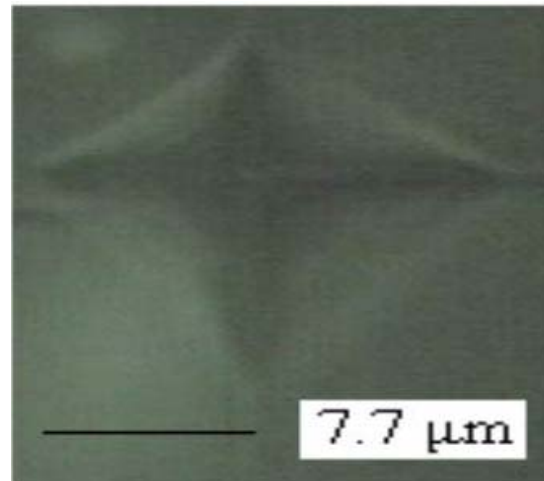

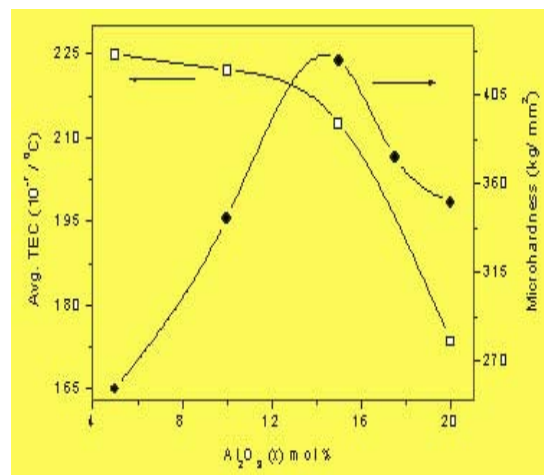*Fig. 4. Typical Vickers' impression on the glass sample surface*

Fig.5. Dependence of average thermal expansion coefficient and microhardness on composition of x Al_2O_3 (1-x) $NaPO_3$ glasses

Table 1: Density, molar volume, glass transition temperature, microhardness, thermal expansion coefficient and optical gap for different NAP glass samples.

Composition (Nominal) Na_2O-Al_2O_3-P_2O_5 (mol %)	Density (gm/cm^3)	V_M. (cm^3)	T_g (^{o}C)	MH Gpa	TEC 10^{-7}/^{o}C (30-300 ^{o}C)	E_{opt} (eV)	O/P Ratio
47.5-5-47.5	2.489	40.96	300	2.55	224.79	3.45	3.15
45-10-45	2.608	39.09	383.5	3.42	221.98	3.32	3.33
42.5-15-42.5	2.691	37.89	445.2	4.22	212.41	3.13	3.52
41.25-17.5-41.25	2.57	39.71	--	3.73	203.35	--	3.63
40-20-40	2.52	38.42	404.9	3.50	173.29	3.51	3.75

Optical gaps for different glass samples as measured from transmission characteristics were found to be in the range 3.13 to 3.51eV. It initially decreased with alumina content upto 15mol% and then increased. This behaviour of various physical properties is thought to be due the change in the average aluminum coordination number from six Al(6) to four Al(4) (i.e. Al (OP) $_6$/Al (OP) $_4$ ratio) along with the changes in polyhedra linkages in the glass network due to change in O/P ratio, which was evident from FTIR measurement

Glass ceramics

Magnesium aluminium silicate glass- ceramics:
The glass-ceramics based on the magnesium aluminium silicate system belong to an important class of advanced technological materials, having a wide range of applications[22-24]. A study has been carried out to investigate the effects of composition and processing temperatures in MAS glass ceramic. Table-2 gives the nominal composition, density, Tg and average TEC of the base glass. Glass transition temperatures of base glasses decrease and thermal expansion coefficients increase with the increase in the content of MgF_2. On the other hand, glass transition temperatures of the base glasses increase and thermal expansion coefficients decrease with the increase in the content of MgO. The average TEC of base glass seems to be dependent on the content of Mg. The sample having maximum Mg concentration shows the lowest TEC. It seems that as MgO /SiO_2 ratio increases, a more rigid glass network is formed (evident from high value of Tg i.e. 664.9^{o}C for batch-IV), which increases the bond strength and decreases the local vibration -O- resulting in low TEC.

Table 2: Nominal compositions, density and the average TEC of different batch samples

Batch	SiO_2/ M-oxide	MgO (mol%)	MgF_2 (mol%)	Density (gm / cc) (Base glass)	Tg (^{o}C)	Average TEC (10^{-6}/ ^{o}C) (Base glass)
Batch-I	1.137	12.85	0.00	2.501	653.6	7.937
Batch-II	1.127	12.85	6.6	2.55	610.8	8.35
Batch-III	1.129	12.85	13.2	2.605	599.8	8.38
Batch–IV	0.764	25.7	6.6	2.593	664.9	7.25

The glasses processed at different temperatures produced different phases thus affecting the physical properties. Fig. 6 shows the XRD patterns for glass-ceramics processed at different temperatures.
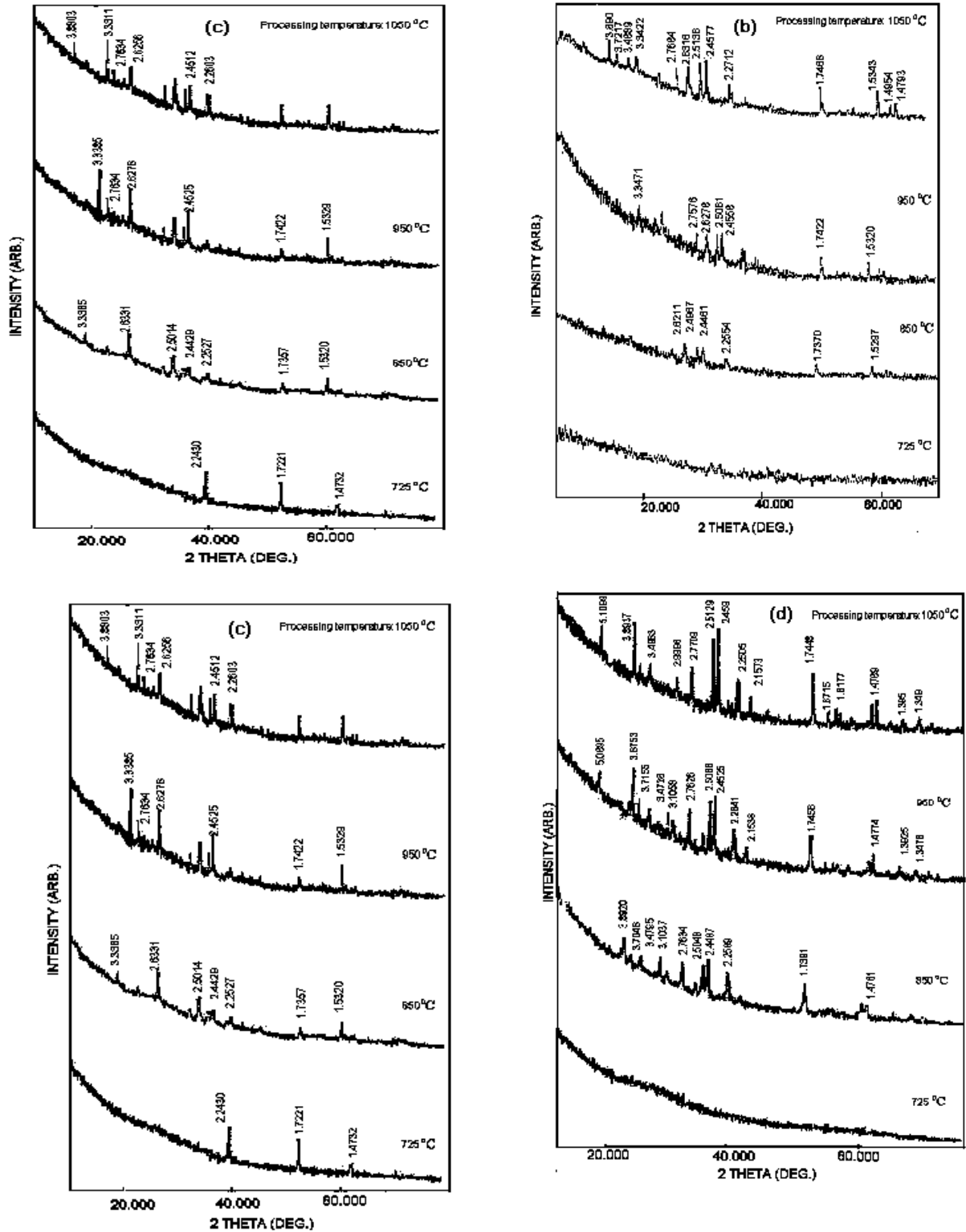

Fig.6 XRD patterns at different processing temperatures; (a) Batch-I, (b) Batch –II, (c) Batch-III and (d) Batch-IV

The thermal expansion coefficients for different batch samples after processing at different temperatures are found out. Dependence of average TEC (30-300 ^{o}C) as a function of processing temperatures for all the batches is shown in Fig. 7. The TEC of the base glass of batch-I (7.936 x 10 $^{-6}$/^{o}C), increases rather slowly with processing temperature, reaching to 8.6 x10 $^{-6}$/^{o}C at 1050°C. It is interesting to note that, although XRD measurements do not show any crystalline phase formation up to 850°C, there is an increase in TEC. This might be due to molecular/atomic rearrangements in the material due to processing temperature.
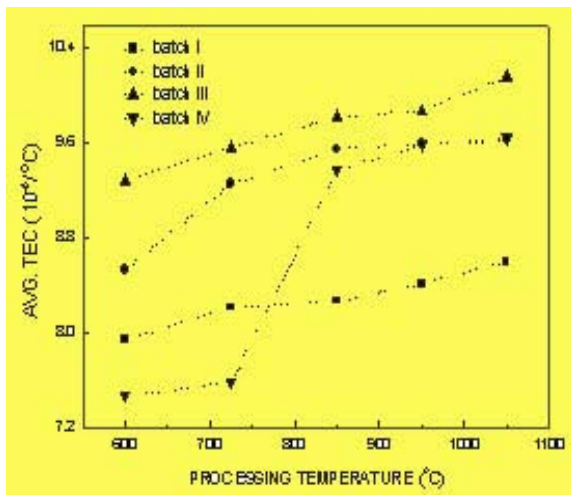

Fig.8. SEM photograph of batch-II glass-ceramic sample processed at 1050°C

There is a slow increase up to 725°C and then rises sharply to 9.37 x 10 $^{-6}$/^{o}C at processing temperature of 850°C and again attains a value 9.643 x 10 $^{-6}$/^{o}C after processing at 1050°C. However, sharp rise in TEC is due to the formation of Mg_2SiO_4 phase, which has higher thermal expansion coefficient[25]. Best machining characteristics were seen with increased fluoroplogopite phase giving platelike crystallites[16] as shown in SEM micrograph shown in Fig.8. Photographs of various MAS glass-ceramics samples and components fabricated using in-house prepared material are shown in Fig. 9.

Fig. 7 Average TEC Vs processing temperatures for batches- I to IV.

TEC of the base glass of batch-II is to found be 8.35 x10^{-6}/^{o}C, which gradually increases to 9.6 x 10^{-6}/^{o}C after processing at 1050°C. This increase in TEC is due to formation of different crystalline phases at different processing temperatures. The TEC of the base glass of batch-III is about the same (8.38 x 10 $^{-6}$/^{o}C) as for batch-II and also follows the similar dependence of TEC with processing temperature but has higher basic TEC. This is thought to be due to higher percentage of fluorophlogopite phases formed due to increased content of nucleating agent. The TEC batch-IV samples varies in somewhat complex manner as evident from Fig. 8.
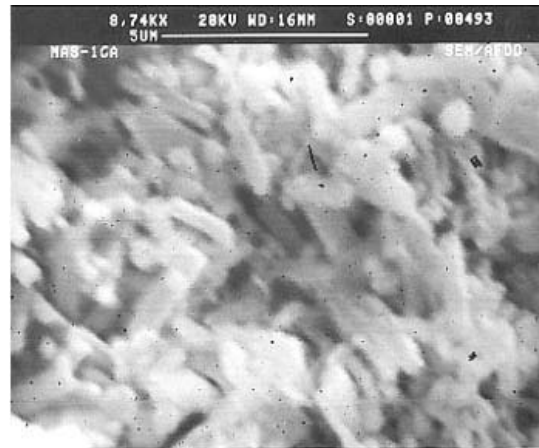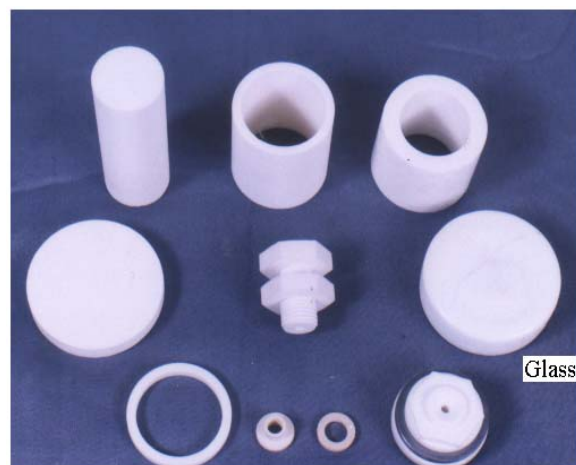

Fig. 9. Photographs of different MAS glass-ceramics and some fabricated components

Table 3. Density, Molar volume, Vicker's hardness number and average TEC for glass-ceramics in Li_2O–ZnO–SiO_2–P_2O–Na_2O–B_2O_3 system

Sample no.	ZnO/ (ZnO+SiO2)	Density (gm cm^{-3})	Molar Volume (cm^3 mol^{-1})	Hardness (GPa)	TEC (30-450ºC) (10^{-7}/ºC)
LZSH-03-1	0.10	2.62	21.90	6.56	125
LZSH-03-2	0.15	2.67	21.77	6.37	130
LZSH-03-3	0.20	2.70	21.74	6.12	132
LZSH-03-4	0.25	2.73	21.72	5.93	164
LZSH-03-5	0.31	2.82	21.27	5.79	185

Lithium zinc silicate glass ceramics: Glass-ceramics derived from the base glass of Li_2O-ZnO-SiO_2-Na_2O and B_2O_3, etc. have attracted a lot of attention to researchers not only because they can be prepared with a wide range of thermal expansion coefficients (from 50×10^{-7} to 200×10^{-7} /°C) by controlling heat treatments but also because of some interesting basic properties. The various constituent oxides in the base glass have their own specific functions. The introduction of Na_2O and ZnO in the glass composition modifies thermo physical properties, including reduction in viscosity increase in thermal expansion and B_2O_3 acts as glass network former [26]. LZS glasses containing Li_2O-ZnO-SiO_2-Na_2O-B_2O_3-P_2O_5 were prepared. The effect of ZnO/ (ZnO+SiO$_2$) ratio on various thermo-physical properties was investigated by changing the ratio from 0.1 to 0.31(Table-3). Density (ρ) was found to increase from 2.62 to 2.82 gm cm^{-3} while microhardness (*VHN*) decreased from 6.56 to 5.79 GPa with increase in ZnO/(ZnO+SiO$_2$) ratio in the glass-ceramics. Average thermal expansion coefficient in the temperature range 30 to 450°C increased from 125×10^{-7} to 185×10^{-7}/^{o}C. The increase in expansion coefficient and decrease in microhardness are thought to be due to the formation of different phases, which in turn influence the rigidity/bonding in the glass-ceramics. The

material has been used for the fabrication of hermetic seal with copper.
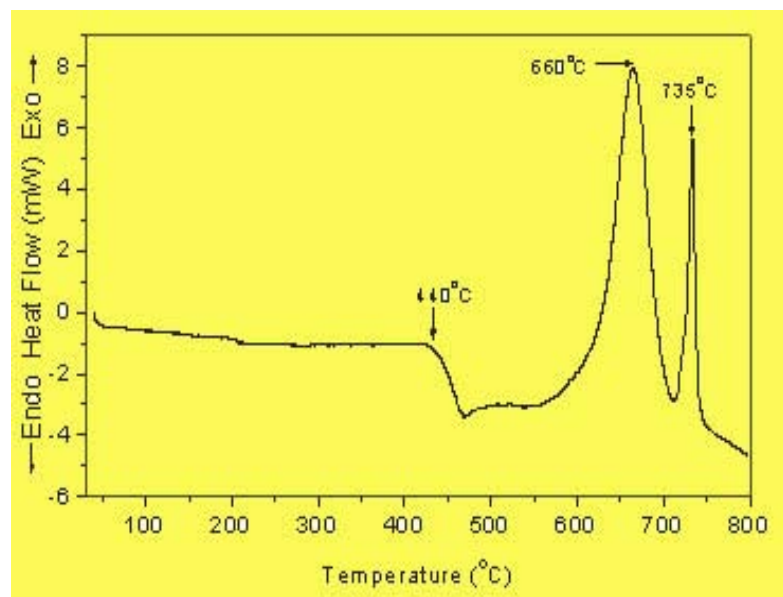
Fig. 10. DTA curve for LZS glass sample

Figure 10 shows a typical DTA curve taken on the virgin LZS glass under present investigation. The endothermic base line shift at 440°C gives the glass transition temperature. Two sharp exothermic peaks at 660°C and 735°C are the two crystallization peaks. XRD patterns for all the samples under present investigations are shown in Fig.11. Crystalline peaks corresponding to the different crystalline phases are marked with different symbols and major crystalline phases namely cristobalite, $Li_3Zn_{0.5}SiO_4$ and Li_2SiO_3 are identified. It is noted that the intensity of cristobalite and $Li_3Zn_{0.5}SiO_4$ crystalline phase increases whereas the intensity of Li_2SiO_3 crystalline phase is

Fig. 11. XRD patterns for glass-ceramics in Li₂O-ZnO-SiO₂-Na₂O-B₂O₃-P₂O₅ v system

Fig. 11. XRD patterns for glass-ceramics in Li_2O-ZnO-SiO_2-Na_2O-B_2O_3-P_2O_5 v system

decreased with increase in $ZnO/(ZnO+SiO_2)$ ratio (sample nos. LZSH-03-1 to LZSH-03-5).
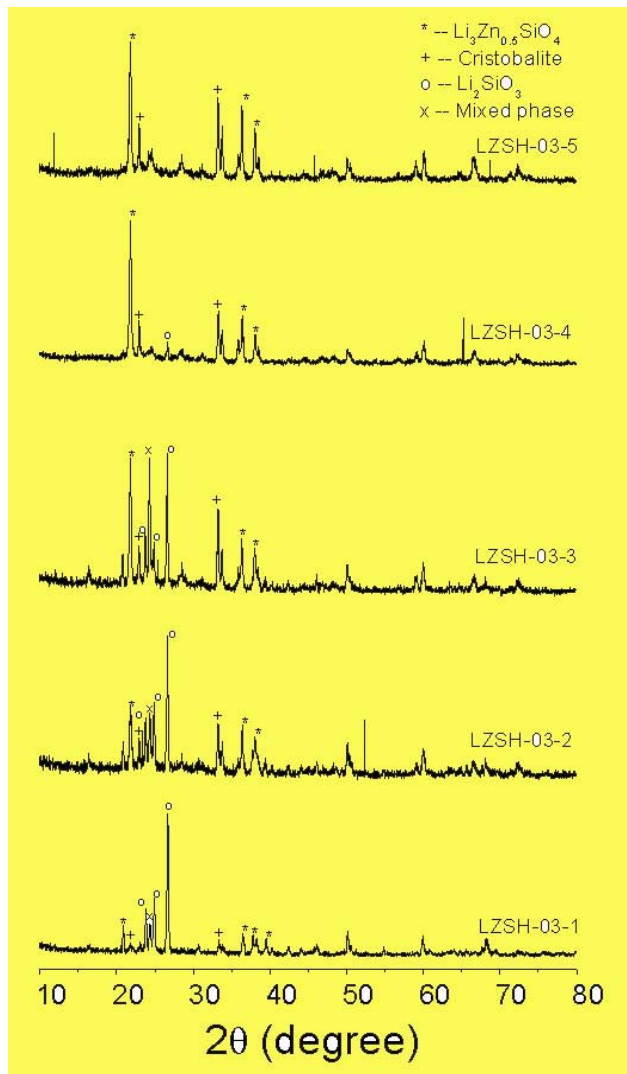
Figure 12 shows variation of microhardness and thermal expansion coefficient with $ZnO/(ZnO+SiO_2)$ ratio. Decrease in microhardness and increase in TEC with more $ZnO/(ZnO+SiO_2)$ ratio is the glass-ceramic reflect that glass network becomes less rigid as silica content decreases with increase in $ZnO/(ZnO+SiO_2)$ ratio present in the glass-ceramic.

This decreasing trend can also be understood in the light of the XRD results as explained above. It was already pointed out that $Li_3Zn_{0.5}SiO_4$ crystal phase increases and Li_2SiO_3 crystal phase decreases with more $ZnO/(ZnO+SiO_2)$ ratio in the glass-ceramics. The increase in $Li_3Zn_{0.5}SiO_4$ phase which has lower bond strength than Li_2SiO_3 phase may be the responsible for decrease in the hardness. It also gives strong evidence that microhardness is a bond sensitive property [26].

Fig. 12. Variation of microhardness and TEC with ZnO/(ZnO+SiO₂) ratio.

Fig.13. Photograph of LZS glass-ceramic to metal seal

In the fabrication of seal, the hold up time at the melting temperature has been found to have significant effect on sealing behavior. The seal fabricated with optimal heating schedule and dwell time at melting temperature was found to withstand a vacuum of 10^{-6} torr with helium leak rate of less than 3×10^{-10} torr litre/sec. Figure 13 shows the photograph of a GCM seal.

Acknowledgement

References

1. W.D. Kingery, H.K. Bowen and D.R. Uhlmann, Introduction to Ceramics (John Wiley & sons, NY, 1976)

2. P.W. McMillan, Glass Ceramics, (AP Lond. 1964)p 2, and 2nd Edition(1979)

3. G. Partridge and T. Hales, in: Surfaces and Interfaces – British Ceramic Proceeding : 48, (Eds. R Morrel and G Partridge, Inst. Ceramics, UK, 1991) p161

4. B.L. Metcalfe, I W Donald and D J Bradley, ibid p 177

5. W.J. McCraken in: Corrosion of Glass, Ceramics, and Ceramic superconductors, (Eds. D C Clark and B K Zoitos, Park Ridge: Noyes,1992)p 432.

6. W Donald, J. Mater. Sci., 28(1993) 2841.

7. A.W.A. EI-Shennawi, A.A. Omar & A.R. EI-Ghannam, , Ceram. Int.17(1991)25

8. Lj Radonjie and lj Nikolic, J. Eur.. Cerm. Soc. 7(1991)11

9. W. Donald, B.L. Metcalfe, D.J. Wood and J.R. Copley, J. Mater. Sci., 24 (1989) 3892

10. E. Demirkesen and E. Maytalman, Ceramics International 27 (2001)99

11. R.K. Brow, T.M. Alam, D.R. Tallant, and R.J. Kirkpatrik, MRS Bull., Nov. (1998)63

12. J.A. Wilder, J. Non-cryst. Solids 38/39(1980)879

13. N.Bandhopadhyay, S.S. Tamhankar, M.J. Kirschner, Eur. Pat. Appl. EP 311308

14. V.K. Shrikhande, V. Sudarsan, G.P. Kothiyal, and S.K. Kulshrestha, J. Non-cryst. Solids, 283(2001)18

15. M. Goswami, T. Mirza, A. Sarkar, S. Manikandan, Sangeeta, S.L. Verma, K.R. Gurumurthy, V.K. Shrikhande, and G.P. Kothiyal, Bull. Mat. Sci., 23{2000)

16. M. Goswami, A. Sarkar, T Mirza, V.K. Shrikhande, Sangeeta, K.R. Gurumurthy, and G.P. Kothiyal, Ceramic International, 28(2002)585

17. V. Sudarsan, V.K. Shrikhande, G.P. Kothiyal, and S.K. Kulshrestha, J. Phys.: Condens. Matter, 14(2002)6553

18. Y.B. Peng and D.E. Day Glass Technol. 32 (1991) 166

19. R.K. Brow and D.R. Tallant J. Non-Cryst Solids 222 (1997) 396

20. R.K. Brow, R J Kirkpatrick and G.L. Turner J. Am. Ceramic. Soc. 73 (1990)2293

21. R K Brow, R J Kirkpatrick and G LTurner J. Am. Ceram. Soc. 76(1993) 919

22. D.G. Grossman, J. Am. Ceram. Soc., 55(1972)446

23. D.S. Baik, K.S. No, J S Chun, , J. Am. Ceram. Soc., 78(1995)1217

24. D.S. Baik, K.S. No, J S Chun, Y.Y. Yoon, H.Y. Cho, J. Mater. Sci., 30(1995)1801

25. J.D. Cawley, W.E. Lee, Materials Science and Technology, (M Swain, Ed, 1994) Vol. 11, p.69

26. P.W. McMillan, Glass Ceramics(Academic Press, London, 2nd edn.)197

27. J. Zarzycki, Materials Science and Technology, (Weinheim (Ed), 1991,New York),Vol. 9 p.667

The author was honoured with the MRSI Medal Lecture award for the year 2003 at 14th Annual General Meeting of Materials Research Society of India (MRSI) held at BARC during February 11-13, 2003.

About the author ...

Dr G P Kothiyal, *Head, Glass and Ceramics Technology Section of TPPED, BARC, joined BARC in 1970 after completion of Post Graduate Training in Physics from 13th batch of BARC Training School, and took up research in the area of solid state physics/materials science. The MRSI Medal Lecture award for the year 2003 has been conferred upon him for his outstanding contributions in the field of materials science and engineering. He has also been honoured recently (2002) for his remarkable editing ability by Indian Society of Health, Environment, Education and Research (ISHEER), Jodhpur Chapter. Dr Kothiyal has been associated with the editorial board of "Vaigyanik", a quarterly Journal of Hindi Vigyan Sahitya Parishad, BARC, for the last twenty years and is currently its Chief Editor. Earlier he was honoured by a title of 'Vigyan Vachaspati' by Vigyan Parishad Prayag in 1999, for his contributions in the field of science communication/ popularisation in Hindi. He has published more than 130 papers in International/National journals/proceedings in the area of materials science. He is a recognised PhD guide in Physics from University of Mumbai.*

ELECTROPHORETIC STUDY OF DNA FOR DETECTING DRUG INDUCED CANCER CELL DEATH

Pratip Shil and P.B. Vidayasagar
Department of Physics, University of Pune, Pune

and

K.P.Mishra
Radiation Biology and Health Sciences Division
Bhabha Atomic Research Centre

Introduction

Gel electrophoresis is a physical technique widely used in Molecular Biology for the study of macromolecules like proteins, DNA and RNA. This technique is based on the electrostatic mobility of molecules under the influence of electric field. The velocity of migration (v) of a biomolecule in an electric field depends on the applied electric field strength (E) , the net charge on the biomolecule (z) and the frictional coefficient (f) as :

$$v = E.z/f \qquad (1)$$

The frictional force f depends on both the mass and shape of the biomolecule and the viscosity of the medium . Assuming spherical shape of the biomolecule with radius r, the force is given by

$$f = 6\,\pi\eta r \qquad (2)$$

This implies that the molecules with smaller masses will experience lesser frictional force and travel greater distances under the effect of the electric field whereas molecules with greater mass will travel shorter distances. This enables the separation of the molecules on the basis of molecular weight. The separation is usually carried out in a porous gel that governs the magnitude of separation. Chemically inert materials like polyacrylamide or agarose are used for gel preparation and choosing various concentrations of the material can control the pore size.

This technique is of immense importance in molecular biology for its ability to separate molecules on the basis of their molecular weight. This technique is also very important in cancer research as it can be used to investigate the changes in cancer cells at the molecular level over a wide range including expression of proteins, fragmentation of DNA, etc.

Electrophoresis, Liposomal Encapsulation of Anti-cancer Drug and Cytotoxicity to Cancer Cell

Anticancer drugs can kill cancer cells either by initiating apoptosis or necrosis. Apoptosis or programmed cell death is characterized by the fragmentation of the DNA molecules into units with multiples of 180 base pairs. DNA fragmentation being a biochemical hallmark of apoptosis is an important parameter for studying the effectiveness of anticancer drugs or treatment protocol. Cellular DNA isolated from apoptotic cells and subjected to gel electrophoresis show a ladder pattern in the gel with fragmented DNA molecules, having different molecular weights, arranged in bands separated from each other. In the present study

electrophoresis technique has been used to investigate the effect of anticancer drug Doxorubicin on human Leukemia cells HL60 both as free drug and as liposome –encapsulated form.

HL60 cells in culture conditions were treated with different concentrations(concentrations: 0-10 µg/ml) of Doxorubicin hydrochloride both as free drug and as liposome- encapsulated form and incubated. At different incubation times post treatment cells were lysed and cellular DNA was isolated using biochemical protocols. The isolated DNA samples were then subjected to gel electrophoresis in agarose gel. The fragmentation of DNA was detected from the formation of ladder pattern in the gel (after electrophoresis) in treated samples, indicating apoptosis -- cell death. In case of free drug, the appearance of the first fragmented DNA ladder in electrophoresis occurs for incubations of 23, 16 and 8 hrs respectively for drug concentrations 1, 5 and 10 µg/ml whereas in case of liposomal

drug this appears at 16, 8 and 4 hr respectively for the concentrations of 1,5 and 10 µg/ml. The result indicated enhanced cytotoxicity and apoptosis for liposome-mediated delivery of the drug. Electrophoresis method has been used effectively to detect drug-induced apoptosis.

Conclusions

Cancer cells are characterized by their resistance to apoptosis due to various factors. The DNA of apoptotic cells shows unique fragmented pattern in gel electrophoresis experiments. Electrophoresis has proved a powerful molecular method to distinguish between normal and apoptotic cells. Analysis of DNA fragmentation pattern also allows to distinguish between normal and transformed cells. Liposome encapsulated antitumor drugs have been shown to be efficiently delivered to target cells and produce apoptosis *in vitro* using electrophoresis method.

Mr Pratip Shil received the R. Chandrashekhar Memorial Foundation's Dr. (late) M.R. Bhide Award for Best Paper presentation in Raman Memorial Conference held at the University of Pune

---

About the authors ...

Mr Pratip Shil did his MSc. in Physics with Biophysics as specialization from the Department of Physics, University of Pune, and is currently working as JRF under the BARC- Pune University Collaborative Research Program .

Dr P.B.Vidyasagar is currently Professor (Biophysics) in the Department of Physics, University of Pune, and is also the Director, School of Basic Medical Sciences, University of Pune. He is also Senior Associate, Abdus Salam International Center for Theoretical Physics, Trieste , Italy.

Dr Kaushala Prasad Mishra joined BARC in 1969 through 12th batch Training School in Chemistry and is internationally known for his contributions in the area of Free Radical Biology and Radiation Biology. His major research interests concern the mechanism of radiation damage to normal and tumor cells and its modification by chemical and physical agents. More recently, focus of his research has been concerning the role of ROS in oxidative stress induced apoptotic cell death relevant to radioprotection and cancer radiotherapy. Currently, Dr Mishra is the Head, Radiation Biology and Health Sciences Division of BARC. He has edited a book titled **Radiobiology and Biomedical Research**. Together with his colleagues, Dr Mishra has designed and developed a Cell Electroporator for biomedical research and applications, which is under Technology Transfer from this Centre. He has received several professional recognitions for his significant research contributions in the area of Radiation Biology and Life Science. Dr Mishra is a Fellow of National Academy of Sciences, India, Vice President of Bioelectrochemical Society of India, Past President of Section of New Biology, 88th Indian Science Congress, a Member of the Executive Council of Asia Pacific ESR/EPR Society, General Secretary, Indian Biophysical Society, Vice President of Society of Free Radical Research of India, Council Member, International Association of Radiation Research. He was invited as Visiting Scientist to several Universities/Institutions in India and abroad.

PULSE RADIOLYSIS STUDIES OF 5-HYDROXY INDOLES WITH ·NO₂ RADICALS

G. H. Naik, K. I. Priyadarsini and Hari Mohan
Radiation Chemistry & Chemical Dynamics Division
Bhabha Atomic Research Centre

Abstract

The reactions of ·NO₂ radical with substituted 5-hydroxy indoles (5-hydroxy indole, 5-hydroxy tryptophol, 5-hydroxy tryptophan, 5-hydroxy tryptamine and 5-hydroxy-N(ω)-methyl tryptamine) were studied using nanosecond pulse radiolysis technique in the pH range of 5-10. In all these cases the transient species showed λ_{max} at 420 nm with shoulder in 350 - 370 nm region and attributed to indoloxyl radical and ·NO₂-adduct respectively. The bimolecular rate constant for formation of transient species was observed to increase from 10^5 M^{-1} s^{-1} to 10^7 M^{-1} s^{-1} with pH from 5 to 10. The transient absorption band at 420 nm was observed to decay by first order kinetics. Steady state analysis showed formation of stable nitrated indole absorbing at 420 nm.

Introduction

NO₂ radical is produced in the body during physiological processes such as nitric oxide oxidation, peroxidase catalysed reactions etc. It is a key player in cellular nitrosative stress [1]. It can undergo variety of reactions like recombination with radical species, addition to double bonds, electron transfer and hydrogen abstraction. Since H-abstraction and addition across the double bond requires high activation energy these reactions are found to be less common as compared to radical recombination and electron transfer reactions [2]. It has high reactivity towards biomolecules such as DNA, proteins and enzymes [3]. 5-hydroxy indoles form an important class of biomolecules and are found in significant amounts in the central nervous system. Free radical induced oxidative modification of these compounds and their metabolites are being implicated in neurodegenerative diseases [4-6]. With these objectives, the reactions of ·NO₂ radical with substituted 5-hydroxy indoles have been studied.

Experimental
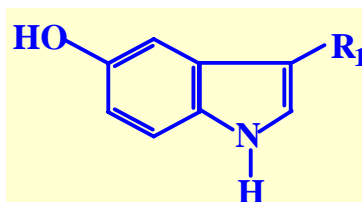
¹HI	R_1	=	H
HTe	R_1	=	CH₂CH(OH)NH₂
HTn	R_1	=	CH₂CH(COOH)NH₂
HTl	R_1	=	CH₂CH₂OH
HMT	R_1	=	CH₂CH(OH)NHCH₃

Scheme : 1

Feshly prepared aqueous solutions of 5-hydroxy indole (HI), 5-hydroxy tryptophol (HTl), 5-hydroxy tryptophan (HTn), 5-hydroxy tryptamine (HTe) and 5-hydroxy-N(ω)-methyl tryptamine (HMT) [scheme 1] were used for each experiment. pH was adjusted with NaOH/HClO₄ in phosphate buffer. Pulse

radiolysis studies were performed with high energy electron pulses (7 MeV. 50 ns) obtained from a linear electron accelerator. The bimolecular rate constant values were determined from the linear regression plot of pseudo-first order rate constant (k_{obs}) versus solute concentration.

NO_2 radicals were generated on radiolysis of N_2-saturated solution of KNO_2 (20 mM) and KNO_3 (160 mM) as shown by reactions 1 and 2. Steady state γ-radiolysis experiments were carried out with a ^{60}Co source (dose = 7.9 Gy min^{-1}).

$$NO_2^- + \cdot OH \rightarrow \cdot NO_2 + OH^- \qquad (1)$$

$$NO_3^- + e_{aq}^- \rightarrow NO_3^{2-} \rightarrow \cdot NO_2 + 2 OH^- \quad (2)$$
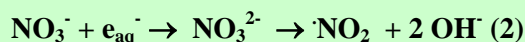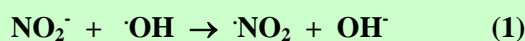
Results and Discussion

Pulse radiolysis studies

The reaction of $\cdot NO_2$ radical with HTl showed the formation of a transient absorption band at 420 nm with a shoulder in 350 – 370 nm region (Fig. 1a). The reaction at lower pH was slow and much lower transient absorbance was seen at pH 7 (Fig. 1b) and 5 (Fig. 1c).

The transient absorption band at 420 nm was observed to decay by first order kinetics with k = 5.3 s^{-1} (inset of Fig. 1). The nature of the transient spectrum and decay kinetics were similar to the transient species formed on reaction of $N_3^\cdot$ with HTl. The transient species (Fig 1a) is assigned to indoxyl radical produced by one-electron oxidation followed by deprotonation at the OH group. The reaction of $\cdot NO_2$ radical with other substituted 5-hydroxy indoles (scheme 1) at pH 9 also showed the formation of transient absorption band at 420 nm. In all these cases, the reaction at lower pH was slow and the transient absorbance was small. However the decay of the transient species formed on reaction of $\cdot NO_2$ radical with
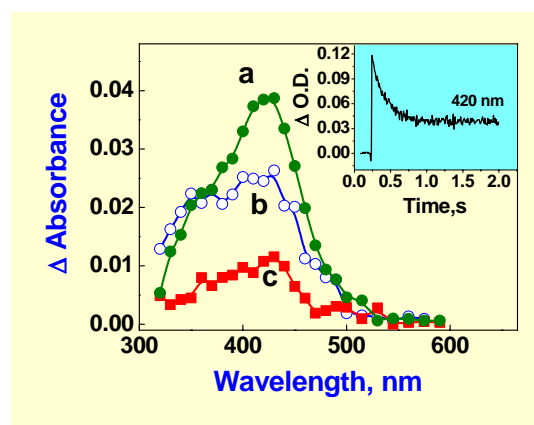
Fig. 1   Difference transient absorption spectra obtained of reaction of $\cdot NO_2$ radical with HTl at pH 9 (a); pH 7 (b) and pH 5 (c). Dose per pulse= 13 Gy. Inset shows the absorption-time plot for the transient at 420 nm (pH 9; dose per pulse = 40 Gy).

different substituted 5-hydroxy indoles was different. The decay of the indoloxyl radical produced from HTe, HTn and HMT was in the range of $(5 – 9) \times 10^2$ s^{-1}.while the indoloxyl radical produced from HI and HTl was in the range of 5 - 6 s^{-1}. The difference in decay rate of the indoloxyl radical of different 5-hydroxy indole may be due to the fact that $\cdot NO_2$ may have different sites of reaction. In case of 5-hydroxy indole containing amino substituent, $\cdot NO_2$ radical may not only cause oxidation but also react with the amino group present in the side chain to cause deamination or nitrosation [7].

Steady state γ- radiolysis

The stable end products formed on reaction of $\cdot NO_2$ radical with substituted 5-hydroxy indoles was carried out by using steady state γ-radiolysis technoque. The absorption spectra were recorded in 300 – 600 nm region. Before γ–irradiation, the aqueous solution showed a peak at 350 nm and with very little absorption after 400 nm region (Fig 2a). On γ–irradiation, increased absorption was seen in 330 – 360 and 420 – 500 nm region (Fig 2b, 2c). The dimerisation reaction takes place through radical-solute reaction. One-electron oxidized species (indolyl radical) react
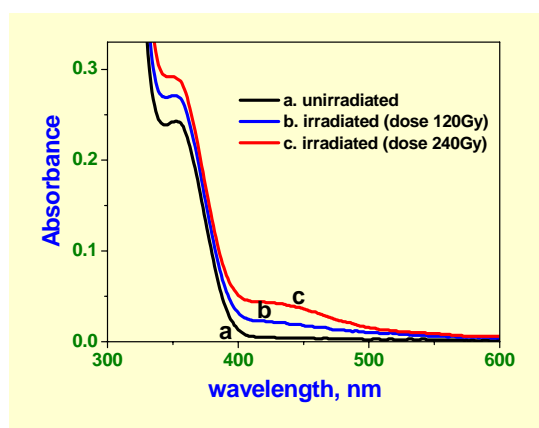
Fig .2 Optical absorption spectyra of N₂-saturated aqueous solution (pH 9) of HTl (550 μM) containing NaNO₂ (10 mM) and NaNO₃ (160 mM) before (a) γ–irradiation; after γ-irradiation with (b) 120 Gy and (c) 240 Gy γ–dose.

Scheme 2

with parent indole to form dimeric products. Thus γ-radiolysis studies showed that ·NO₂ radicals are able to induce not only one-electron oxidation but also nitration of the indole ring.

Conclusion

The 420 nm absorption is attributed to the one-electron oxidized species (indoloxyl radical). The absorption in 350 – 370 nm is due to the addition product (Scheme2). The yield and the rate of formation of transient species decreased with increasing pH from 5 to 9. The transient species formed from 5-hydroxy indoles containing amino group, decayed faster which may be due to the reaction of ·NO₂ radical with the amino group causing deamination or nitrosation. Steady state radiolysis showed the formation of stable products absorbing in 330 – 360 nm and 420 – 500 nm region.
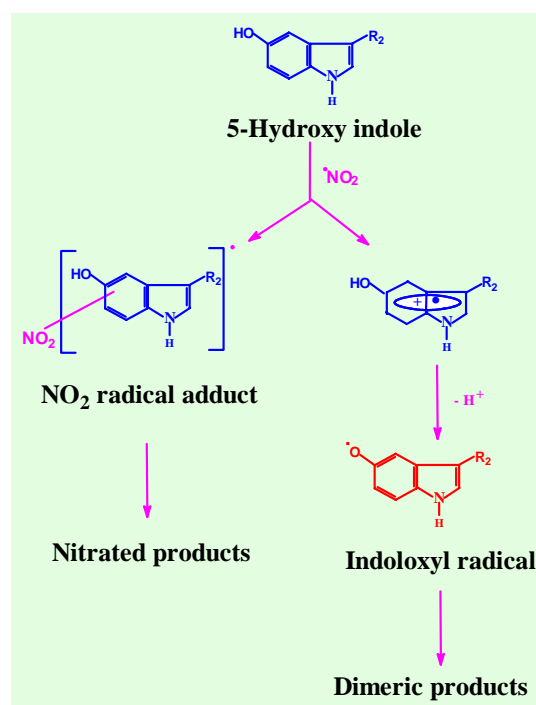
References

1. O Augusto, M. G. Bonini, A. M. E. Amanso, C. C. Linares, S. L. Santos, De Menezes, Free Radic Biol Med., 32, 841, 2002.
2. E. Ford, M. N. Hughes, P. Wardman, Free Radic Biol Med. 32, 1314, 2002.
3. T. Herraiz, J. Galisteo, Free Radic Res., 38, 323, 2004.
4. G. Dryhurst, Chem. Rev., 90,795, 1990.
5. P. G. Hela, N. R. Anipindi, K. I. Priyadarsini, P. O' Neill, J. Phys. Chem., 103, 8606, 1999.
6. G. H. Naik, K. I. Priyadarsini, H. Mohan, Phys. Chem. Chem. Phys., 4, 5872, 2002.
7. B. Blanchard, M. Dendane, J. F. Gallard, C. Houee-Levin, C. A. Karim, D. Payen, J. M. Launay, C. Ducrocq. Nitric Oxide, 1, 1442, 1997.

This paper was adjudged as one of the Best Posters in the National Symposium on Radiation & Photochemistry (NSRP 2003) held at IIT Kanpur during March 3 – 5, 2003.

About the authors ...

Mr Ganesh Naik *received his M.Sc degree in Organic Chemistry from Somaiya College, Mumbai University, in 2000. He is a DAE fellow working in Radiation Chemistry and Chemical Dynamics Divison, BARC. He is persuing his Ph.D degree in the subject entitled, 'Study of Free Radicals and Excited States of Some Important Biomolecules'.*

Dr Indira Priyadarsini *joined BARC in 1983. She obtained her Ph. D. in Radiation and Photochemistry in 1990. She has co-authored more than 70 papers in international journals on radiation chemistry, photochemistry and radiation biology. Employing fast reaction techniques, she has been studying the free radical reactions involving antioxidants, radio protectors and radio sensitizers in model systems. She is currently working on the elucidation of mechanism of antioxidant action involving natural products and herbal extracts.*

Dr Hari Mohan *joined BARC in 1967. Since then, he is actively involved in the study of fast reaction kinetics using accelerators and lasers. His current research interests include free radical reactions of halogenated and sulfur compounds and biomolecules of natural origin. He has co-authored more than 150 research papers in international journals. Presently, he is the Head, Radiation Chemistry Section of Radiation Chemistry & Chemical Dynamics Division, BARC.*

ONE-ELECTRON OXIDATION OF SELENOUREA IN AQUEOUS SOLUTION

Beena Mishra, K. I. Priyadarsini and Hari Mohan
Radiation Chemistry & Chemical Dynamics Division
Bhabha Atomic Research Centre

A b s t r a c t

One-electron oxidation of selenourea in aqueous solution has been studied using pulse radiolysis technique. The hydroxyl radicals react with a bimolecular rate constant of 9.9×10^9 M^{-1} s^{-1} and showed the formation of a transient absorption band with λ_{max} at 410 nm. The absorbance at 410 nm is observed to depend on solute concentration. The transient showed reactivity towards oxygen (k= 8.6×10^7 M^{-1} s^{-1}). Specific one-electron oxidants ($N_3^{\cdot}$, $Br_2^{\cdot-}$, $Cl_2^{\cdot-}$, $I_2^{\cdot-}$) and also $H^{\cdot}$ atom showed the formation of similar transient species. Based on these studies, the transient absorption band is assigned due to the solute dimer radical cation formed by 2-centre 3-electron bonding between two selenium atoms.

Introduction

S ulfur compounds are biologically important molecules as they are involved in many physiological functions. One of the factors responsible for their activity is their ability to react with reactive oxygen free radicals like hydroxyl radicals. On oxidation, organic sulfides produce dimer radical cations via a complex sequence of reactions involving α-thio radicals, OH-adduct and monomer radical cation [1]. The radiation chemistry of thiourea has been studied to understand its application as radioprotective agent and corrosion inhibitor. Selenium belongs to the same group and it is therefore interesting to see how selenium behaves on oxidation. With this objective, we have studied in detail the reactions of hydroxyl radicals and specific one-electron transfer agents with selenourea (SeU).

Experimental

The solutions of selenourea (Aldrich Chemicals) were prepared in nanopure water in phosphate buffers. Freshly prepared solutions were used for each experiments. Pulse radiolysis experiments were carried with high energy electron pulses (7 MeV, 50 ns) obtained from a linear electron accelerator. An aerated aqueous solution of KSCN was used to determine the dose delivered per pulse and it was kept close to 8 Gy. The reaction of $^{\cdot}$OH radical was carried out in N$_2$O-saturated aqueous solution where e_{aq}^- is quantitatively converted to $^{\cdot}$OH radicals (N$_2$O + $e_{aq}^- \rightarrow$ $^{\cdot}$OH + OH$^-$ + N$_2$). The reaction with specific one-electron oxidants was conducted under conditions such that the $^{\cdot}$OH radicals do not react with the solute and only the one-electron oxidants react with the solute. The reaction with H. atom was carried out at pH 1 in N$_2$-saturated solution containing tert-butyl alcohol to scavenge $^{\cdot}$OH radicals ($^{\cdot}$OH + (CH$_3$)$_3$COH $\rightarrow$ $^{\cdot}$CH$_2$(CH$_3$)$_2$COH + H$_2$O).

Results and Discussion

Figure 1 shows the transient absorption spectra obtained on pulse radiolysis of N$_2$O-saturated aqueous solution of selenourea, which exhibits λ_{max} at 410 nm. The transient absorbance at
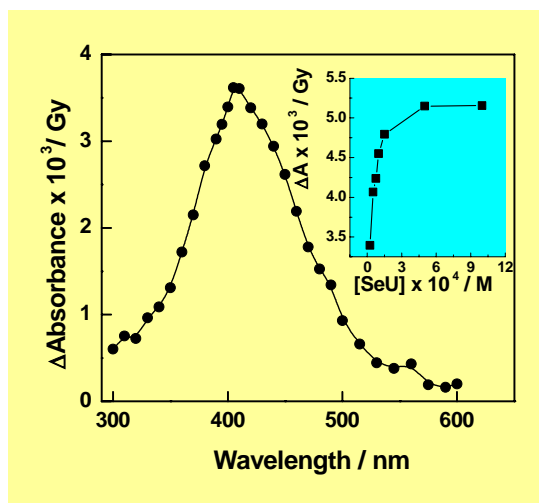
Fig. 1 Difference transient optical absorption spectrum obtained on pulse radiolysis of N_2O-saturated aqueous solution (pH 7) of SeU (50 μM). Inset show variation of absorbance at 410 nm as a function of SeU concentration.

410 nm was observed to increase with solute concentration (inset of Fig 1), suggesting the formation of a dimeric species. The rate constant for the reaction of ·OH radicals with SeU was determined by competition kinetic studies using 2-propanol (IP) as the standard solute. Using a value of $k_{IP + OH} = 1.9 \times 10^9$ M^{-1} s^{-1}, the bimolecular rate constant was determined to be 9.9×10^9 M^{-1} s^{-1} (Table 1).

Table 1: Kinetic and spectroscopic properties of dimer radical cation formed on reaction of ·OH radicals with selenourea

Parameters	Values
λ_{max} / nm	410
Bimolecular rate constant / M^{-1} s^{-1}	9.9×10^9
Association constant / M^{-1}	7.9×10^4
Second order decay constant (2k) / M^{-1} s^{-1}	3.3×10^9

The transient absorption band at 410 nm was observed to decay by second order kinetics with a 2k value of 2.7×10^9 M^{-1} s^{-1}. The decay was observed to be faster in the presence of oxygen (Fig 2). The pseudo-first order rate constant (k_{obs}) increased linearly with oxygen concentration (inset of Fig 2). The slope of the linear plot gave a bimolecular rate constant of 8.6×10^7 M^{-1} s^{-1}.
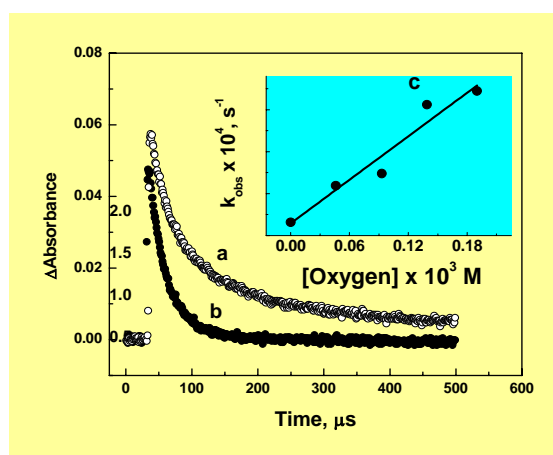
Fig. 2 Absorption-time profiles at 410 nm formed on pulse radiolysis of aqueous solution of SeU (1 mM, pH 7) in (a) N_2O and (b)N_2O-O_2. Inset shows variation of pseudo- first-order rate constant (k_{obs}) as a function of oxygen concentration.

The reaction with specific one-electron oxidants ($Cl_2^{·-}$, $Br_2^{·-}$, $I_2^{·-}$, $N_3^·$) produced transient absorption spectra with λ_{max} at 410 nm and the transient absorbance was observed to increase with SeU concentration in each case. The nature of the transient optical absorption spectrum obtained on reaction of ·OH radical with SeU was similar to that obtained on reaction with specific one-electron oxidants. Therefore the transient absorption band (Fig 1) is assigned to one-electron oxidized species of SeU.

Pulse radiolysis of N_2-saturated acidic (pH 1) aqueous solution of SeU (0.3 mM) containing tert-butyl alcohol (0.3 M) showed the formation of a transient absorption band at 410 nm. The transient absorbance at 410 nm was also observed to increase with SeU concentration.

The rate constant for the reaction of H· atom with SeU was determined to be 2.1×10^9 M^{-1} s^{-1}. The HO$_2$· radical was also observed to react with SeU with the formation of transient absorption band at 410 nm.

Based on these studies and the data available in literature on organic sulfur compounds, the transient absorption band at 410 nm is assigned to dimer radical cation, formed by 3-electron bonding between two selenium atoms (scheme 1).
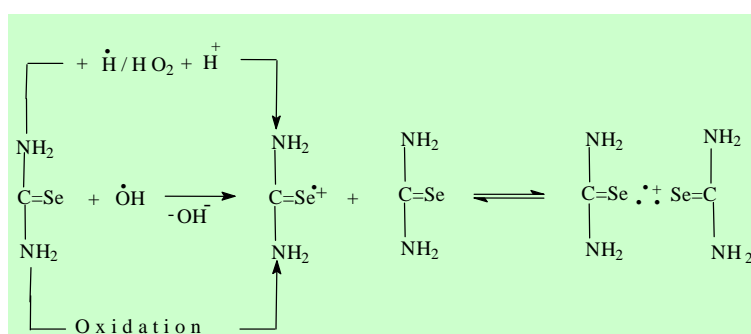
Scheme 1

The equilibrium constant (K) for the equilibrium process was determined by following equation [2].

$$\frac{A_0}{A} = 1 + K^{-1}\left[SeU\right]^{-1}$$

where A and A$_o$ are the absorbance at 410 nm at any given concentration of SeU (6×10^{-6} – 1×10^{-3} M) and the saturation absorbance of SeU (1×10^{-3} M) respectively. The plot of (A$_o$/A) – 1 against [SeU]$^{-1}$ gave a straight line with slope = 1/K. The equilibrium constant for the formation of dimer radical cation was evaluated to be 7.9×10^4 M^{-1}.

Conclusions

Hydroxyl radicals and specific one-electron oxidants react with selenourea to form a transient broad absorption band at $\lambda_{max} = 410$ nm and is assigned to dimer radical cation. Unlike organic sulfur compounds, the dimer radical cation of selenourea reacts with moleculae oxygen. H·/HO$_2$· also react to form dimer radical cation following H-abstraction reaction. The results also confirm that like sulfur, selenium formed 2-centre 3-electron bonding between two selenium atoms.

References

1. K.D. Asmus, in S-centered radicals, Z. B. Alfassi (Ed.) John Wiley: New York, p.142 (1999).
2. W. Wang, M. N. Schuchmann, H. P. Knolle, W. J. von Sonntag, C. von Sonntag, J. Am. Chem. Soc., 121, 238 (1999).

This paper was adjudged as one of the Best Posters in the National Symposium on Radiation & Photochemistry (NSRP 2003) held at IIT Kanpur during March 3 – 5, 2003.

About the authors ...

Ms Beena Mishra *received her M.Sc. degree in Chemistry with specialization in Inorganic Chemistry from Institute of Science, Mumbai, in 2001. She stood second in M.Sc. in Mumbai University. She is a DAE fellow working in Radiation Chemistry & Chemical Dynamics Division, BARC. She is persuing her Ph.D. degree in the subject entitled, "Free radical and transient studies of some biologically important organic and organometallic compounds".*

Dr Indira Priyadarsini *joined BARC in 1983. She obtained her Ph. D. in Radiation and Photochemistry in 1990. She has co-authored more than 70 papers in international journals on radiation chemistry, photochemistry and radiation biology. Employing fast reaction techniques, she has been studying the free radical reactions involving antioxidants, radio protectors and radio sensitizers in model systems. She is currently working on the elucidation of mechanism of antioxidant action involving natural products and herbal extracts.*

Dr Hari Mohan *joined BARC in 1967. Since then, he is actively involved in the study of fast reaction kinetics using accelerators and lasers. His current research interests include free radical reactions of halogenated and sulfur compounds and biomolecules of natural origin. He has co-authored more than 150 research papers in international journals. Presently he is the Head, Radiation Chemistry Section of Radiation Chemistry & Chemical Dynamics Division, BARC.*

PERFORMANCE EVALUATION OF HYPERSTOICHIOMETRIC $(U_{0.45}Pu_{0.55})C$ FUEL FOR FBTR FROM ITS OUT OF PILE PROPERTIES

A.K. Sengupta, J. Banerjee, T. Jarvis, T.R.G. Kutty, R. K. Bhagat, K. Ravi and S. Majumdar
Radiometallurgy Division
Bhabha Atomic Research Centre

A b s t r a c t

Some of the important out-of-pile thermo physical and thermo mechanical properties data like solidus temperature, coefficient of thermal expansion, thermal diffusivity/thermal conductivity and hot hardness of hyperstoichiometric mixed carbide fuel of Mark II composition [$(U_{0.45}Pu_{0.55})C$] have been generated as a function of temperature for prediction of its in-reactor performance. The out-of-pile chemical compatibility of the fuel with SS316 (20% cold worked) cladding material and sodium coolant has also been established experimentally. From the thermophysical properties data generated and out-of-pile chemical compatibility experiments it has been concluded that the Mark II fuel can be operated at a high power and linear heat rate without causing any clad breach.

Introduction

Hyperstoichiometric $(U_{0.3}Pu_{0.7})C_{1+x}$, the driver fuel for FBTR, has been replaced by hyperstoichiometric [$(U_{0.45}Pu_{0.55})C_{1+x}$] fuel to operate the reactor at full power (40 MW$_{th}$) and higher linear rate. Evaluation of the out-of-pile thermo physical and thermo mechanical properties of this, so far unknown fuel, is very important and essential. This will help to predict the in-pile performance of the fuel, to develop a computer code for whole core accident analysis and for reactor fuel pin design. Some of the thermo physical and thermo mechanical properties of concern are solidus temperature, coefficient of thermal expansion, thermal conductivity/diffusivity and hot hardness. It is also important to know the out-of-pile chemical compatibility of the fuel with the clad and coolant. In the present investigation, these properties of hyperstoichiometric $(U_{0.45}Pu_{0.55})C$ fuel have been generated as a function of temperature and its out-of-pile chemical compatibility with SS316 (20%CW) cladding and sodium coolant have been established experimentally.

Experimental

Material: Mixed carbide fuel samples were prepared by conventional powder metallurgy route where mixed carbide clinkers were prepared by vacuum carbothermic reduction of a mixture of UO_2 and PuO_2 powders. This was followed by milling, pre-compaction, granulation, final compaction and sintering. The sintered mixed carbide pellets contained less than 5000ppm of oxygen impurity and varying amount of (5-15 w%) M_2C_3 phase. The details of the mixed carbide fuel fabrication steps and characterization procedure have been given in reference 1.

Solidus temperature: The solidus temperature was estimated in a horizontal dilatometer when the sintered pellet was heated up to 2010^{0}C in

flowing argon gas and the change in length was monitored as a function of temperature (Fig 1a & b). The solidus temperature of this fuel was approximated to be ~ 1920^{0}C. Beyond this temperature a high rate of shrinkage of the material was observed, which could be attributed to the gradual melting of the pellet. This was confirmed by visual observation of the pellet after cooling to room temperature, which showed the pellet had lost its geometry due to melting.
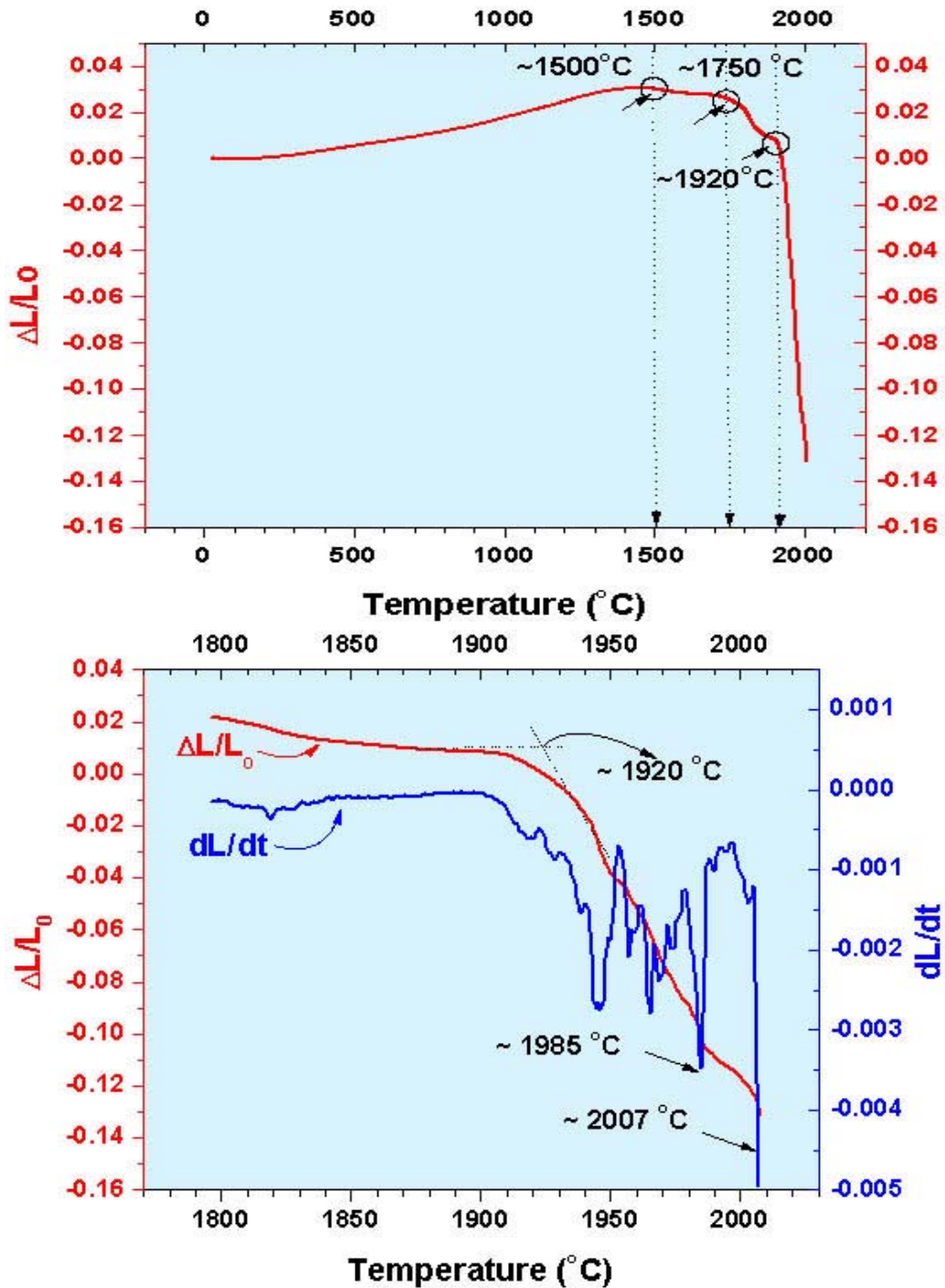
Fig. 1 a) Softening behavior of $(U_{0.45}Pu_{0.55})$ when continuously heated up to 2010C in a dilatometer; b) magnified high temperature end of the same curve.

Thermal Expansion: Percentage Thermal Expansion [$(\Delta L/L_0) \times 100$] data were generated between 300K-1800K and can be expressed by the following [2]:

$$[(\Delta L/L_0) \times 100]_T = -0.3333 + 7.1528E\text{-}4.T + 7.6889E\text{-}7.T^2 - 2.2249E\text{-}10.T^3 \quad (1)$$

where L_0 is initial length of sample, ΔL is change in length and T is temperature (K).

Thermal Conductivity: Thermal conductivity was derived from the experimentally measured thermal diffusivity data by laser flash method, specific heat from the literature and density. The thermal conductivity data (k) of the fuel can be expressed by [3] :

$$k(W/m.K) = 4.4946 + 0.0081.T - 5.1314E\text{-}6.T^2 + 3.4997E\text{-}9.T^3 \ (600°C \text{ to } 1650°C) \quad (2)$$

It was observed that thermal conductivity increases with increase in temperature.

Hot Hardness: Hot hardness was measured using a high temperature micro hardness tester with a Vickers Pyramid indenter to predict the softening behavior of the fuel and the onset temperature of thermal creep deformation. The details of the equipment and the procedures are given in reference 4. The plot of hardness vs. temperature indicates a gradual decrease in hardness with temperature. The plot of modulus compensated hardness vs. homologous temperature shows three distinct regions (see Fig 2) indicating different softening mechanism corresponding to each region [5].

Fig. 2 Modulus-compensated hardness (H/G) vs. homologous temperature (T/Tm) plot for the fuel.

Out-of-pile chemical compatibility: Fuel-Clad-Compatibility experiments were carried out by isothermal heating (973K and 1123K for 1000 hrs) of miniature capsules containing sintered hyperstoichiometric mixed carbide pellets in contact with SS316 (20%C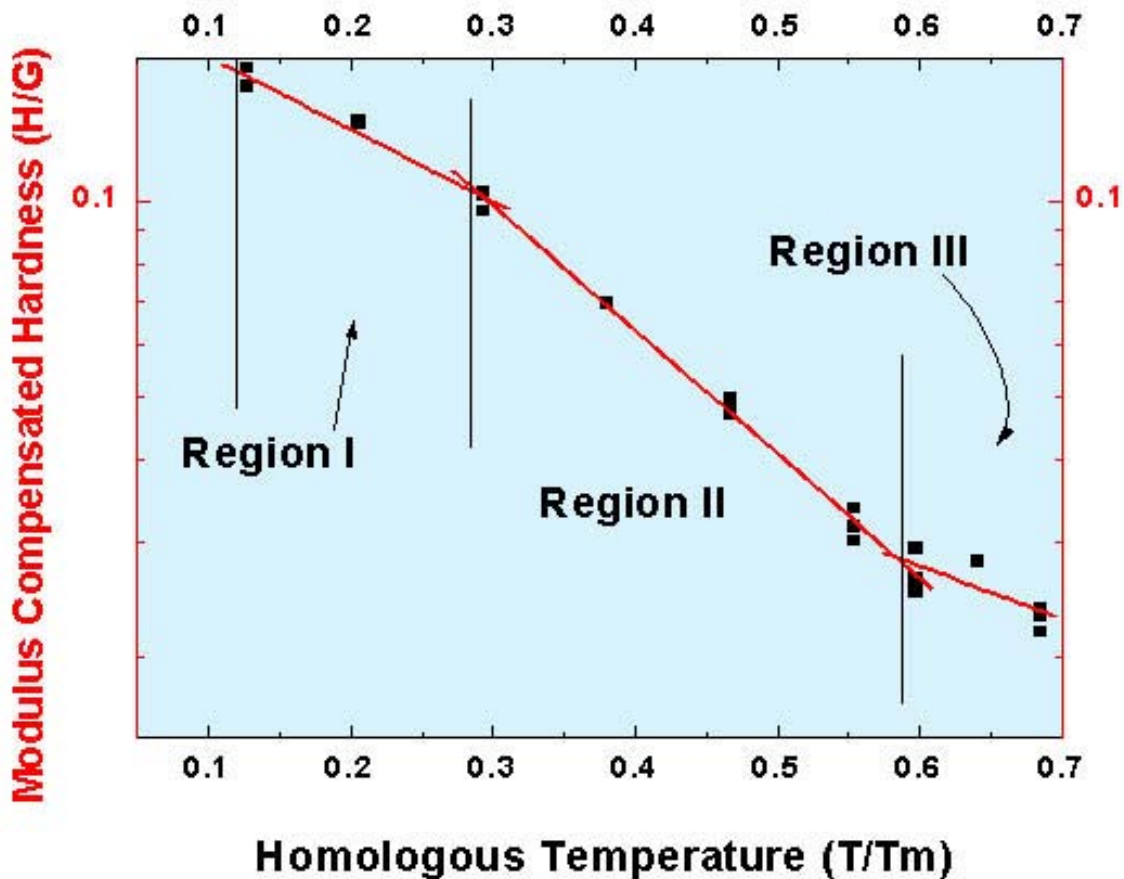W) cladding material in the form of a disk sealed under helium atmosphere by TIG welding. The design of the compatibility capsule was the same as has been used in an earlier study [6]. After the compatibility experiments, visual examination of the SS316 disks, cladding tubes and fuel pellets did not show any apparent chemical reaction as there was no bonding between the fuel pellets and the cladding disks. The depth of carburisation was also insignificant. Microhardness measurement along the cross section of the tube and disk show very minor hardness gradient from the pellet / clad interface compare to the bulk of the samples. It was established that there was excellent compatibility between the fuel and the cladding material and clad carburization was insignificant (<12μm).

The fuel-clad-coolant compatibility capsule design is shown in Fig 3. The capsule has two chambers, separated by a SS- 316 filter. Chamber-1 contains a perforated SS-316 cladding tube, in which 4 numbers of sintered carbide fuel pellets are loaded. Chamber-2 contains titanium sponge ('oxygen' getter) and sodium (coolant) rod. Sodium was allowed to come in chember-1 where it comes in intimate contact with cladding material and the fuel. Capsules were heated in this condition at 883K for 1000 and 2000hrs. After the experiments, sodium was leached out both from pellet and the cladding material. The clad and fuel were observed to be in good physical condition. Metallographic examination revealed a very narrow reaction layer near clad-coolant interface (Fig 4). Hardness profile of the SS316 (20% cold worked) cladding material from the fuel/clad interface is shown in Fig 5.
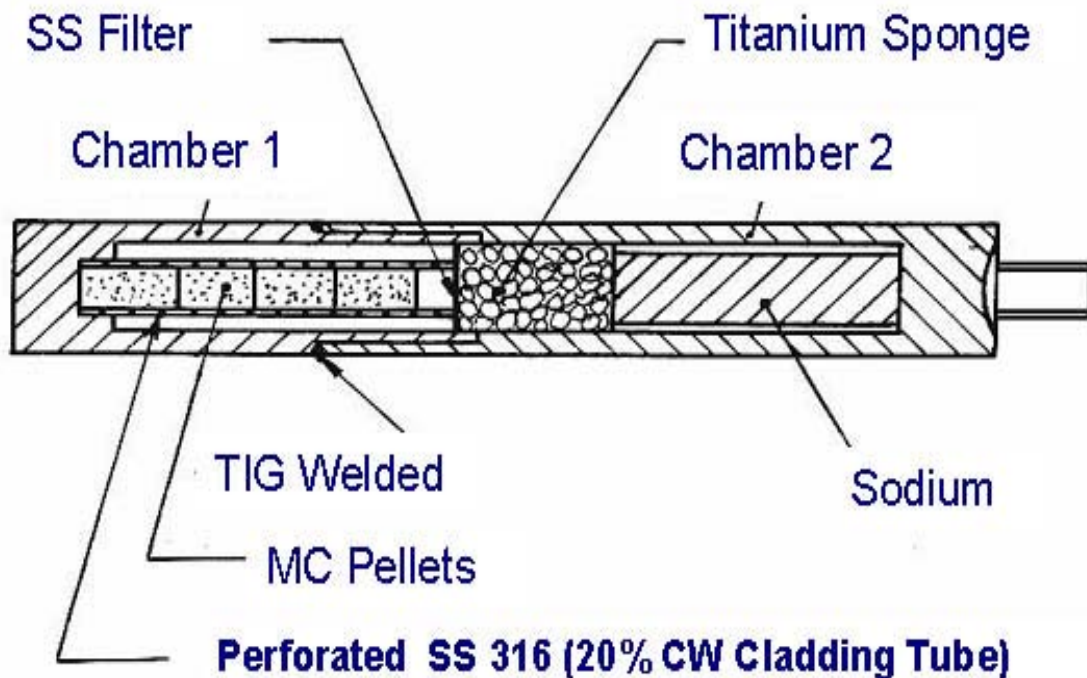
Fig. 3 Schematic diagram of fuel-clad-coolant compatibility capsule
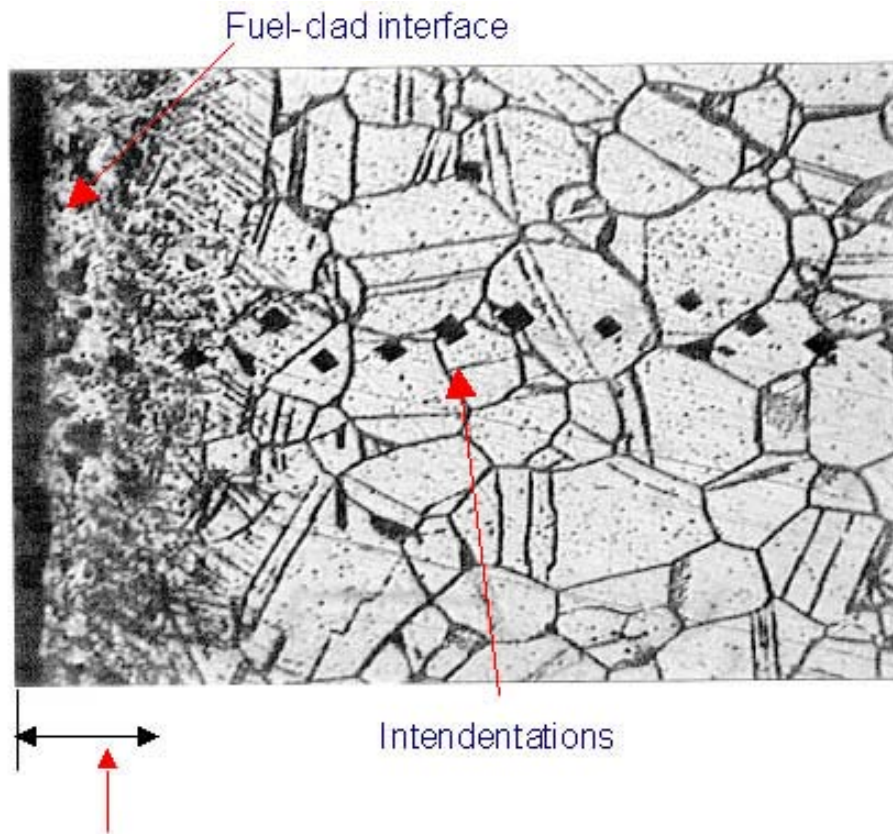
Fig. 4   Photomicrograph of SS-316 (20% CW) showing Vicker's indentation after fuel-clad-coolant compatibility experiment.
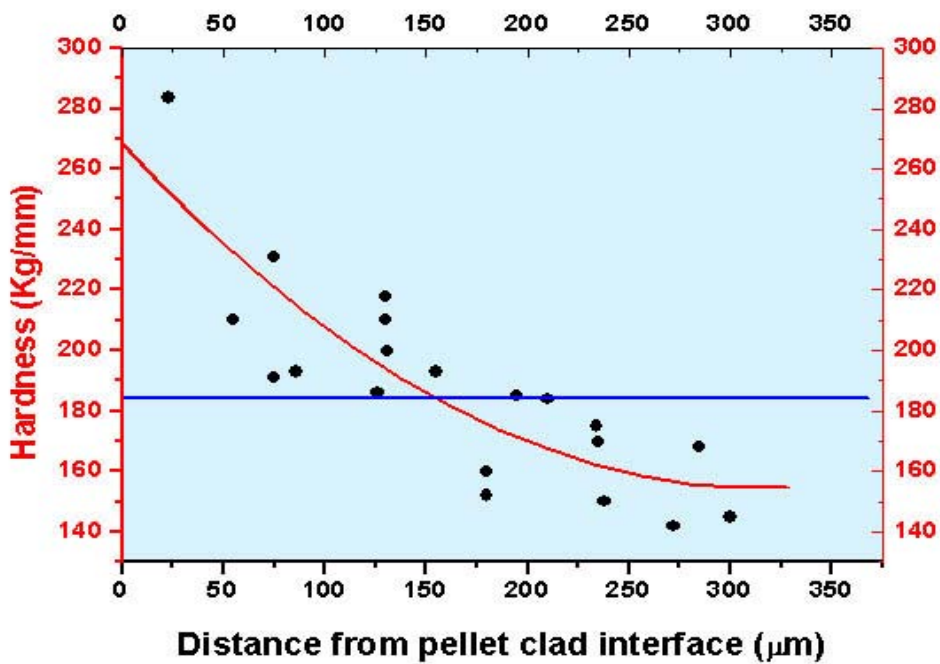

Fig. 5   Hardness profile of SS316 (20%cold worked) cladding from fuel/clad   interface

Discussions

The experimentally measured out-of-pile properties of $(U_{0.45}Pu_{0.55})C_{1+x}$ fuel and its compatibly with SS 316 cladding material and sodium coolant reveals that this fuel has higher solidus temperature (~1920ºC) than $(U_{0.3}Pu_{0.7})C_{1+x}$ (Mark I) fuel (~1875ºC). Moreover, Mark II fuel, having lower PuC content, have higher thermal conductivity and lower linear thermal expansion coefficient compared to Mark I fuel. These properties indicate that Mark II fuel can be operated at a higher reactor power and linear heat rating without any center melting. The higher solidus (melting) temperature of Mark II fuel could lead to lowering of thermal creep and swelling at any particular temperature. However, a lower thermal expansion of the fuel could allow sufficient time for the fuel-clad gap closure for generation of back stress for the thermal creep to occur. The plot of modulus compensated hardness vs. temperature indicates a sharp change in slope at considerably lower temperature indicating even an early onset of thermal creep could be a possible phenomenon. It is known that the 'C' potential of Mark II fuel is higher than that of Mark I fuel. So it is expected that Mark II fuel could be more carburizing when fuel-clad contact is established. However, low p_{co} of Mark II fuel (because of lower 'O' solubility) would reduce the possibility of gas phase carburization of the clad. Out-of-pile fuel-clad and fuel-clad-coolant compatibility experiments indicate that during the residence time of the fuel in the rector, clad carburization will not be of much concern and the possibility of a breach in clad due to clad carburization will not cause any hindrance for the operation of the fuel.

Conclusions

- FBTR Mark II fuel ($(U_{0.45}Pu_{0.55})C_{1+x}$ has higher melting point, higher thermal conductivity and lower coefficient of thermal expansion (than Mark I fuel of 30% UC +70% PuC composition).
- This fuel could be operated at higher power & higher linear heat rating without centre melting.
- Higher melting point could lead to lower thermal creep rate & lower swelling.
- Lower thermal expansion coefficient may need more time for fuel-clad gap closure.
- Mark II fuel has higher "C" potential and may be prone to clad carburization. However, experimental finding indicate that the extent of clad carburization is not severe to cause any breach of clad during the residence time of the fuel.

References

1. C. Ganguly, P.V. Hegde and G. C. Jain, "Fabrication of $(Pu_{0.55}U_{0.45})C$ fuel pellets for the second core of the fast breeder reactor in India", *Nuclear Technol,* 105, 346(1994).
2. A. K. Sengupta, J. Banerjee, R. K. Bhagat, R. Ramachandran, S. Majumdar and D. S. C. Purushottam, "Thermal expansion data of $(Th,U)O_2$ fuel", *BARC/2000/E/008*, Bhabha Atomic Research Center, India (2000).
3. A. K. Sengupta, S. Majumdar, C. Ganguly, D.S.C Purushottam and P. R. Roy, "Determination of some important thermophysical properties of $(U_{0.3}Pu_{0.7})C$ fuel", *Am. Ceramic. Soc. Bull.*,67[7], 1057 (1986).
4. A.K. Sengupta, U. Basak And C. Ganguly, "Hot hardness of hyperstoichiometric mixed Uranium Plutonium monocarbide, *J .Mater. Sci. Letters* 6, 20 (1987).
5. A. K. Sengupta, J. Banerjee, T. Jarvis, T. R. G. Kutty, K. Ravi And S. Majumdar, *Nucl. Tech*, Vol 142, No 3, 260-269 (2003).
6. C. Ganguly, A. K. Sengupta, "Out-of-Pile Chemical compatibility of Hyperstoichiometric $(Pu_{0.7}U_{0.3})C$ with Stainless Steel Cladding and Sodium Coolant, *J. Nucl. Mater*, 158, 159 (1988).

About the authors ...

Dr A. K. Sengupta *BE, metallurgy, University of Calcutta, 1971; MTech (Met.E) IIT Kanpur, 1976; PhD, metallurgical engineering, IIT Mumbai. Presently, He is Head, Fuel Property Evaluation Section, RMD, BARC. His area of research is studies on high temperature thermophysical and thermomechanical properties of nuclear fuels and also fuel-clad and fuel-clad-coolant chemical compatibility for thermal and fast reactors.*

Mr J. Banerjee *BE, metallurgy, University of Calcutta, 1989. He works in Radiometallurgy Division, BARC. His areas of research are out-of-pile thermophysical and thermomechanical properties of fuels for thermal and fast reactors. His area of interest also includes development, fabrication, and characterization of nuclear fuels materials.*

Mr T. Jarvis *BSc, physics, University of Calicut, 1979; AMIE metallurgy, Institution of Engineers, 1990. He works in Radiometallurgy Division, BARC. His areas of research   are thermophysical and thermomechanical properties like thermal conductivity,thermal expansion, etc. of fuels for thermal and fast reactors.*

Mr T. R. G. Kutty *BSc, physics, Kerala University, 1970; MSc engineering, 1990; PhD; metallurgical engineering,1996, IIS, Bangalore. He works in Radiometalllurgy Division, BARC. His field of interest is thermophysical and thermomechanical properties, evaluation of fuels and structural materials, and   densification behaviour and kinetics of sintering of thermal and fast reactor fuels.*

R. K. Bhagat *MSc, physics, Nagpur University, 1979; AMIE metallurgy, Institution of Engineers, 1991. He works in Radiometallurgy Division. His field of interest is thermophysical and mechanical properties of nuclear fuel and out-of-pile chemical compatibility of fuel-clad-coolant of advanced reactor.*

K. Ravi   *BSc, physics, Madras University, 1981. He works in Radiometalllurgy Division, BARC. His fields of interest are thermophysicsal and mechanical properties of nuclear fuel and cladding materials, and also out-of-pile chemical compatibility of fuel-clad-coolant of fast reactor.*

S. Majumdar *B.E, metallurgy, University of Calcutta, 1967. He is Head, Radiometallurgy Division, BARC. He worked extensively in the field of research, development, fabrication, characterization, and out-of-pile property evaluation of plutonium, thorium and uranium based nuclear fuels, both for thermal and fast reactors.*

AUTOLYTIC DEGRADATION OF CHICKEN INTESTINAL PROTEINS

P. Harikumar and S.N. Jamdar
Food Technology Division
Bhabha Atomic Research Centre

Abstract

Chicken intestine possesses proteolytic activities (cathepsin B, D, H, L, aminopeptidases and alkaline proteases) comparable to that in organ tissues like liver and spleen, which could degrade the tissue proteins extensively (70-80%). The autolytic degradation was found to be optimum at pH 2.5 and 60ºC. Analysis by SDS PAGE showed a time dependent degradation of proteins to low molecular weight (<10 kDa) products. Kinetic studies employing specific inhibitors indicated that the degradation (90-94%) of proteins at acidic pH is governed largely by pepstatin sensitive proteases. The acidic extract of the tissue was found to hydrolyze albumin, casein and soybean proteins efficiently. Results point to the possible application of tissue autolysis for obtaining protein hydrolysates from chicken intestine. Chicken intestine could also serve as a potential source of much needed proteolytic enzymes for food and pharmaceutical applications.

Introduction

Animal tissues are endowed with endo and exo peptidases, which play vital role in determining the quality attributes and storage characteristic of meat and fishery products (Huss, 1995; Jiang, 1998; Kristensen and Purslow, 2000). The significance of proteolytic enzymes in food industry is ever increasing with the advent of modern food preservation techniques such as radurization (Hwang and Hau, 1995) and high-pressure treatments (Claude and Culioli, 1997), which do not inactivate enzymes. Tissue proteases also assume importance, as they are involved in postmortem breakdown of polypeptides leading to textural and flavor changes in meat products (Toldra and Flores, 2000). Modification of the quality attributes of flesh foods during postmortem storage (Sakai and Matsumoto, 1981; Jiang, 1998; Hurtado et al., 1999; Visessanguan et al., 2001) is effected by a process called tissue autolysis, which involves the action of proteolytic enzymes on these

proteins. Autolytic degradation of proteins in fish and meat has been a subject of wide interest due to its applicability in the modification of quality attributes of foods and in the preparation of value added products such as protein hydrolyzates, sauce and silages (Ledward and Lawrie, 1984; Haard et al., 1994; Rao et al., 1996).

Byproducts of poultry industry, which include viscera, bone, blood, head, feet and feather, together constitute 28-30% of the total weight (Panda and Singh, 1980;Ockerman and Hansen, 2000). Intestine, which accounts for 20-30% of the processing wastes (Panda and Singh, 1980) is a potential source of proteins, lipids (Rao et al., 1996, Ockerman and Hansen, 2000) and tissue proteases (Raju et al., 1997). However, this commodity has not found favor with consumers, mainly due to aesthetic and hygienic reasons. Hence, presently, the bulk of this waste is being either discarded or partly used in animal feeds. In India, poultry industry is growing steadily and is estimated to produce annually

more than 65,000 tons of intestine (Rao et al., 1996). Although some attempts have been reported for preparing hygienised animal feed products from chicken intestine (Giri et al., 2000), no systematic attempt seems to have been made to utilize proteins and proteolytic enzymes from this valuable byproduct. One of the major objectives of our laboratory is to standardize suitable procedures to retrieve proteins from chicken intestine using tissue autolysis. The present paper reports the kinetics of interaction of chicken intestinal proteases with tissue proteins during autolysis as well as the potential of using intestinal proteases for the degradation of protein substrates from other sources.

Materials and Methods

Chicken intestine, liver, spleen and skeletal muscle were brought from the local abattoir. Intestine was washed thoroughly by flushing with tap water so as to remove the undigested material. All the tissues were stored at -20°C until use.The homogenates (200mg tissue/ml) were prepared in suitable buffers using Polytron homogenizer at setting of 5 for 2.0 minutes.

Protease assays

Activities of cathepsin B, cathepsin L, cathepsin H and cathepsin D were determined according to Barrett and Kirschke (1981) and the activity of alkaline protease was determined as per Thakore and Harikumar (1995).

Autolysis

Intestinal homogenates were allowed to undergo autolysis at pH 2.0, 2.5, .0, 6.3, 7.0 and 8.5 and temperatures 28, 37, 50, 60, 70 and 77°C. The TCA soluble peptides were estimated from autolysate at regular time interval.

Analysis of autolytic degradation by SDS-PAGE

Aliquots of the autolysate were subjected to SDS-PAGE (Weber and Osborn 1969) at regular intervals and were stained with coommassie blue R 250.

Proteolytic activity of intestinal acid protease

A crude preparation of the intestinal tissue was used as enzyme source. A 1%Hb, 1% Bovine serum albumin (BSA), 1% Human serum albumin (HSA), 5% Casein and 1% SPI (with respect to protein content) were used as substrate for the enzyme. The stock solution of the substrates was prepared in 0.1M glycine-HCl buffer pH 2.5. The reaction system consisted of 30µl of crude preparation, 470 µl 0.1M glycine-HCl buffer pH 2.5 and 500 µL of stock solution of the substrate. The assay mixture was incubated at 50°C for 15 minutes. The enzyme reaction was stopped by adding 1ml of cold TCA (10%).

Degradation profile of SPI by SDS PAGE

Soybean protein isolate (SPI) was prepared using isoelectric precipitation method the method of Qi et al. (1997). The degradation of SPI (2% solution in Gly-HCl pH 2.5) by a crude extract of chicken intestine was analysed using SDS PAGE during a incubation period of 60 minutes.

Protein

The protein content was determined by Miller's method (1959) using bovine serum albumin as the standard.

Results and Discussion

High levels of cathepsins, aminopeptidases and alkaline proteases observed in chicken intestine (Table 1) shows that it is a rich source of proteolytic enzymes. The specific activities of the enzymes in intestinal tissue were 1.5 to 3 fold higher than that in skeletal muscle, liver and spleen. Assuming that these enzymes in chicken are distributed largely among liver, spleen, skeletal muscle and intestine, the yield in intestine could be estimated (Table 1 parenthesis) as 36-64%. The protein content of the intestine calculated in terms of dry weight of the tissue was 57-60%. Chicken intestine being a good source of both proteins and proteolytic

Table 1 Levels of proteases in chicken tissues

Enzyme	Specific activity (nmoles/mg protein /h)			
	Liver	**Spleen**	**Skeletal Muscle**	**Intestine[a]**
Cathepsin B	31.5 ± 0.30	22.1 ± 0.37	1.9 ± 0.11	69.5 ± 0.78 (48%)
Cathepsin D	2230 ± 60.00	2260 ± 24.00	73 ± 2.00	4700 ± 37.00 (53%)
Cathepsin H	110 ± 3.90	93.2 ± 1.23	17.2 ± 0.54	310 ± 4.68 (39%)
Cathepsin L	631.5 ± 30.25	412.0 ± 35.00	83.6 ± 14.50	843.9 ± 61.00 (27%)
Phe-Arg aminopeptidase	179.5 ± 7.40	198.5 ± 1.14	6.4 ± 0.36	408.8 ± 8.24 (34%)
Ala aminopeptidases	81.6 ± 2.90	49.4 ± 4.33	11.6 ± 0.15	169.2 ± 4.17 (66%)
Leu aminopeptidases	69.9 ± 4.30	63.3 ± 1.81	9.1 ± 0.14	165 ± 8.03 (36.6%)
Pro aminopeptidases	22.4 ± 1.30	15.7 ± 0.734	5.7 ± 0.77	46 ± 2.62 (34%)
Tyr aminopeptidases	63.7 ± 2.00	46.9 ± 2.53	8.5 ± 0.53	190.9 ± 14.52 (38.5%)
Alkaline Proteases	126 ± 15.60	213.7 ± 12.61	28.7 ± 1.60	1346 ± 10.30 (64%)

[a] *Values in parenthesis represent the yield of the enzymes in the intestine, considering the sum of the activity associated with all the four tissues, as 100%.*

enzymes, the possibility of autolytic degradation of proteins becomes strong, which in turn, could serve as a means to retrieve value added protein products from this otherwise underutilized source.
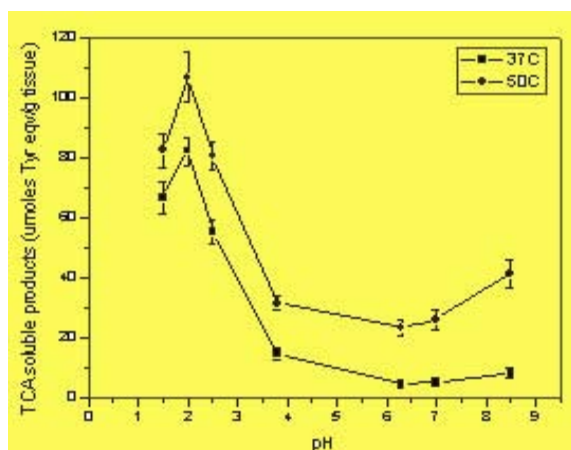
Fig.1 Effect of pH on protein degradation by autolysis at 37°C and 60°C. Tissue homogenates were held at pH 2.0 to 8.5 and TCA soluble products were determined after 2h.

The autolytic degradation of proteins was found to be pH dependent (Fig.1) exhibiting optimum at pH 2.5 with a minor peak at pH 8.5.

Protein hydrolysis was the least at neutral pH range (6.5-7.0). Similar dependence of autolytic degradation on pH has been reported in squid (Sakai and Matsumoto, 1981) and octopus arm muscle (Hurtado et al., 1999). The major enzymes responsible for protein degradation at acidic pH could be intracellular proteases such as cathepsin D and E while that at pH 8.5 could be alkaline proteases. Incorporation of protease inhibitors (pepstatin at pH 2.5 and STI at pH 8.5) or heat treatment (90°C for 20 minutes) abolished the autolytic degradation of proteins (data not shown), showing thereby that the protein degradation is indeed enzymatic and not mediated by factors such as acidic pH or temperature changes. This contention is supported by the data on the influence of

temperature (Fig.2 and Fig.4), pH (Fig.3) and protease inhibitors (Fig.5) on tissue autolysis.
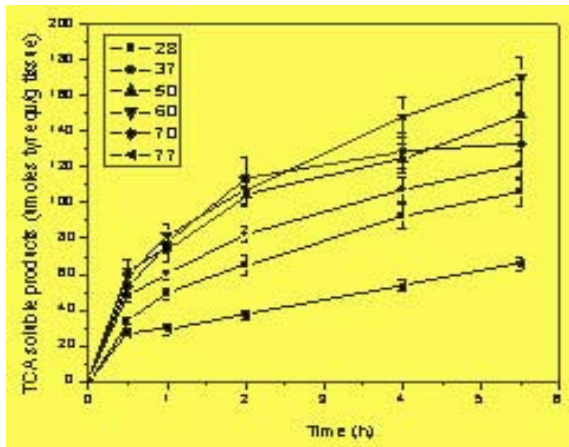
Fig.2 Kinetics of protein degradation by autolysis at different temperatures Autolysis was carried out at pH 2.5 by incubating tissue homogenate at a temperature range of 28-77°C. TCA soluble products were determined at regular intervals from 0 to 5.5 h.
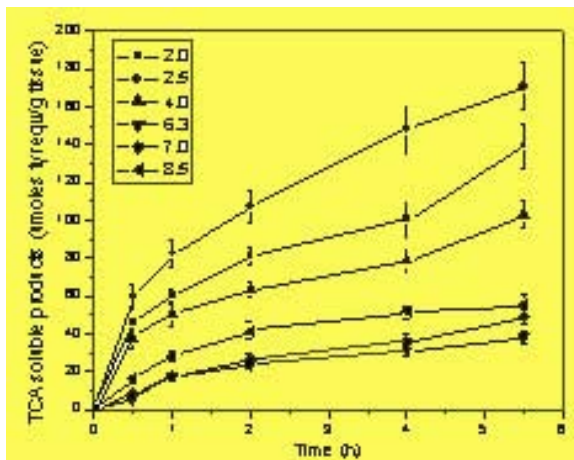
Fig.3 Kinetics of protein degradation by autolysis at different pH values. Autolysis was carried out at 60°C by incubating tissue homogenate prepared in respective buffers at pH 2.5 to 8.5. TCA soluble product were determined at regular intervals from 0 to 5.5 h.

The kinetics of autolysis at different temperatures (Fig.2) showed that the degradation of proteins increased steadily with temperature from 28°C to 60°C as a function of time up to 2h, attaining a plateau thereafter. At higher temperature (77°C), the autolysis was markedly

reduced apparently due to heat inactivation of enzymes. The negative influence of temperature on autolysis was also discernible during incubation beyond 2h at 70°C. Data on the hydrolysis of proteins as a function of time at different pH values is depicted in Fig.3. As expected from the data in Fig.1, the rate of protein degradation was highest at pH 2.5 with a gradational decrease as the pH was raised to 7.0, with a spurt of activity at alkaline pH.
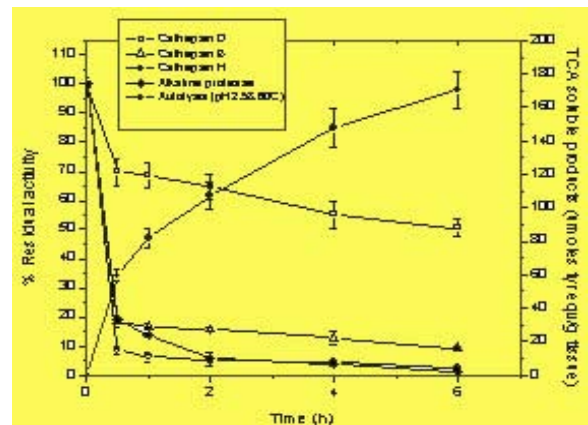
Fig. 4 Residual activity of enzymes during autolysis. Autolytic mixture was incubated at 60°C and pH 2.5. Aliquots were withdrawn at regular intervals to estimate the levels of TCA soluble products and the activity of cathepsin D, cathepsin B, cathepsin H and alkaline protease as given in Materials and Methods.
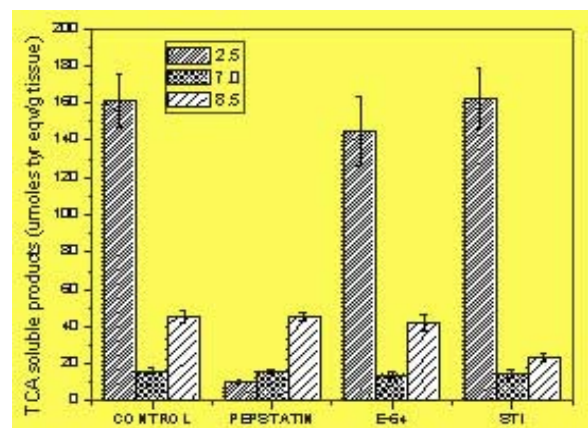
Fig. 5 Effect of protease inhibitors on autolysis. Autolysis was carried out as described in Materials and Methods. Autolytic mixture was pre-incubated with respective inhibitors [pepstatin (20μM), soybean trypsin inhibitor (100μg/ml) and E-64 (20μM)] for 15 min before starting autolysis.

The patterns of degradation of tissue proteins observed by us at different temperatures and pH values are in agreement with the reports of Shahidi et al. (1995) who showed that the enzymatic hydrolysis of fish muscle proteins is characterized by an initial rapid phase, during which a large number of peptide bonds are hydrolysed, followed by a decrease in hydrolysis reaching a stationary phase. The decreased rate of hydrolysis observed at higher (2-6h) time intervals could be ascribed to factors such as enzyme inactivation, product inhibition (Rebeca et al., 1991; Shahidi et al., 1995, Kristinsson and Rasco, 2000) and auto-digestion of the enzymes (Mullally et al., 1995).

The optimum activity at pH 2-2.5 and 60°C, suggests that acid proteases, especially cathepsin D could be predominantly involved in the degradation of chicken intestinal proteins. Among intracellular proteases, cathepsin D is noted for its optimum activity at highly acidic pH value (Conner, 1998) and high temperatures (Iodice et al., 1966; Draper and Zeece, 1989). Data presented in Fig 4 supports the involvement of cathepsin D in tissue autolysis. It could be seen that unlike cathepsin B, cathepsin H and alkaline protease, the activity profile of cathepsin D follows a pattern similar to that exhibited by autolysis. This enzyme retained more than 50% of its activity throughout the period of autolysis (6h), while other enzymes lost their activity rapidly (within 30 minutes) even as the tissue autolysis has reached only 30% and been rising steadily. These results, as reported by Iodice et al. (1966) and Barrett (1970), indicated that cathepsin D from poultry tissue is relatively stable.

The assumption that cathepsin D is responsible for autolysis is confirmed by the investigations on the effect of specific protease inhibitors on the release of TCA soluble products (Fig.5), as well as on the electrophoretic patterns of autolytic end products (Fig 6A, B and C). At pH 2.5, tissue autolysis was inhibited 95% by pepstatin, while it was unaffected by the cysteine

protease inhibitor, E-64 or by the serine protease inhibitor, STI. This is in agreement with the observation of Sakai and Matsumoto (1981) who observed that the inhibition of autolytic degradation of proteins in squid mantle muscle by pepstatin was markedly higher than that by inhibitors such as STI, PMSF, iodoacetate and leupeptin. It could be observed from Fig.5 that no significant autolysis takes place at pH 7.0. At pH 8.5 however, about 30% of autolytic activity was observed, which is inhibited partially (30-35%) by STI and unaffected by pepstatin and E-64 indicating the contribution of serine proteases in tissue autolysis at alkaline pH. The influence of pH on the pattern of degradation of tissue proteins is affirmed by the resolution of peptides on SDS PAGE (Fig.6A, B and C). Data in Fig.6A, B and C represent SDS PAGE profile as a function of time at pH 2.5, 7 and 8.5 respectively. Bands corresponding to myosin heavy chain (MHC), alpha actinin (AA), actin (A) and myosin light chain (ML) are clearly observed before autolysis. Autolysis at pH 2.5 caused degradation of all the major proteins (205 to 66 kDa) within 2 h (Fig.6A, lane 5) to molecular size<45 kDa. By 6h (Fig.6A, lane9), the hydrolysis was near completion with progressive increase in the accumulation of smaller molecular weight (<29 kDa) products, the major component being ≤10 kDa. As observed by Ladrat et al. (2003); Nielsen and Nielsen (2001) and Matsumoto et al. (1983) our results provide evidence for the involvement of cathepsin D in the degradation of proteins like MHC, tropomyosin, α-actin. However, our results differ from these reports in that an exhaustive degradation of proteins to molecular sizes > 10 kDa was observed by us, while these authors indicated degradation of proteins to the molecular sizes of 30-160 kDa by cathepsin D. The involvement of other proteases in the generation of low molecular weight products (10kDa) could be ruled out, since pepstatin, which is a specific inhibitor for cathepsin D, could abolish the formation of 10 kDa products. It is interesting to note that in the presence of
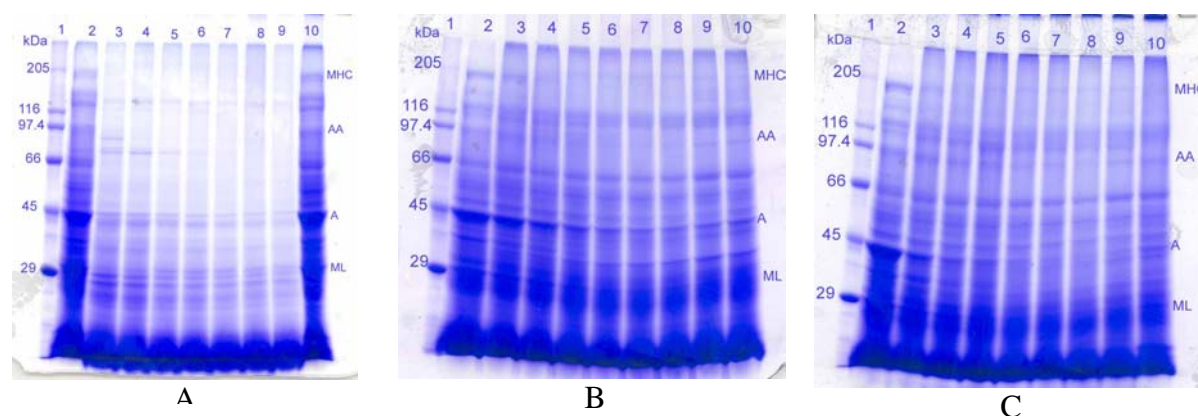
Fig. 6 Electrophoretic pattern of proteins after autolysis at (A), pH 2.5; (B), pH 7.0; (C), pH 8.5.Autolysis was carried out as described in Materials and Methods. M, myosin; AA, alpha-actinin; A, actinin; ML, Myosin Light Chain. Lanes: (1) Molecular weight standards (2) 0h, (3) 0.5h, (4) 1h, (5) 2h, (6) 3h, (7) 4h, (8) 5h, (9) 6h, (10) 6h with pepstatin (A), E-64 (B), or STI (C).

pepstatin no degradation of tissue proteins was observed even after 6h (Fig.6A, lane 10), while E-64 (Fig.6B, lane 10) or STI (Fig.6C, lane 10) did not affect the degradation profiles of tissue proteins. Although disappearance of MHC (205 kDa) was observed at all the pH ranges, further degradation of medium size peptides (116 to 29kDa) was observed only at acidic pH. This would indicate that although limited fragmentation of high molecular weight proteins such as MHC could be effected by acid, neutral as well as alkaline proteases, degradation of medium size peptides (116 to 45 kDa) to lower molecular weight products (>29kDa), needs the intervention of cathepsin D. The above observations are not entirely surprising considering the known versatility of this enzyme in degrading of polypeptides of varied sizes (Ladrat et al., 2003; Nielsen and Nielsen, 2001; Conner, 1998; Matsumoto et al., 1983). The PAGE pattern (Fig.6A) along with the data in Fig.2 and 3 clearly establishes that the chicken intestinal proteins could be exhaustively degraded by acidic endogenous enzymes. It further implies that chicken intestinal proteases could be potentially used for retrieving proteins by converting them to soluble peptides. This observation is in conformity with that of Fonkwe and Singh (1996) and Surowka and Fik (1994),

who indicated that proteases could be useful for the recovery of proteinaceous substances from poultry products. These authors used extraneous proteolytic enzymes such as papain and pepsin for protein degradation, in our autolytic procedure equally efficient degradation of proteins is achieved by endogenous enzymes. Moreover the acidic pH used, while in our autolytic process being an effective hurdle, could effect microbial hygienization of the autolytic end products. Studies in our laboratory have shown that the samples obtained after autolysis are indeed devoid of viable bacteria (data not shown). As acidic proteases are known to constitute the major proportion of hydrolytic enzymes in animal tissues (Raju et al., 1997; Ikeda et al., 1985; Sakai and Matsumoto, 1981; Jiang et al., 1990; Hurtado et al., 1999), our studies on proteolysis by tissue autolysis assumes greater practical significance.

Application of proteolytic reactions for the preparation of value added products from, byproducts of fish (Kristinsson and Rasco, 2000; Pavlisko et al., 1999; Haard, 1992; Haard and Simpson, 1994), poultry (Surowka and Fik, 1992; Surowka and Fik, 1994; Raju et al., 1997; Giri et al., 2000) and meat (Ledward and Lawrie, 1984; Ockerman and Hansen, 2000) has been

indicated by many investigators. Mahendrakar et al. (1991) have shown that autolytic reactions can be used for the preparation of silage from poultry viscera. However, the biochemical mechanisms underlying the autolytic reactions have not received much attention in the above reports. In this context, our observations on the kinetics of autolysis and involvement of specific proteases in protein degradation during tissue autolysis in chicken intestine is noteworthy.

The data presented in Table 2 shows that chicken intestinal proteases could degrade proteins from other sources also.

Table 2 Proteolytic activity of intestinal extract on different substrates at 50 C and pH 2.5

Substrate	Specific activity[a]
Hemoglobin	16.7
BSA	8.6
HSA	6.1
Casein	7.0
SPI	6.7

[a] specific activity is expressed as μmoles tyrosine eqv./h/mg protein. The values represents mean of three independent experiments.

The efficiency of degradation was in the order Hemoglobin>BSA>casein>HSA>SPI. Fig. 7 depicts the electrophoretic profile of the degradation products of soybean proteins. At the end of 60 minutes all the bands above 24 kDa, except that near 55 kDa disappeared resulting in the production of low molecular weight bands (<14 kDa). The reasons for the resistance to hydrolysis of proteins near 55kDa are not clear at present. The enzymatic nature of protein degradation is apparent from the observation that the incubation of enzyme (lane 9) or protein (lane 10) alone under identical conditions did not yield any low molecular weight bands.
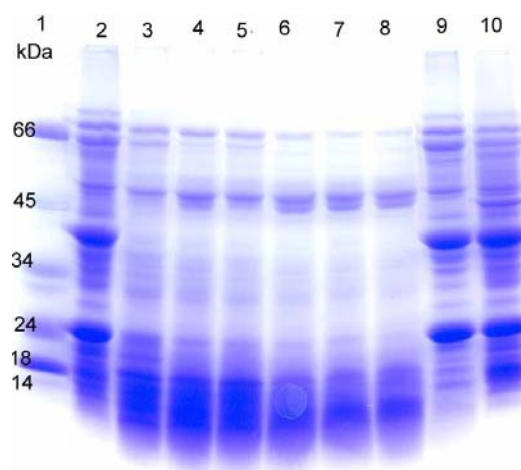
Fig. 7   *Degradation pattern of SPI by chicken intestinal acid protease at pH 2.5 and 50 °C. Lanes (1): molecular weight standards; (2): 0h; (3): 10 min; (4): 20 min; (5): 30 min; (6): 40 min; (7): 50 min;(8): 60 min; (9) substrate blank (substrate added after the incubation period); (10) enzyme blank (enzyme added after the incubation period).*

The foregoing results clearly establish that chicken intestine is an excellent source of acid proteases, which could exhaustively degrade endogenous as well as exogenous proteins. We envisage that the autolytic reactions defined in our paper could serve as basis for standardizing an inexpensive procedure for the retrieval of proteins from poultry intestine. Further, chicken intestine could serve as a source of not only animal proteins but also proteolytic enzymes with potential applications in food industry.

References

1. Barrett, A.J., 1970. Cathepsin D, purification of isoenzymes from human and chicken liver. Biochem. J. 117, 601-607.
2. Barrett, A. J., 1977. Cathepsin D and other carboxyl proteases. In: Barrett, A. J., (Ed.). Proteinases in Mammalian cells and Tissues. North- Holland Biomed press, Amsterdam, pp. 209-248.

3. Barrett, A. J., Kirschke, H., 1981.Cathepsin B, Cathepsin H and Cathepsin L. Methods Enzymol. 80, 535-561.

4. Claude, C.J., Culioli, J., 1997. Effects of high pressure on meat: A review. Meat Sci. 46 (3), 211-236.

5. Conner, G.E., 1998. Cathepsin D. In: Barrett, A., J., Rawling, N., Woessner, J.F., (Eds), Handbook of proteolytic enzymes. Academic press, New York, pp. 828-836.

6. Draper, A.M., Zeece, M.G., 1989. Thermal stability of cathepsin D. J. Food Sci. 54 (6), 1651-1652.

7. Fonkwe, G., Singh, R.K., 1996. Protein recovery from mechanically deboned turkey residue by enzymic hydrolysis. 31(6), 605-616

8. Giri, S.S., Sahoo, S.K., Sahu, A.K., Mukhopadhyay, P.K., 2000. Nutrient digestibility and intestinal enzyme activity of *Clarias batrachus* (Linn.) juveniles fed on dried fish and chicken viscera incorporated diets. Bioresour. Technol. 71,97-101.

9. Haard, N.F., 1992. A Review of proteolytic enzymes from marine organisms and their application in food industry. J. Aqua. Food Prod. Tech. 1, 17-34.

10. Haard, N.F., Simpson, B.K., Sikorski, Z.E., 1994. Biotechnological Application of Seafood Proteins and other Nitrogenous Compounds In: Sikorski, Z.E., Pan, B.S., Shahidi, F., (Eds). Seafood Proteins. Chapman and Hall, New York, pp. 202.

11. Haard, N.F., Simpson, B.K., 1994. Proteases from aquatic organisms and their uses in the seafood industry. In: Martin, A.M., (Eds.), Fisheries Processing: Biotechnological applications. Chapman & Hall, London, pp. 133-154.

12. Hurtado, J.L., Borderias, J., Montero, P., An, H., 1999. Characterisation of proteolytic activity in octopus (*Octopus vulgaris*) arm muscle. J. Food Biochem. 23, 469-483.

13. Huss, H.H., 1995. Quality and quality changes in fresh fish. FAO fisheries Technical paper 348, pp. 39-50.

14. Hwang, H.I., Hau, L.B., 1995. Effects of ionizing radiation on the enzyme activities and ultra structural changes of poultry. Radiat. Phys. Chem. 46 (4-6), 713-716.

15. Ikeda, T., Watabe, S., Yago, N., Horiuchi, S., 1985. Comparative biochemistry of acid proteinase from animal origins. Comp. Biochem. Physiol. 83B, 725-730.

16. Iodice, A.A., Leong, V., Weinstock, I.M., 1966. Separation of cathepsin A and D of skeletal muscle. Arch Biochem. Biophys. 117, 477-486.

17. Jamadar, V.K., Jamdar, S.N., Dandekar, S.P., Harikumar, P., 2003. Purification and characterization of aminopeptidase from chicken intestine. J. Food Sci. 68, 438-443.

18. Jiang, S., Wang, Y., Gau, B., Chen, C., 1990. Role of pepstatin –sensitive proteases on the postmortem changes of Tilapia (*Tilapia nilotica* X *Tilapia aurea*) muscle myofibrils. J. Agric. Food Chem. 38, 1464-1468.

19. Jiang, S., 1998. Contribution of muscle proteinases to meat tenderization. Proc. Natl. Sci. council ROC. part B Life Sci. 22 (3), 97-107.

20. Kristensen, L., Purslow, P.P., 2000. The effect of ageing on the water holding capacity of pork: role of cytoskeletal proteins. Meat Sci. 58, 17-23.

21. Kristinsson, H.G., Rasco, B.A., 2000. Fish Protein Hydrolysates: Production, Biochemical and Functional Properties. Crit. Rev. Food Sci. Nutr. 40, 43-81.

22. Ladrat, C., Verrez-Bagnis, V., Noel, J., Fleurence, J., 2003. In vitro proteolysis of myofibrillar and sarcoplasmic proteins of white muscle of sea bass (*Dicentrarchus labrax* L.): effects of cathepsin B, D and L. Food Chem. 81, 517-525.

23. Ledward, D.A., Lawrie, R.A., 1984. Recovery and utilization of by-product proteins of the meat industry. J. Chem. Tech. Biotechnol. 34B, 223-228.

24. Mahendrakar, N.S., Khabade, V.S., Rao, J.R., Latha, R., Dani, N.P., 1991. Influence

of feeding fish and poultry viscera silages to broilar chicks and their performance and meat quality. Int. J. Anim. Sci. 6, 19-26.

25. Miller, G.L., 1959. Protein determination for large number of samples. Anal. Chem. 31, 964.

26. Matsumoto, T., Okitani, A., Kitamura, Y., Kato, H., 1983. Mode of degradation of myofibrillar proteins by rabbit muscle cathepsin D. Biochim. Biophys. Acta 755, 76-80.

27. Mullally, M.M., O'Callaghan, D.M., Fitzgerald, R.J., Donnelly, W.J., Dalton, J.P., 1995. Zymogen activation in pancreatic endoproteolytic preparations and influence on some whey protein hydrolysate characteristics. J. Food Sci. 60, 227- 233.

28. Nielsen, L.B., Nielsen, H.H., 2001. Purification and characterization of cathepsin D from herring muscle (*Clupea harengus*). Comp. Biochem. Physiol. 128B, 351-363.

29. Ockerman, H.W, Hansen, C.L., 2000. Poultry By- products. In:Ockerman, H.W., Hansen, C.L., (Eds.), Animal By product processing and utilization. CRC press, New York, pp. 439-455.

30. Panda, B., Singh, R.P., 1980. Processing and utilization of poultry industrial by-products. By-products from food Industries: utilization and disposal. In: Association of Food Technologist, India, Symposium proceedings. pp. 58-63.

31. Pavlisko, A., Silvia, D.V., Coppes, Z., 1999. Enzymatic digestion of muscle from manhaden (Brevoortia spp.) at different pHs. J. Food Biochem. 23, 451-467.

32. Qi, M., Hettiarachchy, N.S., Kalapathy, U., 1997. Solubility and emulsifying properties of soy protein isolates modified by pancreatin. J. Food Sci 62 (6), 110-1115.

33. Raju, A.A., Rose, C., Rao, N.M., 1997. Enzymatic hydrolysis of tannery fleshings using chicken intestine proteases. Anim. Feed Sci. Technol. 66, 139-147.

34. Rao, J.R., Mahendrakar, N.S., Chakrabarty, N.M., Raghavan, S.L., 1996. Utilisation of fermented fish and poultry offals in feed for common carp (*Cyprinus carpio*). Seaood Export J. 27(3), 17-23.

35. Rebeca, B.D., Pena-Verra, M.T., Diazcastaneda, M.,1991. Production of fish protein hydrolysates with bacterial proteases; Yield and nutritional value. J. Food Sci. 56, 309-314.

36. Sakai, J., Matsumoto, J.J., 1981. Proteolytic enzymes of squid mantle muscle. Comp. Biochem. Physiol. 68B, 389-395.

37. Shahidi, F., Han, X.Q., Synowiecki, J., 1995. Production and Characteristics of protein hydrolysates from capelin (*Mallotus villosus*). Food Chem. 53, 285-293.

38. Surowka, K., Fik, M., 1992. Studies on the recovery of proteinaceous substances from chicken heads. I. An application of neutrase to the production of protein hydrolysate. Int. J. Food Sci. Tech. 27, 9-20.

39. Surowka, K., Fik, M., 1994. Studies on the recovery of proteinaceous substances from chicken heads. II. Application of pepsin to the production of protein hydrolysate. J. Sci. Food Agric. 65, 289-296.

40. Thakore, D., Harikumar, P., 1995. Total proteolytic profiles in buffalo kidney cortex lysosomes. Proc. Indian Natn. Sci. Acad. 61B, 371-376.

41. Toldra, F., Flores, M., 2000. The use of muscle enzymes as predictors of pork meat quality. Food Chem. 69, 387-395.

42. Visessanguan, W, Menino, A.R., Kim, S.M., An, H., 2001. Cathepsin L: A predominant heat activated proteinase in arrowtooth flounder muscle. J. Agric. Food Chem. 49, 2633-2640.

43. Weber, K., Osborn, M., 1969. The reliability of molecular weight determination by dodecyl sulfate polyacrylamide gel electrophoresis. J. Biol. Chem. 244, 4406-4412.

This paper won the 1ˢᵗ Prize in the poster session in the area of Animal Products at 5ᵗʰ International Food Convention (IFCON 2003) held at Mysore during December 5-8, 2003

About the authors ...

Dr P. Hari Kumar *is presently the Head, Flesh Food Biochemistry Section, Food Technology Division, BARC. He joined BARC in 1967 after graduating from the University of Kerala and obtained MSc and PhD degrees from the University of Mumbai. He has carried out Post-doctoral research at Roche Institute of Molecular Biology, Nutley, New Jersey, USA (1982-1984) and at University of Medicine and Dentistry, New Jersey, USA (1998 – 1999) on "The role of lysosomal proton AtPase and Ca^{2+} in the regulation of intracellular protein catabolism." His major contribution is in understanding the structure-function relationships of lysosomal proteases and their role in regulating the quality attributes of irradiated flesh foods and in the preparation of value added products from poultry and fish processing wastes.*

Mr Sahayog Jamdar, *MSc (Microbiology) from University of Mumbai, joined BARC in 1996 through BARC Training School (39ᵗʰ batch) and is working in the Flesh Food Biochemistry Section, Food Technology Division, BARC. He is currently pursuing PhD on the project entitled "Structure function relationships of proteases and protein degradation."*

DESIGN AND FABRICATION OF PHOTOCHEMICAL REACTOR FOR SCALING UP OPERATION OF LASER ISOTOPE SEPARATION PROCESS

P. Mathi, A.K. Nayak, V. Parthasarathy and S.K. Sarkar
Laser & Plasma Technology Division
Bhabha Atomic Research Centre

and

Lala Abhinandan and R. Bhatnagar
Centre for Advanced Technology, Indore

Introduction

Natural carbon consists of two stable isotopes, viz. C-13 (1.11%) and C-12 (98.89%). Carbon-13 is an important isotope as a tracer in chemistry, life sciences, medicine and biochemical synthesis. Although the current world production of C-13 at 90% concentration is about 10 kg per annum, an optimistic projection of hundred fold increase in the market demand is anticipated in view of rapid development of routine medical applications such as breath tests and whole body NMR. As a spin-off, C-13 depleted carbon (C-12 content 99.9%) can be used to make 'super diamond'. The current method of C-13 separation by very low temperature (-205°C) distillation of carbon monoxide has inherent drawbacks such as huge distillation tower, low separation factor, high energy consumption thus leading to a high production cost. In view of the growing demand for carbon isotopes, we are actively engaged in developing laser photochemical methods.

Laser isotope separation (LIS) by infrared laser chemistry of polyatomic molecules has come a long way since its discovery. The process has been successfully demonstrated for the separation of isotopes of many light elements like hydrogen, carbon, oxygen, silicon and sulphur. The last decade has witnessed a considerable effort in scaling up of the process by adopting various strategies for improving both the throughput and separation factor [1]. The photochemical reactor (PCR) plays a major role in the process scaling up. In the present paper, we will highlight our current efforts in the design and fabrication of a PCR for the macroscopic separation of various isotopes.

System Description

Based on our laboratory scale studies [2], a prototype facility was built which has the following major components and the flow sheet for this process is given in Fig 1.

1. Laser and accessories include various optical elements like windows, gratings, mirrors, lenses etc, detectors of energy and temporal profile, oscilloscopes and control electronics.

2. Photochemical reactor (PCR) includes Herriott multipass refocusing cell (MPRF) in flow configuration with circulatory pump / blower, mass flow meter, metering valves, pressure transducer etc.

3. Product separator / collector include (i) cryogenic distillation column and (ii) preparative gas chromatograph.
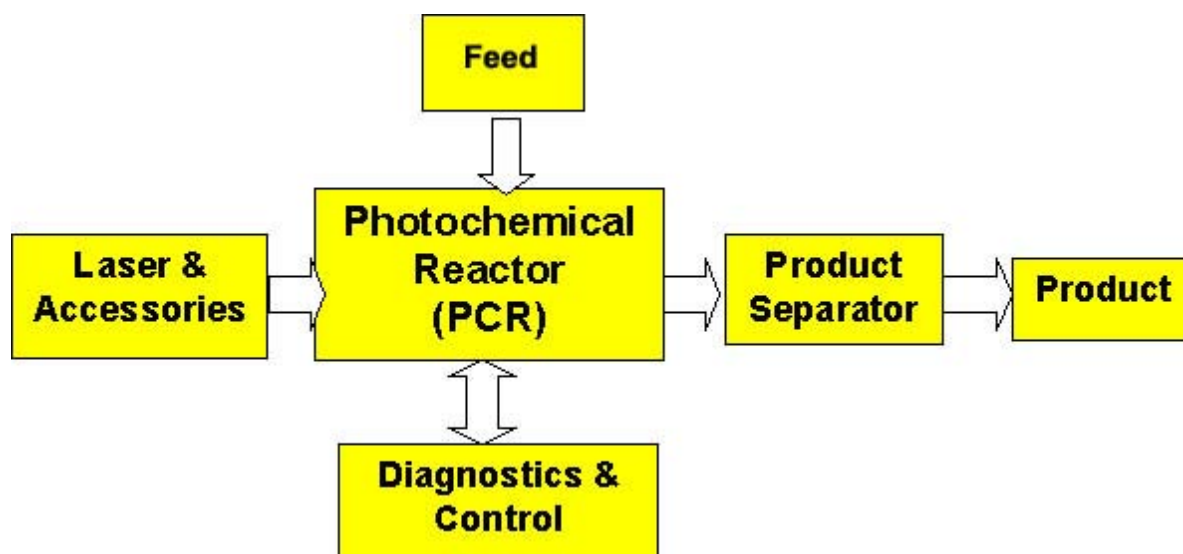
Fig 1. Process flow sheet

4. Diagnostics includes FTIR spectrometer, gas chromatograph and quadrupole / time-of-flight mass spectrometer
5. Feed includes gas handling system with purifier etc

The photochemical reactor (PCR) has been designed keeping in view of the criteria of (i) efficient photon utilization and (ii) selectivity loss due to working with higher pressure sample and higher laser repetition rate. When the target isotopic species is present in very low concentration, use of laser photons can be efficiently done with a long absorption path length of the sample. At high pressure, dissociation selectivity gets drastically degraded due to processes like collisional energy transfer between the selectively excited isotope and the undesired ground state species. The selectivity also deteriorates due to heating of the sample while working with high rep rate laser.

The multipurpose PCR (Fig. 2) made of ss consists of three identical modules (each having 50 cm length) and is suitable for use with different mirror systems of various radii of
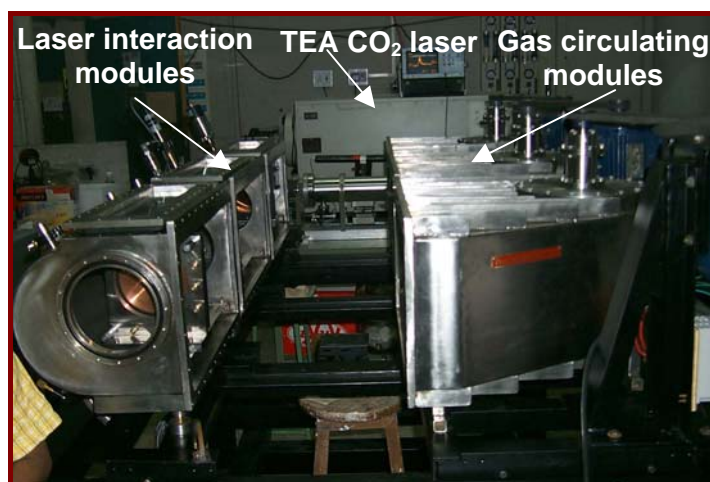
Fig 2. A Prototype Photochemical Reactor (PCR) facility for Molecular Laser Isotope Separation

curvature ranging from 10 to 100 cm depending on the fluence requirement of the laser chemistry process. Each module has a laser interaction chamber (LIC) and a gas blower chamber (GBC). The multi-pass, re-focusing (MPRF) Herriott configuration is a stable optical resonator consisting of two coaxial concave mirrors. A pair of high reflectivity (≥ 98.5 %) copper mirrors (six inch diameter) with a protective layer of SiO_2 / Cu are mounted inside LIC for efficient photon utilization. With proper design and alignment every reflection refocuses
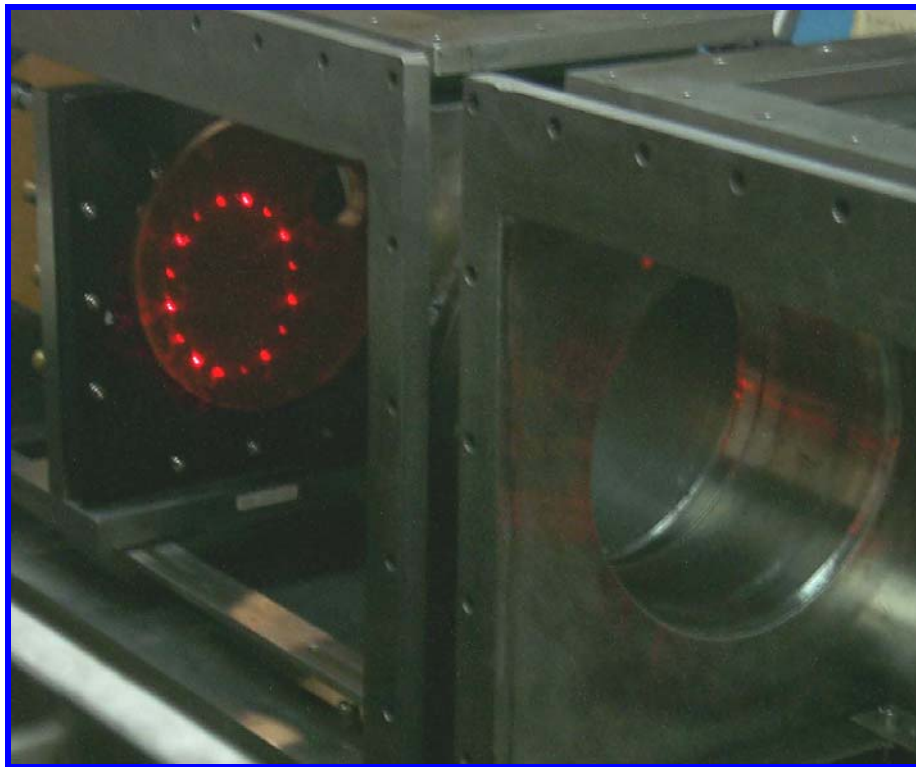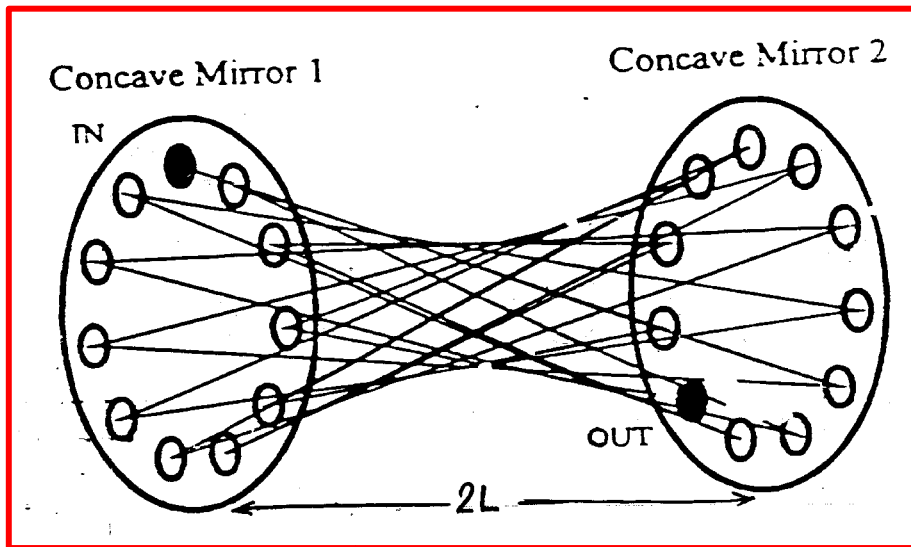
Fig 3. Foot print of laser beam in multipass refocusing Herriott optics

the beam to the same waist radius in the central plane between the mirrors. Fig 3 shows the footprint of the He-Ne laser on the Cu mirror.

The requirement of a circulatory system was evaluated for working with high rep rate laser. This system having a capacity 50 m^3 / hr

working with 100 Torr sample pressure would be able to replace the irradiated zone thrice between the successive laser pulses to eliminate the non-selective heating with high rep rate laser. To meet this requirement, the GBC of each module incorporated an appropriate centrifugal blower for circulating the process gases during

irradiation. The centrifugal blower can be driven at desired speeds using a variable frequency control unit. Flow velocities were measured at different locations in LIC along the length and the height which varied in the range of 2–5 m/s and a typical velocity profile is shown in Fig 4.
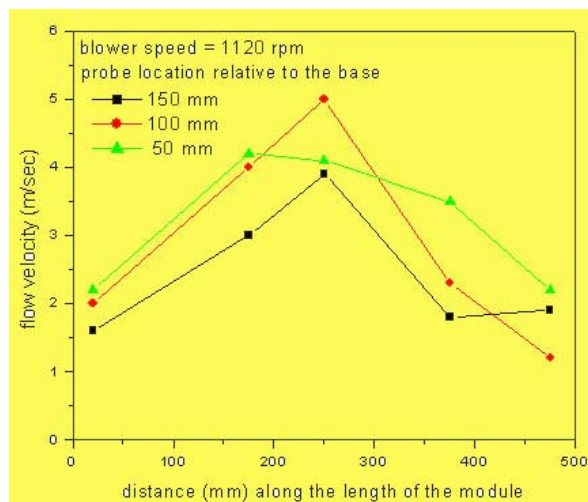
Fig 4. *Flow velocity patterns in the central module of the PCR*

Results and Discussion

In the multi pass, refocusing arrangement, a total number of thirteen passes could be obtained with the process TEA CO_2 laser [1 J, 10 Hz, 9P(22) line]. This resulted in better dissociation yield by more than an order of magnitude in absolute terms compared to that obtained with the single pass cell experiments. A simulation of the C-13 species depletion of a PCR batch as a function of the number of pulses can be evaluated for both the single and multi pass cases using our experimental data and is shown in Figure 5. It illustrates the great leverage obtained in reducing the irradiation time by deploying multi pass Herriott optics to obtain a certain degree of conversion of the C–13 species at a given selectivity. Therefore, processing of a moderate batch size of 280 litres in a reasonable time can conveniently be effected by employing the multipass Herriott optics.
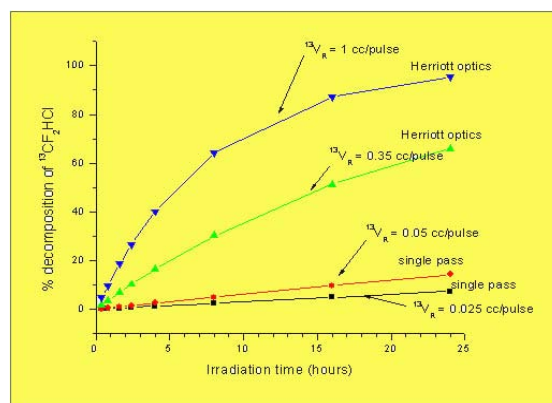
Fig 5. *Plot of C-13 species depletion as a function of irradiation time for single and multipass cases*

We have gained a lot of operational experience for successfully carrying out the LIS runs in the PCR. There is scope for further improvement in the reaction volume per pulse by judiciously adjusting the beam waist size, focal zone depth etc for the right combination of the focusing optics and the inter mirrors' separation distance. For example, by increasing the $^{13}V_R$ further to 1 cm^3 $pulse^{-1}$ from the current value of 0.35 cm^3 $pulse^{-1}$, one can realize a 40 % decomposition in the C –13 species in about 4 hours irradiation time. However, even with current moderate value of $^{13}V_R$ = 0.35 cm^3 $pulse^{-1}$, we would be able to induce 30% decomposition in a 8 hour batch run. This would correspond to a processing of about 100 mg of carbon with a 40% C – 13 content.

In summary we have developed a prototype facility for laser separation of carbon isotopes and this facility has generated database, operating experience and trained manpower in the general area of laser processing of high value and strategic materials.

References

1. V. Parthasarathy, A.K. Nayak, S.K. Sarkar, Proc. Indian Acad. Sci. (Chem. Sci.) 114 (2002) 639

2. V. Parthasarathy, S.K. Sarkar, N.V. Iyer, K.V.S. Rama Rao, J.P. Mittal, Appl. Phys. B, 56 (1993) 321

This paper received the Best Poster award at the National Symposium on Radiation and Photochemistry (NSRP – 2003) held at Department of Chemistry, IIT Kanpur, during March 3 – 5, 2003

About the authors ...

Ms P.Mathi *joined the Laser and Plasma Technology Division, BARC, after graduating from the 44th batch of BARC Training School. Her field of work is laser enrichment of various light elements at macroscopic levels.*

Dr Akshya Kumar Nayak *obtained his M.Sc from Utkal University in 1980 and joined the Multi Disciplinary Research Section in 1982 after completing the training at BARC Training School. He got his Ph.D from University of Mumbai in 1992. His Post-Doctoral work (1993 – 1995) at National Institute of Science and Technology, Gaithersburg MD, USA with Dr. A.Fahr involved the measurements of UV-VUV absorption cross sections of hydrocarbon compounds. His current research interest includes the study of dynamics and collisional effects on multiphoton dissociation, determination of radical – radical and radical – molecule gas phase rate constants by kinetic absorption technique and laser isotope separation.*

Dr Venkatachari Parthasarathy *joined BARC in 1975 after his Master's degree in Chemistry from IIT Kanpur. He received his Ph. D degree from the University of Mumbai in 1986 and had a post-doctoral fellowship at the Ecole Polytechnique Federale de Lausanne, Switzerland, during 1987 – 1988. His current research is focused on laser enrichment of various light elements at macroscopic levels in the L &PT Division, BARC.*

Dr. Sisir K. Sarkar *joined BARC in 1974 and currently heads Molecular Isotopic Photochemistry Section of Laser & Plasma Technology Division, BARC. Dr. Sarkar did his post-doctoral work at Columbia University, New York, with Prof. J.W.Flynn in the area of chemical dynamics using high-resolution semiconductor diode laser. He has worked as visiting scientist at the P.N.Lebedev Physical Institute & Institute of Spectroscopy, Russia, Kyoto Institute of Technology, Japan, and Institute of Chemical Process Fundamentals, Czech Republic, with various laser systems including Free Electron Laser. His research interest includes laser selective photophysics and photochemistry in nuclear fuel cycle, chemical dynamics, spectroscopy and laser development.*

Dr Lala Abhinandan *graduated from Institute of Technology, BHU, in Chemical Engineering in 1977 and joined the 21st batch of BARC Training School in the same year. After completion of training, he joined MDRS and worked on the development of high temperature system for generation of atomic beam. Later, he participated in the development of Nitrogen, Carbon dioxide, Copper vapour and Excimer laser systems. He was awarded PhD by IIT, Bombay, in 1999 for his work on 'Laser Curing of Powder Coatings'. His current interest includes study of laser induced chemical reactions.*

Dr R.Bhatnagar *is the former Head of Laser System Engineering Division, CAT, Indore. He was the architect of high power copper vapour laser (CVL) development programme.*

RADIOPROTECTIVE AND ANTIOXIDANT PROPERTIES OF INDIAN MEDICINAL PLANT, *Terminalia arjuna*

J. C. Tilak and T.P.A. Devasagayam
Radiation Biology & Health Sciences Division
Bhabha Atomic Research Centre

and

S. Adhikari
Radiation Chemistry & Chemical Dynamics Division
Bhabha Atomic Research Centre

A b s t r a c t

Using rat liver mitochondria as model systems, we examined the radioprotective and antioxidant effects of the Indian medicinal plant Terminalia arjuna. *Various sohxlet fractions of the bark and the medicinal formulation arjunsal besides an active ingredient, baicalein, were examined for their ability to protect both rat liver mitochondria and cardiac homogenate against radiation and oxidative stress apart from their ability to scavenge radicals and for ferric reducing/antioxidant power. Among the various extracts from arjunsal the ones from organic solvents were found to be the most effective in DPPH, ABTS and FRAP assays. In* T. arjuna *bark, the methanolic extract showed the highest antioxidant activity. Radioprotection studies also showed that the methanolic extract was the most effective. Baicalein showed antioxidant as well as radioprotective activity. To look at the possible mechanisms for the observed antioxidant/radioprotective effects pulse radiolysis was performed to examine the reactions of baicalein with various radiation-related and biologically relevant reactive species such as hydroxyl radical ($^{\bullet}OH$), azide radical ($N_3^{\bullet}$), lipid peroxyl radical ($LOO^{\bullet}$), trichloro methyl operoxyl radical ($CCl_3O_2^{\bullet}$) and thiyl ($RS^{\bullet}$) radical. Baicalein reacts with these radicals at almost diffusion controlled rates. The bimolecular rate constants for the reaction of these radicals were in the order of 10^9 $dm^3mol^{-1}s^{-1}$. The above results indicate that various preparations from* T. arjuna *and its component baicalein have significant radioprotective and antioxidant activities and the ability to react with radiation-derived or radiation-related reactive species may be the factor responsible.*

Introduction

In an aerobic environment, all animals and plants require oxygen and hence reactive oxygen species (ROS) are ubiquitous. It is established that excess generation of ROS is involved in structural alterations of cellular molecules leading to cytotoxicity and cell death. This eventually results in a variety of biological phenomena such as mutation, carcinogenesis, ageing, radiation or UV exposure, inflammation, ischemia-reperfusion injury, atherosclerosis, diabetes mellitus and neurodegenerative disorders (Yoshikawa et al, 2000).

Exposure to physical and chemical agents including ionizing radiation can result in excess ROS generation. Low LET (low energy transfer) radiation such as γ-rays can cause damage through ROS generation. The living systems comprised of aqueous media are prone to impairment due to radiolysis of water yielding hydroxyl radical ($^{\cdot}OH$), hydrated electrons (e^-_{aq}), hydrogen peroxide (H_2O_2), etc. In presence of

oxygen, other reactive species such as superoxide radical ($O_2^{.-}$), singlet oxygen ($^1O_2$) are also produced. In biological systems, cellular membranes are made up of polyunsaturated fatty acids (PUFA). They are highly prone to damage by ROS by process known as lipid per oxidation, which drastically alters the biomembranes structurally and functionally. It also generates highly toxic byproducts which can act at places away from their site of generation. Another important type of damage to cellular membranes can be induced by peroxyl radicals ($ROO^{.}$). this reactive species is predominant in LOOH-dependent lipid peroxidation. 2.2'-Azobis (2-amidinopropane) dihydrochloride (AAPH) on thermal decomposition in presence of oxygen gives rise to peroxyl radicals which can initiate the chain of lipid peroxidation.

Among the subcellular organelles, mitochondria are crucial sites for energy generation and ATP synthesis by tetravalent reduction of oxygen by mitochondrial cytochrome oxidase. There are also important sites of ROS generation (such as $O_2^{.-}$). Besides affecting ATP synthesis, it can compromise energy transduction by faultily synthesized proteins or lead to DNA fragmentation etc. (Yoshikawa et al, 2000). The oxidative damage to mitochondria can also lead to membrane permeability transition, cytochrome c release and dysfunction of mitochondria associated with decrease in membrane potential, respiratory control , apoptosis etc. (Yoshikawa et al, 2000). Hence the mechanistic study of membrane damage induced by ROS in relation to various human ailments and its prevention by antioxidants from natural dietary sources is very important.

There are several Indian medicinal plants known for their beneficial therapeutic effects which also might have antioxidant properties (Tilak et al, in press). *Terminalia arjuna* is one of these plants credited fro its cardiotonic and cardioprotective properties. The bark of the tree is used in 'Ayurvedic' system of medicines for over three centuries, primarily as cardiac tonic besides cure

for haemorrhages, fractures, diarrhoea, ulcers and acne (Kirtikar and Basu, 1984). It has also been known to possess antimutagenic, anti-ischemic, hypocholesterolemic, cardioprotective, and antioxidant abilities. In the present study, the radical scavenging activities and membrane protective abilities of *T. arjuna* extracts, as well as baicalein, its active ingredient, were examined.

Materials And Methods

Materials

Ascorbic acid, aluminum chloride,2,2'-azobis-3-ethylbenzthia zoline -6- sulfonic acid (ABTS) diammonium salt, β-phycoerythrin, 1,1'-diphenyl-2-picrylhydrazyl (DPPH), ethylene diamine tetra acetic acid (EDTA), ferric chloride, Folin-Ciocalteu reagent, hydrogen peroxide, methylene blue, myoglobin, potassium ferricyanide, potassium phosphate (monobasic and dibasic), sodium carbonate, α-tocopherol, trolox (6-hydroxy-2,5,7,8-tetramethylchroman-2-carboxylic acid), 1,1,3,3-tetraethoxypropane, 2,4,6-tripyridyl-s-triazine (TPTZ), 2-thiobarbituric acid and trichloroacetic acid were purchased from Sigma Chemical Co., U.S.A. 2.2'-Azobis (2-amidinopropane) dihydrochloride (AAPH) was from Aldrich Chemical Co., U.S.A. Other chemicals used in our studies were of the highest quality commercially available from local suppliers.

Methods

Preparation of the Arjunsal extracts : 'Arjunsal' is an herbal preparation of *T. arjuna,* known for its cardiotonic properties which is commercially available. In this study we have used two different extracts of arjunsal, using aqueous and mixture of organic solvents such as acetone, chloroform, methanol, isopropyl alcohol and water. Both the extracts were prepared by stirring the total extract of arjunsal in the respective solvents at room temperature for 2 hrs.

Preparation of T. arjuna *bark extracts :* The Soxhlet extracts of *T. arjuna* were prepared by taking the bark free of dust and other impurities. It was sun-dried and finely powdered. Depending on the increasing order of polarity of the solvents, sequential extraction was done using benzene, chloroform, acetone, methanol and methanol-HCl using Soxhlet apparatus. The bark powder was extracted with each solvent for 8-10 hours to remove the soluble matter. The aqueous extract was prepared by stirring the bark powder in distilled water for 4 hours and then filtering it.

Isolation of mitochondrial fraction from rat liver: Three months old female Wistar rats (weighing about 250 ± 20 g) were used for the preparation of mitochondria (Devasagayam et al, 1986). In brief, rat livers were homogenized in 0.25 M sucrose containing 1×10^{-3} mol dm^{-3} EDTA. The homogenate was centrifuged at 3000 x g for 10 min to remove cell debris and the nuclear fraction. The resultant supernatant was centrifuged at 10,000 x g for 10 min to sediment mitochondria. This pellet was washed thrice with 5 mM potassium phosphate buffer, pH7.4, to remove sucrose. Protein was estimated and pellets were suspended in the above buffer at the concentration of 10 mg protein/ml.

Exposure of rat liver mitochondria to radiation and agents for inducing oxidative stress : Oxidative damage was induced by exposure to γ-rays from a ^{60}Co source (dose rate 65 Gy/min, BARC, Mumbai). The mitochondria (final concentration 2 mg/ml) were suspended in 5 mM phosphate buffer (pH 7.4) and exposed to radiation with and without extracts or baicalein. The dose selected was 450 Gy at which optimum damage was obtained. The unexposed samples served as controls.

Peroxyl radical-induced lipid peroxidation was observed using azobis- amidinopropane hydrochloride. In the system for treating mitochondria to AAPH, mitochondria (final concentration 0.2 mg/ml) were incubated with AAPH (final conc. 10 mM) at 37°C for 30 min in a shaker-water bath with continuous bubbling of oxygen.

Biochemical assays

After exposure of mitochondria to oxidative stress, the products of lipid peroxidation were measured as lipid hydroperoxides (LOOH) and thiobarbituric acid reactive substances (TBARS). The lipid hydroperoxides were measured by using FOX (Ferrous Oxidation in Xylenol orange) II method. FOX II reagent contains 90% (v/v) methanol, which facilitates lipids to solubilize. Concentration of LOOH is then calculated with the help of standard graph using H_2O_2. FOX II gives ε for hydroperoxides as 4.46×10^4 M^{-1}cm^{-1}. TBARS were measured immediately after the treatment (Devasagayam, 1986). On addition of TBA reagent comprising of 0.5% thiobarbituric acid, 10 % trichloroacetic acid, 2 mM EDTA, 0.63 M hydrochloric acid and the samples were boiled for 20 min. The pink coloured TBARS formed were estimated spectroflurometrically using excitation at 532 nm and emission at 553 nm, after accounting for appropriate blanks. Malonaldehyde standard was prepared by the acid hydrolysis of tetramethoxypropane. The superoxide dismutase (SOD) activity was also estimated. Data were presented as mean $\pm$ SE. Significance of inter-group differences was determined by Student's *t* test (two-tailed). A *p* value of $p < 0.05$ was considered statistically significant.

Ferric Reducing Antioxidant Power (FRAP) assay

The ferric complexes reducing ability of the extracts by FRAP assay were measured at low pH. The stock solutions of 10×10^{-3} mol dm^{-3} TPTZ in 40×10^{-3} mol dm^{-3} HCl, 20×10^{-3} mol dm^{-3} FeCl$_3$. 6H$_2$O and 0.3 mol dm^{-3} acetate buffer (pH 3.6) were prepared. The FRAP reagent contained 2.5 ml TPTZ solution, 2.5 ml ferric chloride solution and 25 ml acetate buffer. It was prepared freshly and warmed to 37°C.

Then, 900 μl of FRAP reagent was mixed with 90 μl of D/W and 30 μl of test sample/methanol/DW/standard solutions. The reaction mixture was then incubated at 37°C for 30 min and absorbance was recorded at 595 nm. The concentration of $FeSO_4$ was in turn plotted against concentrations of the standard antioxidants (L-ascorbic acid and Trolox).

DPPH radical scavenging assay

Determination of the scavenging effect on $DPPH^.$ was carried out with different extracts. In this method a commercially available and stable free radical $DPPH^.$, which is soluble in methanol, was used. In its radical form, $DPPH^.$ has an absorption band at 515 nm, which disappears on reduction by an antioxidant compound. The calibration curve was plotted with % $DPPH^{.+}_{SCAVENGED}$ versus concentration of the standard antioxidants (L-ascorbic acid and Trolox).

ABTS radical scavenging assay

In the spectrophotometric assay, the inhibition of radical formation by the extracts was determined by using the ferrylmyoglobin/$ABTS^{.+}$ protocol. The calibration curve was plotted with lag time in seconds versus concentration of the standard antioxidants (L-ascorbic acid and Trolox).

Pulse radiolysis studies

The pulse radiolysis system using 7 MeV electrons has been described earlier (Mukharjee, 1997). The dosimetry was carried out using an air-saturated aqueous solution containing 5×10^{-2} mol dm^{-3} KSCN ($G\varepsilon = 23,889$ dm^3 mol^{-1} cm^{-1} per 100 eV at 500 nm). The kinetic spectrophotometric detection system covered the wavelength range from 250 to 800 nm. The optical path length of the cell was 1.0 cm. The width of the electron pulse was 50 ns and the dose was 16 Gy per pulse. Alkaline pH was obtained by adding NaOH only. High purity (> 99.9 %) N_2O, from BOC India Pvt. Ltd. was used.

Results

Fig. 1 presents data on the antioxidant properties of arjunsal extracts as assessed by standard assays for measurement of inhibition of radical formation and radical scavenging. The aqueous extracts were compared to water-soluble antioxidant, ascorbic acid (AEAC), while the solvent extracts were expressed in terms of Trolox (TEAC), an ethanol soluble standard antioxidant, equivalent.
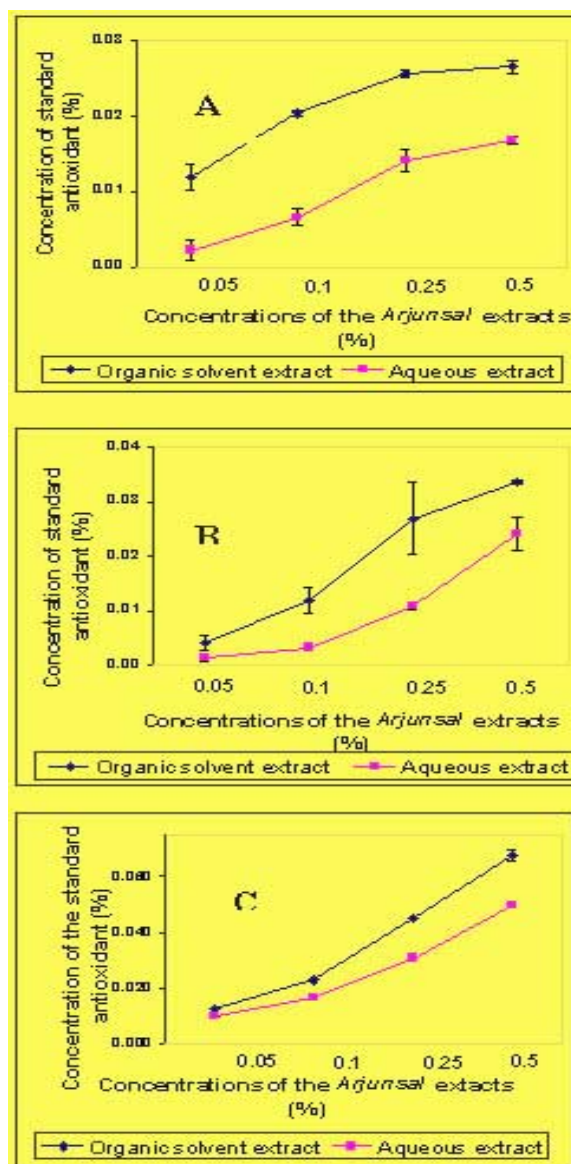

Fig. 1: Antioxidant abilities of arjunsal extracts with a) FRAP, b) DPPH scavenging and c) ferrylmyoglobin /ABTS assays

The results of FRAP assay were presented in Fig. 1a. The aqueous and organic solvent extracts of arjunsal were used with the concentrations ranging from 0.05% to 0.5%. Both the extracts show concentration dependent increase in their ferric reducing capacities. The organic solvent extract was more potent (TEAC-0.24) than aqueous one (TEAC-0.04). Fig 1b presented the data on DPPH radical scavenging abilities, while Fig.1c showed the data on inhibition of formation of ABTS radical measured by ferrylmyoglobin/ABTS assay. Among the arjunsal extracts, the organic solvent extracts were superior to the aqueous ones.

The data on antioxidant properties of *T. arjuna* extracts were presented in Fig.2. Three different concentrations of *T. arjuna* were used i.e. 0.05, 0.1 and 1% and concentration dependent effect of the extracts in terms of their antioxidant potential was observed. Fig. 2a showed the data on ferric reducing activities as assessed by FRAP assay. In this, methanolic extract possessed the highest ferric reducing property (TEAC-0.37) followed by methanolic-HCl, acetone, aqueous and chloroform. The results of DPPH radical scavenging were presented in Fig. 2b, showing methanolic-HCl extract to be the most potent scavenger (TEAC-0.7) followed by methanolic, aqueous, acetone and chloroform. Fig.2c showed the data on ferrylmyoglobin/ABTS assay, in which methanolic extract was highly significant (TEAC-0.34) in inhibiting formation of ABTS radical.

Aqueous, methanolic-HCl, acetone and chloroform extracts also showed significant antioxidant activities in the decreasing order.

The data on radiation- and AAPH-induced lipid peroxidation products and their inhibition by *T. arjuna* (final concentration 0.1 %) extracts were shown in Table 1. A dose of 450 Gy resulting in a significant increase in peroxidation was selected for the studies. Mitochondria were exposed to 450 Gy with and without *T. arjuna*
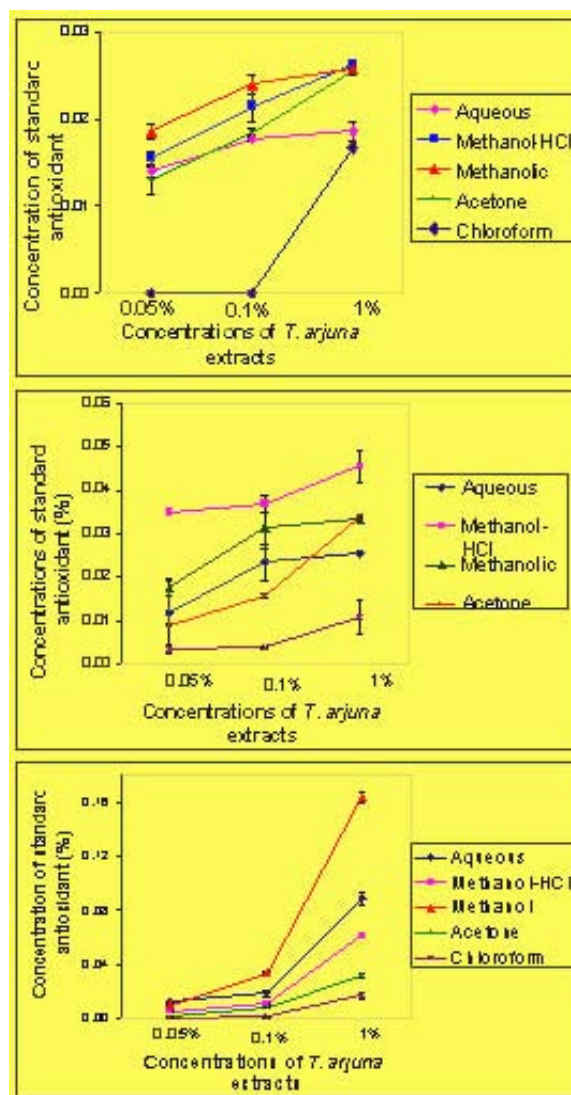
Fig. 2 Antioxidant abilities of Sohxlet extracts of T. arjuna *bark with a) FRAP, b) DPPH scavenging and c) ferrylmyoglobin /ABTS assays*

extracts. Methanolic extract was observed to be the most potent in protection against lipid peroxidation by inhibiting TBARS formation by 100 % and LOOH formation by 90 %. This was followed by methanolic-HCl, acetone and aqueous extracts of *T. arjuna.* In case of AAPH-induced TBARS and LOOH formation again methanolic one was found to be the most significant protector with 82 and 72 % protection respectively, followed by methanolic-HCl, aqueous and acetone extracts of *T. arjuna.*

Table 1: **Effect of *T. arjuna* extracts on radiation and AAPH-induced formation of TBARS and LOOH in rat liver mitochondria.**

	γ-radiation exposure		AAPH treatment	
	TBARS (nmoles/mg protein)	LOOH (nmoles/mg protein)	TBARS (nmoles/mg protein)	LOOH (nmoles/mg protein)
Control	0.550 ± 0.134	2.98 ± 0.12	0.888 ± 0.134	2.39 ± 0.32
Treatment	3.217 ± 0.374	18.66 ± 3.54	4.163 ± 0.222	23.084 ± 1.59
Treatment + Aqueous	0.834 ± 0.123	10.96 ± 1.82	1.284 ± 0.295	10.208 ± 0.42
Treatment + Methanolic-HCl	0.417 ± 0.177	3.22 ± 3.974	0.400 ± 0.144	7.0308 ± 1.13
Treatment + Methanolic	0.167 ± 0.286	4.48 ± 1.93	1.450 ± 0.117	6.960 ± 1.48
Treatment + Acetone	0.934 ± 0.112	4.09 ± 1.04	0.917 ± 0.057	7.0308 ± 1.53
Treatment + Chloroform	1.022 ± 0.543	3.51 ± 1.25	1.300 ± 0.148	6.612 ± 1.43
Treatment + Benzene	0.700 ± 0.215	5.94 ± 2.25	2.817 ± 0.247	7.242 ± 0.88

TBARS- thiobarbituric acid reactive substances; LOOH- lipid hydroperoxides

Values are mean $\pm$ SE from 4 different experiments.

* p < 0.001 compared with radiation treatment.

The data on the effect of baicalein on radiation- and AAPH-induced oxidative damage in terms of LOOH formation in rat liver mitochondria were shown in Table 2. When mitochondria were exposed to γ–rays at 450 Gy with and without baicalein, there was a significant enhancement in LOOH formation at the dose of 450 Gy. Baicalein at concentrations of 5 and 10 μM, was observed to possess a significant ability to inhibit LOOH formation induced by both radiation and AAPH. When exposed to radiation, the inhibition by baicalein of 5 and 10 μM were 48 % and 68 % respectively. The enhanced formation of LOOH owing to radiation exposure at 450 Gy was effectively reduced by baicalein even at 5 μM. Lowering of LOOH was also observed with baicalein at concentration of 5 and 10 μM on AAPH treatment in rat liver mitochondria.

Table 2: **Effect of baicalein on radiation and AAPH-induced formation of LOOH in rat liver mitochondria**

	LOOH (nmoles/mg protein)	
	γ-radiation exposure	AAPH treatment
Control	3.73 ± 0.32	4.58 ± 0.43
Treatment	25.52 ± 1.72	16.49 ± 1.82
Treatment + 5 μM baicalein	15.08 ± 0.81	10.44 ± 0.49
Treatment + 10 μM baicalein	10.70 ± 1.44	9.63 ± 1.07

Table 3: **Effect of baicalein on radiation and AAPH-induced formation of superoxide dismutase (SOD) activity in rat liver mitochondria**

	SOD (Units/mg protein)	
	γ-radiation exposure	AAPH treatment
Control	2.27 ± 0.15	4.60 ± 0.18
Treatment	0.24 ± 0.22	1.92 ± 0.11
Treatment + 1 μM baicalein	1.30 ± 0.36	3.56 ± 0.06
Treatment + 5 μM baicalein	1.56 ± 0.21	4.03 ± 0.12
Treatment + 10 μM baicalein	1.88 ± 0.25	4.10 ± 0.06
Treatment + 50 μM baicalein	2.05 ± 0.45	4.26 ± 0.05

SOD- superoxide dismutase

Values are mean ± SE from 4 different experiments.

* $p < 0.001$ compared with respective radiation treatment.

Superoxide dismutase activity was significantly reduced by radiation exposure as well as AAPH treatment as shown in Table 3. As with lipid peroxidation baicalein caused significant inhibition of damage. It also significantly protected the enzyme against oxidative damage in a concentration dependent manner. At concentrations of 1, 5, 10 and 50 μM, the protection against damage was 52, 65, 80 and 89% respectively. With AAPH treatment the percentage protection by baicalein were 61, 79, 81 and 87 % for 1, 5, 10 and 50 μM concentrations. Thus increasing protection was observed with increasing concentrations of baicalein.

The ability of baicalein to scavenge ROS generated by radiolysis of water was demonstrated using pulse radiolysis. Baicalein has significant abilities to react with $^{.}OH$, with a bimolecular rate constant of 3.7×10^9 dm^3 mol^{-1} s^{-1}. The studies also reveal that with azide radical it gives the rate constant of 1.34×10^9 dm^3 mol^{-1} s^{-1}. Azide radical ($N_3^{.}$) is highly selective and reacts with phenolic compounds by univalent oxidation giving rise to aroxyl (phenoxyl) radical. Since the transient absorption spectra for $^{.}OH$ and $N_3^{.}$ radicals were similar, it is evident that baicalein reacts with these radicals by single

electron transfer reactions. Our study also shows that baicalein also has a fairly high rate constant with a model peroxyl radical i.e. trichloromethylperoxyl radical (8.5×10^7 dm^3 mol^{-1} s^{-1}). Linoleic acid peroxyl radical is very relevant in biological systems and baicalein forms transient with $LOO^{.}$ at 100 μs at 450 nm.

Discussion

Many plants are known to have beneficial therapeutic effects as noted in the traditional Indian system of medicine, *Ayurveda*. However, they have received little attention for their radioprotective as well as antioxidant activities. Medicinal plants can protect against harmful effects of ionizing radiation. Natural plant extracts or pure compounds are safe ingredients, which do not have any toxic effects. *T. arjuna* is a well-known cardiotonic, cardio protective plant and used in India for centuries. It is used as a cure for various heart disorders such as congestive heart failure, coronary artery disease, myocardial necrosis, angina, atherosclerosis and ischemia-reperfusion injury besides having hypolipidaemic activity. It was shown that 500 mg capsule of bark extract is a safe and effective remedy for patients suffering from refractory congestive heart failure. Because of its high

calcium content it is given in all types of hemorrhages. When given with honey, it is known to promote union of fractures. The other beneficial properties include anti-pyretic, anti-allergic, antimutagenic, antigenotoxic, antitumor, chemo preventive and antioxidant effects. Therefore the aim of the present study was to evaluate radioprotective and antioxidant effects of *T. arjuna* and its active ingredient baicalein.

In biological systems, oxidative stress *in vitro* can be generated using various physical/chemical agents. Among them, ionizing radiation such as γ-rays is an important source. The exposure of biological systems to radiation results in radiolytic cleavage of water yielding ·OH, ·H, e^-_{aq} etc. In presence of oxygen even $O_2^{·-}$, H_2O_2, $^1O_2$ are also produced. Thermal decomposition of an azo-initiator (AAPH) in presence of oxygen gives rise to a constant source of peroxyl radicals. These free radicals can initiate lipid peroxidation. In this paper, we have demonstrated that ROS induce significant lipid peroxidation in the model system i.e. rat liver mitochondria as measured by LOOH, an unstable intermediate, which further breaks down to stable aldehydes and react with thiobarbituric acid (TBA) to form TBARS, the final stable end product (Girotti, 1990). Apart from enhancing lipid damage, radiation and AAPH treatments lead to inactivation of antioxidant enzymes such as superoxide dismutase (SOD).

Our results have shown that methanolic and aqueous extracts of *T. arjuna* as well as baicalein, when present during radiation exposure, can prevent the damage to the cell membranes. At a concentration of 1 mg/ml, methanolic Soxhlet extract of *T. arjuna* could prevent against lipid damage in terms of TBARS and LOOH formation. Whereas, at 1 mg/ml, methanolic-HCl Soxhlet extract of *T. arjuna* significantly inhibited the formation of TBARS and LOOH when present during the AAPH-induced damage.

Plants are complex mixtures of compounds and no single compound can provide the observed activity. Plant extracts can be characterized by polyvalent formulations and interpreted as additive, or, in some cases, potentiating (Kulkarni, 1997). The exact mechanism of action of *T. arjuna* is not known. However, it can scavenge free radicals produced by γ-radiation and other sources of oxidative stress. Thus it reduces the radiation-induced damage to cellular biomolecules including genome. Our studies with the bark of *T. arjuna* show that the observed cardioprotective effects may be due to the antioxidant properties seen at different levels.

Majority of flavonoids in *T. arjuna* including baicalein are soluble in methanol, and are capable of protecting against oxidative damage by scavenging free radicals. Hence free radical scavenging capacities were measured by standard assays like DPPH and ferrylmyoglobin/ABTS assays. The ferric reducing capacities were also determined using FRAP assay. The trolox/ascorbic acid equivalent antioxidant capacities were calculated and *T. arjuna* as well as arjunsal extracts possessed fairly high T/AEAC scores. If LDL oxidation plays a key role in pathogenesis of atherosclerosis, then its inhibition by antioxidants should prevent atherosclerosis (Halliwell and Gutteridge, 1997; Yoshikawa et al, 2000). Considering the activities of free radicals and concentrations of substrates, the phenolic compounds from natural sources are promising candidates for drugs for atherosclerosis, depending on their reactivity towards free radicals, localization, mobility in lipoprotein and fate of its radicals. Baicalein is a naturally occurring flavone from the medicinal plant *T. arjuna*. Our results show that baicalein possess significant antioxidant properties in terms of radical scavenging and ferric reducing activities efficiently protects mitochondrial membrane against radiation damage. These

observations suggest that baicalein is a potent radioprotector in biological systems.

The significant Trolox equivalent antioxidant capacity (TEAC) values of the extracts in ferric reducing and radical scavenging assays might be responsible for inhibition of lipid peroxidation. Thus it can protect against radiation induced cell death. *T. arjuna* has been reported to possess antioxidant, anti-lipoperoxidative and anti-radical properties. *T. arjuna*'s active constituents include tannins, triterpenoid saponins, gallic acid, ellagic acid, oligomeric proanthocyanidines, phytosterols, Ca, Mg, Zn, Cu besides flavonoids such as arjunone, arjunolone, luteolin, baicalein etc. (Anonymous, 1999). Most of these compounds have been reported to possess antioxidant activities (Ratty and Das, 1988). Further baicalein has also been reported to have antioxidant properties (Gao et al., 1996; Shieh et al., 2000). Therefore antioxidant properties of *arjunsal, T. arjuna* extracts and baicalein observed earlier and in the present study might have contributed to the observed radioprotective action in the present study.

References

1. Yoshikawa T, Toyokuni S, Yamamoto Y, Naito Y, (Eds.). *Free Radicals in Chemistry Biology and Medicine*. London: OICA International, 2000.

2. Tilak JC, Devasagayam TPA, Lele RD. *Res. Commun. Pharmacol. Toxicol.* (in press).

3. Kirtikar KR, Basu BD, *Indian Medicinal Plants,* Vol, 1 & 2. Allahabad, 1984.

4. Devasagayam TPA, Kamat JP, Mohan H, Kesavan P C. *Biochim Biophys Acta* 1996;1282: 63-70.

5. Mukharjee T. 1997. In *Atomic, Molecular and Cluster physics*. Ahmad SA (ed). Narosa: New Delhi; 299-316.

6. Girotti AW, Geiger PG, Thomas JP. *Free Rad. Biol. Med.* 1990;**9**: 76.

7. Kulkarni RD. *Principles of pharmacology in Ayurve*da, Ram Sangram Graphics, Mumbai, 1997.

8. Halliwell B, Gutteridge JMC, Free Radicals in Biology and Medicine. Oxford: Oxford University Press, 1997.

9. Anonymous. *Terminalia arjuna. Altern. Med. Rev.* 1999, **4**, 436-437.

10. Ratty AK, Das NP. *Biochem Med Metabol Biol.* 1988, **39**, 69-79.

11. Gao D, Sakurai K, Katoh M, Chen J, Ogiso T. *Biochem. Mol. Biol. Int.* 1996, **39**, 215-255.

12. Shieh DE, Liu LT, Lin CC. *Anticancer Res.* 2000, **20**: 2861-2866.

This paper received the Best Poster award in the International Conference on "Free Radicals and Antioxidants in Health & Disease", held at Lucknow during February 10-12, 2003

About the authors ...

Ms Jai C. Tilak *received her M.Sc. degree in Biotechnology from Ruia College, Mumbai, in 2000. She was a topper during her Graduation and Post Graduation from the same college. At present, she is a DAE fellow attached with Radiation Biology and Health Sciences Division, BARC, pursuing her Ph.D. on a project entitled "Studies on the antioxidant effect of natural compounds from Indian medicinal plants."*

Dr T.P.A. Devasagayam *joined BARC in 1975 after completing BARC Training School in Biology and Radiobiology. At present he is with Radiation Biology and Health Sciences Division of BARC. He is deeply involved in research related to Human Health and Radiation Biology. He has done his Post-Doctoral work at the University of Dusseldorf, Germany and at Wayne State University, USA. He holds the post of Honorary Secretary General of SFRR-India Chapter and also Vice-President of EMSI-India.*

Dr S. Adhikari *joined BARC Training School in 1990 (34th batch). After successful completion of the one-year orientation course, he joined the then Chemistry Division in 1991. Since then he has been involved in studying radiation chemistry biologically important molecules in microheterogeneous media. He is the recipient of the prestigious IUPAC (International Union of Pure and Applied Chemistry) Prize for Young Chemists. His recent research interest is the free radicals induced damage in bio-systems and the mechanistic aspect of the antioxidant activity of natural antioxidants.*

MECHANISMS RESPONSIBLE FOR THE ANTIOXIDANT PROPERTIES OF CHLOROPHYLLIN: A PULSE RADIOLYSIS STUDY

K.K. Boloor and T.P.A. Devasagayam
Radiation Biology & Health Sciences Division
Bhabha Atomic Research Centre

and

Hari Mohan
Radiation Chemistry & Chemical Dynamics Division
Bhabha Atomic Research Centre

A b s t r a c t

Chlorophyllin, the water-soluble analogue of the ubiquitous green pigment chlorophyll has been shown to be a potent antioxidant and radioprotector under both in vitro and in vivo conditions. It is a potent protector of membrane damage and prevents protein oxidation, lipid peroxidation besides depletion of thiols induced by radiation, photosensitization and other oxidants. To analyze the possible mechanisms involved, we have studied the reaction of chlorophyllin with biologically relevant radical species in the form of linoleic acid peroxyl radical (LOO$^\bullet$), chloroperoxyl radical (CCl$_3$O$_2$$^\bullet$), azide radical (N$_3$$^\bullet$) and thiyl radical (RS$^\bullet$). The summary of results obtained are given below: Pulse radiolysis studies show that these radicals (CCl$_3$O$_2$$^\bullet$, N$_3$$^\bullet$, RS$^\bullet$) react with chlorophyllin in a similar way producing transient absorption bands at 370 nm and in the region of 430-450 nm with bleaching at 410 nm. The one electron oxidized species was long lived without any decay upto 1 millisecond. The high rate constant values reveal that chlorophyllin is able to scavenge these radicals effectively. However, the reaction of LOO$^\bullet$ radical with chlorophyllin was slow and the yield of one-electron oxidized species of chlorophyllin was also small. This indicates that inhibition of lipid peroxidation observed with chlorophyllin may involve other mechanisms.

Introduction

In recent years there has been an increased interest in areas related to newer developments in the prevention of disease especially those involving natural compounds with antioxidant activities. These antioxidants neutralize free radicals or their activities. Oxidative stress involving the enhanced generation of reactive oxygen species (ROS) including free radicals and other related reactive species has been implicated in a variety of toxicities and ailments [Ames, 1993; Sies, 1996; Yoshikawa et al. 2000]. ROS have been implicated as possible causative factors for more than 100 diseases. These include cardiovascular ailments, neural disorders, diabetes, various forms of cancer, hepatitis, urolithiasis, tissue injury and immune disorders [Sies, 1996; Thomas & Kalyanaraman, 1997; Yoshikawa et al. 2000; Klaunig & Kamendulis, 2004]. Hence compounds with potent antioxidant activity can help in the prevention/cure of diseases as well as in toxicities. Such compounds, especially derived from natural sources and capable of minimizing oxidative damage *in situ,* have

potential uses to control human diseases. These compounds, capable of interacting with DNA, cellular membranes and other biomolecules have potential protective properties against deleterious free radicals [Sies, 1996; Packer & Ong, 1998; Surh, 2003].
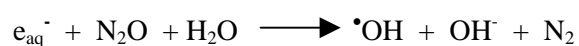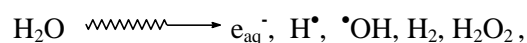
Chlorophyllin is a water-soluble analogue of chlorophyll, the ubiquitous photosynthetic green pigment present in food materials of plant origin as well as in nutritional supplements such as extracts from *Spirulina* and *Chlorella vulgaris*. Chlorophyll has been credited with several beneficial properties. Chlorophyllin (CHL), has proved to be better than the parent compound as evident from studies employing model systems [Negishi, 1997; Dashwood et al, 1998]. It possesses highly potent antioxidant activity [Sato et al, 1984; Sato et al, 1985; Kamat et al, 2000; Kumar et al, 2001]. It has been used, without apparent toxic side effects, to treat a number of human ailments. As a food pigment it can be widely used in cakes, beverages, sweets, ice creams etc. On a daily basis, it is used in green toothpaste and cosmetics. It has been found to exhibit anticarcinogenic and antimutagenic properties. Our earlier studies have shown chlorophyllin to be a potent antioxidant against oxidative stress induced by radiation, photosensitization and peroxynitrite as measured by inhibition of lipid peroxidation, protein oxidation, DNA damage and restoration of endogenous antioxidants [Kamat et al, 2000; Kumar et al, 2001].

Though its scavenging ability of primary radicals such as hydroxyl radical, superoxide and singlet oxygen has been established, its ability to react with biologically important secondary radicals such as peroxyl radicals and thiyl radicals has not been examined. The present investigation is towards this objective. The secondary radicals studied in the present investigation are lipid peroxyl radicals (LOO·), chloroperoxyl radical (CCl$_3$O·) and thiyl radicals (RS·). Peroxyl radicals are able to abstract hydrogen atom from another lipid molecule (adjacent fatty acid), especially in the presence of metals such as copper and iron, thus causing an autolytic chain reaction. LOO· can combine with H to give LOOH and this reaction characterizes the propagation stage of lipid peroxidation. Chloroperoxyl radical has been used as a representative peroxyl radical and also for its inherent simplicity in performing experiments. The action of cytochrome P450 system on toxicants like CCl4 generates trichloromethyl radical which is able to react with oxygen to give chloroperoxyl radical. Thiols are present in living systems which in addition to participating in cellular redox processes also take part in scavenging free radicals. This reaction is known as an antioxidant reaction. The thiyl radicals thus generated in living systems are considered to be reactive oxidants as they are able to initiate lipid peroxidation by abstracting bis-allylic hydrogen from poly-unsaturated fatty acids. The thiyl radicals can also add to the double bond leading to efficient cis/trans isomerization of mono and polyunsaturated fatty acids.

Materials and Methods

The pulse radiolysis system using 7 MeV electrons has been described earlier [Mukharjee, 1997; Scotl et al, 1993]**.** The dosimetry was carried out using an air-saturated aqueous solution containing 5 x 10^{-2} mol dm^{-3} KSCN (Gϵ = 23,889 dm^3 mol^{-1} cm^{-1} per 100 eV at 500 nm) [Buxton and Stuart, 1995]. The kinetic spectrophotometric detection system covered the wavelength range from 250 to 800 nm. The optical path length of the cell was 1.0 cm. The width of the electron pulse was 50 ns. Time-dependent absorbance differences were recorded on a digital oscilloscope. High purity (> 99.9 %) N$_2$O, from BOC India Pvt. Ltd. was used.

$$H_2O \rightsquigarrow e_{aq}^-, H^\bullet, {}^\bullet OH, H_2, H_2O_2 ,$$

$$e_{aq}^- + N_2O + H_2O \longrightarrow {}^\bullet OH + OH^- + N_2$$

•Chloroperoxyl radical (CCl3OO·) was generated by the reaction of carbon tetrachloride

(CCl4) with oxygen. ·CCl4 generates trichloromethyl radical (·CCl3) which is able to react with oxygen to give CCl3OO·. This radical species was generated in aerated water-isopropanol-acetone (50:40:10 v/v) mixtures containing carbon tetrachloride by the following reactions:

H·, or OH· + $(CH_3)_2CHOH \longrightarrow$
$(CH_3)_2C· OH + H_2$ or H_2O

e aq- + $(CH_3)_2CO \longrightarrow (CH_3)_2CO^-$

$CH_3)_2CO^- + H_2O \longrightarrow (CH_3)_2C· OH + OH^-$

$(CH_3)_2C· OH + CCl4 \longrightarrow (CH_3)_2CO +$
$CCl_3· + H+ Cl-$

$CCl_3· + O_2 \longrightarrow CCl_3OO·$
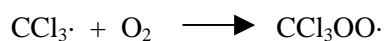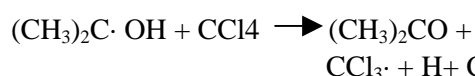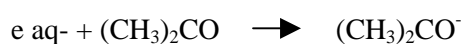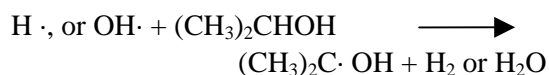
Lipid peroxyl radical was generated by pulse radiolysis carried out in aerated aqueous solution containing 2 x 10-2 mol dm-3 linoleic acid.

LH + ·OH $\longrightarrow$ L· + H2O
L· + O_2 $\longrightarrow$ LOO·

Thiyl radicals were generated on pulse radiolysis of cystein (10-3 M) in N2O saturated solution containing chlorophyllin (6.5 x 10-5 M).

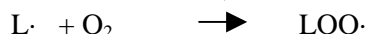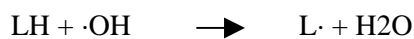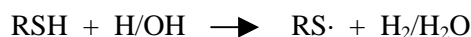RSH + H/OH $\longrightarrow$ RS· + H_2/H_2O

• Azide radicals were generated on pulse radiolysis of N_2O-saturated aqueous solution of NaN_3 (0.1 M).

N_3^- + ·OH $\longrightarrow$ $N_3·$ + OH^-
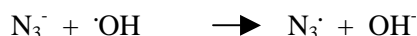
The bimolecular rate constants were calculated by plotting pseudo-first order rate of formation of the transient against the concerned solute concentration. The uncertainty in the measurement in bimolecular rate constant is <10%. The transients obtained in the pulse radiolysis study were used to characterize the product radical. The rate constants determined and presented in the text are not mere radiation chemical parameters, but they reflect on the efficiency of scavenging free radicals and the ease with which competing reactions occur.

Results and Discussion

Figure 1 shows the transient optical absorption spectrum obtained on reaction of $N_3·$ with chlorophyllin, One-electron oxidized species is observed to have transient absorbtion bands at 320, 370 and in the region of 430-450 nm with bleaching at 410 nm. The one-electron oxidized species is observed to be stable at least upto 1ms and recovery of bleaching is also not observed in this time scale.

Fig. 1

Fig. 2

Chloroperoxyl radicals are also observed to react with chlorophyllin with a bimolecular rate constant of ~7x108 M-1S-1 and the transient absorbtion spectra was similar to that obtained on reaction with azide and thiyl radicals. Azide radicals are observed to react with chlorophyllin

with a bimolecular rate constant of 1x109 M-1 S-1 as determined from the growth of the transient band at 360 nm and bleaching of ground state absorbtion at 400 nm.

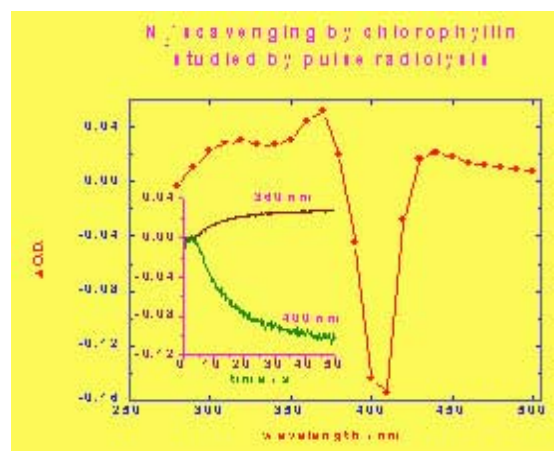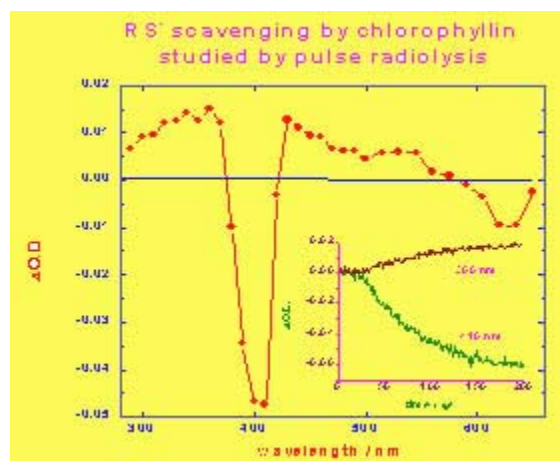Thiyl radicals generated on pulse radiolysis of cystein (10-3 M) in N2O saturated solution of chlorophyllin (6.5 X 10-5 M) showed the formation of a transient band ~370 nm with bleaching at 410 nm with a bimolecular rate constant of ~ 2 X 108 m-1 s-1. The spectra is similar to that obtained on reaction with azide radicals, but only the rate constant value was lower.

Table 1: **Reaction rate constants of various radicals studied with chlorophyllin determined using pulse radiolysis**

Reaction of CHL with	Rate constant $(dm^3\ mol^{-1}\ s^{-1})$
$N_3{}^\cdot$	1×10^9
$CCl_3O_2{}^\cdot$	7×10^8
$RS^\cdot$	2×10^8

Pulse radiolysis studies reveal that chloroperoxyl, azide and thiyl radicals react with chlorophyllin in similar way. The high rate constant values reveal that chlorophyllin is able to scavenge chloroperoxyl, azide and thiyl radicals effectively.

Values are mean ± S.E. of 4experiments. LOOH – lipid hydroperoxide.

[Kamat JP, Boloor KK & Devasagayam TPA Chlorophyllin as an effective antioxidant against membrane damage *in vitro* and *in vivo*. *Biochimica et Biophysica Acta* 1487, 113-127, 2000]

However the reaction of LOO· radical with chlorophyllin was slow and the yield of one-electron oxidized species of chlorophyllin was also small. Our earlier studies have indicated chlorophyllin to be a potent protector of lipids and proteins in rat liver mitochondria (Table 2).

Table 2 : Protective effect of chlorophyllin against radiation-induced lipid peroxidation and inactivation of superoxide dismutase as compared to established antioxidants at equimolar concentration of 50 μM

Treatment	Lipid peroxidation (nmoles LOOH/mg protein)	Superoxide dismutase (units/mg
Control	7.38 ± 0.17	6.37 ± 0.10
Rad	43.55 ± 1.54	1.50 ± 0.17
Rad+CHL	20.15 ± 3.71	5.25 ± 0.14
Rad+Asc	40.21 ± 1.47	3.00 ± 0.28
Rad+GSH	25.50 ± 1.83	4.80 ± 0.10
Rad+Mann	35.66 ± 2.01	2.62 ± 0.21
Rad+t-BuOH	34.39 ± 1.25	2.25 ± 0.43

This indicates that inhibition of lipid peroxidation observed with chlorophyllin may involve other mechanism apart from radical scavenging.

References

1. Ames B.N., Shigenaga M.K., Hagen T.M. Oxidants, antioxidants and the degenerative diseases of ageing. *Proc. Natl. Acad. Sci. USA*. 1993, 90, 7915-7922.

2. Buxton G.V., Stuart C.R. Re-evaluation of the thiocyanate dosimeter for pulse radiolysis. *J. Chem. Soc. Faraday Trans.* 1995, 91, 279-281.

3. Dashwood R.H., Negishi T., Hayatsu H., Breinholt V., Hendricks J., Bailey G. Chemopreventive properties of chlorophylls towards aflatoxin B$_1$: a review of antimutagenicity and anticarcinogenicity data in rainbow trout. *Mutat. Res*.1998, 399, 245-253.

4. Kamat J.P., Boloor K.K., Devasagayam T.P.A. Chlorophyllin as an effective antioxidant against membrane damage *in vitro* and *in vivo, Biochim. Biophys. Acta* 2000, 1487, 113-127.

5. Kumar S.S., Devasagayam T.P.A., Bhushan B., Verma N.C. Scavenging of reactive oxygen species by chlorophyllin: an ESR study. *Free Rad. Res*. 2001, 35, 563-574.

6. Mukharjee T. 1997. In *Atomic, Molecular and Cluster physics*. Ahmad SA (ed). Narosa: New Delhi; 299-316.

7. Negishi T., Rai H., Hayatsu H. Antigenotoxic activity of natural chlorophylls. *Mutat. Res.* 1997, 376, 97-100.

8. Packer L., Ong A.S.H. (Eds.) *Biological Oxidants and Antioxidants:Molecular Mechanisms and Health Effects*, AOCS Press, Champaign, 1998.

9. Sato M., Imai K., Kimura R., Murata T. Effect of sodium copper chlorophyllin on lipid peroxidation. VI. Effect of its administration on mitochondrial and microsomal lipid peroxidation in rat liver, *Chem. Pharm. Bull. (Tokyo).* 1984, 32, 716-722.

10. Sato M., Imai K., Kimura R., Murata T. Effect of sodium copper chlorophyllin on lipid peroxidation. VIII. Its effect on carbon tetrachloride-induced liver injury in rats. *Chem. Pharm. Bull. (Tokyo).* 1985, 33, 3530-3533.

11. Scotl S.L., Chen W.J., Bakac A., Espenson J.H. Spectroscopic parameters, electrode potentials, acid ionisation constants and electron exchange rates of the 2,2′-azinobis(3-ethylbenzothiazoline-6-sulfonate) radicals ad ions. *J Phys Chem* 1993, 97, 6710-6714.

12. Sies H. (Ed.) *Antioxidants in Disease, Mechanisms and Therapy*, Academic Press, New York, 1996.

13. Surh Y.J. Cancer chemoprevention with dietary phytochemicals. *Nature Rev. Cancer* 2003, 3, 768-780.

14. Thomas C.E., Kalyanaraman B. (Eds.). *Oxygen Radicals and The Disease Process*. Harwood Academic Publishers, The Netherlands, 1997.

15. Yoshikawa T., Toyokuni S., Yamamoto Y., Naito Y. (Eds.) *Free Radicals in Chemistry Biology and Medicine*, OICE International Saint Lucia, 2000.

This paper won the Best Poster award at the International Conference on "Role of Free Radicals and Anti-oxidants in Health and Disease" held at Lucknow during February 10-12, 2003

About the authors ...

Dr K.K. Boloor *received his Ph.D. degree carried out under the guidance of Dr T.P.A. Devasagayam from Radiation Biology and Health Sciences Division, BARC, on 'Mechanisms and modulation of membrane damage induced by ionizing radiation and reactive oxygen species'. Presently, he is working as a senior research scientist in Vimta Laboratories, Hyderabad.*

Dr T.P.A. Devasagayam *joined BARC in 1975 after completing BARC Training School in Biology and Radiobiology. At present, he is with Radiation Biology and Health Sciences Division of BARC. He is deeply involved in research related to Human Health and Radiation Biology. He has done his Post-Doctoral work at the University of Dusseldorf, Germany and at Wayne State University, USA. He holds the post of Honorary Secretary General of SFRR-India Chapter and also Vice-President of EMSI-India.*

Dr Hari Mohan *joined BARC in 1967. Since then, he has been actively involved in the study of fast reaction kinetics using accelerators and lasers. His current research interests include free radical reactions of halogenated and sulphur compounds and biomolecules of natural origin. He has co-authored more than 150 research papers in international journals. Presently, he is the Head, Radiation Chemistry Section of Radiation Chemistry and Chemical Dynamics Division, BARC.*

ANTIOXIDANT EFFECTS OF *Convolvulus pluricalus* IN RAT BRAIN MITOCHONDRIA AGAINST OXIDATIVE DAMAGE INDUCED BY GAMMA RADIATION AND PHOTOSENSITIZATION

Jayashree P. Joshi and Jayashree P. Kamat
Radiation Biology & Health Sciences Division
Bhabha Atomic Research Centre

H. Mohan
Radiation Chemistry& Chemical Dynamics Division
Bhabha Atomic Research Centre

and

G. Chintalwar and S. Chattopadhyay
Bioorganic Division
Bhabha Atomic Research Centre

Abstract

Aqueous and methanolic extracts of natural herb, Convolvulus pluricalus (CP) was monitored for their antioxidant ability against photosensitization and radiation induced damages in rat brain mitochondria. Both the extracts of CP (50 μg /ml assay) showed significant protection against the formation of the lipid peroxidation product, TBARS. Protein oxidation and degradation of proteins was shown to be significantly high following photosensitization, while CP extracts could effectively modify these damages. Exposure of plasmid DNA pBR322 to gamma radiation resulted in enhanced formation of single strand breaks (SSB). Simultaneous treatment of pBR322 DNA with CP extracts during radiation effectively prevented the damage. Further, these extracts also showed inhibition against stable radicals, 2, 2'- azino-bis (3- ethylbenzthiazoline-6- sulfonic acid (ABTS) and 1, 1-diphenyl-2-picryl hydrazyl (DPPH). The scavenging capacity of the extracts was quantified by pulse radiolysis experiments. Hence, Convolvulus pluricalus may emerge as potent antioxidant/radioprotector, capable of scavenging singlet oxygen, hydroxyl radical, as well as other stable radicals, ABTS and DPPH.

Introduction

Oxygen derived reactive oxygen species (ROS) and their adverse effects are inevitable for aerobic organisms. Cellular constituents, lipids, proteins and DNA are the crucial targets for ROS attack. Overexpression of ROS is being implicated in several degenerative diseases [1,2]. Therefore intake of antioxidants from natural origin with less toxicity (compared to synthetic antioxidant) in relation to human health is useful. Plants have several phytochemicals/micronutrients with creditable medicinal values useful in ayurveda [3]. Since photosensitization, as well as radiation exposure can result in oxidative stress through reactive oxygen species (ROS) [4,5], the aim of the present study was to evaluate the effect of phytoconstituents of the medicinal plant, *Convolvulus pluricalus* (Family-

Convolvulaceae, Fig.1) The plant occurring in the plains of North India is a known intellect-promoter, psycho-stimulator and an excellent brain/ cardio-tonic [6].

Materials and Methods

Fig.1 *Convolvulus pluricalus (Shankhapushpi)*
Family: leguminoceae
Plant part used: whole herb
Habitat: This plant generally occurs in the plains of North India and has creditable medicinal values

Assessment of oxidative damage

Oxidative damage to lipids was studied by monitoring formation of TBARS while protein oxidation and degradation of mitochondrial proteins were assessed by measuring carbonyl contents [4,5] and SDS PAGE [7] respectively. Plasmid pBR322 was exposed to γ radiation at 6 Gy with and without CP extracts and protection by CP was assessed by gel electrophoresis and quantification. Assays of DPPH and ABTS were carried out by standard methods [8,9].

Results and Discussion

Membrane peroxidation and protein oxidation

Due to the high contents of polyunsaturated fatty acids, membranes are prone to the attack by ROS forming several peroxidation products which are toxic to cells. One of the stable products is thiobarbituric acid reactive substances (TBARS). Using photosensitization system the antioxidant potential of CP extracts was monitored using the TBARS assay. A significant increase in TBARS was demonstrated when mitochondria were exposed to photosensitization for 15 min. Simultaneous addition of methanolic or aqueous extracts of CP (50 μg /ml) in independent experiments during photosensitization could prevent TBARS formation effectively. The results demonstrated about 40% decrease in TBARS levels by both the extracts of CP (Fig 2).
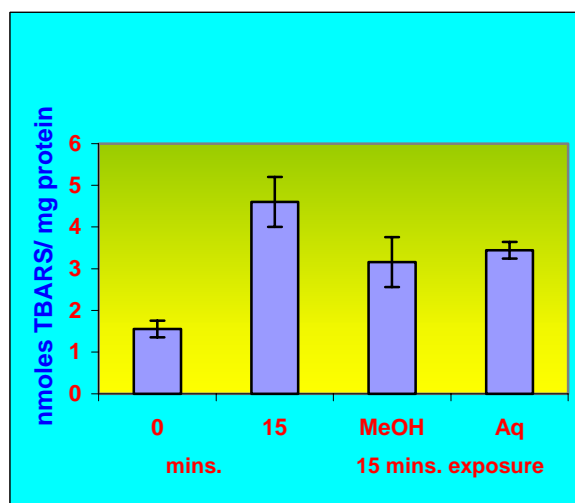
Fig 2: *Photosensitization induced formation of TBARS in rat brain mitochondria and prevention by CP*

Oxidation of protein due to ROS is one of the important and deleterious reactions of membrane proteins implicated in several diseases including aging [10]. Photosensitization showed enhanced formation of protein carbonyls, the index of protein oxidation. The extent of formation of protein carbonyls was high at 15 min photo exposure. Presence of CP extracts, however,
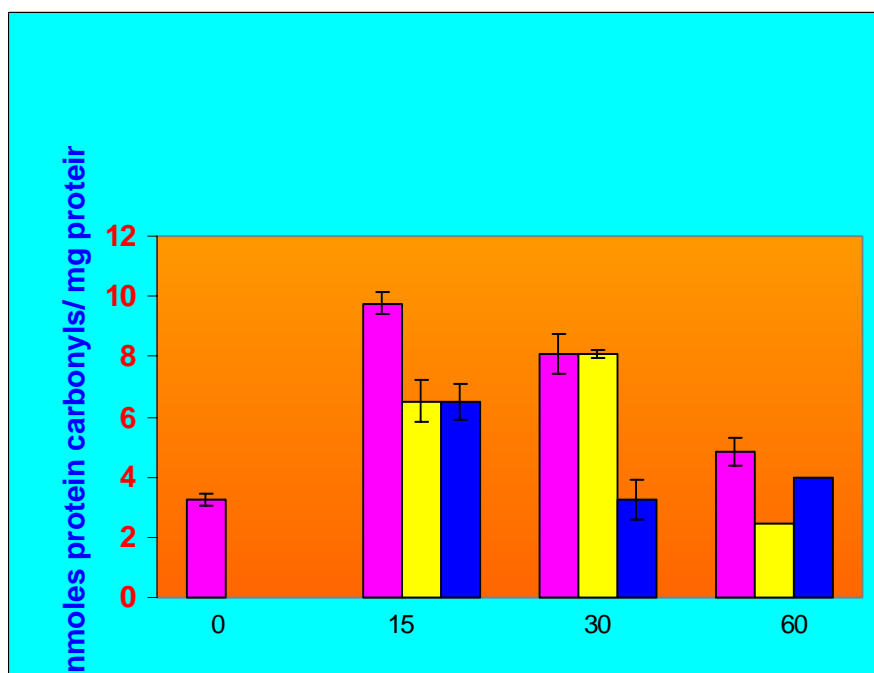
Fig 3 Photosensitization induced formation of protein carbonyls in rat brain mitochondria and inhibition by CP

exerted protective effects against this damage (Fig 3).

Photosensitization also induced time dependent degradation of the mitochondrial proteins. The effect of CP on photosensitization- induced degradation of brain mitochondrial proteins was assessed by SDS PAGE (Fig 4). The intensity of

Fig 4: Photosensitization induced protein degradation and prevention by CP extracts.

protein bands was less in the lanes containing photosensitized samples (exposure time 30 and 60 mins). The intensity was considerably less at 60 min exposure compared to that at 30 min. Photosensitization of mitochondria in presence of CP (50 μg /ml) prevented protein degradation as seen from the higher intensity of bands.

Radiation exposure to plasmid DNA pBR322

Generation of ROS especially through low LET ionizing radiations and its profound damaging effects on cellular system is well known. In the present studies expression of radiation damage and protection of DNA repair mechanism is explored by studying a simple cell free system i.e. plasmid pBR322. The pBR322 DNA was exposed to radiation (6 Gy) with and without CP extracts. Radiation exposure induced single strand breaks (SSB) in closed circular form (CC-Form I) of pBR322 increasing the open circular form (Form II). It is evident from the gel image that CP extracts reversed the effect of radiation by preventing the formation of SSB. The results are compared with unexposed control (Fig 5).
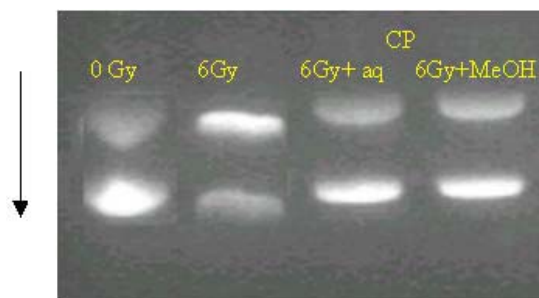
Fig 5: Radiation induced DNA damage and
       prevention by CP and effect of CP extract
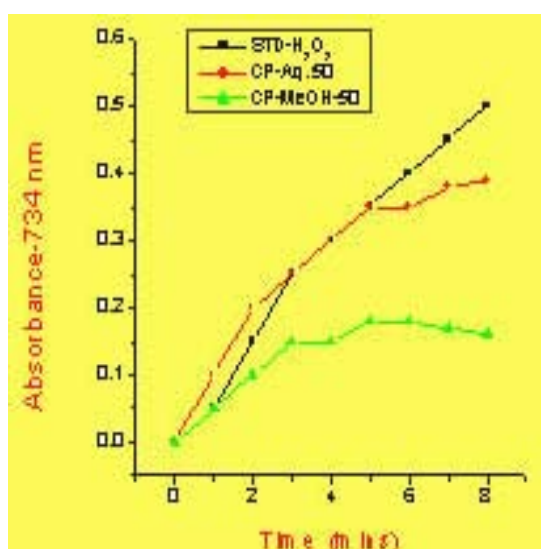
Fig.6a Antioxidant activity of convolvulus
        pluricalus extra by ABTS assay
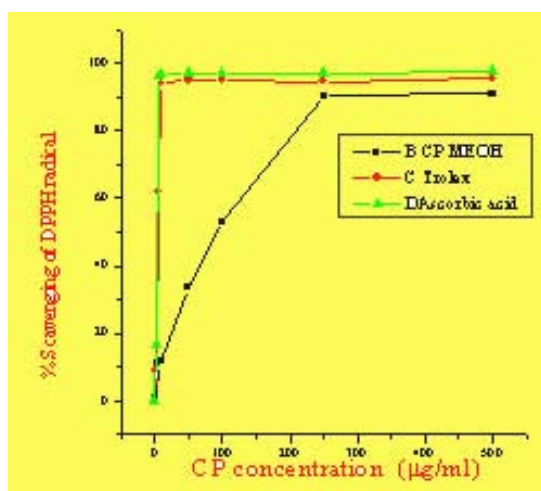
Fig.6b DPPH scavenging capacity of
        convolvulus pluricalus

These extracts also showed inhibition against stable radicals, 2, 2'- azino-bis (3-ethylbenzthiazoline-6- sulfonic acid (ABTS) and 1, 1- diphenyl-2-picryl hydrazyl (DPPH). Scavenging capacity was compared with standard antioxidants (Fig 6). The rate constant of CP by pulse radiolysis technique in presence of ABTS was evaluated as $4\times10^{-4}S.^{-1}$ Thus based on the above results, preparations from *Convolvulus pluricalus* appear to be potent antioxidants, capable of scavenging singlet oxygen, hydroxyl radical, as well as other radicals, ABTS and DPPH.

Acknowledgements

References

1. Halliwell, B., Gutteridge, J.M.C., Free radicals in biology and medicine, Oxford University Press, Oxford 1997.

2. Freidovich, I., Fundamental aspects of reactive oxygen species, or what's the matter with oxygen? *Ann. N.Y. Acad. Sci*.,893,13,1999.

3. Kirtikar, K.R., Basu, B.D., (Eds) Indian Medicinal Plants, Vol – I & II, Publishers Blatter, E., Cauis, J.R. and Mhaskar, K.S., Basu, L.M., Allahabad, India. 1984.

4. Kamat, J.P. Sarma, H.D., Devasagayam, T.P.A., Nesaretnam, K., and Basiron, Y., Tocotrienols from palm oil as effective inhibitors of protein oxidation and lipid peroxidation in rat liver microsomes**.** *Molecular and Cellular Biochemistry,* 170, 131, 1997.

5. Kamat J.P.Boloor, K.K., T.P.A. Devasagayam, Jayashree,B., and Kesavan, P.C. Differential modification by caffeine of oxygen-dependent and independent effects of γ irradiation on rat liver mitochondria. *Int. J. Radiat. Biol*, 76, 1281, 2000.

6. Indurwade, N.H., Biyani, K.R., Evaluation of comparative and combined depressive effect of Brahmi, Shankhpushpi and Jatamansi. *Ind. J. Med Sci.* 54, 339,2000.

7. Lammelli, U.K., Cleavage of structural proteins during the assembly of the head of bacteriophae T4, *Nature* 227,680, 1970.

8. Lim, K.T,. Hu, C., Kitts, D.D., Antioxidant activity of *Rhus verniciflua* strokes ethanol extracts. *Food and Chemical Toxicol.* 39, 229, 2001.

9. Yu, W. T., Ong, C.N., Lag-time measurement of antioxidant capacity using myoglobin and 2,2'-Azinobis(3-ethylbenzthiazoline-6-sulfonic acid): Rationals, Applications and Limitations). *Analytical Biochem.* 275, 217, 1999.

10. Finkel, T., and Holbrook, N.J., Oxidants, oxidative stress and the biology of ageing. *Nature* 408, 239, 2000.

This paper received Best Poster Presentation award in National Symposium on "Radiation & Photochemistry (NSRP-2003)" held at I.I.T.Kanpur, March 3-5, 2003

About the authors ...

Ms Jayashree P Joshi received her M.Sc in Life Sciences, Biotechnology (specialisation) of Mumbai University in 2001. At present, she is a DAE fellow in Radiation Biology and Health Sciences Division, BARC, working for Ph.D.

Dr (Ms) Jayashree P. Kamat had her Ph.D. from the University of Mumbai in 1989. She had a stint of post-doctoral studies at the Wistar Institute and Temple University, Philadelphia, U.S.A. At present, she is deeply involved in exploring radioprotective effects of herbal/ dietary compounds and photodynamic therapy in relation to human health and has published several scientific papers in this area in international journals. She has also collaborative research work with other Divisions of BARC.

Dr Hari Mohan graduated from BARC Training School (Chemistry) in 1967. His main area of research is the study of fast reaction kinetics using electron accelerator and lasers. His current research interests include free radical reactions of biomolecules and natural products.

Dr G. Chintalwar retired from BARC after putting in 38 years of fruitful service in Bioorganic Division, BARC. His main area of research is isolation, identification and characterization of natural products from plants.

Dr S. Chattopadhyay is currently the Head of the Bio-Organic Division, BARC. He received his Ph.D (1989) from the Mumbai University. He has contributed immensely in the fields of asymmetric organic synthesis, biocatalysis, supramolecular chemistry and chemical biology of the oxidative processes. His other research interests include developments of new solvents for metal extraction and bioremediation of radioactive wastes. Besides, he has developed pheromone technology for protection of important crops against several pests and devised a phytohormone technology for use in sericulture. He is the recipient of several awards including the honorary fellowships of the National Academy of Sciences, India, Society for Cancer Research & Communications, the Themis UDCT Diamond Jubilee Distinguished Professor, Indian Chemical Society Award, etc.

VALUE ADDED PRODUCTS FROM RIPE BANANA: BANANA JUICE AND RIPE BANANA POWDER

K. K. Surendranathan, N. K. Ramaswamy, P. Radhakrishna and J. S. Nair
Nuclear Agriculture and Biotechnology Division
Bhabha Atomic Research Centre

A b s t r a c t

Banana is the largest grown fruit crop in India. Introduction of tissue culture techniques in banana cultivation has further enhanced its production. The fruit has a very short post-harvest shelf life because of its highly perishable nature. Unlike the developed countries, in India the development of commodities of consumer interest by value addition of fruits is less than 2 % of the annual agricultural produce. Short shelf life and increased production necessitates development of non-conventional products from banana. This laboratory has developed a bench level technology for extracting almost 60 – 70 % of the total soluble materials of banana in the form of its juice and the left over pulp can be dried into a fine powder.

Introduction

Banana is the largest produced and maximum consumed amongst the fruits cultivated in India. It is known as the 'common man's fruit'. It is highly nutritive and very delicious. India ranks first amongst the banana cultivating countries of the world with an annual production share of 25 % of the total harvest [1]. During the past two decades the large-scale cultivation of this fruit crop has undergone considerable changes. Banana is perhaps one of the major crops, which has accepted tissue culture as a mode of propagation especially in India. Shorter harvest times and enhanced yields have popularized the cultivation of this fruit crop with respect to the area of cultivation and production by tissue culture methods.

Banana when ripened is a soft and delicate fruit with a post-harvest shelf life of 5- 10 days [2]. This makes it prone to injury during transport. Further, release of ethylene during bulk storage makes the fruit ripen faster and the fruits generally rot before reaching its destination. Hence, it has always being considered a 'problem fruit' with respect to transportation. These reasons contribute to a local market glut, resultant price crash and subsequent disinterest among the farming community to cultivate it on a large scale. It is hence important to overcome this problem by generating an increased demand of this fruit crop. Exploring possibilities of converting banana into a cash crop by developing products of commercial interest is one way of solving this problem. In developed countries 40 – 50 % of the annual agricultural produce is converted into value added commodities. However, in India it is less than 2 % annually. Such a situation further necessitates the development of value added products.

Experimental

Fruit juices are the most common and demanding products made out of most of the

fruits. Generally, juices are extracted by simple crushing and / or grinding of fruits. However, in case of banana this process results in a sticky, lumpy mass with no juice. For banana juice production, any variety of banana like Basrai '10 Gy' (developed by tissue culture at BARC), Harichal or Cavendish can be used for extraction. A process has been developed to extract almost 60 – 70 % of the total soluble materials of banana as juice. This process has been patented [3]. Taste panel studies were conducted at Food Technology Division, FIPLY, BARC involving 30 panelists [4]. Products evaluated included banana juice [5], ripe banana powder [6] and products made from ripe banana powder such as banana biscuits, banana cake [7] and banana baby food [6].

Results

This technology is capable of extracting 600 – 700 ml juice from one kg of Basrai '10 Gy' variety; 400 – 500 ml from Harichal variety (Fig. 1), and does not involve addition of any external agents such as water and / or enzyme. The left over pulp retains all the aroma of banana. It can be dried and powdered to give ripe banana powder (Fig. 2). Depending on the variety of banana used, specific gravity of the juice varied from 1.08 – 1.12 and its pH was 4.4 – 4.7. The solid content was found to be 24 – 27 % and it contained between 16 – 28 % sugar. Taste panel studies showed general acceptability of non-conventional products developed from banana [4]. The dry powder can be used as an additive in confectioneries, milkshakes and baby foods. Other products developed from ripe banana powder in our laboratory include biscuits, cake and baby food (Fig.3).
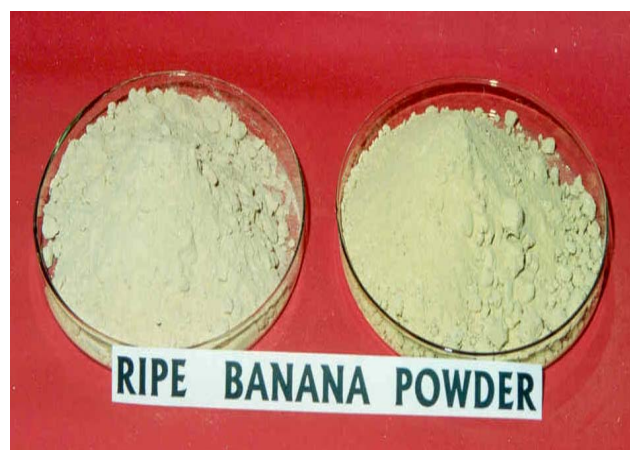

Fig.1

Fig. 2

Fig.3

Conclusion

Scale-up of this technology provides an excellent scope for the development of non-conventional products from banana. The extracted juice after a dilution is ready to serve as nectar and / or after carbonation as a drink. Banana juice also can be used for the production of banana wine by fermentation, which has a lot of commercial value.

Acknowledgements

The authors sincerely thank Mr. Pillay and Mr N. Surve of this Section for their continued excellent technical assistance throughout the course of the work.

References

1. http://r0.unctad.org/infocomm/anglais/banana/market.htm

2. Surendranathan, K. K., Ramaswamy, N. K., and Pendharkar, M. B., Indian J. Biotechnol., 2004, 3, 382-387.

3. Surendranathan, K. K., Ramaswamy, N. K., Chadha, S., and Mitra, R. K., Indian Patent, 2001, No. 189999.

4. Surendranathan, K. K., Ramaswamy, N. K., and Mitra, R. K., in Marwaha, S. S., and Arora, J. K., (eds.), "Biotechnological Strategies in Agro-Processing", Asiatech Publishers Inc., New Delhi, 2003, pp. 432-437.

5. Nair, A. S., B. Tech Project Report, UDCT-BARC, 2000.

6. Jayachandran, T., PG Dip. Diet. Appl. Nutr. Project Report, Nirmala Niketan-BARC, 2000.

7. Cardozo, C., PG Dip. Food Technol. Project Report, Gharda Institute-BARC, 1999.

This paper was given the First Prize for the Best Poster presented at the Seminar on "Regional Agro-Wealth: Opportunities for Value Addition and Exports" organised jointly by Maharashtra Academy of Sciences, Mumbai Chapter, and Bhabha Atomic Research Centre, Mumbai, held at BARC during Mumbai, March 28-29, 2003.

About the authors ...

Dr K. K. Surendranathan retired as Head, Bioprocess Development and Biochemical Applications Section, Nuclear Agriculture and Biotechnology Division (FIPLY), BARC, in May 2004 after a distinguished service of more than three decades. He was actively involved in research related to physiology and biochemistry of ripening of banana and post-harvest biotechnology of fruits. He has more than 60 publications in Journals of National and International repute.

Dr N. K. Ramaswamy currently leads the Section. His areas of research interests include stress physiology and biochemistry of crop plants with an emphasis on photosynthesis. He has three enzymes listed / classified in International Union of Biochemistry and has more than 100 publications in Journals of National and International repute.

Mr P. Radhakrishna joined BARC in 2001 and he working on production of amylase by utilization of agro-wastes.

Mr J. S. Nair joined BARC in 1999 as a DAE Research Fellow after completing his M. Sc. (Biotechnology) from University of Mumbai. His Ph. D. work is on the stress induced alterations of photosynthesis in crop plants.

FABRICATION OF MIXED URANIUM PLUTONIUM CARBIDE FUEL PELLETS FOR FBTR BY DIRECT PROCESSING OF SINTER REJECTS

U. Basak, P.S. Kutty, S. Mishra, S.K. Sharma, K.S. Bhatnagar, R.S. Mehrotra, S. Majumdar and H.S.Kamath
Nuclear Fuels Group
Bhabha Atomic Research Centre

Abstract

Fast Breeder Test Reactor at Kalpakkam uses plutonium rich mixed uranium-plutonium carbide as driver fuel in the form of sintered cylindrical pellets encapsulated in stainless steel cladding tube.The process flowsheet followed for the fabrication of sintered pellets is well established and involves preparation of carbide clinkers by vacuum carbothermic reduction of oxide- graphite mixture followed by processing of crushed clinkers into sintered pellets by powder metallurgical route. The sintered pellets rejected due to physical defects only are crushed and oxidized before further processing into fuel pellets.The present paper highlights a direct processing approach for the fabrication of fuel pellets from sinter rejects. This process does not involve vacuum carbothermic reduction and offers many advantages including substantial reduction in radiation exposure to personnel.

Introduction

Plutonium rich mixed uranium-plutonium carbide fuel of two compositions namely (30%UC-70%PuC) as Mark I and (45%UC-55%PuC) as Mark II are being used as driver fuel in the Fast Breeder Test Reactor (FBTR) at Kalpakkam. Fabrication of these fuel pellets involves the following two major steps :

(i) preparation of mixed uranium-plutonium carbide clinkers by vacuum carbothermic reduction of oxide – graphite mixture

(ii) crushing of clinkers and milling of powder followed by pre – compaction, granulation, final compaction and high temperature sintering in argon – 8% hydrogen gas mixture

In order to fabricate fuel pellets suitable for use in FBTR, process control parameters are required to be followed strictly for maintaining chemical quality of fuel pellets particularly the specifications on carbon, oxygen, nitrogen, Pu/U, M_2C_3 (M = Pu + U) and impurities. Finally, powder batches qualifying the chemical specifications are further processed for the fabrication of fuel pellets. The flowsheet already developed[1,2] and followed for the fabrication of mixed carbide fuel pellets incorporating process control parameters is shown in Fig. 1. The accepted sintered pellets are used for encapsulation and the pellets rejected due to off - dimensions and physical defects such as cracks, chips, surface defects etc. are normally crushed and oxidized before further processing into fuel pellets. By this re-cycling approach, rejects have to undergo the entire process steps (Fig.1) from mixing of oxide – graphite mixture to high temperature sintering once again and this leads to decrease in production throughputs and increase in radiation exposure to personnel.
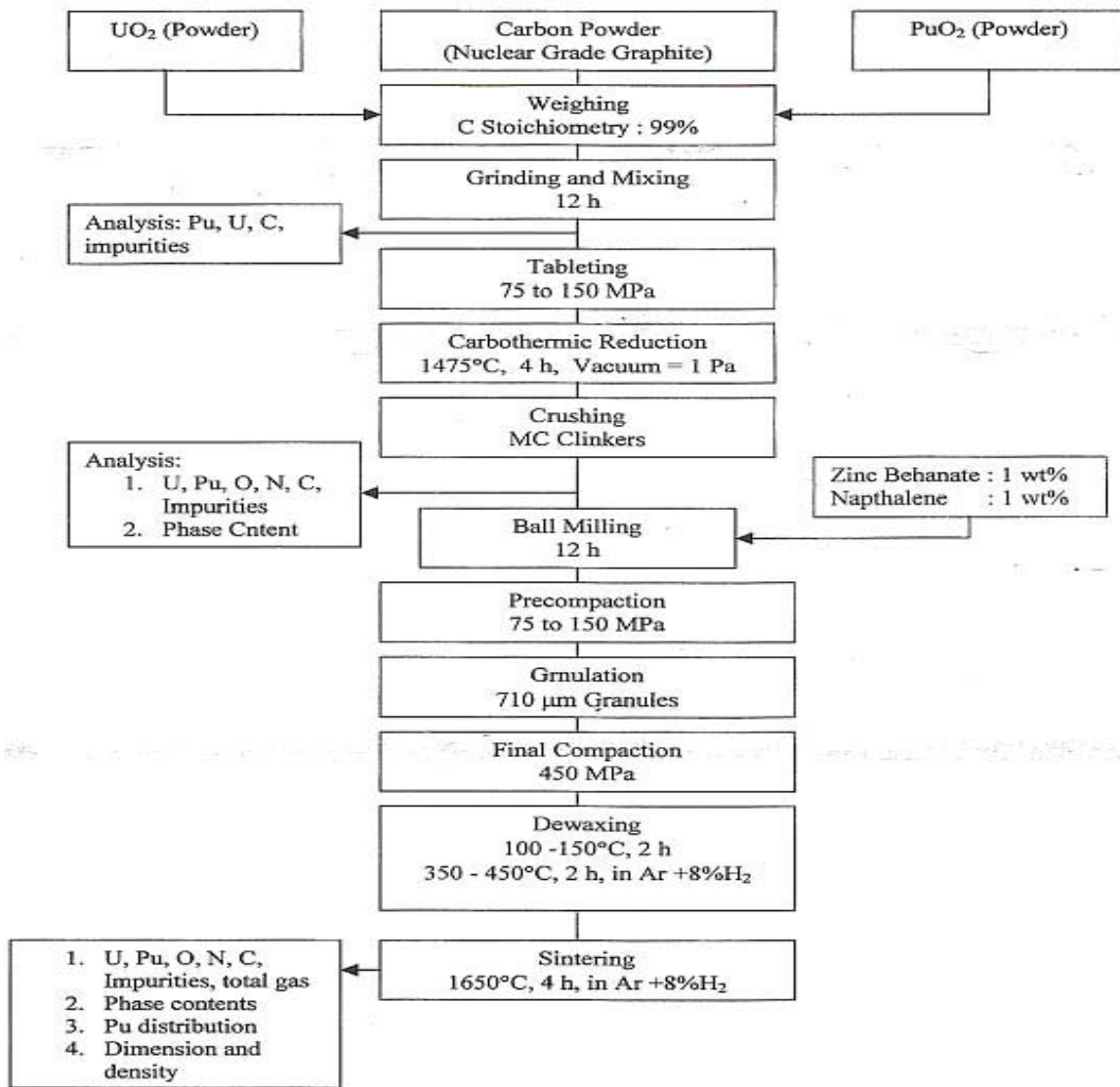
Fig.1 Flow sheet for fabrication of (U,Pu)C pellets for FBTR

Direct processing of chemically accepted but physically rejected sintered pellets has the following advantages:

➢ number of process steps is minimized .
➢ mixing & milling of oxide – graphite mixtures, tabletting and vacuum carbothermic   reduction are not required leading to almost 30% savings in time & energy.
➢ loss of plutonium is minimized
➢ production throughputs is increased

➢ radiation exposure to personnel is reduced

Experimental

The rejected sintered pellets were directly crushed into powders and milled for 10 hours in planetary ball mill.The apparent density of powders was measured by Hall's Flow meter after every two hours of milling. Milled powders were divided into three batches (size: 200gms) and each batch was mixed with binder & lubricant for additional one hour in the following combinations :

Batch A : 1% zinc behanate and 1%
   naphthalene

Batch B : 1.5% zinc behanate and 0.5%
   naphthalene

Batch C : 2% zinc behanate

These powder batches were subjected to pre – compaction at 5 tsi followed by final compaction at ~ 20 tsi. The green pellets were dewaxed at 500° C for two hours with intermittent soak at different temperatures for adequate time in order to ensure complete removal of binder / lubricant. The dewaxed pellets were sintered at 1620ºC for 4 hours in argon – 8% hydrogen atmosphere, maintaining the heating and cooling rates at ~5ºC / min.

Results & Discussions

With progressive milling of powders , the apparent density decreased from 5.97g/cm^3 after two hours to 4.26g/cm^3 after ten hours and the specific surface area measured for the 10 hour milled powder by BET method was 0.32 m^2/g. The characteristics of pellets in terms of linear mass (mass/height), green densities and sintered densities made from different batches are shown in table 1. Densities of sintered pellets obtained from powders mixed with 1% zinc behanate and 1% naphthalene (Batch A) were found to satisfy FBTR fuel pellet specifications. Hence, a large batch (size : 600g) was processed under Batch A condition for the fabrication of sintered pellets for FBTR. Analysis of the critical parameters of sintered pellets before and after re-cycling is shown in table 2. The pellets made from direct processing and satisfying the fuel pellet specifications were used for fuel pin fabrication.

Table 1: Characteristics of (45%UC-55%PuC) fuel pellets fabricated from sinter rejects by direct processing

Batches	Green pellet linear mass(m/h),g/cm	Green density, %T.D	Sintered pellet Linearmass(m/h),g/cm	Sintered density, %T.D
A	1.49	65.90	1.58	87.4
B	1.56	69.03	1.69	93.5
C	1.55	68.83	1.68	94.4

Table 2: Analysis of (45%UC-55%PuC) sintered pellets

Chemical analysis	Before re-cycling (sinter rejects)		After direct processing		FBTR fuel pellet specification
Plutonium (wt%)	(i)	55.41	(i)	55.37	Pu + U = 95 wt% max.
	(ii)	54.82	(ii)	54.74	
Uranium (wt%)	(i)	39.31	(i)	39.26	
	(ii)	39.59	(ii)	39.33	
Carbon (wt%)	(i)	4.92	(i)	4.68	≤ 5.03
	(ii)	4.68	(ii)	4.65	
Oxygen (ppm)	(i)	4251	(i)	4281	≤ 5000
	(ii)	4585	(ii)	4921	
Nitrogen (ppm)	(i)	693	(i)	1123	≤ 2000
	(ii)	1196	(ii)	1603	
M_2C_3 (wt%) M = U + Pu (by XRD)	(i)	11.40	(i)	11.40	5 – 20%
	(ii)	8.0	(ii)	12.40	
Total impurities(ppm)	(i)	668	(i)	849	≤ 3000
	(ii)	707	(ii)	852	

Conclusions

1. Milling of crushed sintered pellets for ten hours resulted in powder characteristics similar to that obtained from crushed clinkers prepared by vacuum carbothermic reduction of oxide – graphite mixtures .

2. 1% zinc behanate and 1% naphthalene as binder- lubricant mixture was found to be optimum for obtaining pellets meeting FBTR fuel pellet specification.

3. Direct processing of sinter rejects improves production throughputs, reduces radiation exposure to personnel and minimizes plutonium losses.

4. Several fuel pins made from pellets fabricated by direct processing of sinter rejects were delivered to IGCAR for use in FBTR.

References

1. Development and fabrication of 70% PuC - 30% UC fuel for the Fast Breeder Test Reactor in India, Nuclear Technology, 72(1), 1986, p. 59-69.C.Ganguly, P.V.Hegde, G.C.Jain, U.Basak, R.S.Mehrotra, S.Majumdar and P.R.Roy.

2. Process control in mixed carbide fuel pellet fabrication for FBTR , Proc.Fast Breeder Reactor Fuel Cycle, RRC, Feb. 10 – 11, 1986. G.C.Jain, P.V.Hegde, U.Basak, S.Majumdar and C.Ganguly.

This paper received the 2ⁿᵈ Best Paper award in 14ᵗʰ Annual Conference of Indian Nuclear Society, INSAC 2003, held at IGCAR during December 17-19, 2003

About the authors ...

Mr U. Basak, *M.Sc.(Tech), Metallurgy, is a graduate from 21ˢᵗ batch of Training School,BARC. His expertise includes development of the processes for the fabrication of ceramic nuclear fuels for thermal and fast reactors.*

Mr P.S.Kutty, *AMIE.(Metallurgy), joined RMD, BARC, in the year 1976.He is involved in the fabrication of mixed carbide fuel for FBTR.*

Mr S. Mishra, *M.Tech.(Metallurgy) is a graduate from 34ᵗʰ batch of BARC Training School. He is involved in fabrication of mixed carbide fuel for FBTR and development of thorium-based fuels for thermal reactors.*

Mr S.K.Sharma, B.Sc, joined BARC in year 1981. He is working for fuel pellets and pin fabrication for FBTR.

Mr K.S. Bhatnagar, B.Sc, joined BARC in year 1981. He is working for fuel pellets and pin fabrication of FBTR.

Dr.R.S. Mehrotra is a graduate from 13th batch of Training School. His expertise is in the field of fast reactor fuel and fuel pin fabrication. He is presently Head of Fast Reactor Fuel Section, Radiometallurgy Division, BARC.

Mr S. Majumdar, B.E., Metallurgy, is a graduate from 11th batch of BARC Training School. His expertise is in the field of fabrication and characterization of nuclear fuels, both for thermal and fast reactors. He is currently Head of Radiometallurgy Division, BARC.

Mr H.S. Kamath, B.E., Metallurgy is a graduate from 13th batch of Training School, BARC. His expertise is in the area of nuclear fuel cycle activities. He is presently Director of Nuclear Fuels Group, BARC.

INELASTIC NEUTRON SCATTERING AND LATTICE DYNAMICS OF NOVEL COMPOUNDS

R. Mittal and S. L. Chaplot
Solid State Physics Division
Bhabha Atomic Research Centre

Abstract

Using a combination of lattice dynamical calculations and inelastic neutron scattering experiments, we have studied the phonon properties of a variety of solids. The materials studied find a wide range of applications, which include the negative thermal expansion materials and other technologically important samples, and also geophysically relevant minerals. Often we have made it possible to provide the predictions of the thermal expansion and the equation of state when experimental data are not yet available. It has been shown that a proper description of negative thermal expansion may require consideration of both the acoustic and optic phonon modes in the entire Brillouin zone.

Introduction

A crystal is described as a perfect periodic three-dimensional array of atoms. However, the atoms are not static at their lattice sites but vibrate about their mean positions with energies governed by the temperature of the solid. The collective motions of atoms in solids form traveling waves (called lattice vibrations), which are quantized in terms of "phonons". The study of lattice vibrations is of considerable interest because several physical properties of crystals like their specific heat, thermal expansion, phase transitions are related to the vibrations of atoms in solids [1-3].

The experimental studies of lattice vibrations are carried out using techniques like Raman spectroscopy, infrared absorption (IR), inelastic neutron scattering, inelastic X-ray scattering, etc. Unlike Raman and infrared studies which probe only the long wavelength excitations in one-phonon scattering, inelastic neutron and X-ray scattering can directly probe the phonons in the entire Brillouin zone. While inelastic neutron scattering is widely used for such measurements, inelastic X-ray scattering has also been recently used at intense synchrotrons sources for the study of phonons in a few materials.

Experimental studies at high pressures and temperatures are often limited and accurate models for the compounds are of utmost importance. A major goal of research therefore has been theoretical predictions of the thermodynamic properties. The success of the models in predicting thermodynamic properties depends crucially on their ability to explain a variety of microscopic and macroscopic dynamical properties. These include an understanding of the crystal structure, elastic constants, equation of state, phonon frequencies, dispersion relations, density of states and thermodynamic quantities like the specific heat and thermal expansion. The experimental neutron and long wavelength optical data are used to test and validate models of interatomic potentials, which in turn have been used to predict thermodynamic properties at high pressures and temperatures.

We have developed models of interatomic potentials for several novel compounds which allow to calculate the structural and dynamical properties as a function of pressure and

temperature. In order to validate the interatomic potentials, we have carried out inelastic neutron scattering experiments on polycrystalline and single crystal samples at different facilities namely, Dhruva reactor, Trombay (India), ILL (France), ISIS (UK) and ANL (USA).

Sections below give brief information about the experimental technique and the lattice dynamics calculations respectively, while the results and discussion, and conclusions are presented later.

Experimental

Inelastic-neutron-scattering (INS) experiments [3] may be performed using both single crystals and polycrystalline samples, which provide complementary information. The single crystals may be used to obtain the details of the phonon dispersion relation (PDR), namely the relation between the phonon energies and their wavevectors, for selected values of the wavevectors. On the other hand, the polycrystalline samples provide the phonon density of state (PDOS) integrated over all wave vectors in the Brillouin zone. The inelastic-neutron-scattering experiments require much larger-sized samples (single crystals of the order of 1 cm^3 and powder samples of about 10 cm^3 upwards) than those used in optical spectroscopies. Measurements of the phonon dispersion relations and density of states can in principle be carried out using both reactors as well as spallation sources. However, thermal neutrons (E ~ 25 meV) from a nuclear reactor are best suited for the measurements of the acoustic and low-frequency optic modes in a single crystal. On the other hand, the high energies of neutrons from a spallation source enable measurements over the entire spectral range and are best exploited for the measurements of the phonon density of states.

Lattice Dynamical Calculations

Lattice dynamical calculations [2] of the vibrational properties may be carried out using either a quantum-mechanical ab-initio approach

or an atomistc approach involving semiempirical interatomic potentials. However, due to structural complexity of the compounds which we have studied, detailed calculations are carried out using semiempirical models. The interatomic potentials consist of Coulombic and short-ranged Born-Mayer type interactions. The parameters of the potentials have been evaluated using the structural and dynamical equilibrium conditions as well as other known experimental data. The optimized parameters are used for lattice dynamics studies of the system.

Results and Discussion

Negative thermal expansion compounds: ZrW_2O_8, HfW_2O_8 and $ZrMo_2O_8$

The compounds ZrW_2O_8, HfW_2O_8 and $ZrMo_2O_8$ are of considerable interest [4] due to their large isotropic negative thermal expansion (NTE) in their cubic phase over a wide range of temperatures up to 1443 K, 1050 K and 600 K, respectively. This remarkable feature makes these compounds potential constituents in composites to adjust thermal expansion to a desired value. Thermal expansion in insulating materials is related to the anharmonicity of lattice vibrations. We have carried out lattice dynamical calculations for these compounds using a transferable interatomic potential [4-8]. The phonon frequencies as a function of wave vectors in the entire Brillouin zone and its volume dependence in quasiharmonic approximation are calculated. The calculations predicted that large softening of the phonon spectrum involving librational and translational modes below 10 meV would be responsible for NTE in these compounds. In order to check our prediction we have carried out high-pressure inelastic neutron scattering experiments [8-10] at several pressures up to 2.5 kbar on polycrystalline samples of ZrW_2O_8 and $ZrMo_2O_8$ using IN6 spectrometer at ILL, France. In case of ZrW_2O_8 at 1.7 kbar, phonon softening of about 0.1-0.2 meV is observed (Fig. 1) for
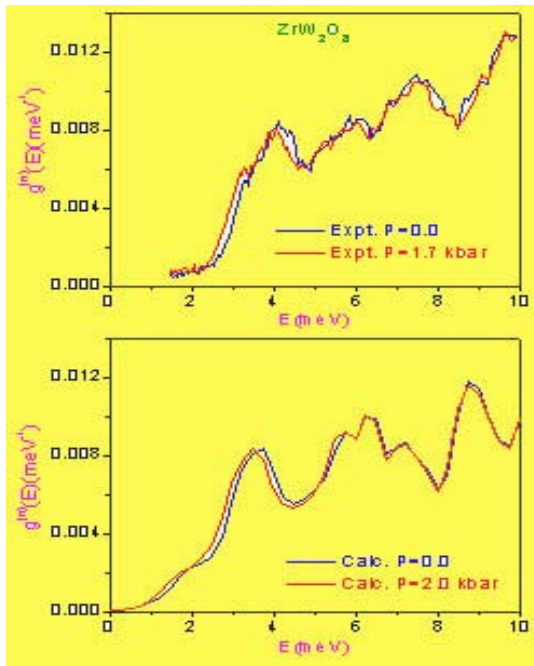
Fig. 1 The comparison between the calculated and experimental inelastic neutron scattering spectra for cubic ZrW_2O_8. The experimental data for cubic ZrW_2O_8 is at 160 K and at pressures of 0.0 and 1.7 kbar. The experimental spectra at P=0.3 kbar and 1.0 kbar fall in between those of P=0 and 1.7 kbar, and have not been shown here for the clarity (after Ref. [9]).

phonons below 8 meV. Similar shift is observed for $ZrMo_2O_8$ at 2.5 kbar. The Grüneisen parameters of phonon modes have been determined as a function of their energy. The experiments validate our lattice dynamical calculations (Fig. 1). In order to check the quality of interatomic potential model the phonon density of states data has also been recently obtained upto 160 meV for HfW_2O_8 using time of flight technique at IPNS (USA) in collaborative experiments [7].

Silicate mineral zircon, $ZrSiO_4$

Zircon, $ZrSiO_4$ is an important host silicate mineral for radioactive elements uranium and thorium in the earth's crust. Since it is a natural host for the radioactive elements in the crust, it is a potential candidate for nuclear waste storage. High pressure and temperature stability of zircon is therefore of considerable interest.
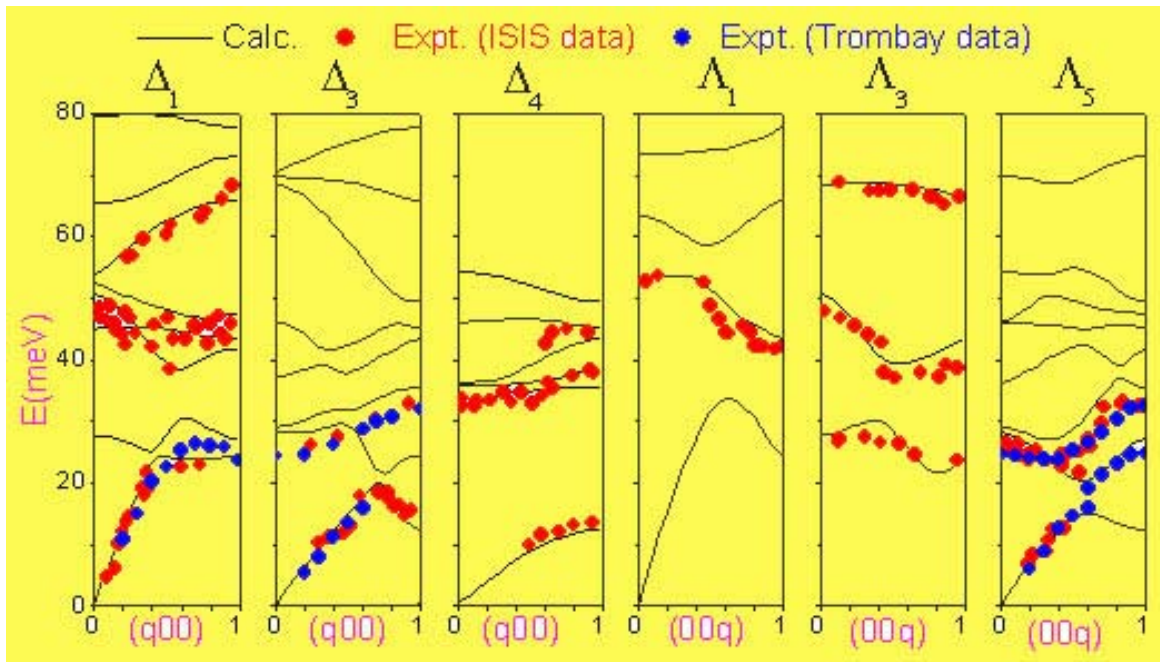

Fig. 2 The experimental phonon data (symbols) in $ZrSiO_4$ along with the lattice-dynamical calculations (lines). The red and blue circles give the phonon peaks identified in the experiments at the ISIS spallation neutron source at U. K. and at Dhruva reactor, Trombay respectively (after Ref. [11, 12]).

The phonon dispersion relation has been measured (Fig. 2) in zircon (ZrSiO₄) from neutron experiments at Dhruva reactor, Trombay, at low energies upto 32 meV [11]. The measurements at high energies require good resolution and high intensity of the neutron beam. We have further extended the measurements upto 70 meV (Fig. 2) using the time of flight technique [12] at ISIS, UK. These extensive phonon measurements upto 70 meV provide a rare example of such studies carried out using a pulse neutron sources on any material. Such extensive measurements have been performed on only a few mineral systems even using a continuous reactor source. A lattice dynamical model was used to plan the experiments and analyze the data, as well as to calculate the elastic constants, long-wavelength phonon frequencies and thermal expansion [13]. The calculations are in good agreement with the experimental data.

Quartz structure compound FePO₄

The quartz structure compound FePO₄ is of interest to understand the nature of bonding in tetrahedral coordinated phosphates. Detailed lattice dynamical studies [14] involving experimental inelastic neutron scattering measurements and theoretical shell model calculations of the vibrational and thermodynamic properties have been undertaken for FePO₄. The calculations are in good agreement with numerous experimental data including phonon density of states measurements (carried out in our collaboration) and thermal expansion for FePO₄. The calculated pressure variation of phonon frequencies shows that a zone boundary mode at (1/3,1/3,0) becomes soft at 4 GPa, which may be associated with the mechanical instability of the quartz structure of FePO₄ at high pressure.

Mineral garnets

Garnets are rock-forming minerals and are important constituents of the upper crust, upper mantle and the transition zone. Garnets are also hosts for aluminium in the upper mantle.
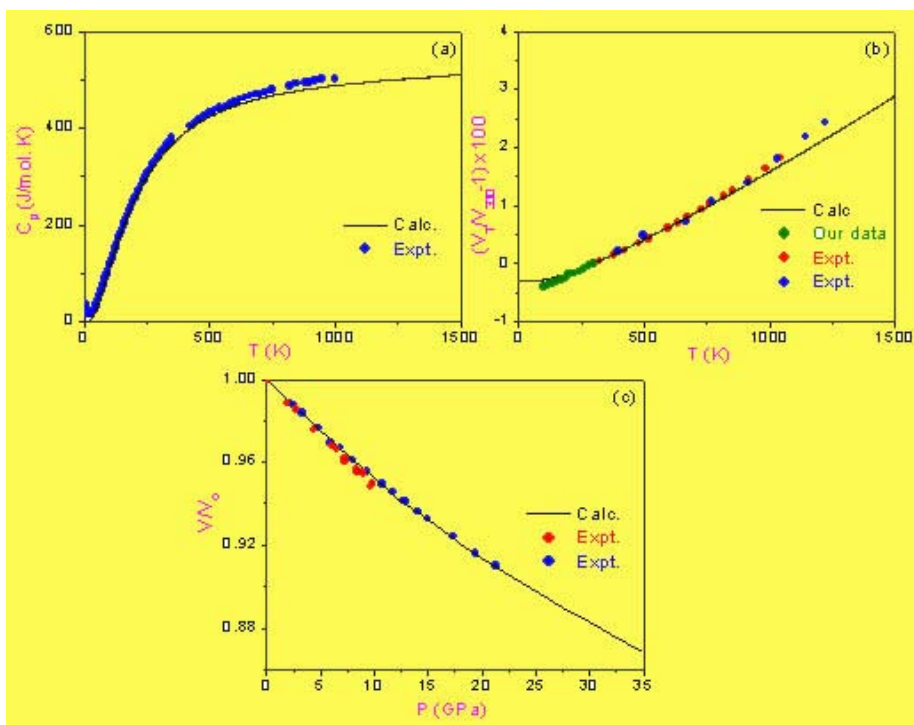
Fig. 3 Comparison of the calculated (full line) (a) specific heat, (b) thermal expansion and (c) equation of state of the garnet mineral almandine Fe₃Al₂Si₃O₁₂ with available experimental data (symbols). The references for the experimental data are available in Ref. [16] (after Ref. [16]).

The lattice dynamical calculations of various microscopic and macroscopic phonon properties of the aluminosilicate garnets almandine, pyrope, grossular and spessartine (given by $M_3Al_2Si_3O_{12}$, where M=Fe, Mg, Ca or Mn,

respectively) are carried out using a transferable interatomic potential [13, 15, 16]. These studies are fairly involved as hese garnets have complex crystal structures (cubic, space group $Ia\bar{3}d$) with 80 atoms/primitive cell. The calculated neutron-weighted density of states are in overall good agreement with measurements (carried out in our collaboration) for almandine and data available for other garnet minerals from the literature. Due to their structural similarities, the phonon spectra of these garnets are overall similar. Subtle differences are however observed in their phonon densities of states arising from the vibrational contributions from the Fe, Mg, Ca and Mn atoms, respectively in almandine, pyrope, grossular and spessartine. The calculations have enabled a microscopic interpretation of the available experimental data and the transferable potentials have been extremely useful in deriving the various thermodynamic properties (Fig. 3) at high pressure and temperatures.

X-ray image storage materials MFX (M=Ba, Sr, Pb; X=Cl, Br, I), and intermetallics Zr₂M (M=Ni, Fe)

Neutron inelastic scattering experiments to determine the phonon density of states, and lattice dynamical calculations of thermodynamic properties were successfully carried out [17,18] for X-ray image storage materials MFX (M=Ba, Sr, Pb; X=Cl, Br, I) using a transferable interatomic potential based on a shell model. The model is validated by the inelastic neutron scattering measurements of phonon density of states for BaFCl (Fig. 4) carried out using the triple axis spectrometer at Trombay. The model is then transferred to BaFBr, BaFI, SrFCl, SrFBr, PbFCl and PbFBr by changing only the potential parameter associated with the radii of Sr, Pb, Br and I atoms. The differences in the calculated phonon spectra in these compounds arise from both mass and potential variations, and are shown to manifest in the thermodynamic properties. We have made it possible to provide

predictions on the thermal expansion and the equation of state in these compounds wherever experimental data are not yet available.
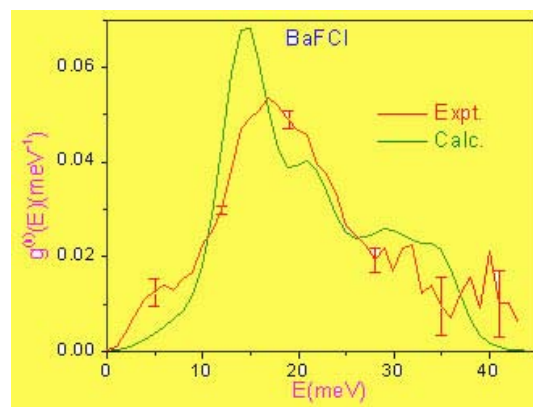
Fig. 4 The experimental and calculated neutron-weighted phonon density of states for BaFCl. The multi-phonon contribution has been subtracted from the experimental data to obtain the experimental one-phonon spectrum. The calculated spectra have been convoluted with a Gaussian of FWHM of 4 meV in order to correspond to the energy resolution in the experiment (after Ref. [17]).

Intermetallic compounds Zr₂Ni and Zr₂Fe show superconductivity at 1-2 K. Lattice dynamical calculations and measurements of the phonon density of states were carried out [19-21] in these materials in order to understand the electron-phonon interaction.

Conclusions

A combination of lattice dynamics calculations and inelastic neutron scattering measurements have been successfully used to study the phonon properties and their manifestations in thermodynamic quantities like the specific heat, thermal expansion and equation of state. The experiments validate the models and the models in turn have been fruitfully used to calculate the phonon spectra and various thermodynamic properties at high pressures and temperatures. The calculations have been very useful in the planning, execution and analysis of the experiments and have enabled microscopic

interpretations of the observed data. These studies have also been exploited to study the anomalous properties like large negative thermal expansion in various compounds.

References

1. S. L. Chaplot, N. Choudhury, S. Ghose, M. N. Rao, R. Mittal, P. Goel, European Journal of Mineralogy 14, 291 (2002).

2. G. Venkataraman, L. Feldkamp and V. C. Sahni, *Dynamics of perfect crystals*, MIT Press, Cambridge (1975).

3. P. Bruesch, *Phonons: Theory and experiments II*, Springer-Verlag, Berlin, Heidelberg, New York, (1986).

4. R. Mittal and S. L. Chaplot, Phys. Rev. B 60, 7234 (1999) and references therein.

5. R. Mittal and S. L. Chaplot, Solid State Communication 115, 319 (2000).

6. S. L. Chaplot and R. Mittal, Phys. Rev. Lett. 86, 4976 (2001).

7. R. Mittal, S. L. Chaplot, A. I. Kolesnikov, C. -K. Loong and T. A. Mary, Phys. Rev. B 68, 54302 (2003).

8. R. Mittal, S. L. Chaplot, H. Schober, T. A. Mary and A. P. Wilkinson, Acta Cryst. A 58, C334 (2002).

9. R. Mittal, S. L. Chaplot, H. Schober and T. A. Mary, Phys. Rev. Lett. 86, 4692 (2001).

10. R. Mittal, S. L. Chaplot, H. Schober and T. A. Mary, Neutron News 13, 36 (2002).

11. R. Mittal, S. L. Chaplot, Mala N. Rao, N. Choudhury and R. Parthasarathy Physica B 241, 403 (1998).

12. R. Mittal, S. L. Chaplot, R. Parthasarathy, M. J. Bull and M. J. Harris, Phys. Rev. B 62, 12089 (2000).

13. S. L. Chaplot, R. Mittal, E. Busetto and A. Lausi, Phys. Rev. B 66, 64302 (2002).

14. R. Mittal, S. L. Chaplot, A. I. Kolesnikov, C. -K. Loong, O. D. Jayakumar and S. K. Kulshreshtha, Phys. Rev. B 66, 174304 (2002).

15. R. Mittal, S. L. Chaplot, N. Choudhury and C.-K. Loong, Phys. Rev. B 61, 3983 (2000).

16. R. Mittal, S. L. Chaplot and N. Choudhury, Phys. Rev. B 64, 94302 (2001).

17. R. Mittal, S. L. Chaplot, A. Sen, S. N. Achary and A. K. Tyagi, Phys. Rev. B 67, 134303 (2003).

18. R. Mittal, S. L. Chaplot, A. Sen, S. N. Achary and A. K. Tyagi, Appl. Phys. A 74[S], S1109 (2002).

19. R. Mittal, S. L. Chaplot, K. R. Rao and P. Raj, Physica B 222, 233 (1996).

20. H. G. Salunke, R. Mittal, G. P. Das and S. L. Chaplot, J. Phys Condensed Matter 9, 10137 (1997).

21. R. Mittal, S. L. Chaplot, H. G. Salunke, G. P. Das, P. Raj, A. Sathyamoorthy, K. Shashikala and S. K. Dhar, Physica C 320, 239 (1999).

This paper received the second prize in XXI Colloquium for Young Physicists, 2003 of the Indian Physical Society held at Saha Institute of Nuclear Physics, Kolkata, during August 22-23, 2003.   The thesis presentation by Dr Mittal including this work was selected for the Indian Physics Association "Best Thesis" award in the DAE-Solid State Physics Symposium held at Jiwaji University, Gwalior, during December 26-30, 2003.

About the authors…

Dr R. Mittal *joined the 34ᵗʰ batch of BARC Training School after completing M.Sc. (Physics) from H. N. B. Garhwal University. Subsequently he joined the Solid State Physics Division, BARC, in 1991. Since then, he is involved in inelastic neutron scattering experiments and lattice dynamics computations.*

Dr S. L. Chaplot *is from the 18ᵗʰ batch of BARC Training School. He works in the Solid State Physics Division in the areas of neutron scattering, lattice dynamics and computer simulations.*

FEASIBILITY STUDIES ON QUANTIFICATION OF SPECTRALLY INTERFERED SULPHUR (S) IN THORIA (ThO$_2$) MATRIX FOLLOWING CHARGE DISTRIBUTION BY SPARK SOURCE MASS SPECTROMETRY (SSMS)

V.L. Sant, S.K. Mishra and S.K. Aggarawal
Fuel Chemistry Division
Bhabha Atomic Research Centre

Introduction

Nuclear grade ThO$_2$ is presently being used as a blanket material in fast breeder reactor (FBR) for producing fissile ^{233}U and for the purpose of flux flattening of pressurised heavy water reactors (PHWRs)[1]. ThO$_2$-PuO$_2$ ($\leq$ 4 %) and ThO$_2$-^{233}UO$_2$ ($\leq$ 4 %) are proposed fuels for India's third generation advanced heavy water reactor (AHWR)[2]. Any processed thoria sample has to pass stringent specification limit (1.5ppm$_w$ boron equivalent) for overall impurity as a part of chemical quality control (CQC) exercise in the nuclear technology. Sulphur is one of the critical non-metallic trace elements, which has been individually specified. Presence of sulphur amounts in excess of specified level ($\geq$ 50 ppm$_w$) are known to cause the shattering of ThO$_2$ pellets during the sintering process[2] Determination of sulphur content is thus significant and forms an essential part of chemical characterization of ThO$_2$ [4].ThO$_2$ being refractory in nature, different instrumental, spectroscopic methods reported in the literature for sulphur determination do not conform to their applicability at ppm level in ThO$_2$ matrix. SSMS with photo plate detection was, therefore, used for the purpose.

SSMS was chosen mainly because of its capability of providing trace elemental concentration at lowest detection limits (sub-ppm) at very high exposures without resorting to their pre-concentration or encumbersome ion exchange separation from the matrix.

Determination of trace constituent sulphur, particularly in nuclear grade ThO$_2$, by SSMS is a challenging task for different reasons. Firstly, Th being mono-isotopic, gets saturated on photo plate at very high exposures. Secondly, higher amounts of oxygen and carbon (from supporting material graphite) present in the sample make determination of sulphur difficult. Molecular oxygen species ^{16}O^{16}O, ^{16}O^{17}O, ^{17}O^{17}O, ^{18}O^{16}O, ^{18}O^{18}O & ^{12}C3 interfere with ^{32}S, ^{33}S, ^{34}S and ^{36}S at mass numbers 32, 33, 34 and 36 respectively. Besides, there is instrumental limitation in resolving these interfering species due to the inadequate resolution (R ~ 1000). Thirdly, unlike metallic constituents, charge distribution of non-metallic S in the spark plasma of refractory matrices is not well studied.

In the present work, a new approach based on a correlation between experimentally measured (S^{n+}/Th$^+$) intensity ratios and the ionization energy (IE) of the respective charged state 'n' of S has been investigated [4] to compute the intensity ratio due to (S$^+$/ Th$^+$) at IE = 10.36 eV for effecting oxygen molecular ion interference correction. Extrapolation of the linear curve obtained further at IE=0 provides the estimate of

the fraction (S^0/Th^+) of neutral S atoms in the ion beam of thoria samples. This fraction of atomic (S^0) species along with those fractions in different charged states S^{1+}, S^{2+}, $S3+$ and S^{4+} together constitutes total concentration of trace element S in the ion beam of sample without requiring the use of calibration factor RSC (Relative Sensitivity Coefficient), generally deduced from the analysis of the matrix (Th) matched impurity (S) standard, for the quantification purpose.

Experimental

ThO_2 sample was mixed with high purity graphite powder (1:1 w/w) for the preparation of cylindrical electrodes. Electrodes were sparked in JEOL-JMS-01BM2 SSMS and mass spectra were recorded on Ilford Q_2 photo-plates. The range of recorded exposures was between 1×10^{-13} and 1×10^{-7} coulombs. Exposed photo plates were developed and evaluated.

Results and Discussion

Table 1 shows the Charge Distribution (CD) data obtained for ^{33}S and ^{34}S in the given thoria sample by photo-plate evaluation method due to Franzen et.al. al. [5]. Intensities of the ionic species of charged states up to 4+ could be measured. Exposure values corresponding to zero Seidel function (50% transmission) for matrix thorium and charged states 4+, 3+ & 2+ of ^{33}S & ^{34}S were obtained from their transmission curves are given in rows 2, 4, 6 & 7 respectively whereas corresponding intensity ratios S^{n+}/Th^+ are seen in rows 1, 3 & 5. Intensity ratios were calculated by taking reciprocal of the exposures (intensity α 1/exposure) and applying appropriate corrections for the charged states, line width and mass response of the photo plate emulsion same were converted in to the atom ratios. CD of ^{32}S was not considered because of an isobaric interference from major $^{16}O^{n+}$ at the charged states $^{32}S^{2+}$ & $32S^{4+}$ Moreover for $^{36}S^+$, non-detection due to least abundance or an overlapping of $^{36}S^{n+}$ (n=3, 2 & 4) species with $^{12}C^+$, ^{18}O and $^{18}O^{2+}$ due to inadequate resolution, CD for ^{36}S also couldn't be considered.

Table 1: Charge Distribution of Sulphur (S) in ThO$_2$

Isotope Exposure	^{33}S	^{34}S	{ I.E. }^{a}
Th^+	1.60361E-12		
S^{2+}	3.1917E-9	5.7299E-10	{ 23.4 eV}
Atom Ratio (S^{2+}/Th^+)	2.5122E-4	1.4007E-3	Mean + σ 8.2594E-4 ±5.747E-4
S^{3+}	2.9799E-9	1.9781E-8	{ 35.0 eV}
Atom Ratio (S^{3+}/Th^+)	1.7938E-4	2.7023E-5	*Mean + σ* 1.0320E-4 ±7.6179E-5
S^{4+}	8.2307E-7	1.1680E-7	{ 47.3 eV}
Atom Ratio (S^{4+}/Th^+)	1.2409E-6	3.4324E-6	Mean + σ 2.3367E-6 ±1.0957E-6

[a]Ref: CRC Hand Book of Chemistry & Physics by D.R.Lide (4-29, 1999-2002)
Atom Ratios corrected for charge distribution, emulsion sensitivity & line width.

CDs for ^{32}S & ^{36}S not considered for isobaric interference due to $^{16}O^{n+}$, $^{18}O^{n+}$ & $12C_n$.

Intensity ratios were calculated by taking reciprocal of the exposures (intensity α 1/exposure) and applying appropriate corrections for the charged states, line width and mass response of the photo plate emulsion same were converted in to the atom ratios. CD of ^{32}S was not considered because of an isobaric interference from major $^{16}O^{n+}$ at the charged states $^{32}S^{2+}$ & $32S^{4+}$ Moreover for $^{36}S^{+}$, non-detection due to least abundance or an overlapping of $^{36}S^{n+}$ (n=3, 2 & 4) species with $^{12}C^{+}$, ^{18}O and $^{18}O^{2+}$ due to inadequate resolution, CD for ^{36}S also couldn't be considered.

In Fig. 1, plot of abundance of $^{34}S^{n+}$ wrt Th^{+} against the IE of the respective charged state 'n' of S is displayed. Values for neutral atom fraction (S^{0}/Th^{+}) and fraction for singly charged atoms (S^{+}/Th^{+}) w.r.t Th are computed from the extrapolation of the linear plot obtained at X=0 & 10.36 respectively and are added to atom fractions of higher charged states 2+, 3+ & 4+ to
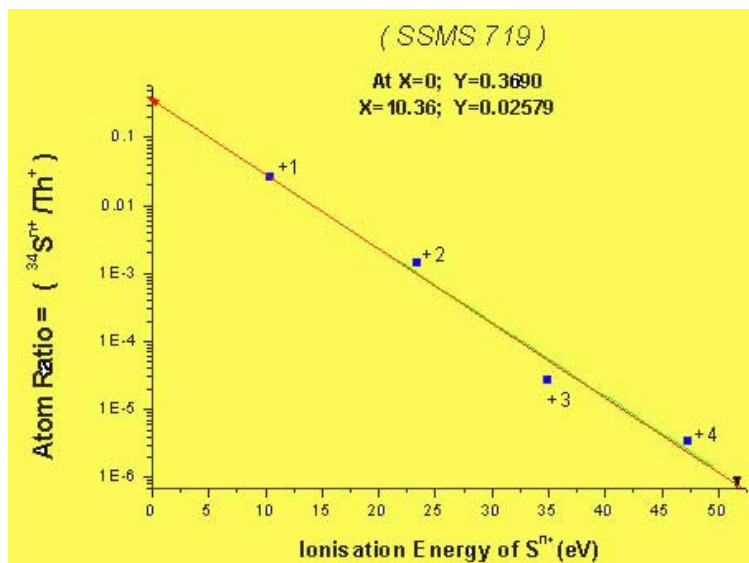
Fig. 1 Correlation of $(^{34}S^{n+}/Th^{+})$ vs. I.E. of S^{n+}

get total concentration of S in the sample. Concentration of S wrt $^{33}S^{n+}$ & $^{34}S^{n+}$ as internal standards was also determined on the basis of their average CDs considered simultaneously in the same manner.

Results obtained for the trace element S in nuclear grade ThO_2 by SSMS are summarized in Table 2 and are compared (+5%) with another independent technique Energy Dispersive X-ray Fluorescence (ED-XRF)[6] when ThO_2 was analysed by the same technique.

Table 2 : Concentration of Sulphur (PPM$_w$) in ThO$_2$ Matrix

Ref. Int. Std.	Analytical Technique			Mean
	SSMS		ED-XRF[6]	
$^{34}S^{n+}$	41.26			
$^{33}S^{n+}$ & $^{34}S^{n+}$	52.58	46.92±5.66 (12 %)	55.90±1.30 (2.3 %)	51.41 ± 5.81 (11%)

Conclusion

Correlation of abundance of sulphur atoms in different charged states S^{2+}, S^{3+} & S^{4+} wrt Th^+ versus respective IEs enabled proper accounting of interfering oxygen present in the sample and provided us with the oxygen interference free concentration (~51 ppm_w) for trace constituent S in ThO_2.

Acknowledgements

Authors are indebted to Dr V.D.Puranik, Head, Environmental Assessment Division for allowing the use of the ED-XRF. Authors are grateful to Mr H.S.Kamath, Director Nuclear Fuels Group, and Dr.V.Venugopal, Head, Fuel Chemistry Division, for their encouragement and interest in this work.

References

1. S.B. Bhoje, IGCAR, Kalpakkam. FBR Programme: Present Status and Perspectives. Invited talk # 28, *10th annual conference of Indian Nuclear Society, [INSAC-99]*, BARC, Mumbai, Aug31-Sept 2,1999.

2. U. M. Basak , M. R. Nair, R. Ramchandran and S. Majumdar, *BARC News Letter (Founder's Day Special Issue 2001), 120-123, 2001.*

3. H. N. Bajpei, C. S. P. Iyer and Das M. Shankar, *Analytica Chimica Acta, 72(1974) 423-425.*

4. V.L. Sant and S.K.Aggrawal; *Proc. 10th ISMAS Workshop on Mass Spectrometry, Intitute of Physics,* Bhubneshwar (Orissa), 229-231, Februrary 25- March1, 2002.

5. B.P. Datta, V.A.Raman, V.L.Sant, P.A. Ramasubramanian, P.M. Shah, K.L. Ramkumar, V.D. Kavimandan, S.K. Aggrawal and H.C.Jain; *Int. Journal of Mass Spectrometry and Ion Processes, 64 (985), 139-158.*

6. S.K. Jha, V.L. Sant, G. Varma, S.K.Aggarawal and V.D.Puranik; *Nuclear & Radio Chemistry Symposium (NUCAR 2003)*-BARC, Mumbai, Feb.10-13, 2003 (Paper accepted for presentation).

This paper received the 2nd Prize in the category of "Nuclear Technology (NT-10)" presented during ISMAS Silver Jubilee Symposium on Mass Spectrometry (ISMAS-SJS-2003) held at National Institute of Oceanography, Goa, during January 27-31, 2003

About the authors ...

Mr V. L. Sant *is presently working in Fuel Chemistry Division, BARC. He is specialised in the field of solid state mass spectrometry and actively involved in chemical quality control (CQC) of nuclear fuels and other high purity nuclear grade materials for the last 28 years. Utilizing expertise in Spark Source Mass Spectrometry (SSMS) in particular, he has developed and standardised different quantification and spectral interference correction methodologies for the critical trace constituents of the variety of matrices specified in the nuclear technology. His other sphere of activity comprises determination of burn-up of uranium and thorium based reactor fuels and recovery of plutonium from different types of nuclear wastes. He has more than 50 publications in international journals and symposia.*

Mr Suman K.Mishra *is presently working in Laser & Plasma Technology Division, BARC. He joined Fuel Chemistry Division, BARC, in 2002. His areas of interest include HPLC, Mass Spectrometry and Laser Optics.*

Dr S.K. Aggarwal *is currently, Head, Mass Spectrometry Section of the Fuel Chemistry Division, BARC. He received his B.Sc. (Hons.) from Guru Nanak Dev University, Amritsar, in 1972 with two Gold Medals. He joined the 16th batch of BARC Training School in 1972 and received the Homi Bhabha Award. He did his Ph.D. from Mumbai University in 1980. He is a coauthor of 300 scientific publications, which include 100 articles published in reputed journals. Dr Aggarwal has participated in several international and national conferences and in different international intercomparison experiments. He is a specialist in the field of atomic mass spectrometry and alpha spectrometry and is interested in various mass spectrometric techniques. His other areas of interest include electrochemistry and solvent extraction. He represents India in the Executive Committee of International Mass Spectrometric Conferences. He has visited several countries in America, Europe and Australia as an expert as well as for delivering lectures. He is a recognised Ph.D. Guide of the Mumbai University.*

A SIMPLE METHOD FOR ISOLATION OF DNA FROM PLANTS SUITABLE FOR LONG TERM STORAGE AND DNA MARKER ANALYSIS

E. Nalini and N. Jawali
Molecular Biology and Agriculture Division
Bhabha Atomic Research Centre

and

S.G. Bhagwat
Nuclear Agriculture and Biotechnology Division
Bhabha Atomic Research Centre

Abstract

DNA based markers have extensively been used in genome mapping. Restriction Fragment Length Polymorphism (RFLP) markers were the first to be used for this purpose. With the advent of Taq DNA Polymerase, PCR-based markers have become popular since they require less time, effort and expense for molecular mapping. PCR based studies such as in construction of a linkage map, estimating genetic diversity in a germplasm etc. involves a limited number of samples (50-200). Such studies require isolation of sufficiently pure DNA, which is suitable both for the purpose as well as for preserving the same for a considerable period of time. Although the DNA needed per reaction in PCR based markers is very low, the number of PCR reactions to be performed is large and hence a good amount of DNA would be needed for such studies. We have developed a simple method for isolation of DNA from plant tissue (leaf or seed). The method is suitable for isolating DNA from a small to medium number of plant samples. The DNA can be stored for a longer duration. The method involves extraction of DNA using a buffer (pH 8.0) containing Tris (100 mM), EDTA (20 mM), 7 M urea, 0.5 M NaCl and 0.1% β- mercaptoethanol, followed by purification of DNA with phenol, chloroform and Isoamlyalcohol and finally precipitation of DNA by sodium acetate and isopropanol. The protocol is simple and fast as it does not involve time consuming steps such as incubation at higher temperatures, does not require expensive chemicals such as proteinase K, liquid nitrogen etc., and no special equipment is needed.

Introduction

In recent years, considerable emphasis has been placed on the development and use of molecular markers for a variety of objectives. One of the most extensive uses of the molecular markers has been the development of genetic and physical maps of genomes. Molecular markers are also used for a wide range of purposes such as germplasm characterization, genetic diagnostics, characterization of transformants, study of genome organization, phylogenetic analysis, marker-assisted selection, mapping Quantitative Trait Loci (QTL) etc. (Gupta et al, 1999) Till recently this was achieved by Restriction Fragment Length Polymorphism (RFLP) analysis. However, the advent of thermo stable *Taq* DNA Polymerase has led to the development of several PCR- based markers such as Random Amplified Polymorphic DNA (RAPD), Inter Simple Sequence Repeats (ISSR),

Sequence tagged Microsatellite Site (STMS), Amplified Fragment Length Polymorphism (AFLP), etc. Some of the advantages PCR based markers have over RFLP are that they are faster, easier, need less amount of DNA per assay and high purity of DNA is not an absolute requirement as compared to RFLP.

The quality and quantity of DNA required depends upon the objective. In marker assisted selection the number of samples are high but the number of PCR reactions to be performed are few and hence the amount of DNA needed is small and need not be stored for a long duration [McCarthy et al (2002), Guo-Liang Wang et al (1993)]. On the other hand in case of QTL mapping or population studies of RILS, F_2 population etc., the number of PCR reactions to be performed are large and therefore considerable amount of purified DNA would be needed which can be stored for a longer duration.

Although several protocols are available for DNA isolation in wheat [(Stein et al (2001), Dellaporta et al (1983), Sharp, et al (1988), Murray et al (1980), Chunwongse et al (1993), McCarthy et al (2002), Clarke et al (1989), Benito et al (1993), etc.)] and in other plant species [Krishna and Jawali (1997), Hong Wang et al (1993), Xiao-Dong Wong et al (1996), Lange et al (1998), Kamalay et al (1990), Francois Guidet (1994), etc.] all of them either involve elaborate and time consuming steps such as hours of incubation at 65ºC or 37ºC or use of expensive chemicals such as proteinase K, liquid nitrogen etc. Some methods involve use of specific equipment designed especially for DNA isolation. Although the method by McCarthy et al (2002) for DNA isolation does not involve incubation and specific equipment, it is suitable for isolation of DNA from seed material and not for leaf tissue.

In this paper we describe a DNA isolation method suited for isolation of reasonably pure DNA in sufficient amount from wheat leaves that can be stored for a longer duration and lasting for several PCR reactions. The method is rapid involving no incubation steps, expensive chemicals and specific equipment.

Materials and Methods

Materials

Segregating F_2 population obtained from a cross Sonalika X Kalyansona (bread wheat: *Triticum aestivum L* .) was used for this study. Fresh as well as frozen leaf tissue was used in this method. Leaves from one-month-old field grown plants were harvested and brought on ice to laboratory. The leaves were thoroughly washed with tap water and rinsed with distilled water, blot dried and weighed. The leaves were either stored at –70˚C or used directly for extraction.

The chemicals needed for isolation of DNA viz. Tris, EDTA were obtained from Sigma and Sodium chloride, urea, SDS, Isopropanol, sodium acetate, chloroform, Isoamlyalcohol and phenol were of the analytical grade. PCR grade dNTPs were procured from Roche chemicals. Enzyme Taq DNA Polymerase, 10X-assay buffer for Taq DNA Polymerase and Magnesium chloride were obtained from Bangalore Genei Pvt. Ltd. The primers were obtained from Gibco BRL. The agarose used for gel electrophoresis was also obtained from Sigma. The Hoechst dye used for DNA estimation was procured from Amersham Pharmacia biotech.

Methods

DNA from the samples was isolated as follows. Around 0.5 g of leaf tissue was placed in a mortar and homogenized with 2 ml of extraction buffer. The extraction buffer (pH 8.0) consisted of 100 mM Tris, 20 mM EDTA, 0.5 M NaCl, 7 M Urea, 0.1% β-mercaptoethanol and 2% SDS. Long fibers of the tissue were retained back after crushing and the homogenate was transferred to a 2 ml-microfuge tube. An equal volume of phenol:chloroform :Isoamlyalcohol (25:24:1) was added to the tubes and mixed well by gently

shaking the tubes. The tubes were centrifuged at room temperature for 15 min at 15,000 rpm. The upper aqueous phase was collected in a new tube and an equal volume of chloroform: Isoamlyalcohol (24:1) was added and mixed.

The upper aqueous phase obtained after centrifuging at room temperature for 10 min at 15,000 rpm was transferred to a new tube. The DNA was precipitated from the solution by adding 0.1 volume of 3 M Sodium acetate pH 7.0 and 0.7 volume of Isopropanol. After 15 min of incubation at room temperature the tubes were centrifuged at 4ºC for 15 min at 15,000 rpm. The DNA pellet was washed twice with 70% ethanol and then very briefly with 100% ethanol and air-dried. The DNA was dissolved in TE (Tris-Cl 10 mM pH 8.0, EDTA 1 mM). To remove RNA 5 µl of DNAse free RNAse A (10 mg/ml) was added to the DNA.

Estimation of DNA

The amount of DNA in the RNAse treated mixture was estimated by measuring the fluorescence emission using the dye Hoechst. Since the dye binds specifically to double stranded DNA, the presence of small fragments of degraded RNA in the sample did not interfere with the measurements. The fluorescence intensity was measured at emission maximum of 546 nm using the fluorimeter Hoefer DyNA Quant 200. The amount of DNA was estimated by comparing the emission intensity obtained using a known amount of standard DNA (100 µg/ml) (provided by Amersham) which acts as the reference. The DNA was also observed on 2% agarose gel by electrophoresis using 1X TBE buffer. The DNA fragments were stained with ethidium bromide and viewed under UV light and subsequently photographed. The quantity of the DNA was estimated against a marker (λHindIII, 100 ng/µl) which was also loaded in the gel along with the DNA. The DNA was further used for PCR.

PCR Analysis

AP-PCR ANALYSIS: AP-PCR amplification was carried out in a volume of 25 µl containing 100 ng of template DNA, 2 mM $MgCl_2$, 25 pmoles of primer SS26.1 (5'-GAA\GGG\TAA\TTC\ AGA\GCC\A -3'), 2.5 µl of 10X assay buffer which includes (10 mM Tris (pH 9.0), 50 mM KCl, 1.5 mM $MgCl_2$, and 0.01% Gelatin), 0.2 mM each of dNTPs and 1 unit of Taq DNA Polymerase. The PCR amplification was carried out in an Eppendorf Mastercycler-Gradient thermal Cycler as follows: 1 cycle of 5 min at 94ºC, 5 min at 45ºC and 5 min at 72ºC, and 35 cycles of 1 min at 94ºC, 1 min at 45ºC and 1 min at 72ºC, followed by a final 10 min extension at 72ºC.

ISSR ANALYSIS: PCR amplification of template DNA using a 3′ anchored ISSR primer was carried out in a volume of 25 µl. The reaction mixture contained 100 ng of template DNA, 2 mM $MgCl_2$, 25 pmoles of the primer SSR11.2 (5'-GAC\AGA\GAC\AGA\GAC\A (C\T)C -3') 2.5 µl of 10X assay buffer which included (10 mM Tris (pH 9.0), 50 mM KCl, 1.5 mM $MgCl_2$, and 0.01% Gelatin), 0.2 mM each of dNTPs and 1 unit of Taq DNA Polymerase. The PCR amplification was carried out on an Eppendorf Mastercycler-Gradient thermal Cycler as follows: 1 cycle of 5 min at 94ºC, 5 min at 50ºC and 5 min at 72ºC, 45 cycles of 1 min at 94ºC, 1 min at 50ºC and 1 min at 72ºC followed by a final 10 min incubation at 72ºC.

The PCR products obtained by AP-PCR and ISSR were separated on 2% agarose gel by electrophoresis using 1X TBE buffer. The DNA fragments were stained with ethidium bromide and viewed under UV light and subsequently photographed (Sambrook et al 1989).

Results and Discussions

To check the efficiency and reliability of the procedure, the DNA was isolated from leaves of 150 wheat plants. The amount of the leaf sample

used varied from 0.5 g to 0.6 g. By using mortar and pestle one person could easily isolate DNA from 48 samples in a day. On an average 200 μg of DNA was obtained and significant positive correlation was observed between the leaf weight in the range 0.5 g to 1.0 g and the DNA isolated indicating the reliability of the protocol. The efficiency of the protocol is indicted by the quantity of the DNA obtained which is comparable to the yield obtained by other extraction protocols [Stein et al (2001), Clarke et al (1989)]. Considering that 100 ng is required for one PCR reaction the amount of DNA obtained is sufficient for 2000 reactions.

The suitability of the DNA isolated as a template in PCR amplification reactions such as AP-PCR and ISSR was analyzed. The AP-PCR amplification product profiles using 19mer primers using DNA as template from F_2 plants was analyzed. The DNA isolated from all the 150 plants yielded consistently amplified products. As an example the products obtained from the parents and some F_2 plants using primer SS26.1 are shown in Fig.1. A polymorphic band was detected between the parents which segregated among the F_2 individuals in the ratio 2.75:1 that is close to the expected value of 3:1 with a chi-square value of 0.32 at significance level of 1%. The results showed that the DNA isolated by the above method is reliable and sufficiently pure to be used in AP-PCR analysis to study genetic segregation.

The results also showed that the DNA isolated by this protocol produced consistent and reliable ISSR profiles with several 3′ anchored ISSR primers. Fig.2 shows an example of ISSR profiles obtained from F_2 plants using the primer SSR11.2 As in the case of AP-PCR analysis, the bands that were polymorphic between the parents showed segregation in the F_2 population. DNA isolated using the above method and stored at 4ºC for over a year was used in AP-PCR and ISSR analysis to check its quality. The results showed that all the 150 samples yielded amplification products with their profiles being the same as obtained earlier.
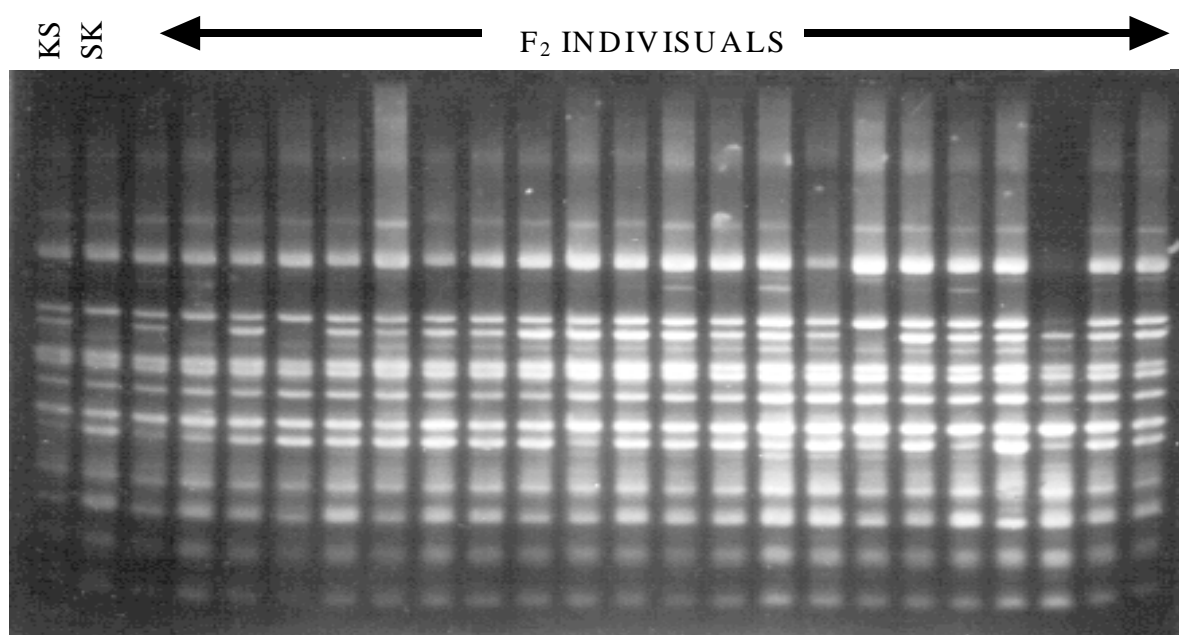

Fig. 1 AP- PCR analysis of 22 F_2 plants of wheat (Triticum aestivum) derived from a cross between Sonalika (Sk) X Kalyansona (Ks). The PCR products were analyzed as indicated in Materials and Methods. The polymorphic band showing segregation has been indicated.
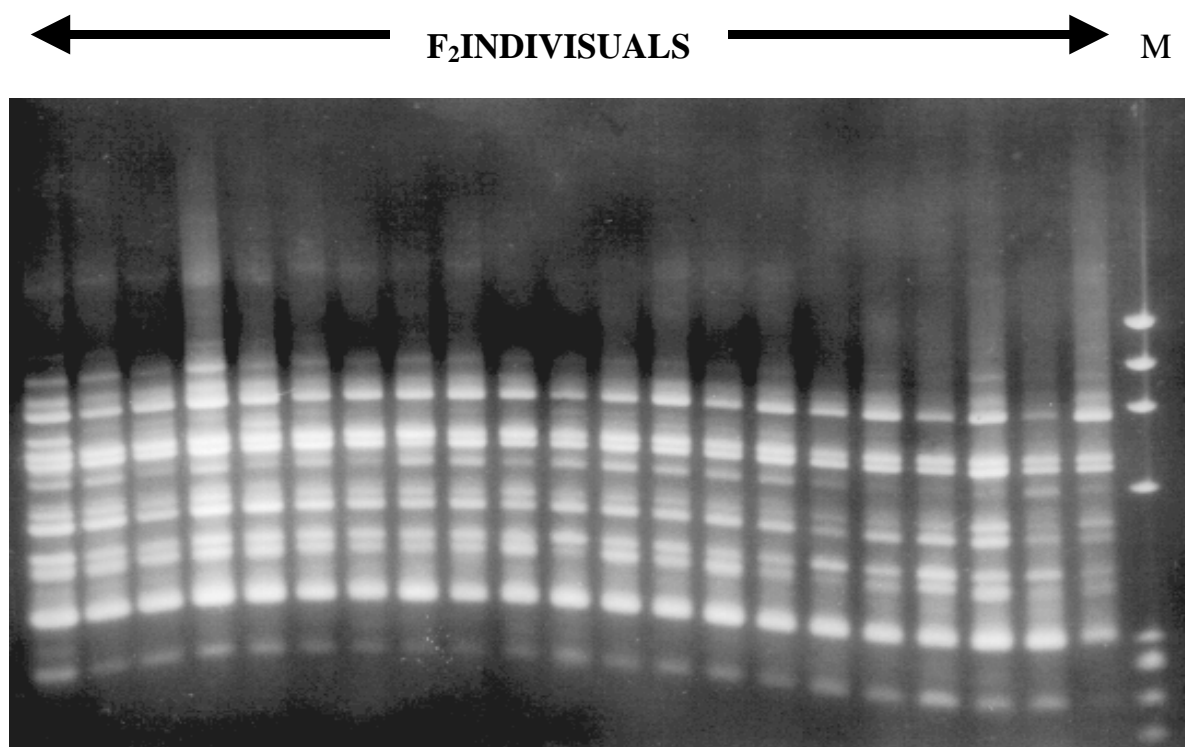
◄━━━━━━━━━━━━━━ **F₂INDIVISUALS** ━━━━━━━━► M

Fig. 2 ISSR analysis of 21 F₂ plants of wheat (Triticum aestivum) derived from a cross between Sonalika X Kalyansona. Lane M: Φx174 DNA digested with Hae III. The polymorphic band showing segregation has been indicated.

DNA isolated from plants often contains certain compounds that inhibit PCR amplification reactions (Krishna and Jawali 1997, McCarthy et al 2001, etc.). In this method Sodium chloride and β-mercaptoethanol were added in the extraction buffer to take care of the polysaccharides and the polyphenols in the leaf tissue which are the compounds which could contribute to the inhibition of the DNA amplification during PCR reactions. Hence there were no additional steps needed for the removal of these compounds [McCarthy et al (2002), Maliyakal, E.J et al 1992, Oard, J.H. et al (1992) Shirzadegan et al (1991)]. The presence of the enzyme RNAse A in the DNA solution does not hamper the amplification. Hence repurification of the DNA is not needed. (Sharp et al 1988).

While this method was designed especially for isolating DNA from leaf tissue of hexaploid wheat for marker analysis, it was also found to be suitable for wheat seeds, and from leaf and seed material of mungbean, mustard, sesbania. (data not shown). Our experience showed that the DNA isolation protocol could be successfully applied to a broad range of plant species.

The advantages of this procedure over existing methods are its simplicity, rapidity of isolation and reduction in the cost. DNA could be isolated from 48 samples by one person within a day as the protocol did not involve time consuming steps such as incubation at 65ºC or 37ºC. In addition the protocol did not require liquid nitrogen that may not be easily available in many laboratories. All chemicals used are inexpensive and equipments used are available in the laboratories. The method is best suited for isolating DNA from a small to medium sized population, and where storing for a longer duration of time is required.

References

1. Benito, c., Figueiras, A.M., Zaragoza, C., Gallego, F.J. and de la Pena, A. 1993. Rapid identification of Triticeae Genotypes from single seeds using the polymerase chain reaction. Plant Mol. Bio. 21:181-183.

2. Chunwongse, J., Martin, G.B. and Tanksley, S.D. 1993. Pre-germination genotypic screening using PCR amplification of half-seed. Theor. Appl. Genet. 86:694-698.

3. Clarke, B.C., Moran, L.B. and Appels, R. 1989. DNA analysis in wheat breeding. Genome. 32:334-339.

4. Dellaporta, S.L., Wood, J. and Hicks, J.B. 1983. A plant DNA Minipreparation version 2. Plant Mol. Bio. Rep. 1: 19-22.

5. Francois Guidet. 1994. A powerful new technique to quickly prepare hundreds of plant extracts for PCR and RAPD analyses. Nucl. Acid Res. Vol 22, No. 9: 1772-1773.

6. Guo-Liang Wang, Rod, A.W. and Paterson, A.H. 1993. PCR amplification from single seeds, facilitating DNA marker-assisted breeding. Nucl. Acid Res. Vol 21, No 10: 2527.

7. Gupta, P.K., Varshney, R.K., Sharma, P.C. and Ramesh, B. 1999. Molecular markers and their applications in wheat breeding. Plant Breeding. 118: 369-390.

8. Hong Wang, Meiqing Qi, and Cutler, A.J. 1993. A simple method of preparing plant samples for PCR. Nucl. Acid Res. Vol21, No 17: 4153-4154.

9. Kamalay, J.C., Tejwani, R. and Rufener II, K.G. 1990. Isolation and analysis of Genomic DNA from single seeds. Crop. Sci. 30:1079-1084.

10. Krishna, T.G. and Jawali, N. 1997. DNA Isolation from single or half seeds suitable for Random Amplified Polymorphic DNA Analyses. Anal. Biochem. 250: 125-127.

11. Lange, D.A., Penuela, S., Denny, R.L., Mudge, J., Concibido, V.C., Orf, J.H. and Young, N.D. 1998. A plant DNA isolation protocol suitable for polymerase chain reaction based marker-assisted breeding. Crop. Sci. 38: 217-220.

12. Maliyakal, J.E. 1992. An efficient method for isolation of RNA and DNA from plants containing polyphenolics. Nucl. Acid Res. Vol 20, No 9: 2381.

13. McCarthy, P.L. and Berger, P.H. 2002. Rapid identification of transformed wheat using a half-seed PCR assay prior to germination. Biotechniques. 32: 560-564.

14. Murray, M.G. and Thompson, W.F. 1980. Rapid isolation of high molecular weight plant DNA. Nucl. Acid Res. Vol 8, 19: 4321-4325.

15. Oard, J.H. and S. Dronavalli. 1992. Rapid isolation of rice and maize DNA for analysis by random-primer PCR. Plant Mol. Biol. Rep. 10:236-241.

16. Sambrook, J., Fritsch, E.F., and Maniatis, T. 1989. Molecular cloning: A laboratory Manual. II ed[n]. Cold Spring Harbour Laboratory. Press, Cold Spring Harbour, N.Y.

17. Sharp, P.J., Kreis, M., Shewry, P.R. and Gale, M.D. 1988. Location of β-amylase sequences in wheat and its relatives. Theor. Appl. Genet. 75: 286-290.

18. Shirzadegan, M., Christie, P. and Seemann, J.R. 1991. An efficient method for isolation of RNA from tissue cultured plant cells. Nucl. Acid Res. 19:6055.

19. Stein, N., Herren, G. and Keller, B. 2001. A new DNA extraction method for high-throughput marker analysis in a large genome species such as *Triticum aestivum*. Plant Breeding. 120: 354-356.

20. Xiao-Dong Wang, Zi-Ping Wang, and Yu-Ping Zou.1996. An Improved Procedure for the Isolation of Nuclear DNA from Leaves of Wild Grapevine Dried with Silica Gel. Plant Mol. Bio. Rep. 14(4)

This paper was awarded the second prize for Best Poster presentation at the National Symposium on "The Role of Biotechnology in the Development of the Indian Economy" at Vaze College, Mumbai, during February 22-23, 2003

About the authors ...

Ms Nalini Eswaran, *SRF, DAE-Mumbai University collaborative fellowship, is a first rank holder in M.Sc. degree in Life Sciences (Biomacromolecules, specialization) from Mumbai University in the year 2001. She was awarded the DAE-Mumbai University collaborative fellowship for doing her Ph.D., in 2001. She is carrying out her research project entitled "Genetic Linkage Map of Bread Wheat with an emphasis on Genes Controlling Plant Morphology" in the Molecular Biology Division of BARC under the guidance of Dr Narendra Jawali. She was presented with a 'Certificate of Appreciation' and a memento at the above symposium.*

Dr Narendra Jawali *obtained M.Sc., Degree in Biochemistry from Central College, Bangalore University, Bangalore in 1975. He joined the 19th batch of Training School in the Biology and Radiobiology discipline. He obtained his Ph.D. in 1988 from Mumbai University. He is working in the Molecular Biology Division of the Bioscience group, BARC. His research interests are plant and microbial molecular genetics.*

Dr S.G. Bhagawat *did his M.Sc. in Botany from Poona University, Pune, in the year 1975. He joined the 19th batch of Training School in the Biology and Radiobiology discipline. He did his PhD. on "Grain protein variation in wheat". Currently, he is working in the Nuclear Agriculture and Biotechnology Division of the Bioscience group, BARC. His research interests are genetics and genetic improvement of wheat.*

ALTERATIONS IN MITOCHONDRIAL FUNCTIONS IN DAMAGED HUMAN MITRAL VALVE

Santosh Shinde, A.J. Tendolkar and Neela Patil
Department of Biochemistry, L.T.M.M.C and L.T.M.G.H., Mumbai

and

K Pasupathy and K P Mishra
Radiation Biology and Health Sciences Division
Bhabha Atomic Research Centre

The mitral valve is the inflow valve into the left side of the heart, which allows blood to move the left atrium into the left ventricle. Myocardial function depends on ATP supplied by oxidation of several substrates. In adult heart, this energy is obtained primarily from fatty acid oxidation through oxidative phosphorylation. However, the energy source may change depending on several factors such as substrates availability, energy demands, oxygen supply and metabolic condition of an individual. Myocardial recovery from ischemic injury requires a substantial generation of energy to repair damage to cellular processes and allow for return of contractile force after reperfusion. The mitochondria are the subcellular sites of this vital energy generating function their recovery from ischemic injury is of fundamental importance. Cardiac mitochondria are complex structure and this complexity is particularly evident in the molecular structure of the crista membrane, which organizes the enzyme molecules that are responsible for phosphorylation and that ensure the efficiency of energy generation. There is not much information available on mitochondrial function in human mitral valve from normal or from diseases. The present studies analysed the relationship between preoperative clinical conditions (as per New York Heart Association) and extent of mitochondrial enzyme activities in damaged human mitral valve in various heart diseases such as rheumatic heart disease and bacterial endocarditis.

39 patients were studied for routine valvular heart surgery. The defect arising out of all possible causes namely Rheumatic Heart Disease (RHD) and Bacterial Endocarditis (BE). Human mitral valves from autopsies were taken as control. Mitochondrial Oxygen Consumption and enzymes like Cytochrome oxidase (COx), Succinate dehydrogenase (SDH), Malate dehydrogenase (MDH), Citrate synthase (CS) and ATPase were determined.

Mitochondrial Oxygen Consumption and COx, SDH, MDH, CS and total ATPase were highly affected in diseased originating Bacterial Endocarditis (BE). On the other hand as per New York Heart Association (NYHA) preoperative clinical classification, all the mitochondrial enzymes were significantly impaired in class IV. Results correlated well with the condition of the patients who are clinically classified stage I, II, III and IV of New York Heart Association (NYHA) depending upon the Volume overload.

This paper received 3ʳᵈ prize in the "Molecular Medicine" category at the 10ᵗʰ Federation of Asia and Oceanic Biochemists and Molecular Biologists Congress, held at IISc, Bangalore, during December 7-11, 2003.

About the authors ...

Mr Santosh Shinde passed his M.Sc. in 1999 from Institute of Science, University of Mumbai, Mumbai. He is working in the Department of Biochemistry at L.T.M.G. Hospital, Sion, Mumbai. He is currently pursuing his Ph.D. at BARC. His research activities are : (1) Inborn error of metabolism (like galactosemia, MPS, Organic/Aminoaciduria), (2) Pre/Post-natal diagnosis of genetic disorders (neural tube defect). (3) Biochemical markers during cardiac surgery, and (4) Mitochondrial function in cardiac and neurosurgery.

Dr Anil G Tendolkar is the Professor and Head, Department of Cardiovascular Thoracic Surgery (CVTS), L.T.M.Medical College, Sion, Mumbai. He has done his M.S. in General Surgery and M.S. in Thoracic Surgery. His research interests are : (i) Beating Heart surgery (ii) Congenital Heart Diseases and (iii) Mitochondrial studies.

Dr (Ms) Neela D. Patil is the Professor and Head, Department of Biochemistry, L.T.M.Medical College, Sion., Mumbai. She did her Ph.D. from University of Mumbai in 1983. Her research interests are : (i) Mitochondrial Function (ii) Metabolic Disorder and Cardiovascular Diseases and Atherosclerosis.

Dr Ms Karpagam Pasupathy did her Ph.D. from BARC in 1983 and is working in Radiation Biology and Health Sciences Division, BARC. Her research interests are (i) using yeast as a Test System to study action of radioprotectors, (ii) Radiation induced Cell Cycle Alteration in yeast, (iii) Mitochondrial functions, and (iv) Mitochondrial DNA replication. She has more than 40 publications in International and National Peer-Reviewed Journals.

*Dr Kaushala Prasad Mishra joined BARC in 1969 through 12ᵗʰ batch Training School in Chemistry and is internationally known for his contributions in the area of Free Radical Biology and Radiation Biology. His major research interests concern the mechanism of radiation damage to normal and tumor cells and its modification by chemical and physical agents. More recently, focus of his research has been concerning the role of ROS in oxidative stress induced apoptotic cell death relevant to radioprotection and cancer radiotherapy. Currently, Dr Mishra is the Head, Radiation Biology and Health Sciences Division of BARC. He has edited a book titled **Radiobiology and Biomedical Research**. Together with his colleagues, Dr Mishra has designed and developed a Cell Electroporator for biomedical research and applications, which is under Technology Transfer from this Centre. He has received several professional recognitions for his significant research contributions in the area of Radiation Biology and Life Science. Dr Mishra is a Fellow of National Academy of Sciences, India, Vice President of Bioelectrochemical Society of India, Past President of Section of New Biology, 88ᵗʰ Indian Science Congress, a Member of the Executive Council of Asia Pacific ESR/EPR Society, General Secretary, Indian Biophysical Society, Vice President of Society of Free Radical Research of India, Council Member, International Association of Radiation Research. He was invited as Visiting Scientist to several Universities/Institutions in India and abroad.*

ON-LINE MONITORING OF CO₂ LASER WELDING USING OPTICAL EMISSION SPECTROSCOPY

C.S. Viswanadham and G.L. Goswami
Laser Processing & Advanced Welding Section
Bhabha Atomic Research Centre

and

M. Arumugam
Centre for Laser Technology
Anna University, Guindy, Chennai

Introduction

The plumes formed during high power laser welding contain the atomic and ionic species of the workpiece material and the ambient shielding gas. The relative distribution of these species depends upon the energy exchanges occurring during the welding process. This distribution can be determined by spectroscopic methods, thus providing a valuable method of online process monitoring. However, it would require a large database of welding parameters and their respective spectral signatures to ultimately arrive at a correlation. Rapidly measurable spectral signatures will be required when such correlations are required to be adapted to process control. In this context, it might be useful to explore empirical parameters related to the spectral line characteristics. There were numerous studies on optical emission spectroscopy of laser welding plasmas[1-5], but relatively fewer[5] studies dwell upon the correlations between the spectra and the laser welding parameters. In this study, it has been found that a definite correlation exists between the intensity of spectral lines of specific elements (Cr, Fe and Ni) and the laser power during the CO₂ laser welding of stainless steel AISI 316.

Experimental

An MLI make 5 kW CO₂ laser model ML-5000 with its associated CNC stage was used to perform bead-on-plate welds on a sheet of stainless steel AISI 316. The chemical composition of the workpiece material is shown in Table 1. Argon was used as the shielding gas. The laser was allowed a warmup period of 2 hours between the starting of the discharge and the experiments. Fig. 1 shows the schematic diagram of the experimental setup. The light from the welding plume was focussed optically on to the fiber optic probe connected to the input slit of a 257 mm focal length spectrograph (Acton Research). A grating selectable through software from amongst 300 lines/mm, 600 lines/mm or 1200 lines/mm dispersed the light into its spectrum. On the output side of the spectrograph, a 1024 X 256 pixel CCD detector recorded the spectrum. All these operations were controlled by a computer that also stored the spectra. Winspec® software from Princeton Instruments Inc was used to process the spectra. Further processing of the spectra, including background fitting, background subtraction, and peak detection were done by software developed in-house. The experimental conditions are summarized in Table 2.
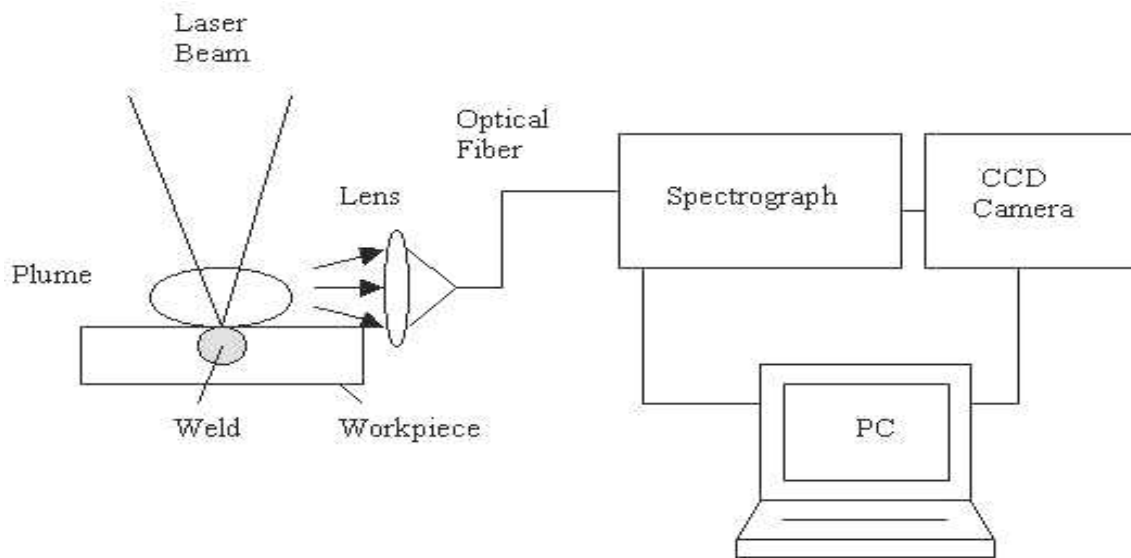
Fig.1. The Experimental Setup

Table 1: Composition of workpiece	
Element	Weight percentage
Fe	68.0
Cr	17.0
Ni	12.0
Mo	2.5
C	0.10

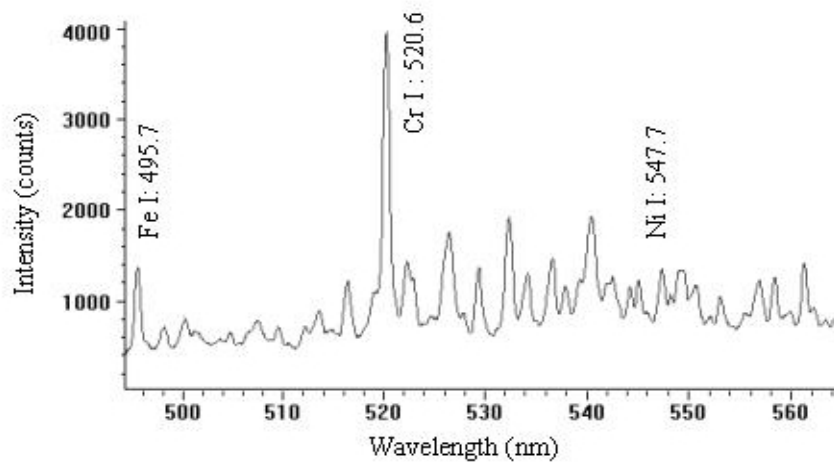| **Table 2: Experimental conditions**	
Welding	Spectroscopy
Laser power: 500 to 1100 W (in steps of 50 W)	Grating: 1200 lines / mm
	Exposure time: 10 ms
	No. of spectra / minute: 165
Welding speed: 0.5 mm/s	Filters: none
Weld duration: 60 s	
Shielding gas: Ar	

Fig.2. Typical spectrum from laser welding plume for laser power of 900 W

Results and Discussion

A typical spectrum obtained for a laser power of 900 W is shown in Fig. 2. Several peaks belonging to the prominent constituents of the steel, i.e., Fe, Cr and Ni were identified. The intensities of the lines were seen to have a definite correlation with the laser power.
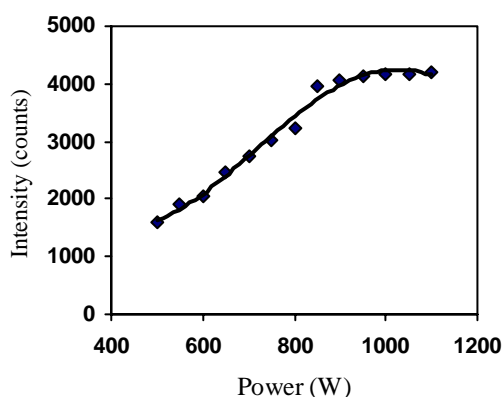

Fig.3. The variation of Cr-I 520.6 nm line with laser power

Typically the variation is like that shown in Fig. 3, where the intensity of Cr I – 520. 6 nm line is plotted against the laser power. The intensity of a spectral line from a certain element is directly related to the amount of that element present in the plume during laser welding. The amount of the element which gets vaporized due to the laser power would increase with the power upto certain power, but later due to complete evaporation, there would be a saturation behaviour. This trend can be seen in the fig.3. Using such correlations, it is possible to monitor for beam power fluctuations during laser welding, especially for the pre-saturation power levels. With further work, it might be possible to identify spectral signatures which are sensitive over a larger power range.

References

1. T.J. Rockstroh and J. Mazumder, J. Appl. Phys. **61** (1987) 917.
2. J. Mazumder, T.J. Rockstroh and H. Krier, J. Appl. Phys. **62** (1987) 4712.
3. A. Poueyo-Verwaerde, R. Fabbro, G. Deshors and A.M. de Frutos, J. Appl. Phys. **74** (1993) 5773.
4. D. Lacroix, G. Jeandel and C. Boudot, J. Appl. Phys. **81** (1997) 1.
5. M.M. Collur and T. Debroy, Met. Trans. **20B** (1989) 277.

> *This paper was awarded a Poster Prize in National Laser Symposium 2002 held during December 2002 at Thiruvananthapuram*

About the authors ...

Chebolu Subrahmanya Viswanadham (M.Sc. Physics, IIT Madras, 1980) graduated from the 24th batch of BARC Training School with Physics discipline. His current interests include laser materials processing, laser micro-machining, materials characterization, process modeling and online process monitoring using optical and acoustic techniques.

M. Armugam (M.Tech. Laser Technology, Anna University, 2001) has been a M.Tech. student in Laser Technology at the Centre for Laser Technology, Anna University, Chennai.

Gyanottam Lal Goswami (B.E. Metallurgy, University of Roorkee, 1970) graduated from the 14th Batch of BARC Training School with Metallurgy discipline. He has made important contributions in nuclear fuel fabrication, thermodynamics of nuclear materials, and laser materials processing. He is currently the Head of Laser Processing & Advanced Welding Section of the Nuclear Fuels Group, BARC.

HYDRODYNAMIC CONSIDERATIONS OF REVERSE OSMOSIS MEMBRANE MODULES & THEIR MERITS AND DEMERITS WITH RESPECT TO THEIR APPLICATIONS

S.A. Tiwari, K.P. Bhattacharyya, D. Goswami, V.K. Srivastava and M.S. Hanra
Desalination Division
Bhabha Atomic Reserach Centre

Abstract

Generally four types of membrane modules namely, Tubular; Plate and Frame; Spiral Wound and Hollow Fine Fiber configurations are popularly known in any pressure driven membrane based separation processes such as Micro-filtration (MF), Ultra-filtration (UF), Nano-filtration (NF) & Hyper-filtration or Reverse Osmosis (RO). At BARC, the developmental work on few modules along with the membrane material synthesis have been done. The utilization of these membrane modules in chemical, food, pharmaceutical and water based desalination industries are growing day by day.

Hydrodynamic considerations play an important role in selection of the right module for any given application. The paper discusses the merits and demerits of various modules. This also dwells upon the structural configuration of each module for better understanding towards the operability and maintainability of various modules during their applications.

Introduction

The development of synthetic polymer with semi permeable properties for application in RO/NF based pressure driven membrane process has always been a challenging task and work on the same had been started in few national R & D centers including BARC. As the basic principle suggests for housing of these membranes in certain form of configuration and pressurizing the modules at more than the osmotic pressure of the feed under consideration required for development of various modules[1,2]. In literature, the tubular RO/UF membranes are among the oldest used industrially. Subsequently the development of plate and frame; spiral wound and hollow fine fiber modules were made giving higher effective membrane area per unit volume of module space[3]. All these have different hydrodynamic characteristics, leading to the advantages and disadvantage in there various applications. At BARC, Trombay the development work of three types of modules namely Ttubular, Plate & Frame and Spiral Wound have been done and some salient features are described here along with hydrodynamic characteristics of these modules.

RO Modules Development at BARC

The RO modules are the building block of any RO plant and it could be any of the currently known four types of modules namely Tubular, Plate & Frame; Spiral Wound or Hollow fine fiber. These modules are generally connected in series and parallel combination to give an optimum flux and salt rejection without leading to excessive concentration polarization in any plant of medium to large sizes.

Tubular Module

The description of tubular module with fourteen tubes each of 1.25 meter length and 18 mm internal diameter made up of fiber glass reinforced porous plastic tube and using CA 2.5 membrane have been reported earlier[4,5,6]. Other membrane material can also be suitably casted in tubular form. The total area of the membrane packed in single module is about 1 m². The typical membrane densities in tubular form are in the range of 60 – 160 m²/m³.. The standard velocity range of feed flow is 0.5 ft/sec to 1.5 ft/sec but even higher value upto 5 ft/sec are also acceptable at the cost of higher pressure drops in few specific applications with high turbidity solutions particularly in food & pharmaceutical industries This corresponds to a minimum volumetric feed flow of about 2.3 lpm and maximum feed flow of about 23 lpm with an optimum range of 5 – 10 lpm feed flow rate. However, based on Reynolds number generally the tubular module system works in turbulent zone only. An assembly of tubular RO modules is shown in Fig. 1.
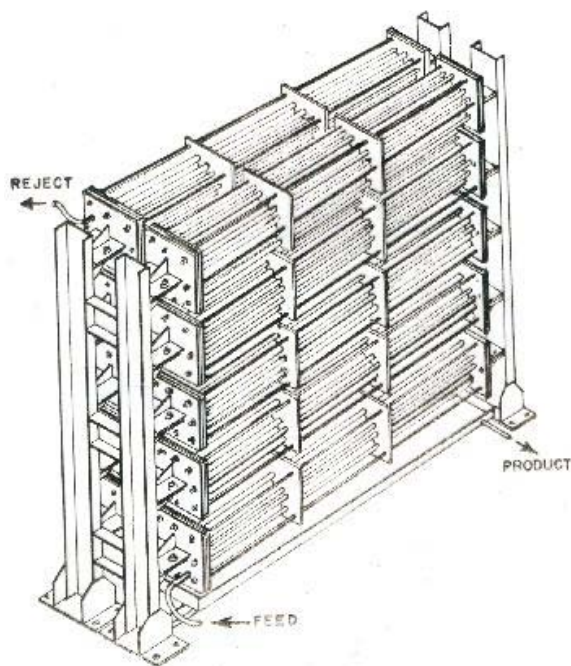

Fig.1 Assemby of Tubular RO Module.
Plate & Frame Module.

Plate & Frame Module

The description of Plate and Frame type module with 80 – 100 plates, comprising of approximate membrane area of 8 m² were reported earlier [7,8,9]. As it is evident from these reports that simply by changing the membrane type of different membrane materials for UF/NF/RO, this type of module can be used for brackish water, seawater, effluent water desalination purposes and other industrial applications.

Table 1 : Typical specification of a plate module

Nominal Permeate Flow	3.5 LPM (5 m³/day)
Maximum Feed Flow Rate	9 LPM
Feed Water TDS	5000 ppm, NaCl
Feed Water pH	5 – 6
Feed Water Temperature	25 °C(Max. 35 °C)
Feed Water Turbidity	1 NTU (max.)
Feed Water SDI_{15}	< 5
Normal Feed Water Flow Rate	7 LPM
Applied Pressure Normal	30 Kg/cm² (Max. 45 Kg/cm²)
Permeate Recovery	50 %
Salt Rejection Average	90 %
Membrane Material	CA
Permeate TDS	≈ 500 ppm
Reject TDS	≈ 9500 ppm
Membrane Area	≈ 8 m²
No. of plates	100

Table 1 gives a typical specification of a plate module. Generally membrane-packing density in such modules are in the range of 60 – 150 ft²/ft³ (200 – 500 m²/m³) and a volumetric flow rate of 2 – 11 lpm are recommended. It is a peculiar module in which a feed flow velocity generally varies from 0.8 to 2.6 ft/sec and a combination of turbulent and laminar flow zones are achieved.

Table 1 gives a typical specification of a plate module. Generally membrane-packing density in such modules are in the range of 60 – 150 ft^2/ft^3 (200 – 500 m^2/m^3) and a volumetric flow rate of 2 – 11 lpm are recommended. It is a peculiar module in which a feed flow velocity generally varies from 0.8 to 2.6 ft/sec and a combination of turbulent and laminar flow zones are achieved. At the entry point to each plate it is turbulent and at the active surface it is laminar zone. Studies have shown that an optimum range of feed flow rate is 5 – 9 LPM at which the permeate flux is best.

The disadvantage in this module configuration has been the uneven tightening of the 4 tie rods leading to leakage in the assembled module in which permeate spacer is placed between the two membrane using a partition plate. However, no feed spacer is used in such modules, but pressure plates have in built dents creating turbulence promoters in such modules. Fig.2 shows as assembled plate & Frame module. A modified version of Plate & Frame modules with single central bolt tie rod in disc tube was first developed by (DDS) Danish Sugar Corporation and ROCHEM Company in which permeate flows through the porous support plate which is connected to the central tubing. Each stack consists of 10 – 80 membranes giving higher membrane area. These modules have found wide application in food, pharmaceutical as well as in water desalination industries.
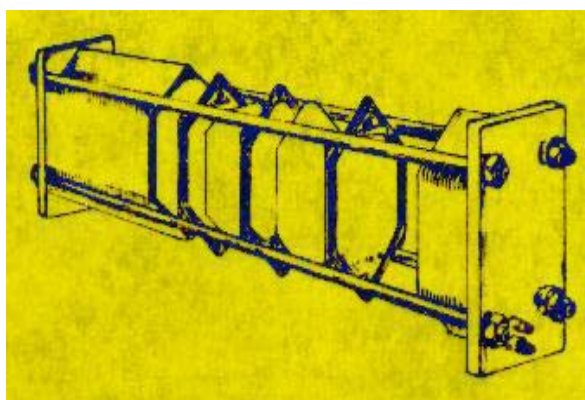
Many details of spiral wound module designs are available in literature[3]. The development of such module is reported earlier from BARC using wet and dry RO/UF/NF membranes made from CA/PA/PS/PAH membrane polymers. So far standard sizes of 2.5 " and 4.0" diameter and 12", 25" and 40" long elements are made and tested. In this design two sheets of membranes are placed one on each side of porous polyester fabric material, which serves as permeate spacer. The three pieces are thus sealed with epoxy around the edges of three sides to form an envelope. The remaining open side is attached to a perforated product water collector tube. A woven mesh of polypropylene mesh sheet which serves as spacer for feed flow region and also as a turbulence promoter in the feed solution, is laid on one side of membrane envelop before rolling them in cylindrical bundle connected to telescopic seal and flow distributor on both ends. Higher diameters of 8"& 8.5" are also made and used in large scale application of these modules and many companies around the world mainly USA, Japan have come with this type of development. This type of membrane module provides a typical packing density of about 800 m^2/m^3 (245 ft^2/ft^3) and a feed flow rate of 0.8 to 1.6 ft/sec is used giving turbulent flow zone throughout inside the module.

Fig.2 Assembly of Plate Module.
Spiral Wound Module.

Fig.3 Typical Spiral Wound module.

Fig.3 shows a typical view of a 2.5" diameter and 12" length spiral module housed in metal and FRP pressure tubes.

Hollow Fine Fibre

Dupont (USA) B9 and B10 Permasep permeaters with aromatic polyamide membrane materials spun into hollow fibers with an inside diameter of 42 µm and outside diameter of 80 – 90 µm are reported. Subsequently HFF module based on CTA membranes are also reported from Toyobo Company, Japan and are in commercial use. These modules though offer highest membrane packing density in the range of 2000 – 8000 ft^2/ft^3 but their productivity is not too far different from that of spiral wound module because of low flux densities. Because of high packing density, these modules are susceptible to particulate plugging and hence fouling leading to flux decline under continued service condition unless more extensive pretreatment are given to remove the suspended and particulate matter prior to RO treatment. This operate in laminar zone and require a low feed flow rate in the range of about 0.016 – 0.02 ft/sec.

Results and Discussions

Table 2 gives the comparison of general hydrodynamics and other characteristics of various membrane modules. A minimum feed flow usually corresponds to the maintaining low concentration polarization (β factor) less than 1.2. The maximum feed flow corresponds to pressure drop across the module, which is generally kept less than 10 psi per element. The membrane separation being based on the flim theory does depend on interfacial properties; morphology of membrane and hydrodynamic condition and governs the transport properties of solute and solvent in any feed solution. Higher the Reynolds number gives improved salt

rejection but an optimum flux range for any given membrane module.

Table-2 : Comparison of different types of module configurations.

Technical Parameters	Spiral Wound	Hollow Fine Fiber	Plate & Frame	Tubular
Compactness (m^2/m^3)	+ +	+++	+	-
Ease of cleaning -- Insitu -- Back flush	+++ -	- +	+ -	++ -
Degree of pretreatment required $(SDI_{15}$ tolerance	+ (<5)	- (<3)	+ (5-6)	+++ (6 or more)
Pressure drop	++	+	-	+++
Dead Volume (m^2/m^3)	+	+++	+	-
Cost of module	+++	++	+	-
% Recovery per element	10-25	30-60	2-3	0.2-2

Acknowledgement

References

1.   Misra B.M. et al.: 'Promise of RO membrane for desalination', Symposium on membrane, organized by Indian Academy of Science, New Delhi, Nov., 1974.

2. Ramni M.P.S.; 'Prospects of RO Technology in India', presented at Indo – FRG Workshop on Desalination, 1981.
3. Sourirajan S. and Matsuura T.; 'Reverse Osmosis /Ultra filtration Process principles', National Research council of Canada, Ottawa 1985.
4. Thomas K.C. et al.: Design of a 10 m^3/day RO plant on tube bundle concept', Proc. 3rd National Cconference on Seawater Desalination', CSMCRI, Bhavnagar, pp 163 – 170, Feb. 1984.
5. Patra R.N. et al.: ibid, pp 49 – 53
6. Prabhakar S. et al.: 'RO for production of boiler feed water for power plants', Indian Journal of Technology, vol. 25, pp 405 – 410. Sept 1987.
7. Prabhakar S. et al: Operational experience of RO plants for drinking water in Indian village', Desalination 65 (1987) pp 361 – 372.
8. Goswami D. et al..: 'RO for treatment of effluent water from a fertilizer plant', Proc. National seminar on water management in process Industries' organized by IICHE, Trichur Regional Center. Ernakulam, Oct 19, 1989
9. Goswami D. et al.: 'Ship borne RO Plant based on Indigenous membrane', Proc. National conference on synthetic membranes and their applications', CSMCRI, Bhavnagar, Nov. 29-30, 1991.
10. DDS – RO System, DK – 4900 Nakskov, Denmark: Leaflet.
11. DT-RO module system, Rochem Separation System, USA: Leaflet.
12. Balasubramaniyan et al., 'In-house development of spiral wound membrane element at BARC', Proc. Annual seminar on Desalination and Water Management', Feb 27' 1999.

This paper was given the Best Paper award at the Chemical Engineering Congress – 2003 held at Bhubaneswar in December 2003

About the authors ...

Mr Sushil Tiwari *of Separation Technology Section of Desalination Division, BARC, is a Chemical Engineer of 41st batch of BARC Training School. He is involved in Membrane-based desalination projects in Desalination Division, BARC.*

Mr K P Bhattacharyya *of Separation Technology Section of Desalination Division, BARC, is a Chemical Engineer of 39st batch of BARC Training School. He is involved in Membrane-based desalination projects in Desalination Division.*

Mr D.Goswami *of Separation Technology Section of Desalination Division, BARC, is a Chemical Engineer of 25 [th.] batch of BARC Training School. He is involved for past 22 years in design, development and application of membrane separation in the field of desalination. He is involved in a number of desalination projects. The 1800 m^3/day seawater RO plant at Kalpakkam as a part of Nuclear Desalination project, with which he is involved right from its inception, was inaugurated by the ex-Prime minister Mr Atal Behari Vajpayee in the year 2002 and is running satisfactorily catering to the needs till date.*

Mr   V.K.Srivastava, *presently   Head,   Thermal   Desalination   Section,   Desalination Division,BARC, a postgraduate Chemical Engineer from 20 [th.] batch of BARC Training School. He has worked in a number of projects related with Nuclear power Agro-Industrial Complex concept in the field of Membrane-based Separation Processes, Electro-Thermal Phosphorous Technology & Thermal Desalination and about 40 papers/publications are there to his credit. He is currently involved in Nuclear Desalination Demonstration Project at Kalpakkam.*

EXPERIMENTS FOR RECOVERY OF URANIUM FROM SEAWATER BY HARNESSING TIDAL ENERGY

A.K. Saxena
Desalination Division
Bhabha Atomic Research Centre

Introduction

In the last century, uranium has universally gained acceptance as primary energy source. Currently it caters to approximately 16% of the electricity generation globally. Uranium has been projected as the main workhorse of future when the fossil energy reserves dwindle by the middle of this century. The terrestrial distribution of uranium ore occurrence is grossly uneven. With a large coastline, India, Japan, Korea and a few other nations have a larger stake in exploiting the 4 billion tones of uranium locked in seawater [1]. Compared to terrestrial mineralisations, this seawater serves as practically inexhaustible resource for uranium [2]. The greatest of the scientific and technological challenges in extracting uranium from seawater are lying in finding a technology that gives a net positive energy balance in terms of electricity produced from the so recovered uranium and the other is the cost of production.

This paper deals with the Indian efforts on both these issues. The initial success of extracting about 800 μg uranium by harnessing the Tidal Wave Power in the year 1999-2000 using electron beam grafted amidoxime as a super specialty adsorbent has been described [3,4]. The engineering flow sheet has been developed for a 1500 times scale up facility with an output of about 100 g/yr uranium. The mechanical design of the contactor arrays has been validated in actual marine conditions. Broad details of the

pilot plant under commissioning at Trombay (India) are also discussed.

Basic Adsorption Mechanism

During seventies and eighties the Initial investigations on the possibilities of recovery of uranium from seawater have been done using inorganic adsorbents [5, 6].

Promising Inorganic adsorbents that have attracted the attention of researchers on this topic are given below in the Table-1:

Table-1 : Uranium loading - Inorganic adsorbents

|	Inorganic adsorbents	U-Loading
1	Hydrous zirconium oxide	13 μg/g
2	Hydrous tin oxide	17
3	Silica Titania gel	27
4	Hydrous lanthanum oxide	38
5	Hydrous iron (III) oxide	60
6	Hydrous aluminum oxide	61
7	Hydrous titanium oxide (after > 60 days storage)	200
8	Zinc carbonate	540
9	Hydrous titanium oxide (freshly precipitated)	1550
10	Bentonite and titanic acid	--
11	Titanyl sulphate	--
12	Trioctyl phophene oxide	--

The above listed inorganic adsorbents suffer the limitations of adsorption rate and insufficient mechanical stability. Extensive investigations are being carried out in parallel on organic

adsorbents as well. Uranium loadings of various organic adsorbents of interest identified so far by various research groups around the world are listed in Table-2.

Table-2 : Uranium loading of Organic adsorbents

	Organic adsorbents	U-Loading
1	Polystyrene acetylene phosphoric acid	24 μg/g
2	Formaldehyde copolymer	45
3	Poly glyco tri amino phenol	45
4	PTO	50
5	Macrocyclic hexacarboxylic acid	70
6	Hyphan on cellulose	80
7	Oxamidoxime terephtalic acid	240
8	Macrocycloimide resin	930
9	Resorcinol arsenic acid	1112
10	Poly Acrylamid Oxime (PAO)	3600
11	Calixarenes	2-123 mg/g
12	Bioactive mass	--

The Poly Acrylamid Oxime (PAO) has been picked up as the best bet for our studies [7] since July 99. This organic adsorbent preferentially extracts heavy metal ions by chelating process. A non-woven polypropylene fibre substrate is irradiated with electron beam to create grafting sites on the polymer chain. The substrate is then treated with acryl polymer to achieve grafting of the cyano group on those sites. In the next step the cyano group of the acryl polymer is reacted with hydroxylamine to convert them into amidoxime groups. These amidoxime groups trap the loosely bonded uranyl ion from the uranyl tricarbonate present in the ionic form i.e. UO_2 $(CO_3)_3^{4-}$ in seawater. The adsorption mechanism [8] as per stoichiometric conditions is as given in the Fig.1 below.
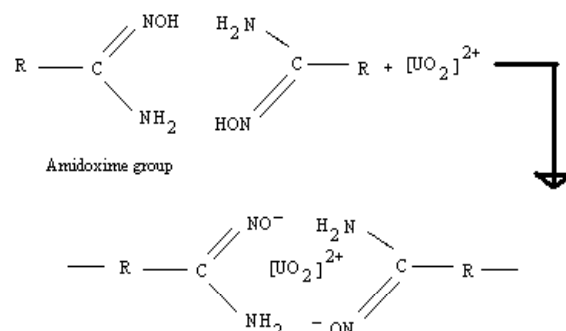

Amidoxime group

Two amidoxime groups capture one uranyl ion

For every two molecules of polyacrylamidoxime (PAO) one uranium atom is captured. Thus theoretically PAO should have an extraction capability of 3.6 kg U/kg PAO.

Description of the First Set of Campaign of Lab-scale Experiments

Substrate: During lab-scale experiments, many types of fiber cross sections and geometry were evaluated for their efficacy for grafting purposes. Polyester and polypropylene fiber materials were shortlisted for further experiments. Finally experiments are done using polypropylene fiber of 1.5 denier cross section as stem material in non-woven felt form. Electron Beam Radiation induced grafting of acrylonitrile on the stem fibre was carried out to optimize the parameters for maximized % grafting. The solution viscosity and temperature were also found to be important factors. Conversion of grafted acrylonitrile into amidoxime was done. PAO was synthesized on the substrate as follows in Figure 2.
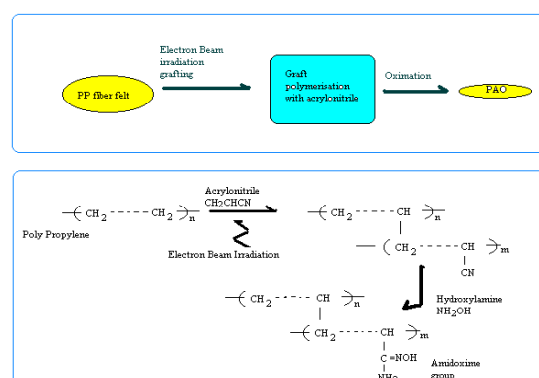
The PAO thus synthesized was conditioned with alkaline treatment to impart it hydrophylicity and thus enhance adsorption characteristics. The tokens of size 75x70x2 mm thick and 150x150x2 mm thick were used.

Process flow chart: Adsorption and Elution cycles were developed. The major unit processes are:Electron-Beam Irradiation of the substrate; Grafting of acrylonitrile; Dissolving of excess AN & drying; Oximation; Alkalination; Submergence in sea; Retrieval from sea; Defouling; Elution and Conversion to yellow cake.

Experimental results: Initial experimental campaigns were carried out on lab scale to establish the process and material parameters under actual marine conditions. The summary is as shown in table-3. Corrosion, bio-fouling and their combined effect on the adsorption kinetics and mechanical properties of the materials used in the suspension assembly and the substrate were studied and their compatibilities vis a vis

seawater and process chemicals used were established.

Table-3 : Summary of Experimental results

| Parameter	Campaign-1	Campaign-2	Campaign-3	Campaign-4
Substrate mm	75x70x2	75x70x2	150x150x2	150x150x2
% Grafting	130%	130%	100%	100%
Alkalination	2-4 hrs	2-4 hrs	4 hrs	4 hrs
Submergence	260 hrs	260 hrs	400 hrs	366 hrs
Elution	2 hrs	2 hrs	400 hrs	366 hrs
Analysis of elute µg/ml				
Vanadium	0.06 to 0.2	0.02 to 1.5	0.5 to 3.3	0.61 to 0.87
Uranium	ND	0.35 to 0.93	0.22 to 0.65	0.09 to 0.67
Uranium collected µg/gm of PAO	ND	75.97	12	12
Total	800µg			

Process Flow Sheet for 100gU/year Experimental Facility

Based on initial success of extracting about 800 µg of uranium by harnessing the tidal wave using electron beam grafted amidoxime as adsorbent, the Process flow sheet for scaled up facility to extract 100gU/year has been developed. The process flow scheme is as shown below.
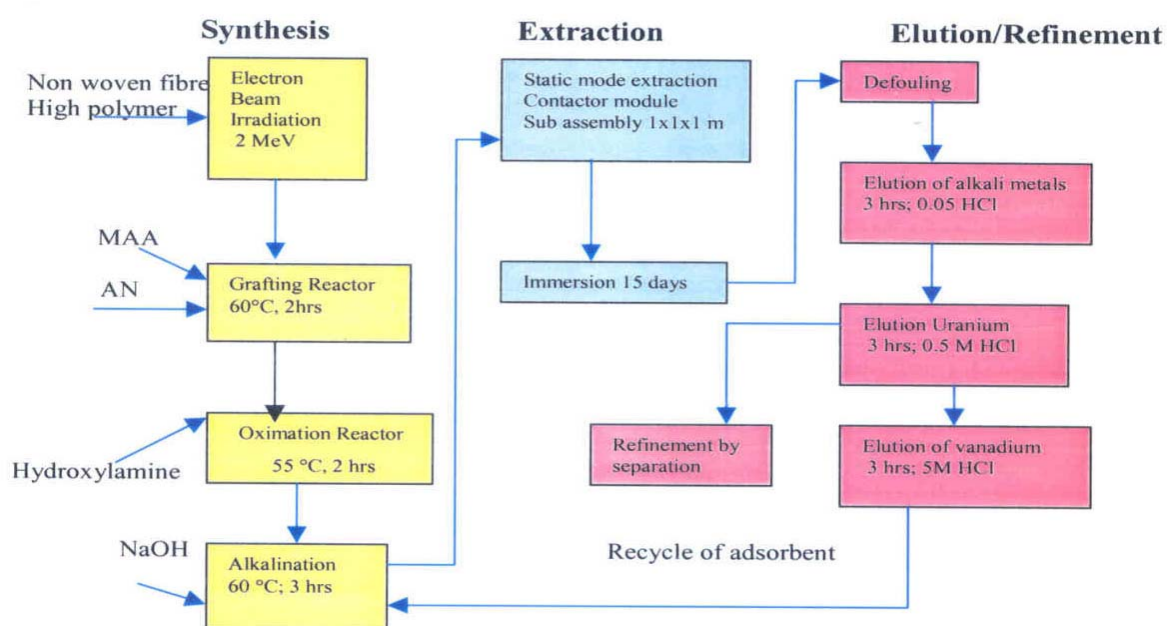
Design description of substrate: The size of the scaled up substrate is 1000 x 1000 x 1.5mm thick. The substrate is made with fiber of 1 denier cross-section and 300 grammes of fibre per square meter. The apparent area of the surface is 2 m^2. The actual area of substrate is 100 m^2 for the fiber diameter considered.

Contactor Array Design: Three types of Contactor Array (CA) designs have been tried as shown in fig.4 below:
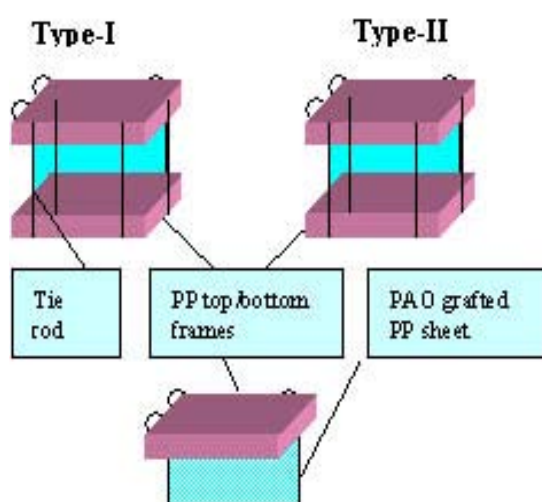
Type I: The design consists cubical box type with top and bottom polypropylene frames to house the hangers for hanging the substrate sheets with polypropylene tie rods. The CA is of size 1000 x 1000 x 1000 mm. The Substrates are of size 1000 x 1000 x 1.5mm with electron beam grafted amidoxime for adsorption. The CA accommodates 27 nos. of substrates. A gap of 25 mm is maintained between the substrate sheets. The sheets are mounted on cPVC pipes, which are hung on polypropylene grooved frames. Eyebolts are provided for facilitating anchoring and mooring during extraction cycle with the help of nylon ropes and for subsequent handling.
Type II: The design is similar to type I, except for the SS-316 tie rods in place of PP tie rods.
Type III : The design is similar to Type I except that it has no bottom frame and no tie rods.

Description of Unit operations: The flow sheet involves the following unit processes:

Stitching of the substrate: The standard substrate roll of non-woven PP fibre felt is cut to size and the pieces are stitched on the cut edges. The substrate is then sent for irradiation.

Electron beam irradiation of the substrate: Polypropylene fibre substrate is irradiated to a dose of ~ 20 Mrads in the ILU-6 Electron Beam Irradiator.

Grafting of acrylonitrile: Acrylonitrile is grafted on the irradiated PP fibre substrate by immersing it in a grafting reactor having acrylonitrile monomer dissolved in di methyl formamide (DMF) solvent to have a 50 to 70% solution. The grafting reactor is of deep design so that the solvent renders a very small evaporation surface. Process is carried out at temperature of 60°C under atmosphere of commercial nitrogen purge and pressure maintained is atmospheric to slightly positive i.e. a couple of mm WC.

The Dissolver Tank has DMF only and dissolving of ungrafted monomer is done at room temperature. Grafting Reactor and Dissolver Tank have 'Relief holes' and have capacity of 130 litres each.

Coils have been provided to heat the mixture using a hot water facility. The grafting is over in about 2 hours. The fibre substrate is then taken out from the Grafting Reactor and put in the Dissolver Tank. In about an hour, the solvent dissolves the non-grafted excess acrylonitrile monomer and homopolymer. The grafted substrates are dried in a drying chamber.

Oximation: The Oximation Reactor is an SS-304L cylindrical tank with FRP lid, graphite rupture disc and vent nozzle. It has an SS-304L immersion coil to heat the vessel using 1.5bar wet-steam. Temperature measurement and control through a thermostat to cut-in or cut-off the steam supply to the heating coil is provided. The Oximation Reactor is charged with ~1000 litres of methanol and ~800 litres of DM water.

Then about 100 to 150 kgs of hydroxylamine hydrochloride flakes are added to the bath gradually in ~1hour time. The circulation pump is used to get a homogeneous solution.

The Contactor Assembly type CA-III with ACN grafted PP fibre substrates is then lowered into the reactor. The FRP lid is then put on the reactor. Steam is used to heat the bath. The reaction is slightly endothermic.

Alkalination: The Alkalination Reactor is of ~2500 litres capacity covered with a removable FRP lid. The reactor is lagged from outside. About 2000 litres of DM water is charged to the reactor and 40 to 100 kg caustic lye is added to it gradually. The dissolution is slightly exothermic. Forced circulation is maintained through a mini pump for ~1 hour. Steam sparging is done with 1.5bar wet saturated steam to maintain the temperature. The amidoximated CA-III assembly is lowered into the reactor. The duration of reaction varies from 2 hours to 6 hours.

Submergence in and retrieval from the Trombay estuary: The alkalinated assembly is transported to CIRUS jetty head. It is slinged as a cradle using 18Φ nylon ropes for submergence in the seawater. The top frame level of CA-III is kept at an average depth 0.5m below the lowest tide level expected during the submergence period. The submergence period is 10 to 20 days. A total of maximum 12 such assemblies will be there at any given time contacting the tidal waves in the sea.

Defouling & Elution: After the sub-mergence operation the cradle assembly is taken out from sea and brought to the plant. The assembly is mounted in the Defouling Tank and washed using 5bar water jet.

Assembly is then moved to Elution Reactor. The Reactor is filled with ~ 1500 litres of DM water and then ~200 litres of commercial HCl of 30% grade is transferred in it gradually. Circulation pump is kept on for the entire

duration of the elution process. Reactor temperature is maintained for about 10 to 24 hrs. Uranium gets eluted in the solution in the form of uranium chloride. The same HCl solution is used for eluting uranium from more assemblies till the concentration of uranium in the solution builds up to ~ 1000 ppm.

Process safety requirements: Acrylonitrile monomer (ACN) and di methyl formamide (DMF) related hazards are addressed with the approach to have minimal quantity in working vessels and working areas. Vapors generation is reduced.
➢ By using deep design reactors and
➢ Keeping provision of nitrogen blanketing.
The vapours from drying chamber are exhausted out using a blower and a discharge stack.
Methanol vapors are condensed and recycled in the oximation process.

Spillages are contained with dykes and drains appropriately.

The discarded substrate sheets do not have any chemical hazard. These are dealt with as non-biodegradable, non-radioactive solid waste.

The operators / technicians while handling hazardous chemicals will use full facemask with vapour filters. In addition they shall also wear apron, rubber hand gloves and rubber boots.

Feasibility Studies on 100Te per year plant

The Refueling requirement of 2 x 220 MWe capacity nuclear power plants based on PHWR technology and operating at ~80% capacity factor is around 80 tonnes of uranium per year [2]. A conceptual process design and cost benefit analysis is carried out for a 100 Te per year 'uranium from seawater' plant. It includes the costs for off shore and on shore civil works, major process equipment and consumption of chemicals, substrates etc.
Salient features of the Project: The adsorption capacity assumed for PAO is 1 g of Uranium per kg of adsorbent. The radiation processing of the

substrate is done at 20 Mrad level to achieve 130% grafting. The total cycle time considered is 20 days and 17 cycles per year is assumed. The requirement of adsorbent material is 5900 tonnes based on current state of technology. About 17,400 contactor arrays of size 4x4x4m will be used. Land area requirements for the on shore units 30x120 M for PAO synthesis and 90x120 M for elution. For the offshore unit based on floating system, the area requirement is 300x550m.

Salient features of the costing: The estimated Operating cost is 25 Crores. Thus operating estimated Cost per kg of uranium is just Rs 2500/kg. The Estimated capital cost, based on current status of technology is 335 Crores. A reasonable life span of 50yrs for the offshore and on shore civil works and the electron beam irradiator is assumed. Life of the remainder equipment is taken as 20 years to arrive at the annual fixed costs. This results in Rs. 900/kg of U recovered as the depreciation component of fixed cost. The 20 years lifetime average interest on the basis of 5% pa works out to 3.8% only. Or in other words the impact on the cost of uranium recovered is Rs. 1500/kg. Thus it is likely to be competitive with the current mining costs.

Conclusions

The specially developed organic adsorbent PAO has shown promising results for recovery of uranium from seawater. Pumped circulation schemes are inherently riddled with negative electricity gain, which means that the electricity producing potential of the recovered uranium is less than the electricity spent in its recovery. But harnessing tidal scheme has the advantage of positive electricity gain and the extent of energy gain ratio depends much on the site selection. Feasibility studies on various sizes of pilot scales will help in optimization of process design parameters of adsorbent synthesis and improving the yield of recovered uranium. The various configurations of contactor array designs being

developed to facilitate the operational flexibility at offshore unit of the plant and utilization of tidal energy/waves more efficiently.

Acknowledgements

References

1. Uranium from seawater report, issued by United Kingdom Atomic Energy Authority, October 1976.
2. Kakodkar A, "Chemical Engineering perspectives in Atomic Energy Programme", HL Roy memorial lecture delivered at CHEMCON-2000, Organised by Indian Institute of Chemical Engineers in collaboration Kolkata Regional Centre, Kolkata, December 19-22, 2000.
3. Saxena, A.K. Invited Talk delivered at BARC during progress review on 'Uranium from Seawater' on August 14, 2000.
4. Saxena, A.K., "Uranium from seawater: a new resource for meeting future demands of Nuclear reactors", Indian Chemical Engineering, Section C, Vol 43, No. 3, July –September 2001
5. Generation IV Roadmap – crosscutting fuel cycle R&D scope report, issued by Nuclear Energy Research Advisory committee and the Generation IV International forum, December 2002
6. Seiji S, Hirofumi K and Osamu M, "Selective adsorption of UO^{2+} on a calixarene based polymer resin immobilising uranophiles", Journal of Polymer Science:

Part C: polymer letters, Vol 26, 391-396 (1988).

7. Saxena, A.K. Invited Talk delivered at DD, BARC during progress review on 'Uranium from Seawater' on April 23, 2000.

8. Sugo T, Status of Development for Recovery Technology of Uranium from seawater, Nippon Kaisui Gakkai-Shi, 51 (1) 20 1997.

This paper received the Best Paper award at the Chemical Engineering Congress – 2003 held at Bhubaneswar in December 2003
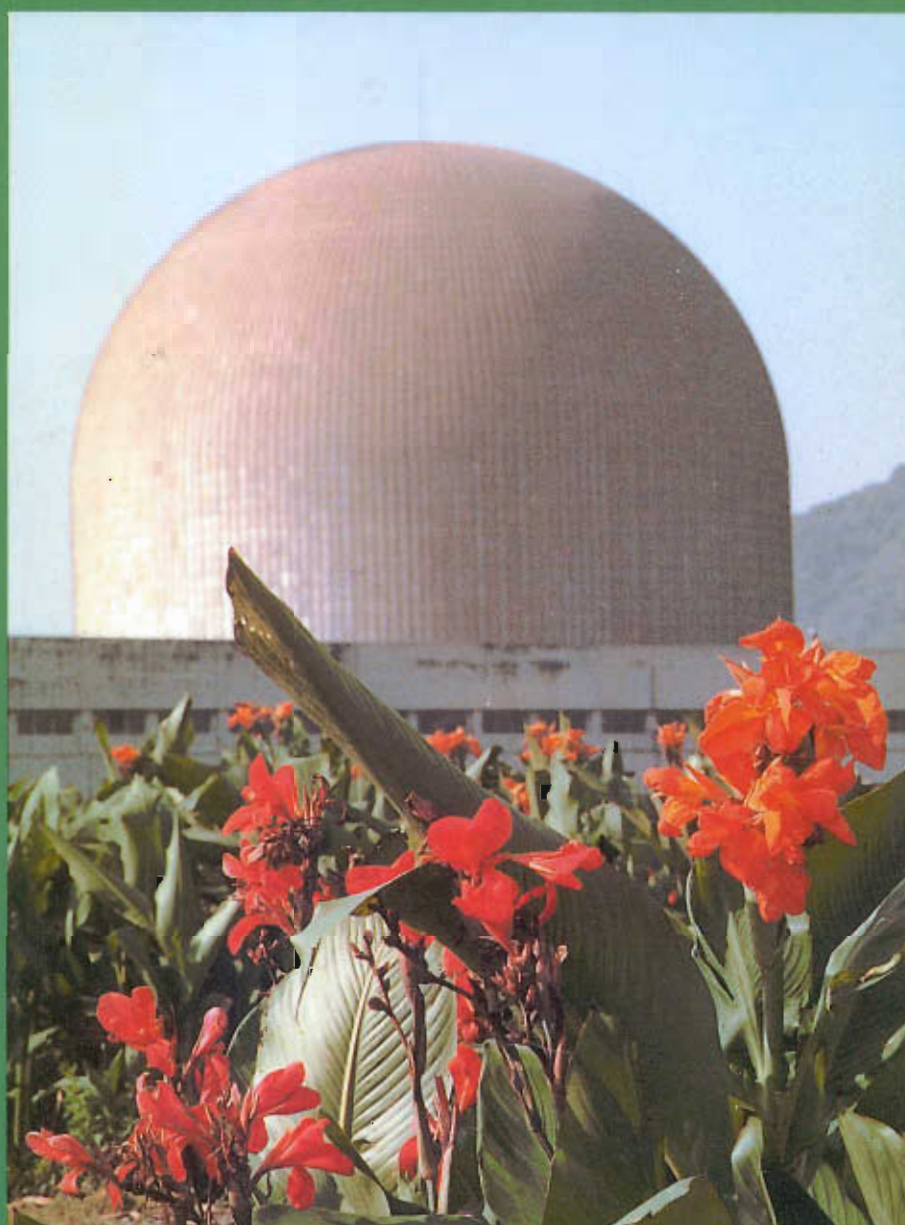

About the author ....

Arun Kumar Saxena graduated from GSITS, Indore, in Engineering in 1968 and joined BARC. He is presently Head, PICUS, Desalination Division, BARC. His professional achievements include:

1. *Outstanding work on Phosphorus Technology with published technical documentation of ~1000 pages on it.*
2. *30 published technical papers.*
3. *Two patents : One on 'Refractory grade carbon' and the other patent on 'Zero leak seals for moving electrodes in submerged arc furnaces.'*
4. *Automation of large capacity seawater desalination plants.*
5. *Presently exploring recovery of 'Uranium from seawater'.*

For more than a decade, he has been serving the Executive Committee of Mumbai Regional Centre (MRC) of Indian Institute of Chemical Engineers in various capacities. For the years 2000 and 2001, he had been its Chairman. As Chairman, he organised a very successful fund raising cum technical event, "Symposium on IT in Chemical Industry- SITCI". During his chairmanship, the MRC received "Best Regional Centre Award" for the year 2001. Earlier as Editor of the MRC bulletin for 3 years, he gave the bulletin a new 'getup and image' of a standard journal. As invited Editor of 'Indian Chemical Engineer', he brought out a special issue on 'Chemical Engineering in Nuclear Technologies' in October 2001.

Mr A.K. Saxena has been the Hon. Vice-President of the National Governing Council of Indian Institute of Chemical Engineers for the year 2002. He was its Hon. Secretary for the year 2001.
In addition to his technical productivity, he is also very actively associated with Lions Clubs International and at present, he is the District Chairman, Information Technology for the North-East Mumbai region.